University of Catania
Department of Civil Engineering and Architecture (DICAR)

Doctoral Programme in Evaluation and mitigation of urban and territorial risks

---

Microwave regeneration of activated carbon saturated with contaminants of emerging concern (CEC)

Erica Gagliano
Ph.D. candidate

Supervisor: **Prof. Paolo Roccaro**
Tutor: **Prof. Pietro Paolo Falciglia**
Research group: **Prof. Tanju Karanfil, Prof. Federico G.A. Vagliandi, Ing. Massimiliano Sgroi**
Coordinator of the Doctoral Programme: **Prof. Massimo Cuomo**

33rd cycle

Academic Year 2020

Summary

In recent decades, the occurrence of contaminants of emerging concern (CEC) at trace levels in water matrixes is under investigation due to their proven or potential adverse effects on human health and the aquatic ecosystems. Amongst anthropogenic CEC, poly- and perfluoroalkyl substances (PFAS) and radioactive 137-Cesium (^{137}Cs) have increasingly received attention due to their high solubility in water, mobility through the environment and bioavailability to terrestrial and aquatic organisms through the food chain. To date, the adsorption is deemed more cost-effective than other advanced processes and the activated carbons (ACs) are extensively recognized as the most common adsorbent materials for both organic and inorganic contaminants. However, ACs saturation is a major issue affecting full-scale treatments. As an alternative to landfill disposal, the regeneration allows the reduction of waste production and the renew of AC adsorption capacity. Generally, the regeneration of exhausted ACs is performed by chemical or conductive thermal processes, although several limitations were widely highlighted. Conversely, Microwave (MW) irradiation is currently figured out as a very effective regeneration technique for exhausted ACs due to the high dielectric nature of ACs (*Chapter 1*). However, further investigations are needed to better explore the efficacy of MW regeneration to a wide group of adsorbates since previous experimental studies were mainly focused on dye compounds.

The overarching goal of the present research is to investigate the innovative regeneration technique based on MW irradiation for saturated ACs. Deeply, the experimental work has been conducted in order to demonstrate the efficacy of MW irradiation (performed at several irradiation power and time) in terms of AC adsorption capacity recovery and textural properties variation.

Moreover, to increase the knowledge on the role of organic matter (OM) during PFAS adsorption and the regeneration processes currently employed for PFAS-saturated adsorbents, the published experimental works are critically reviewed (*Chapter 3*). It can be inferred that granular activated carbon (GAC) adsorption is the most applied technique for PFAS removal at full-scale treatment plant although a fast breakthrough of PFAS (specifically short-chain compounds) was demonstrated. To overcome issues related to GAC replacement it is becoming priority find a suitable regeneration technique for PFAS-saturated GAC.

With this purpose, the applicability of MW irradiation to regenerate PFAS-saturated GAC has been investigated through lab-scale experiments (*Chapter 4*). The results have proven the capability of MW irradiation to desorb long-chain PFAS (i.e., perfluorooctanoic acid (PFOA) and perfluorooctane sulfonic acid (PFOS)) from two commercially available GACs. Rapid temperature increases at short irradiation time, the preservation of GACs porous structure and a good regeneration efficiency throughout several regeneration cycles represent the main key findings. Moreover, the comparison of

MW regeneration efficiencies with the percentages obtained by means of chemical regeneration corroborates the beneficial application of the innovative regeneration technique by means of MW irradiation. Indeed, MW regeneration may allow the overcoming of several drawbacks related to currently employed techniques to manage PFAS-saturated GACs (e.g., the use of organic solvent in chemical regeneration, the costs related to landfill disposal of PFAS exhausted GAC). Based on obtained results, MW irradiation is a promising alternative regeneration technique for PFAS-saturated GACs and further investigations are still required to better understand the PFAS degradation mechanisms.

A novel proof of concept based on MW regeneration coupled with permeable reactive barrier (MW-PRB) for Cs-contaminated groundwater is introduced for the first time. Batch adsorption and column experiments were performed to assess the efficacy of MW irradiation for the regeneration of Cs-saturated GAC (*Chapter 5*). The noticeable Cs removal performance and the low weight loss throughout several adsorption/regeneration cycles claim that MW regeneration of Cs-saturated GAC is a potential effective treatment. A techno-economic analysis is conducted to evaluate the longevity of novel MW-PRB at different scenarios (e.g., simulated Cs field contamination and groundwater velocity) and to provide a comparison of main specific costs between new MW-PRB system and conventional one (*Chapter 6*). The obtained results of techno-economic analysis revealed the MW-PRB feasibility, demonstrating its advantages also in comparison with conventional PRB systems.

The main findings of this research support and promote the feasibility of MW irradiation for the regeneration of saturated ACs. They provide essential information to design and conduct the successive pilot-scale studies. Moreover, some speculations here provided could be helpful to guide the successive scaling-up and to expand the boundaries of full-scale applications (*Chapter 7*).

Table of content

Chapter 1: Literature review and research needs

1. Introduction

In view of sustainable and environmentally friendly development, the essential aims are the reduction of environmental pollution and risks, the protection of natural resources, correct disposal of industrial wastes, and the effective management of water and wastewater treatment plants.

Over the years, illegal discharge activities and ineffective wastewater management have increasingly caused several environmental contaminations worldwide. Drinking water supplies, such as surface water and groundwater, are the compartments mainly impacted by a wide group of contaminants of emerging concern (CEC). CEC have drawn great attention due to their adverse effects on human health and aquatic ecosystems.

Amongst them, per-fluoroalkyl substances (PFAS) and radioactive 137-Cesium (^{137}Cs) are currently under investigation due to their high solubility in water, mobility through the environment, and bioavailability to terrestrial and aquatic organisms through the food chain. Due to the recalcitrant nature of those contaminants, conventional treatments are scarcely applicable or high energy-requiring. Consequently, the implementation of advanced treatments is often required.

The adsorption on activated carbons (ACs) is recognized as the most cost-effective technique for the removal of both organic and inorganic contaminants. However, the performance of full-scale treatments mainly depends on the ACs saturation, which once reached requires the replacement of exhausted ACs with fresh ones. It is paramount to reduce the environmental risk linked to landfill disposal of ACs saturated with harmful substances which may cause the contamination of drinking water supplies (e.g., surface water and groundwater). With this purpose, several regeneration techniques (e.g., chemical, biological and thermal) have been extensively proposed for saturated ACs. However, conventional regeneration techniques own numerous disadvantages and, consequently, further investigations are required in this topic area. Moreover, in order to obtain a good adsorption recovery capacity avoiding the damage of ACs, the development of an effective regeneration technique is needed for both water treatment facilities and ACs manufacturers.

The present research faces the engineering aspects regarding the protection of the natural water resources in order to reclaim the contamination ascribed to human activities through the development of advanced methods and technologies.

In this regard, the overarching goal is to investigate the feasibility of an innovative technology based on microwave (MW) irradiation for the regeneration of AC saturated with CEC.

2. Contaminants of emerging concern (CEC)

The ubiquitous environmental presence of anthropogenic or naturally occurring chemicals, albeit in trace concentrations (ng L^{-1} and μg L^{-1} at contaminated sites), has become an issue of great concern due to the potential harmful impact on human health and on both aquatic and terrestrial life forms. Widely called "contaminants of emerging concern" (CEC), this broad group of chemicals includes both inorganic and organic substances which were not typically included in routine monitoring programs and they could be categorized as water contaminants, due to their known or suspected undesirable effects on humans and ecosystems [1–3].

Two criteria have been proposed for long-term classification of a substance as an emerging contaminant: its persistence in the environment and/or potential harmful human and ecotoxicological effects. However, a substance is not regarded as an emerging contaminant due to the lack of its reported adverse effects, despite the release of a substances may have been going on for a while and it is now widespread in environmental compartments. Conversely, new information regarding ecotoxicological risks may result in reclassification of a well-known contaminant as an emerging contaminant, as occurred in the case of endocrine disruption by nonylphenol [3].

Although some of these synthetic organic compounds such as pharmaceutically active compounds (PhACs), personal care products (PCPs), artificial sweeteners (ASs), fertilizers and pesticides became essential components of modern society, CEC enter the aquatic environment through the water cycle, affecting the quality of drinking water supplies (i.e., groundwater and surface water) [4]. It was demonstrated that the global annual production of anthropogenic chemical increased from 1 million ton in 1930 to 400 million tons in 2000 [3]. Moreover, the existing water treatment facilities (such as wastewater and drinking water treatment plants) are not suited to remove CEC and, in many cases, they represent a route of entry into the environment due to their transformation and not completely degradation. The inclusion of CEC into environmental compartments occurs through several pathways as illustrated in Figure , including the direct discharge of raw and/or treated wastewater from municipal and industrial wastewater treatment plants (WWTPs), landfill leachate, stormwater runoff from urban areas, sewer leakage/sewer overflow, surface runoff in agricultural areas where the reuse of treated wastewater is applied for irrigation purposes [2,3]. Consequently, they have been detected in sewage effluents, groundwaters, surface waters and drinking water sources [5]. Moreover, their occurrence in suspended solids and sediments (both river and marine) has been demonstrated.

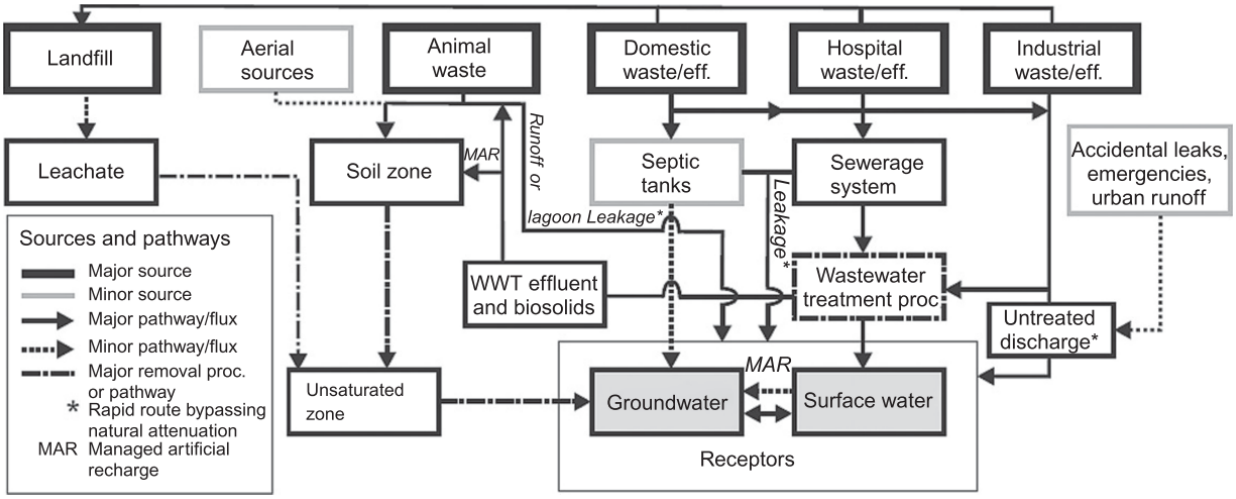

Figure 1 Schematic view of sources and possible pathways of CEC in the environmental compartments [3].

In the last decades, several regulations have been promulgated for controlling: synthetic organic contaminants (e.g., poly- and per-fluoroalkyl substances, PFAS), inorganic contaminants (e.g., perchlorate and arsenic), radionuclides, disinfection by-products DBPs (e.g., trihalomethanes, THMs, and nitrosodimethylamine, NDMA) [6].

Although some CEC have been already regulated such as THMs and NDMA, others are still under investigation and they will be candidates for future regulations due to their potential harmful effects. For instance, in the USA Safe Drinking Water Act Amendments (1996) recommend to publish a contaminant candidate list (CCL) in order to identify potential substances for regulation within a 5-years period [7]. In Europe, the European Directive (98/83/CE) on the quality of water intended for human consumption will set standard limit for PFAS.

However, the occurrence, the risk assessment, and the ecotoxicological data are not available to all CEC, making the prediction of their fate in the aquatic environment difficult [8]. This lack of information could be partially ascribed to the development of a standard analytical method for the entire CEC group [7,9]. Indeed, the analysis of CEC is challenging due to the trace concentrations (usually at part per billion (ppb) or part per trillion (ppt) levels) and the complexity of water matrices (e.g., the presence of organic matter and other compounds in solution) [8]. Furthermore, the extent of CEC may be considered limitless due to the replacement of regulated compounds with new unregulated ones [4].

In summary, CEC are a wide group of compounds which differ widely in their chemical, biological, and physical properties, such as chemical reactivity, biodegradability, and hydrophobicity [10]. Due to their heterogeneity, one single process will not remove all contaminants, and a multi-barrier approach is often suitable to achieve a certain level of water quality. Based on precautionary principles,

advanced techniques must be adopted for the upgrading of water treatment plants, allowing to maximize CEC removal and to face the future drinking water directives and standards.

Amongst the wide group of CEC, poly- and perfluoroalkyl substances (PFAS) and radionuclides, inorganic compounds have drawn great attention due to their occurrence in aquatic environments (such as drinking water supplies, both groundwater and surface water) and potential toxic to animals and human beings.

For each class, specific contaminants (long- and short-chain PFAS and radioactive ^{137}-Cs) were selected as contaminants target in the present research.

Their physical and chemical properties, occurrence and the main processes available for their removal are discussed in the following sections. Lastly, based on the state of art provided, the knowledge gaps and consequently the main research needs are outlined.

Furthermore, as discussed below, by reviewing the previous published works regarding PFAS adsorption (both research and review papers) it was found that more research is needed regarding the adsorption capacities of different adsorbent materials, with particular focus on the role of organic matter and the available techniques for the regeneration of PFAS-saturated AC.

2.1 Poly- and perfluoroalkyl substances (PFAS)

PFAS have been used in products since the 1950s, but were not widely recognized as contaminants until the 2000s. They are used to make stain repellents that are applied to fabrics and carpets, as well as in adhesives, paints, waxes, polishes, metals, electronics, fire-fighting foams, and caulks, and grease-proof coatings for food packaging, including microwave popcorn bags, French fry containers, and hamburger wrappers [11,12]. The chemical structure includes also a charged functional group commonly carboxylic and sulfonic acid attached at one end. Depending on terminal functional group, PFAS can be distinguished in per- fluoroalkyl carboxylic acids (PFCAs) and in perfluoroalkyl sulfonic acids (PFSAs) [13]. An abridged way to distinguishing among PFAS subclasses is that referred to carbon chain length. The terms “long-chain compound” indicates perfluoroalkyl carboxylic acids (PFCAs) with eight or more carbons, and perfluoroalkane sulfonates (PFSAs) with six or more carbons. Whereas, “short-chain” is related to perfluoroalkyl carboxylic acids with seven or fewer carbons o perfluoroalkane sulfonates with five or fewer carbons [14]. It should be noted that PFCAs and PFSAs classification based on chain length is different in terms of number of C atoms. Considering that PFAS bioaccumalution and biomagnification into biota increase with the increasing of carbon chain length, PFSAs are more bioaccumulate than PFCAs with the same chain length [15].

Knowing PFAS physical and chemical properties is essential to understanding their fate and transport in the environment. The strong C-F bound leads to PFAS thermal stability. Whereas, the terminal functional group attached to fluoroalkyl chain provides PFAS chemical stability [13]. PFAS exhibit

mutually hydrophobic and lipophobic properties which are primarily attributed to the low polarizability of fluorine atoms. With the increasing replacement of hydrogen by fluorine as well as the increasing of carbon chain length, PFAS become more chemically inert. On the contrary, their water solubility increases with the decreasing of carbon chain length [11]. Other properties among them resistance to thermal, biological and chemical degradation and redox stability impart unique properties to PFAS [11,13,14].

Due to their intensive industrial production and application, PFAS contamination is the result of consumer products degradation, firefighting activities and fluorochemical manufacturing facilities [12]. PFAS are frequently detected in wastewater influent and effluent, as well as drinking water supplies (e.g., surface water and groundwater) [11,16]. They have been detected at low concentrations in the aquatic environment, ranging from pg L^{-1} to ng L^{-1} [17–19]. The redistribution of PFAS is partially known due to the limited efficiency of conventional wastewater treatment in PFAS removing (e.g., drinking and wastewater treatment plants) and the transformation of PFAS precursor compounds [11,19]. Long-chain compounds such as perfluorooctane sulfonate (PFOS) and perfluorooctanoate (PFOA) are been the most commonly measured PFAS around the world. Although PFOS and PFOA have been banned (Stockholm Convention on Persistent Organic Pollutants, 2010), the total amount of PFAS in the environment is not reduce due to long-chain compounds replacement with short and ultra-short PFAS, and other PFAS alternative compounds are still unidentified [20–22].

Removal of PFAS during water and wastewater treatment processes has been found to be very challenging [11,23]. Indeed, PFAS resist conventional chemical and biological degradation processes in natural and engineered treatment systems due to the stability of perfluoroalkyl chains [11,24]. Adsorption and anion-exchange processes are actually an established technology for PFAS removal, both as single process of point-of-use applications and as step of drinking water treatment plants as well as groundwater remediation [11,19,21,23].

Whereas, other treatment process such as high pressure filtration (i.e., nanofiltration and reverse osmosis) and degradation technologies (e.g., electrochemical oxidation and plasma-based technology) are still in early-stage development and are infeasible for practical applications due to high cost [24,25].

2.2 Radioactive cesium (^{137}Cs)

Radionuclides contamination of drinking water supplies is become a significant and emerging issue. The release of radionuclide into the environment is mainly caused by anthropogenic activities such as nuclear power plant (both common operations and incidental events) and medical facilities. Those activities lead to contaminated surface water and groundwater, as a consequence radionuclide may enter in drinking water production chain [26,27].

Cesium-137 (^{137}Cs) is produced when uranium and plutonium undergo fission after having absorbed neutrons in a nuclear reactor and is detectable and measurable by gamma counting. Small amounts of cesium-137 are released on a regular basis in spent fuel ponds through cracks in the fuel rod that reach the coolant and fuel reprocessing waters, which are all subsequently discharged into the sea as effluents. Consequently, it is a major radionuclide in spent nuclear fuel processing and it represents the most important risk driver after nuclear accident, such as those occurred at Chernobyl and Fukushima [28]. For instance, The Fukushima nuclear power plant accident caused a significant release of Cs radioactive isotopes into the environment (~3 x 10^{16} Bq) [29]. The ^{137}Cs isotope is of special concern due to its high radioactivity and long half-life (~30.4 years). Consequently, it falls in the class "radionuclides emitting beta particles and gamma radiation" with a maximum level of contaminants imposed by EPA of 4 millirems per year in drinking water [30].

Contamination by ^{137}Cs has impacted large areas worldwide and through fall-out processes caused high soil impacts. Cesium is very mobile in aqueous environments due to its high water solubility and consequently it may bind to soil and minerals. Cesium ions can easily be incorporated in terrestrial and aquatic organisms due to its chemical composition similar to potassium and sodium [29]. This promotes accumulation of cesium and contamination through food chain [27]. The radioactive Cs can create an internal hazard into human body, with higher concentration in muscle tissues and lower in bones. In addition, its biological interactions similar to that of potassium have been reported to be responsible to many problems in cardiovascular, immune and respiratory systems [31,32]. Consequently, most of studies regarding nuclear wastes management have been focused on ^{137}Cs. The high solubility and mobility of Cs ions along with their bioavailability to terrestrial and aquatic organisms pose a severe public health concern [33]. Although radioactive Cs has been detected at a low level, drinking water impacted cesium is the primary pathway of Cs in food chain and the decontamination is urgent and a challenging task [27,34].

Amongst physicochemical treatments for decontaminating Cs-impacted water, solvent extraction, ion-exchange and adsorption are the most widely used based on ionic selectivity and efficiency [29,34,35]. Although, solvent extraction using macrocyclic ligand (crown ethers, calix-crowns, chlorinated cobalt dicarbollide) has been shown effective, the full-scale application is very restricted due to the high cost related to equipment and chemicals [36].

Adsorption and ion-exchange is generally preferred to treat large volumes of wastewater, especially when high- purity water is required, due to their cost-effectiveness and easy implementation [29,37].

3. Adsorption processes for CEC removal

Adsorption is one of the most widely used technologies for removing CEC from contaminated aqueous media. It is preferred over other methods because of its relatively simple design, operation, cost effectiveness, and energy efficiency [38,39]. As a whole, two types of interaction are possible between adsorbent and adsorbate: physisorption and chemisorption. The former is a result of attractive forces between adsorbent and adsorbate molecules. Chemisorption provides a stronger bond as it involves the transfer or sharing of electrons between adsorbent and adsorbate species. Specifically, physisorption involves physical adsorption and electrostatic attraction, whereas chemisorption is referred to ion-exchange, precipitation and surface complexation [40].

The adsorption process for removing PFAS and Cs from has been demonstrated to be effective in removing PFAS and Cs from aqueous solutions [29,41]. Amongst several adsorbent materials (commercially available and synthetized ones), activated carbons (ACs) have shown a good applicability for both PFAS and Cs.

Indeed, several clay minerals (e.g., montmorillonite, zeolite, bentonite, vermiculite) or Prussian blue supported materials have been investigated for Cs-removal from groundwater and wastewater [29,42]. However, high concentrations of Na^+ and K^+ ions make the former less effective adsorbents, while the synthetized materials are not recommended due to their non-reusable character or high regeneration costs [42,43].

Adsorption by granular activated carbon (GAC) has been employed as the major treatment process for PFAS removal from wastewater [19,21] and drinking water [11], as well as for groundwater remediation [44]. However, varying performance has been observed in laboratory studies and treatment systems of various scales. It should be highlighted that mostly of adsorption studies have addressed single long-chain PFAS (i.e., PFOA and PFOS) and the evaluation of adsorption efficiency has been explored at high PFAS concentrations, which are not representative of the environmental concentration level [21]. Moreover, prior researches have often been carried out by using deionized water (DI) spiked with selected PFAS, and the effect of organic matter (OM) was not accounted for. Fast breakthrough of PFAS, especially increasingly used shorter chain PFAS, and short service life of GAC filter have been extensively documented [11,45,46].

As an alternative to GAC, anion-exchange resin is currently demonstrated a suitable technology for PFAS removal [11,21,47]. By comparing the adsorption capacities obtained under the same experimental conditions, anion-exchange resin often adsorbs more PFAS than GAC, especially short-chain compounds [45,46]. However, due to the highest capital costs related to full-scale application of anion-exchange resin, GAC is become well-established removal treatment for PFAS removal.

To sum up, the main issues related with PFAS removal through adsorption process are the influence of water matrix (e.g., competing anions, organic matter), frequent regeneration (due to fast breakthrough), and disposal of concentrate with high PFAS concentration [11,46,48]. Consequently, further investigations are strongly advised.

As previously pointed out, the occurrence of PFAS and Cs has been reported in a wide variety of drinking water supplies, including groundwater [11,27,49]. Permeable reactive barrier (PRB) is an effective technology for remediating contaminated groundwater [50–52]. It generally consists in a trench penetrating the aquifer and filled with reactive material, whose hydraulic conductivity is higher than that of the surrounding soils, so that the contaminated plume moves under natural hydraulic gradient and it is passively treated without external energy inputs [51].

Compared to traditional pump-and-treat remediation, PRBs own higher installation costs. However, since PRBs are a passive system, the long-term costs are lower than traditional pump-and-treat operation and maintenance costs which are mainly related to due continuous energy input [53].

The PRB design includes the choose of filling material as well as the site characterization which includes the site geology, hydrology and geochemistry. The filling material of PRB should be (i) reactive, to adsorb the target contaminants; (ii) permeable, to allow water to flow through them; (iii) passive, to work naturally with little maintenance and (iv) cost-effective due to the large amount needed [51]. To meet the conditions required, ACs are widely used materials as PRB filling materials [50,54]. Limited longevity of PRB due to a rapid ACs saturation is the major problem affecting full-scale treatments [51]. Consequently, a frontier and active research issue is coupling PRB with other regeneration processes (e.g., electrochemical and biodegradation) with the aim of extend the PRB longevity[55,56]. However, further investigations are required in this topic area due to the long regeneration times needed for biodegradation and to identify an effective treatment for heavy metals and radionuclides [57].

Furthermore, PRB technological aspects and long-term performance have not been extensively investigated. This gap in our knowledge is all the more problematic because design life has a decisive influence on the economic viability of PRB [58].

4. The main drawbacks of conventional regeneration techniques

Although the widespread use of ACs in the adsorption processes for the removal of both organic and inorganic contaminants is extensively documented, the main limitation during full-scale application is related to its saturation [38,59]. Conventionally, once the adsorption capacity has been exhausted, ACs were incinerated or landfill disposal. However, the disposal of ACs saturated with hazardous contaminants can lead to secondary contamination pathway , whereas the incineration can be considered an uneconomic solution [60]. Consequently, the cost-effectiveness of adsorption process greatly depends on the reuse of ACs. Several regeneration techniques have been developed to desorb both organic and inorganic adsorbed compounds, consequently renewing the ACs adsorption capacity [60–62].

The common regeneration techniques can be categorized into biological, chemical and thermal.

In biological regeneration, the exhausted ACs are placed in contact with a disperse culture of microorganisms, which act the degradation of adsorbates. However, it is mainly related to biodegradable compounds and it requires long treatment times [61,63]. Biological regeneration has been mainly studied in single solute systems and its application at full-scale is not attracted due to the lower regeneration efficiency in the presence of complex aqueous matrix (e.g., drinking water) [60,61].

Chemical regeneration involves the elution of adsorbed compounds using specific extracting agents, mainly chemical solutions. It is usually adopted when there is a risk of ignition or destruction of the adsorptive material such as anion-exchange resin. Moreover, it is not recommended for ACs due to the large investment costs required [63,64].

In spite of being the most widely regeneration technology, conductive thermal regeneration is time-consuming, expensive in terms of energy consumption and it causes loss of a considerable amount of carbons (5 - 15%) due to attrition, burn-off and washout [60,65,66]. Thermal regeneration is currently performed in rotary kilns and fluidized bed furnace at full-scale treatment plant [61]. Briefly, the heating process under mildly oxidizing atmospheric conditions (steam and carbon dioxide) encompasses several steps: (i) evaporation of water, (ii) thermal desorption of volatile compounds (temperatures 100–260 °C), (iii) pyrolysis and carbonization of non-volatile compounds (temperatures 200– 650 °C) and (iv) gasification of pyrolytic residue at high temperatures (~ 800 °C) [60,61,63].

It should be highlighted that the above-mentioned techniques are usually not performed in situ since they have implemented at specialized treatment facilities. As a consequence, the delivery of exhausted GAC at regeneration treatment plants, often for long distance, represents an additional cost [59]. Due to the aforementioned drawbacks, alternative AC regeneration techniques are subject of current investigations.

5. Microwave irradiation: innovative regeneration technique for saturated AC

5.1 Theoretical background of microwave heating

Recently, microwave (MW) irradiation has acquired a great deal of attention in energy and environmental fields [62,67–69]. Developed for communication purposes, it has currently employed as a cost-effective alternative heating technology for several applications, such as mineral processing and extractive metallurgy, drying processing, cement and concrete processing, food industry and oil processing [67,70]. More broadly speaking, MWs are a part of electromagnetic spectrum occurring in the frequency range of 300 MHz to 300 GHz. For industrial and environmental applications, a frequency of 2.45 GHz is generally adopted [59,63].

The growing interest in MW technique is also based on the passive ability of the irradiated matrices to convert a low power irradiation energy into a rapid and large temperature increase. As a matter of fact, during MW irradiation, electric power is partially absorbed by the irradiated matrix and converted into heat, according of the law of Lambert and Beer, generating an exponential decrease of the local electric field with the distance from the MW power [58,64]. This conversion explains the thermal effect associated with the MW irradiation. Moreover, the presence of an alternating electromagnetic field induces the dipolar rotation inside the polar molecules located in the medium (e.g., water), which contributes to heat generation [67,71]. When a medium is irradiated by a MW field, the energy is irreversibly absorbed, bringing to a “volumetric heating”.

Based on the interactions with MW irradiation, materials can be categorized into: conductors, insulators and absorbers [67,70]. Deeply, MW irradiation is reflected from the surface of conductors, for instance metals below to conductor materials [62]. On the contrary, insulators are transparent to MW irradiation. Consequently, the rapid heating through MW irradiation depends on the dissipation factor of the material (loss tangent). Dissipation factor is the ratio of relative loss factor (ε’’) to the dielectric constant (ε’) of a material [63,64]. Dielectric constant is in fact a relative measure of the MW energy density in the material and the relative loss factor accounts for the internal loss mechanisms, i.e. the amount of MW energy that is lost in the material as heat. Therefore, a lossy material with a high ε’’ is easily heated by MW energy [62,67].

It is noteworthy that MW heating differs from conventional heating, where the heat is transferred to the surface of a material and then it is transferred towards the cooler regions by thermal conduction [65,72]. The difference in heat propagation could be visually explained by looking at the obtained temperature profiles after MW irradiation and conventional thermal heating (Figure 2).

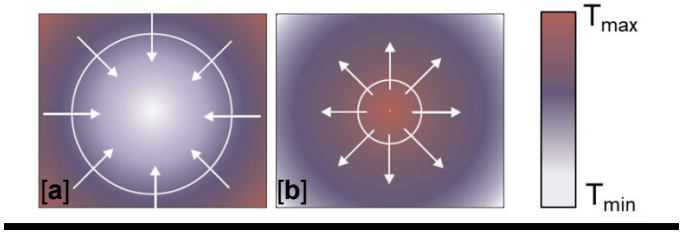

Figure 2 Schematic view of temperature profile and heat direction: conventional heating **[a]** and microwave heating **[b]**.

5.2 Microwave regeneration for saturated adsorbents

To date, MW irradiation has been considered as an effective and alternative technique to regenerate saturated adsorbents (i.e., ACs) due to its capability to heat volumetrically, overcoming the heat transfer limitations that characterize conventional heating [63,66]. MW energy is in fact supplied direct to the carbon bed and it is quickly transformed into heat by dipole rotation and ionic conduction, heating the bulk of the materials throughout the volume [73]. Consequently, the interior part of activated carbon is heated more favorably under MW irradiation, which facilitates the regeneration process [56,58,62].

The major driving force in MW regeneration of saturated ACs is the dielectric nature of carbon which allows the conversion of low power irradiation energy into a rapid and large temperature increase. Furthermore, ACs are suitable materials for MW irradiation due to the delocalized π electrons from sp2-hybridized carbon materials. Specifically, the motion of electrons generates heat through Joule heating within the grain or arc generation at phase boundaries [73]. High mechanical strength and a good resistance towards heat and radiation are other essential features, which promote the MW regeneration of exhausted AC [62,63,73]. MW regeneration offers the possibilities of rapid and precise control of the adsorbent temperature and shorter regeneration time, which implies energy saving [66,74]. The use of MW irradiation for exhausted ACs may avert costly and logistically challenging for ex-situ regeneration of exhausted AC [63].

Several studies have employed MW irradiation for regenerating AC exhausted with organic pollutants (mainly textile dyes and pharmaceutical compounds) and the results are very promising [66,75–78]. Among them, some studies have performed both MW regeneration and conventional thermal regeneration and a comparison between the two techniques was provided [66,75,76,79,80]. As whole, the results demonstrate that the regeneration time is considerably shorter compared to conventional heating and the MW regeneration better preserves AC porous structure than conventional regeneration [66,76,78]. Moreover, the weight loss during MW regeneration occurs to a lesser extent than conventional heating [60,74].

A collection of studies carried out in the regeneration of AC by applying MW technology and the relative regeneration efficiencies are reported in Table 1. The regeneration efficiency (RE, %) of MW irradiation in regenerating exhausted AC (also called adsorption capacity recovery) has been widely

calculated as the ratio between the adsorption capacity of MW regenerated AC and that of virgin one [74,78,81]. As it can be noted the MW experimental conditions such as power (W) or temperature (°C) applied, irradiation time (min), atmosphere (nitrogen, oxidizing or air) and number of regeneration cycles performed as well as the kind of adsorbate (e.g., phenol, textile dyes, salicylic acid) and AC type (e.g., coconut AC, coal-based AC, agricultural-based AC) vary among several experimental studies. As a consequence, a comparison between obtained findings is very challenging. The main results showed high RE values also after several regeneration cycles (Table 1).

Other evidences could be highlighted by looking at experimental studies in which several kind of AC loaded with the same adsorbate were regenerated at the same MW irradiation conditions [74,82].

For instance, Quan et al. [82] demonstrated that, after four cycles of MW regeneration (power of 850 W and irradiation time=5 min), the highest RE was obtained when in coconut-based GAC saturated with Acid Orange 7, followed by almond-based GAC and coal-based GAC. This evidence suggests that the efficiency of MW irradiation also depends on AC characteristics such as their dielectric properties and porous structure.

Table 1 Collection of experimental studies carried out on MW regeneration of exhausted AC.

Adsorbate (Initial concentration at adsorption process, mg L^{-1})	**AC type**	**MW irradiation conditions:** Power (W) or temperature (°C); Irradiation time (min); Atmosphere; Num. cycles (n)	**Regeneration efficiency after n cycles (%)**	**Reference**
Phenol (2000)	Coal-based GAC	850 °C; 4 min; N_2; 6 cycles	30	[66]
Phenol (2000)	Coal-based GAC	850 °C; 4 min; CO_2; 6 cycles	47.8	[66]
Pentachlorophenol, PCP (2000)	Coal-based GAC	850 W; 10; air; 7 cycles	104	[83]
Acid orange 7 (500)	Coconut GAC	850 W; 5; Air; 4 cycles	126.8	[82]
Acid orange 7 (500)	Almond-based GAC	850 W; 5; Air; 4 cycles	94.2	[82]
Acid orange 7 (500)	Coal-based GAC	850 W; 5; Air; 4 cycles	86.8	[82]
Phenol (2000)	Coal-based GAC	850 °C; 4 min; N_2; 6 cycles	26.1	[75]

Table 1 Collection of experimental studies carried out on MW regeneration of exhausted AC (continued).

Adsorbate (Initial concentration at adsorption process, mg L^{-1})	**AC type**	**MW irradiation conditions:** Power (W) or temperature (°C) / Irradiation time (min) / Atmosphere / Num. cycles	**Regeneration efficiency (%)**	**Reference**
Phenol (2000)	Wood-based GAC	850 °C 4 min N_2 6 cycles	46.9	[75]
Salicylic acid (2000)	Wood-based GAC	850 °C 4 min CO_2 6 cycles	98.38	[78]
2,4,5-trichlorobiphenyl, PCB29 (100)	Coal-based GAC	700 W 5 min air 6 cycles	162.7	[84]
2,4-dinitrophenol, DNP (100)	Coal-based GAC	850 °C 4 min CO_2 6 cycles	89	[85]
Methylene Blue, MB (300)	GAC from oil fruit bunches	600 W 3 min N_2 5 cycles	68.3	[86]
2,4,5-trichlorobiphenyl, PCB29 (100)	Coal-based GAC	700 W 5 min air 6 cycles	162.7	[84]
Basic Blue 9, BB9 (1500)	Coconut GAC	200 W 3 min N_2 4 cycles	12	[76]
Acid Blue 93, AB93 (1500)	Coconut GAC	200 W 3 min N_2 4 cycles	27.35	[76]
Basic Blue 9, BB9 (1500)	Bituminous charcoal GAC	300 W 1.5 min N_2 4 cycles	21	[76]
Acid Blue 93, AB93 (1500)	Bituminous charcoal GAC	300 W 1.5 min N_2 4 cycles	38.1	[76]

6. Knowledge gaps and research needs

The above reported literature review allows the identification of several limitations on both adsorption and regeneration processes.

The adsorption on AC is widely established technology for the removal of organic and inorganic CEC (specifically PFAS and Cs). However, its efficiency is related to the presence of organic matter and other co-existing compounds. To date, limited studies have addressed PFAS removal by AC adsorption from real water samples. Indeed, a fast breakthrough of GAC column could occurred due to the presence of both short-chain PFAS and organic matter. Consequently, frequent regeneration is required to renew the adsorption capacity.

Amongst conventional regeneration techniques, their limitations are mainly related to the nature of adsorbate and adsorbents. As previously discussed, chemical regeneration requires a large investment costs and it is largely employed for the regeneration of ion-exchange resin. Furthermore, the high concentrated eluate needs further treatment and its management represents the main drawback. Conversely, the feasibility of microbial regeneration at full scale applications is very limited due to the long treatment time required and the inefficacy of some microorganisms to degrade inorganic adsorbate (i.e., Cs). To date, conventional thermal regeneration is a well-established technique for the regeneration of spent ACs and it is performed conventionally in rotary kilns or vertical furnaces [56]. However, it causes the damage of AC porous structure as demonstrated by the decrease in adsorption capacity with subsequent regeneration due to pore blockage of the adsorbent [59]. Moreover, another disadvantage of conventional thermal regeneration is the loss of considerable amount of AC due to friction [56,59]. Recently, MW irradiation has found relevance in the regeneration of carbonaceous materials due to its unique molecular level heating ability that leads to quick and homogeneous thermal reactions [58].

Based on previous discussion, the main research needs can be summarized as follows:

- Experimental studies regarding the adsorption of PFAS on adsorbent materials need to be critically reviewed with particular focus on the efficiency of adsorbent materials for both long- and short-chain PFAS and on the effect of organic matter during adsorption process. Although the regeneration of adsorbents saturated with PFAS is very challenging, most of previous studied lacked the investigation of suitable regeneration techniques for adsorbent saturated with PFAS.
- The innovative regeneration technique through microwave irradiation needs further investigations as demonstrated by its relevant advantages over conventional regeneration techniques.

- In order to overcome the limitations ascribed to conventional thermal regeneration, the coupling of adsorption and alternative regeneration of exhausted AC to be both conducted in situ are strongly encouraged.
- The potentiality of MW irradiation for regenerating ACs needs further investigations since previous experimental works mainly focused on organic adsorbates (e.g., dyes).
- Further investigation regarding the change in ACs textural properties could be helpful to gain insight into the effect of MW irradiation.
- Due to the fast breakthrough of PFAS and the successive regeneration needed, MW regeneration may allow the long-term performance at full-scale treatment plant.
- The implementation of novel remediation techniques based on MW irradiation is encouraged also for contaminated groundwater, for instance to enhance the longevity of PRB.

References

[1] Rodriguez-Narvaez, O.M., Peralta-Hernandez, J.M., Goonetilleke, A., Bandala, E.R., **2017**. Treatment technologies for emerging contaminants in water: A review. *Chemical Engineering Journal*. 323, 361–380. DOI:10.1016/j.cej.2017.04.106.

[2] Gogoi, A., Mazumder, P., Tyagi, V.K., Tushara Chaminda, G.G., An, A.K., Kumar, M., **2018**. Occurrence and fate of emerging contaminants in water environment: A review. *Groundwater for Sustainable Development*. 6, 169–180. DOI:10.1016/j.gsd.2017.12.009.

[3] Nawaz, T., Sengupta, S., **2018**.Chapter 4 - Contaminants of Emerging Concern: Occurrence, Fate, and Remediation, Elsevier Inc., 2018. DOI:10.1016/B978-0-12-814790-0.00004-1.

[4] Wilkinson, J., Hooda, P.S., Barker, J., Barton, S., Swinden, J., **2017**. Occurrence, fate and transformation of emerging contaminants in water: An overarching review of the field. *Environmental Pollution*. 231, 954–970. DOI:10.1016/j.envpol.2017.08.032.

[5] Tran, N.H., Reinhard, M., Gin, K.Y.H., **2018**. Occurrence and fate of emerging contaminants in municipal wastewater treatment plants from different geographical regions-a review. *Water Research*. 133, 182–207. DOI:10.1016/j.watres.2017.12.029.

[6] Lykins, B.W., Clark, R.M., **1994**. U.S. Drinking-Water Regulations: Treatment Technologies and Cost. *Journal of Environmental Engineering*. 120, 783–802. DOI:10.1061/(ASCE)0733-9372(1994)120:4(783).

[7] Richardson, S.D., **2007**. Water analysis: Emerging contaminants and current issues. *Analytical Chemistry*. 79, 4295–4323. DOI:10.1021/ac070719q.

[8] Petrović, M., Gonzalez, S., Barceló, D., **2003**. Analysis and removal of emerging contaminants in wastewater and drinking water. *TrAC - Trends in Analytical Chemistry*. 22, 685–696. DOI:10.1016/S0165-9936(03)01105-1.

[9] Richardson, S.D., Kimura, S.Y., **2017**. Emerging environmental contaminants: Challenges facing our next generation and potential engineering solutions. *Environmental Technology and Innovation*. 8, 40–56. DOI:10.1016/j.eti.2017.04.002.

[10] Lorenzo, M., Campo, J., Picó, Y., **2018**. Analytical challenges to determine emerging persistent organic pollutants in aquatic ecosystems. *TrAC - Trends in Analytical Chemistry*. 103, 137–155. DOI:10.1016/j.trac.2018.04.003.

[11] Rahman, M.F., Peldszus, S., Anderson, W.B., **2014**. Behaviour and fate of perfluoroalkyl and polyfluoroalkyl substances (PFASs) in drinking water treatment: A review. *Water Research*. 50, 318–340. DOI:10.1016/j.watres.2013.10.045.

[12] Hu, X.C., Andrews, D.Q., Lindstrom, A.B., Bruton, T.A., Schaider, L.A., Grandjean, P., Lohmann, R., Carignan, C.C., Blum, A., Balan, S.A., Higgins, C.P., Sunderland, E.M., **2016**. Detection of Poly- and Perfluoroalkyl Substances (PFASs) in U.S. Drinking Water Linked to Industrial Sites, Military Fire Training Areas, and Wastewater Treatment Plants. *Environmental Science and Technology Letters*. 3, 344–350. DOI:10.1021/acs.estlett.6b00260.

[13] Buck, R.C., Franklin, J., Berger, U., Conder, J.M., Cousins, I.T., Voogt, P. De, Jensen, A.A., Kannan, K., Mabury, S.A., van Leeuwen, S.P.J., **2011**. Perfluoroalkyl and polyfluoroalkyl substances in the environment: Terminology, classification, and origins. *Integrated Environmental Assessment and Management*. 7, 513–541. DOI:10.1002/ieam.258.

[14] ITRC, **2017**. Naming Conventions and Physical and Chemical Properties of Per-and

Polyfluoroalkyl Substances (PFAS). 1–15. DOI:10.1002/ieam.258.

[15] Ahrens, L., **2011**. Polyfluoroalkyl compounds in the aquatic environment: A review of their occurrence and fate. *Journal of Environmental Monitoring*. 13, 20–31. DOI:10.1039/c0em00373e.

[16] Arvaniti, O.S., Stasinakis, A.S., **2015**. Review on the occurrence, fate and removal of perfluorinated compounds during wastewater treatment. *Science of the Total Environment*. 524–525, 81–92. DOI:10.1016/j.scitotenv.2015.04.023.

[17] Pan, C.G., Liu, Y.S., Ying, G.G., **2016**. Perfluoroalkyl substances (PFASs) in wastewater treatment plants and drinking water treatment plants: Removal efficiency and exposure risk. *Water Research*. 106, 562–570. DOI:10.1016/j.watres.2016.10.045.

[18] Quiñones, O., Snyder, S.A., **2009**. Occurrence of perfluoroalkyl carboxylates and sulfonates in drinking water utilities and related waters from the United States. *Environmental Science and Technology*. 43, 9089–9095. DOI:10.1021/es9024707.

[19] Appleman, T.D., Higgins, C.P., Quiñones, O., Vanderford, B.J., Kolstad, C., Zeigler-Holady, J.C., Dickenson, E.R.V., **2014**. Treatment of poly- and perfluoroalkyl substances in U.S. full-scale water treatment systems. *Water Research*. 51, 246–255. DOI:10.1016/j.watres.2013.10.067.

[20] Ateia, M., Maroli, A., Tharayil, N., Karanfil, T., **2019**. The overlooked short- and ultrashort-chain poly- and perfluorinated substances: A review. *Chemosphere*. 220, 866–882. DOI:10.1016/j.chemosphere.2018.12.186.

[21] Du, Z., Deng, S., Bei, Y., Huang, Q., Wang, B., Huang, J., Yu, G., **2014**. Adsorption behavior and mechanism of perfluorinated compounds on various adsorbents - A review. *Journal of Hazardous Materials*. 274, 443–454. DOI:10.1016/j.jhazmat.2014.04.038.

[22] Brendel, S., Fetter, É., Staude, C., Vierke, L., Biegel-Engler, A., **2018**. Short-chain perfluoroalkyl acids: environmental concerns and a regulatory strategy under REACH. *Environmental Sciences Europe*. 30,. DOI:10.1186/s12302-018-0134-4.

[23] Kucharzyk, K.H., Darlington, R., Benotti, M., Deeb, R., Hawley, E., **2017**. Novel treatment technologies for PFAS compounds: A critical review. *Journal of Environmental Management*. 204, 757–764. DOI:10.1016/j.jenvman.2017.08.016.

[24] Trojanowicz, M., Bojanowska-Czajka, A., Bartosiewicz, I., Kulisa, K., **2018**. Advanced Oxidation/Reduction Processes treatment for aqueous perfluorooctanoate (PFOA) and perfluorooctanesulfonate (PFOS) – A review of recent advances. *Chemical Engineering Journal*. 336, 170–199. DOI:10.1016/j.cej.2017.10.153.

[25] Ji, B., Kang, P., Wei, T., Zhao, Y., **2020**. Challenges of aqueous per- and polyfluoroalkyl substances (PFASs) and their foreseeable removal strategies. *Chemosphere*. 250, 126316. DOI:10.1016/j.chemosphere.2020.126316.

[26] Munthali, M.W., Johan, E., Aono, H., Matsue, N., **2015**. Cs+ and Sr2+ adsorption selectivity of zeolites in relation to radioactive decontamination. *Journal of Asian Ceramic Societies*. 3, 245–250. DOI:10.1016/j.jascer.2015.04.002.

[27] Smith, J.T., Voitsekhovitch, O. V., Håkanson, L., Hilton, J., **2001**. A critical review of measures to reduce radioactive doses from drinking water and consumption of freshwater foodstuffs. *Journal of Environmental Radioactivity*. 56, 11–32. DOI:10.1016/S0265-931X(01)00045-5.

[28] Li, D., Kaplan, D.I., Knox, A.S., Crapse, K.P., Diprete, D.P., **2014**. Aqueous 99Tc, 129I and 137Cs removal from contaminated groundwater and sediments using highly effective low-cost sorbents. *Journal of Environmental Radioactivity*. 136, 56–63. DOI:10.1016/j.jenvrad.2014.05.010.

[29] Liu, X., Chen, G.R., Lee, D.J., Kawamoto, T., Tanaka, H., Chen, M.L., Luo, Y.K., **2014**. Adsorption removal of cesium from drinking waters: A mini review on use of biosorbents and other adsorbents. *Bioresource Technology*. 160, 142–149. DOI:10.1016/j.biortech.2014.01.012.

[30] EPA, U., **2000**.National Primary Drinking Water Regulations, 2000.

[31] Olatunji, M.A., Khandaker, M.U., Mahmud, E.H.N.M., Amin, Y.M., Ademola, J.A., Olorode, D.O., **2018**. Remediation of 137Cs radionuclide in nuclear waste effluents by polymer composite: adsorption kinetics, isotherms and gamma irradiation studies. *Journal of Radioanalytical and Nuclear Chemistry*. 316, 933–945. DOI:10.1007/s10967-018-5875-4.

[32] Vipin, A.K., Ling, S., Fugetsu, B., **2016**. Removal of Cs+ and Sr2+ from water using MWCNT reinforced Zeolite-A beads. *Microporous and Mesoporous Materials*. 224, 84–88. DOI:10.1016/j.micromeso.2015.11.024.

[33] Falciglia, P.P., Puccio, V., Romano, S., Vagliasindi, F.G.A., **2015**. Performance study and influence of radiation emission energy and soil contamination level on γ-radiation shielding of stabilised/solidified radionuclide-polluted soils. *Journal of Environmental Radioactivity*. 143, 20–28. DOI:10.1016/j.jenvrad.2015.01.016.

[34] Khandaker, S., Kuba, T., Kamida, S., Uchikawa, Y., **2017**.Adsorption of cesium from aqueous solution by raw and concentrated nitric acid-modified bamboo charcoal, Elsevier B.V., 2017. DOI:10.1016/j.jece.2017.02.014.

[35] Husnain, S.M., Um, W., Woojin-Lee, Chang, Y.S., **2018**. Magnetite-based adsorbents for sequestration of radionuclides: A review. *RSC Advances*. 8, 2521–2540. DOI:10.1039/c7ra12299c.

[36] Figueiredo, B.R., Cardoso, S.P., Portugal, I., Rocha, J., Silva, C.M., **2018**. Inorganic Ion Exchangers for Cesium Removal from Radioactive Wastewater. *Separation and Purification Reviews*. 47, 306–336. DOI:10.1080/15422119.2017.1392974.

[37] Caccin, M., Giacobbo, F., Da Ros, M., Besozzi, L., Mariani, M., **2013**. Adsorption of uranium, cesium and strontium onto coconut shell activated carbon. *Journal of Radioanalytical and Nuclear Chemistry*. 297, 9–18. DOI:10.1007/s10967-012-2305-x.

[38] Tran, H.N., You, S.J., Hosseini-Bandegharaei, A., Chao, H.P., **2017**. Mistakes and inconsistencies regarding adsorption of contaminants from aqueous solutions: A critical review. *Water Research*. 120, 88–116. DOI:10.1016/j.watres.2017.04.014.

[39] Rizzo, L., Malato, S., Antakyali, D., Beretsou, V.G., Đolić, M.B., Gernjak, W., Heath, E., Ivancev-Tumbas, I., Karaolia, P., Lado Ribeiro, A.R., Mascolo, G., McArdell, C.S., Schaar, H., Silva, A.M.T., Fatta-Kassinos, D., **2019**. Consolidated vs new advanced treatment methods for the removal of contaminants of emerging concern from urban wastewater. *Science of the Total Environment*. 655, 986–1008. DOI:10.1016/j.scitotenv.2018.11.265.

[40] Yang, X., Wan, Y., Zheng, Y., He, F., Yu, Z., Huang, J., Wang, H., Ok, Y.S., Jiang, Y., Gao, B., **2019**. Surface functional groups of carbon-based adsorbents and their roles in the removal of heavy metals from aqueous solutions: A critical review. *Chemical Engineering Journal*. 366, 608–621. DOI:10.1016/j.cej.2019.02.119.

[41] Du, Z., Deng, S., Bei, Y., Huang, Q., Wang, B., Huang, J., Yu, G., **2014**. Adsorption behavior and mechanism of perfluorinated compounds on various adsorbents-A review. *Journal of Hazardous Materials*. 274, 443–454. DOI:10.1016/j.jhazmat.2014.04.038.

[42] Abtahi, M., Fakhri, Y., Sarafraz, M., Keramati, H., Conti, G.O., **2018**. Removal of cesium through adsorption from aqueous solutions : a systematic review. *Journal of Advances in Environmental Health Research*. 6, 96–106. DOI:10.22102/jaehr.2018.104959.1048.

[43] Awual, M.R., Yaita, T., Taguchi, T., Shiwaku, H., Suzuki, S., Okamoto, Y., **2014**. Selective cesium removal from radioactive liquid waste by crown ether immobilized new class conjugate adsorbent. *Journal of Hazardous Materials*. 278, 227–235. DOI:10.1016/j.jhazmat.2014.06.011.

[44] Liu, C.J., Werner, D., Bellona, C., **2019**. Removal of per- and polyfluoroalkyl substances (PFASs) from contaminated groundwater using granular activated carbon: a pilot-scale study with breakthrough modeling. *Environmental Science: Water Research & Technology*. 5, 1844–1853. DOI:10.1039/C9EW00349E.

[45] McCleaf, P., Englund, S., Östlund, A., Lindegren, K., Wiberg, K., Ahrens, L., **2017**. Removal efficiency of multiple poly- and perfluoroalkyl substances (PFASs) in drinking water using granular activated carbon (GAC) and anion exchange (AE) column tests. *Water Research*. 120, 77–87. DOI:10.1016/j.watres.2017.04.057.

[46] Zaggia, A., Conte, L., Falletti, L., Fant, M., Chiorboli, A., **2016**. Use of strong anion exchange resins for the removal of perfluoroalkylated substances from contaminated drinking water in batch and continuous pilot plants. *Water Research*. 91, 137–146. DOI:10.1016/j.watres.2015.12.039.

[47] Deng, S., Yu, Q., Huang, J., Yu, G., **2010**. Removal of perfluorooctane sulfonate from wastewater by anion exchange resins: Effects of resin properties and solution chemistry. *Water Research*. 44, 5188–5195. DOI:10.1016/j.watres.2010.06.038.

[48] Appleman, T.D., Dickenson, E.R. V, Bellona, C., Higgins, C.P., **2013**. Nanofiltration and granular activated carbon treatment of perfluoroalkyl acids. *Journal of Hazardous Materials*. 260, 740–746. DOI:10.1016/j.jhazmat.2013.06.033.

[49] De Pourcq, K., Ayora, C., García-Gutiérrez, M., Missana, T., Carrera, J., **2015**. A clay permeable reactive barrier to remove Cs-137 from groundwater: Column experiments. *Journal of Environmental Radioactivity*. 149, 36–42. DOI:10.1016/j.jenvrad.2015.06.029.

[50] Phillips, D.H., **2009**. Permeable reactive barriers: A sustainable technology for cleaning contaminated groundwater in developing countries. *Desalination*. 248, 352–359. DOI:10.1016/j.desal.2008.05.075.

[51] Roehl, K.E., Meggyes, T., Simon, F.-G., Stewart, D.I., **2005**.Long-term permance of permeable reactive barrier, in: J.O. (Univeristy of M. Ngriagu (Ed.), Trace Met. Other Contam. Environ., Elsevier B.V., 2005: pp. 311–321. DOI:10.1016/S0927-5215(05)80016-5.

[52] Naidu, R., Birke, V., **2015**.Permeable Reactive Barrier Sustainable Groundwater Remediation, 2015. DOI:10.1201/9781351228886.

[53] Faisal, A.A.H., Sulaymon, A.H., Khaliefa, Q.M., **2018**. A review of permeable reactive barrier as passive sustainable technology for groundwater remediation. *International Journal of Environmental Science and Technology*. 15, 1123–1138. DOI:10.1007/s13762-017-1466-0.

[54] Erto, A., Lancia, A., Bortone, I., Di Nardo, A., Di Natale, M., Musmarra, D., **2011**. A

procedure to design a Permeable Adsorptive Barrier (PAB) for contaminated groundwater remediation. *Journal of Environmental Management*. 92, 23–30. DOI:10.1016/j.jenvman.2010.07.044.

[55] Careghini, A., Saponaro, S., Sezenna, E., Daghio, M., Franzetti, A., Gandolfi, I., Bestetti, G., **2015**. Lab-scale tests and numerical simulations for in situ treatment of polluted groundwater. *Journal of Hazardous Materials*. 287, 162–170. DOI:10.1016/j.jhazmat.2015.01.028.

[56] Ghaeminia, M., Mokhtarani, N., **2018**. Remediation of nitrate-contaminated groundwater by PRB-Electrokinetic integrated process. *Journal of Environmental Management*. 222, 234–241. DOI:10.1016/j.jenvman.2018.05.078.

[57] Huang, L., Liu, G., Dong, G., Wu, X., Wang, C., Liu, Y., **2017**. Reaction mechanism of zero-valent iron coupling with microbe to degrade tetracycline in permeable reactive barrier (PRB). *Chemical Engineering Journal*. 316, 525–533. DOI:10.1016/j.cej.2017.01.096.

[58] ITRC, **2011**. Permeable Reactive Barrier : Technology Update PRB-5. *Washington, D.C.: Interstate Technology & Regulatory Council, PRB: Technology Update Team*. www.itrcweb.org. www.itrcweb.org.

[59] Marsh, H., Rodríguez-Reinoso, F., **2006**.Activated Carbon, Elsevier S, Elsevier Science & Technology books, 2006.

[60] Zanella, O., Tessaro, I.C., Féris, L.A., **2014**. Desorption- and decomposition-based techniques for the regeneration of activated carbon. *Chemical Engineering and Technology*. 37, 1447–1459. DOI:10.1002/ceat.201300808.

[61] Omorogie, M.O., Babalola, J.O., Unuabonah, E.I., **2014**. Regeneration strategies for spent solid matrices used in adsorption of organic pollutants from surface water: a critical review. *Desalination and Water Treatment*. 57, 518–544. DOI:10.1080/19443994.2014.967726.

[62] Ao, W., Fu, J., Mao, X., Kang, Q., Ran, C., Liu, Y., Zhang, H., **2018**. Microwave assisted preparation of activated carbon from biomass : A review. *Renewable and Sustainable Energy Reviews*. 92, 958–979. DOI:10.1016/j.rser.2018.04.051.

[63] Yuen, F.K., Hameed, B.H., **2009**. Recent developments in the preparation and regeneration of activated carbons by microwaves. *Advances in Colloid and Interface Science*. 149, 19–27. DOI:10.1016/j.cis.2008.12.005.

[64] Woodard, S., Berry, J., Newman, B., **2017**. Ion exchange resin for PFAS removal and pilot test comparison to GAC. *Remediation*. 27, 19–27. DOI:10.1002/rem.21515.

[65] San Miguel, G., Lambert, S.D., Graham, N.J.D., **2001**. The regeneration of field-spent granular-activated carbons. *Water Research*. 35, 2740–2748. DOI:10.1016/S0043-1354(00)00549-2.

[66] Ania, C.O., Menéndez, J.A., Parra, J.B., Pis, J.J., **2004**. Microwave-induced regeneration of activated carbons polluted with phenol. A comparison with conventional thermal regeneration. *Carbon*. 42, 1377–1381. DOI:10.1016/j.carbon.2004.01.010.

[67] Falciglia, P.P., Roccaro, P., Bonanno, L., De Guidi, G., Vagliasindi, F.G.A., Romano, S., **2018**. A review on the microwave heating as a sustainable technique for environmental remediation/detoxification applications. *Renewable and Sustainable Energy Reviews*. 95, 147–170. DOI:10.1016/j.rser.2018.07.031.

[68] Kostas, E.T., Beneroso, D., Robinson, J.P., **2017**. The application of microwave heating in

bioenergy: A review on the microwave pre-treatment and upgrading technologies for biomass. *Renewable and Sustainable Energy Reviews*. 77, 12–27. DOI:10.1016/j.rser.2017.03.135.

[69] Robinson, J.P., Kingman, S.W., Lester, E.H., Yi, C., **2012**. Microwave remediation of hydrocarbon-contaminated soils - Scale-up using batch reactors. *Separation and Purification Technology*. 96, 12–19. DOI:10.1016/j.seppur.2012.05.020.

[70] Remya, N., Lin, J.G., **2011**. Current status of microwave application in wastewater treatment-A review. *Chemical Engineering Journal*. 166, 797–813. DOI:10.1016/j.cej.2010.11.100.

[71] Diprose, M.F., **2001**. Some considerations when using a microwave oven as a laboratory research tool. *Plant and Soil*. 229, 271–280. DOI:10.1023/A:1004819202169.

[72] Sun, J., Wang, W., Yue, Q., **2016**. Review on microwave-matter interaction fundamentals and efficient microwave-associated heating strategies. *Materials*. 9,. DOI:10.3390/ma9040231.

[73] Kim, T., Lee, J., Lee, K.H., **2014**. Microwave heating of carbon-based solid materials. *Carbon Letters*. 15, 15–24. DOI:10.5714/CL.2014.15.1.015.

[74] Sun, Y., Zhang, B., Zheng, T., Wang, P., **2017**. Regeneration of activated carbon saturated with chloramphenicol by microwave and ultraviolet irradiation. *Chemical Engineering Journal*. 320, 264–270. DOI:10.1016/j.cej.2017.03.007.

[75] Ania, C.O., Parra, J.B., Menéndez, J.A., Pis, J.J., **2005**. Effect of microwave and conventional regeneration on the microporous and mesoporous network and on the adsorptive capacity of activated carbons. *Microporous and Mesoporous Materials*. 85, 7–15. DOI:10.1016/j.micromeso.2005.06.013.

[76] Durán-Jiménez, G., Stevens, L.A., Hodgins, G.R., Uguna, J., Ryan, J., Binner, E.R., Robinson, J.P., **2019**. Fast regeneration of activated carbons saturated with textile dyes: Textural, thermal and dielectric characterization. *Chemical Engineering Journal*. 378, 121774. DOI:10.1016/j.cej.2019.05.135.

[77] Foo, K.Y., Hameed, B.H., **2012**. A cost effective method for regeneration of durian shell and jackfruit peel activated carbons by microwave irradiation. *Chemical Engineering Journal*. 193–194, 404–409. DOI:10.1016/j.cej.2012.04.055.

[78] Ania, C.O., Parra, J.B., Menéndez, J.A., Pis, J.J., **2007**. Microwave-assisted regeneration of activated carbons loaded with pharmaceuticals. *Water Research*. 41, 3299–3306. DOI:10.1016/j.watres.2007.05.006.

[79] Pi, X., Sun, F., Gao, J., Zhu, Y., Wang, L., Qu, Z., Liu, H., Zhao, G., **2017**. Microwave Irradiation Induced High-Efficiency Regeneration for Desulfurized Activated Coke: A Comparative Study with Conventional Thermal Regeneration. *Energy and Fuels*. 31, 9693–9702. DOI:10.1021/acs.energyfuels.7b01260.

[80] Çalişkan, E., Bermúdez, J.M., Parra, J.B., Menéndez, J.A., Mahramanlioğlu, M., Ania, C.O., **2012**. Low temperature regeneration of activated carbons using microwaves: Revising conventional wisdom. *Journal of Environmental Management*. 102, 134–140. DOI:10.1016/j.jenvman.2012.02.016.

[81] Wang, J., Peng, X., Luan, Z., Zhao, C., **2010**. Regeneration of carbon nanotubes exhausted with dye reactive red 3BS using microwave irradiation. *Journal of Hazardous Materials*. 178, 1125–1127. DOI:10.1016/j.jhazmat.2010.01.112.

[82] Quan, X., Liu, X., Bo, L., Chen, S., Zhao, Y., Cui, X., **2004**. Regeneration of acid orange 7-exhausted granular activated carbons with microwave irradiation. *Water Research*. 38, 4484–4490. DOI:10.1016/j.watres.2004.08.031.

[83] Liu, X., Quan, X., Bo, L., Chen, S., Zhao, Y., **2004**. Simultaneous pentachlorophenol decomposition and granular activated carbon regeneration assisted by microwave irradiation. *Carbon*. 42, 415–422. DOI:10.1016/j.carbon.2003.12.032.

[84] Liu, X., Yu, G., Han, W., **2007**. Granular activated carbon adsorption and microwave regeneration for the treatment of 2,4,5-trichlorobiphenyl in simulated soil-washing solution. *Journal of Hazardous Materials*. 147, 746–751. DOI:10.1016/j.jhazmat.2007.01.076.

[85] Al-Mutairi, N.Z., **2010**. 2,4-Dinitrophenol adsorption by date seeds: Effect of physico-chemical environment and regeneration study. *Desalination*. 250, 892–901. DOI:10.1016/j.desal.2008.10.035.

[86] Foo, K.Y., **2018**. Effect of microwave regeneration on the textural network, surface chemistry and adsorptive property of the agricultural waste based activated carbons. *Process Safety and Environmental Protection*. 116, 461–467. DOI:10.1016/j.psep.2018.01.022.

Chapter 2: Design of the research

1. Research objectives

Given the research needs described above (Chapter 1, Section 6), the overarching goal of the present research is to investigate the feasibility of an innovative technology based on microwave (MW) irradiation for the regeneration of AC saturated with CEC. Amongst anthropogenic CEC, due to their high solubility in water and bioavailability to terrestrial and aquatic organisms, PFAS and Cs were selected as target contaminates in the present research. Although adsorption on ACs is the most employed technique for their removal, the saturation has a detrimental effect on the long-term performance of ACs at full-scale treatment plants. In order to obtain a good adsorption recovery capacity avoiding the damage of ACs, the development of an effective regeneration technique is becoming paramount for both water treatment facilities managers and AC manufacturers.

Followed by more specifics aims:

- **Objective 1**: to gain insights and increase knowledge related to PFAS adsorption into several adsorbent materials. To study the effect of organic matter (OM) on both long- and short-chain PFAS by critically reviewing the previously published studies. To understand the suitability of the main regeneration techniques currently applied to desorb PFAS from saturated adsorbents.
- **Objective 2**: Considering that GAC adsorption is the most applied technique for PFAS removal, it is priority overcome issues related to the frequent regeneration of PFAS-saturated GAC. With this purpose, MW irradiation is investigated as an innovative regeneration technique for PFAS-saturated GACs, whose regeneration is still a challenging task at full-scale treatment plants.
- **Objective 3**: to investigate the efficiency of MW irradiation for the regeneration of GAC saturated with inorganic compound (i.e., Cs). To understand the desorption mechanisms of Cs during MW regeneration and to assert the variation of GAC porous structure after MW irradiation.
- **Objective 4**: A new proof of concept deals with the coupling of GAC adsorption and MW regeneration, both conducted in-situ, is proposed for the first time. To elucidate the concept of the novel MW based regenerating permeable reactive barrier (MW-PRB) system as combined treatment for Cs-impacted groundwater. To evaluate the feasibility of novel MW-PRB by means of a techno-economic analysis.

2. Thesis organization

This Ph.D. thesis is presented in a manuscript-based format. The main contents of each chapter are described below:

CHAPTER 1 provides the overview of the study background with particular emphasis to the wide group of CEC. An outline of the future needs concludes the chapter.

CHAPTER 2 states the research objectives and provides the summarized outline of the present work, highlighting the original contributions to new knowledge.

CHAPTER 3 addresses Objective 1 and critically reviews the previous published experimental works on PFAS adsorption with particular focus on the effect of OM in the adsorption process and the regeneration techniques available for PFAS-saturated adsorbent.

This chapter has been published as: **Gagliano, E.,** Sgroi, M.; Falciglia, P.P.; Vagliasindi, F.G.A.; Roccaro, P. "*Removal of poly- and perfluoroalkyl substances (PFAS) from water by adsorption: Role of PFAS chain length, effect of organic matter and challenges in adsorbent regeneration*". **Water Research** 171, **115381**, (2020).

CHAPTER 4 deals with Objective 2 and presents the research aiming at investigating the microwave regeneration of PFAS-saturated GAC. Lab-scale tests were conducted to assess the performance of MW irradiation to regenerate two commercially available GACs saturated with PFOA and PFOS, the two mostly detected PFAS. MW regeneration were performed at several irradiation conditions, such as irradiation power and time. The variation of GAC properties (e.g., specific surface area and pore volume) was investigated to assess the effect of MW irradiation on GACs porous structure. The obtained findings were compared and extensively discussed in order to find the best operational conditions for the successive adsorption-regeneration cycles.

The experimental part of this study was conducted at the Department of Environmental Engineering and Earth Science (Clemson University, SC, U.S.A.) in collaboration with Prof. Tanju Karanfil.

CHAPTER 5 addresses Objective 3 and focuses on the regeneration of Cs-saturated GAC through MW irradiation. Batch and fixed-bed column experiments are performed: (i) to calculate the adsorption capacity of selected commercial GAC, (ii) to demonstrate the efficiency of MW irradiation to regenerate Cs-saturated GAC throughout ten successive adsorption/regeneration cycles and also at column dynamic conditions. A new proof concept which couples the GAC adsorption with MW regeneration is proposed for the first time as innovative in-situ remediation technology for Cs-contaminated groundwater.

This chapter has been redrafted from: Falciglia, P.P., **Gagliano, E.**, Brancato, V., Malandrino, G., Finocchiaro, G., Catalfo, A., De Guidi, G., Romano, S., Roccaro, P., Vagliasindi, F.G.A. "*Microwave*

based regenerating permeable reactive barriers (MW-PRBs): Proof of concept and application for Cs removal". **Chemosphere** 251, **126582** (2020).

CHAPTER 6 addresses Objective 4 and it deals with the technical applicability and cost-analysis of novel microwave based regenerating permeable reactive barrier (MW-PRB) as combined treatment for Cs-contaminated groundwater. The design of novel MW-PRB is compared with conventional PRB system in terms of thickness and longevity. The long-term performance of MW-PRB is predicted at different simulated scenarios (e.g., Cs field concentration and groundwater velocity). The comparison of main specific costs between conventional PRB and novel MW-PRB is also provided. This chapter has been redrafted from: Falciglia, P.P., **Gagliano, E.**, Brancato, V., Finocchiaro, G., Catalfo, A., De Guidi, G., Romano, S., Roccaro, P., Vagliasindi, F.G.A. "*Field technical applicability and cost analysis for microwave based regeneration permeable reactive barriers (MW-PRBs) operating in Cs-contaminated groundwater treatment*". **Journal of Environmental Management** 260, **110064** (2020).

CHAPTER 7 presents an overall discussion regarding the main findings obtained. Some future perspectives are also provided, casting the foundations for future research.

Chapter 3: Removal of poly- and perfluoroalkyl substances (PFAS) from water by adsorption: role of PFAS chain length, effect of organic matter and challenges in adsorbent regeneration

Abstract

Poly- and perfluoroalkyl substances (PFAS) are a wide group of environmentally persistent organic compounds of industrial origin, which are of great concern due to their harmful impact on human health and ecosystems. Amongst long-chain PFAS, perfluorooctanoic acid (PFOA) and perfluorooctane sulfonic acid (PFOS) are the most detected in the aquatic environment, even though their use has been limited by recent regulations. Recently, more attention has been posed on the short-chain compounds, due to their use as an alternative to long-chain ones, and to their high mobility in the water bodies. Therefore, short-chain PFAS have been increasingly detected in the environmental compartments. The main process investigated and implemented for PFAS removal is adsorption. However, to date, most adsorption studies have focused on synthetic water.

The main objective of this article is to provide a critical review of the recent peer-reviewed studies on the removal of long- and short- chain PFAS by adsorption. Specific objectives are to review 1) the performance of different adsorbents for both long- and short-chain PFAS, 2) the effect of organic matter, and 3) the adsorbent regeneration techniques. Strong anion-exchange resins seem to better remove both long- and short-chain PFAS. However, the adsorption capacity of short-chain PFAS is lower than that observed for long-chain PFAS. Therefore, short-chain PFAS removal is more challenging. Furthermore, the effect of organic matter on PFAS adsorption in water or wastewater under real environmental conditions is overlooked. In most studies high PFAS levels have been often investigated without organic matter presence. The rapid breakthrough of PFAS is also a limiting factor and the regeneration of PFAS exhausted adsorbents is very challenging and needs more research.

Graphical Abstract

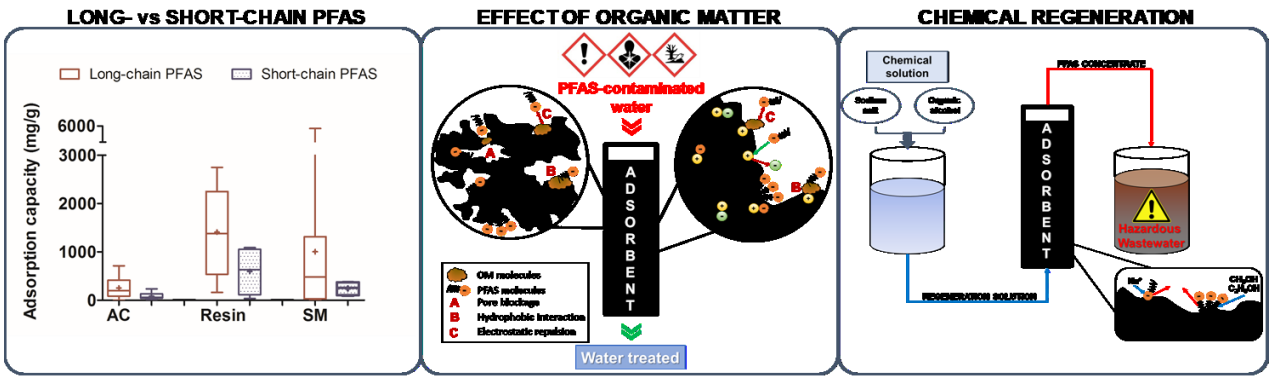

Keywords: Adsorption; anion-exchange; Long- and short- chain PFAS; organic matter; regeneration; adsorption mechanism.

❖ This chapter have been redrafted from:

Gagliano, E., Sgroi, M., Falciglia, P.P., Vagliasindi, F.G.A., Roccaro, P., **2020**. Removal of poly- and perfluoroalkyl substances (PFAS) from water by adsorption: Role of PFAS chain length, effect of organic

matter and challenges in adsorbent regeneration. ***Water Research***. 171, 115381. DOI:10.1016/j.watres.2019.115381

List of abbreviations

Main PFAS and alternative compounds

F-53B	Potassium salt of 6:2 chlorinated polyfluorinated ether sulfonate
FOSA	Perfluorooctane sulfonamide
PFAS	Poly- and perfluoroalkyl substances
PFCAs	Perfluoroalkyl carboxylic acids
PFSAs	Perfluoroalkane sulfonates
PFBA	Perfluorobutanoic acid
PFBS	Perfluorobutane sulfonic acid
PFDA	Perfluorodecanoic acid
PFDoDA	Perfluorododecanoic acid
PFDS	Perfluorodecane sulfonic acid
PFHpA	Perfluoroheptanoic acid
PFHpS	Perfluoroheptane sulfonic acid
PFHxA	Perfluorohexanoic acid
PFHxS	Perfluorohexane sulfonic acid
PFNA	Perfluorononanoic acid
PFNS	Perfluorononane sulfonic acid
PFOA	Perfluorooctanoic acid
PFOS	Perfluorooctane sulfonic acid
PFPeA	Perfluoropentanoic acid
PFPeS	Perfluoropentane sulfonic acid
PFTrDA	Perfluorotridecanoic acid
PFUnDA	Perfluoroundecanoic acid

Adsorbent materials

2-MNPs@FG	Magnetic-nanoparticles attached into fluorographene (mass ratio of MNPs and FG is 3:5)
AC	Activated carbon
ACF	Activated carbon fiber
ARH	Aminated rice husk
BdAC	Bamboo-derived AC
CTF	Covalent triazine-based framework
DFB-CDP	Cross-linked polymer network where β-Cyclodentrix substitutes decafluorobiphenyl (DFB)
Fe_3O_4 NP	Magnetite nanoparticles
Fe_3O_4@SiO_2-NH_2&F_{13}	Silica membrane functionalized with amino group and octyl-perfluorinated chain on the Fe_3O_4 NP surface
GAC	Granular activated carbon
h-BNs	Porous hexagonal boron nitride nanosheets
HDPE	High-density polyethylene

HMS	Hexagonal mesoporous silica
HWC	Hardwood biochar
MIMs	Macromolecular imprinted materials
MIP-CMs	Molecularly imprinted carbon microspheres
MWNT	Multi-walled carbon nanotubes
NIP-CMs	Non-imprinted carbon microspheres
OD-HMS	N-octyldichlorosilane grafted hexagonal mesoporous silica
PAC	Powdered activated carbon
PACFs	Polyacrylonitrile fiber (PANF)-derived activated carbon fibers
PAF-45	Porous aromatic framework constructed from benzene rings
PCMAs	Permanently confined micelle arrays
PEI-f-CMC	Poly(ethylenimine)-functionalized cellulose microcrystals
PS	Polystyrene
PS-COOH	Poly-styrene carboxylic acid
PWC	Pinewood biochar
R-CAC	Reactivated coconut shell-based AC
SWNT	Single walled carbon nanotubes

Other

AE	Anion-exchange
AFFF	Aqueous fil-forming foam
AOPs	Advanced oxidation processes
ATRP	Atom transfer radical polymerization
BET	Brunauer, Emmett and Teller
BSA	Bovine serum albumin
DBP	Disinfection by-products
DI	Deionized water
DMC	Methacryloyloxyethyl trimethyl ammonium chloride
DOC	Dissolved organic carbon
DOM	Dissolved organic matter
DW	Drinking water
DWTPs	Drinking water treatment plants
EBCT	Empty bed contact time
EfOM	Effluent organic matter
EWTP	Electroplating WWTP
FA	Fulvic acids
GW	Groundwater
HA	Humic acids
LW	Lake water
MB	Methylbenzene

MPLs	Microplastics
OM	Organic matter
NDMA	N-Nitrosodimethylamine
NOM	Natural organic matter
NPs	Nanoparticles
PFSOF WWW	Perfluorooctanesulfonyl fluoride washing wastewater
RSSCT	Rapid small-scale column tests
RW	River water
S_{BET}	BET surface area
SDS	Sodium dodecyl sulphate
SeaW	Seawater
$SUVA_{254}$	Specific ultra-violet absorbance at 254 nm
SW	Surface water
TCE	Tri-chloroethylene
TEM	Transmission electron microscopy
TMFA	2-(trifluoromethyl)acrylic acid
TOC	Total organic carbon
WW	Wastewater
WWTPs	Wastewater treatment plants

1. Introduction

1.1 PFAS classification

Poly- and perfluoroalkyl substances (PFAS) are a large group of anthropogenic aliphatic compounds that are of increasing concern worldwide due to their impact on environment and human health. For many decades, they have been used in an array of formulations as surfactants intermediates (i.e., firefighting foams, hydraulic fluids for aircrafts), waterproofing treatment for textiles (i.e., apparel, carpet) and household products (i.e., paper and non-stick cookware coating) [1–3]. PFAS contamination is the result of consumer-product degradation, firefighting activities and discharges of fluorochemical manufacturing facilities [4].

PFAS are made up of a chain of varying carbon length, on which at least one (polyfluoroalkyl acids) or all (perfluoroalkyl acids) of the hydrogen atoms bound to carbon-chain in the nonfluorinated substances have been replaced by fluorine atoms [1]. Their chemical structure also includes a charged functional group commonly carboxylic or sulfonic acids attached at one end. Polyfluoroalkyl acids have also been indicated as "precursors" of perfluoroalkyl ones, hence the non-fluorinated bond provides a biotic or abiotic degradation pathway [5]. Depending on their terminal functional group, PFAS can be distinguished in perfluoroalkyl carboxylic acids (PFCAs) and in perfluoroalkyl sulfonic acids (PFSAs) [1]. However, an abridged way to distinguish among PFAS subclasses is that referred to carbon-chain length. According to the Organization for Economic Co-operation and Development (OECD), the term "long-chain compound" indicates PFCAs with eight or more carbons, and PFSAs with six or more carbons. Whereas, "short-chain" is related to PFCAs with seven or fewer carbons and PFSAs with five or fewer carbons [6]. It should be noted that PFCAs and PFSAs classification, based on chain length, is different in terms of number of carbon atoms. However, PFAS bioaccumulation and biomagnification into biota increase with the increasing of carbon-chain length, PFSAs are more bioaccumulate than PFCAs with the same chain length [7].

1.2 PFAS properties

The knowledge of PFAS physical and chemical properties is paramount to understand their fate and transport in the environment. The C-F bound is the strongest covalent bond in organic chemistry and it leads to PFAS thermal stability [5]. In addition, PFAS exhibit mutually hydrophobic and lipophobic properties, which are primarily attributed to the low polarizability of fluorine atoms. Moreover, the terminal functional group attached to fluoroalkyl chain provides PFAS chemical stability. With the increasing replacement of hydrogen by fluorine as well as the increasing carbon-chain length, PFAS become more chemically inert. On the contrary, their water solubility increases with the decreasing carbon-chain length [8]. PFCAs and PFSAs are characterized by a low vapour pressure, which makes air stripping an unsuitable technique for PFAS removal [2]. With the increasing C-F chain length,

PFAS become more lipophilic as demonstrated by octanol/water partition coefficients (K_{ow}). At environmentally relevant pH, PFAS exhibit anionic species according to their low values of acid dissociation constant (pK_a). Other properties, such as resistance to thermal, biological and chemical degradation and redox stability, impart unique features to PFAS, making them suitable for several industrial applications. Information regarding chemical formulas and Chemical Abstracts Service (CAS) of selected per-fluoroalkyl substances along with their physical and chemical properties are reported in Table 1.

1.3 Occurrence of PFAS in water

In the aquatic environment, PFAS have been detected at low concentrations ranging from pg L^{-1} to µg L^{-1} [2,9] and long-chain compounds, such as perfluorooctane sulfonic acid (PFOS) and perfluorooctanoic acid (PFOA), are the most commonly measured PFAS around the world [5]. Widespread occurrence of PFAS in urban water cycle including wastewater (WW), river water (RW), lake water (LW), drinking water (DW), stormwater, and groundwater (GW) has been demonstrated by several studies [2,10–14]. The amount of PFAS not removed in wastewater treatment plants (WWTPs) and, consequently, released into the receiving environment is a concern for the possible presence of these compounds in water used for potable supply production.

A recent research suggests that the possible impacts of PFAS on GW is linked to the use of treated WW for irrigation [15]. The occurrence and distribution of PFAS remain not completely identified, due to the limited data about the removal efficiency of conventional water treatment plants and about the transformation of PFAS precursor compounds [11,12].

Although the use of PFOS and PFOA has been reduced due to their health impact, the total amount of PFAS introduced into the environment has not been reduced because the long-chain compounds have been replaced by short and ultra-short PFAS [14]. The latter are potentially less bioaccumulated and bioconcentrated through trophic levels as compared to long-chain but they are still environmentally persistent [6,16].

Table 1 Physic-chemical properties of selected PFAS.

Compound name (CAS No.)	Acronym	Formula	MW g mol^{-1}	Log K_{ow}	Solubility in water (mg L^{-1})	Vapor pressure	pKa	Boiling point (°C)	Melting point (°C)	Density (g cm^{-3})
Perfluoroalkyl carboxylic acids (PFCAs)										
Short-chain (C_4-C_7)										
Perfluorobutanoic acid (375-22-4)	PFBA	C_3F_7COOH	214.039[a]	2.31[b]	$2.14 \cdot 10^5$ (at 25 °C)[c]	6.38 mm Hg (25° C)[c]	1.07[b]	121[c]	-17.5[c]	1.651[c]
Perfluoropentanoic acid (2706-90-3)	PFPeA	C_4F_9COOH	264.047[a]	3.01[b]	n.a.	n.a.	0.34[b]	n.a.	n.a.	n.a.
Perfluorohexanoic acid (307-24-4)	PFHxA	$C_5F_{11}COOH$	314.054[a]	3.48[d]	15700 (at 25 °C)[d]	198 mm Hg (at 25 °C)[d]	-0.16[d]	157[d]	n.a.	
Perfluoroheptanoic acid (375-85-9)	PFHpA	$C_6F_{13}COOH$	364.062[a]	4.15[d]	3.65 (at 25 °C)[d]	0.133 mm Hg (at 25 °C)[d]	-2.29[d]	175[d]	30[d]	1.792 (at 20 °C)[d]
Long-chain (C_8-C_{14})										
Perfluorooctanoic acid (335-67-1)	PFOA	$C_7F_{15}COOH$	414.07[a]	4.81[d]	2290 (at 24 °C)	$3.16 \cdot 10^{-2}$ mm Hg (at 25 °C)[d]	-0.5 – 4.2[d]	192[d]	54.3[d]	3300 g mL^{-1} (at 24 °C)[d]
Perfluorononanoic acid (375-95-1)	PFNA	$C_8F_{17}COOH$	464.078[a]	5.48[d]	n.a.	$8.3 \cdot 10^{-2}$ mm Hg (at 25 °C)[d]	-0.21[d]	n.a.	n.a.	n.a.
Perfluorodecanoic acid (335-76-2)	PFDA	$C_9F_{19}COOH$	514.086[a]	6.51[b]	n.a.	n.a.	-5.2[b]	217 (at 740 mmHg)[a]	77 – 78[a]	1.707 (at 68 °F)[a]
Perfluoroundecanoic acid (2058-94-8)	PFUnDA	$C_{10}F_{21}COOH$	564.093[a]	7. 21[b]	n.a.	n.a.	-5.2 [b]	n.a.	n.a.	n.a.
Perfluorododecanoic acid (307-55-1)	PFDoDA	$C_{11}F_{23}COOH$	614.101[a]	7.92[b]	n.a.	n.a.	-5.2[b]	n.a.	n.a.	n.a.
Perfluorotridecanoic acid (72629-94-8)	PFTrDA	$C_{12}F_{25}COOH$	664.109[a]	8.62[b]	n.a.	n.a.	-5.2[b]	n.a.	n.a.	n.a.
Perfluorotetradecanoic acid (376-06-7)	PFTeDA	$C_{13}F_{27}COOH$	717.117[a]	9.32[b]	n.a.	n.a.	-5.2[b]	n.a.	n.a.	n.a.
Perfluoroalkyl sulfonic acids (PFSAs)										
Short-chain (C_4-C_5)										
Perfluorobutane sulfonic acid (375-73-5)	PFBS	$C_4F_9SO_3H$	300.095[a]	1.82 [d]	344 (at 25°C) [d]	$2.68 \cdot 10^{-2}$ mm Hg (at 25 °C)[d]	-3.31 [d]	210 – 212[d]	n.a.	1.811 g mL^{-1} (at 25 °C) [d]
Perfluoropentane sulfonic acid (2706-91-4)	PFPeS	$C_5F_{11}SO_3H$	350.102[a]	n.a.	n.a.	n.a.	n.a.	n.a.	n.a.	n.a.
Long-chain (C_6-C_{14})										
Perfluorohexane sulfonic acid (355-46-4)	PFHxS	$C_6F_{13}SO_3H$	400.11[a]	3.16 [d]	6.2 (at 25°C) [d]	$4.6 \cdot 10^{-3}$ mm Hg (at 25°C) [d]	0.14 [d]	238 - 239 [d]	n.a.	1.841 g L^{-1} [d]
Perfluoroheptane sulfonic acid (375-92-8)	PFHpS	$C_7F_{15}SO_3H$	450.118[a]	n.a.	n.a.	n.a.	n.a.	n.a.	n.a.	n.a.
Perfluorooctane sulfonic acid (1763-23-1)	PFOS	$C_8F_{17}SO_3H$	500.126[a]	4.49[d]	$3.2 \cdot 10^{-3}$ (at 25°C)[d]	$2 \cdot 10^{-3}$ mm Hg (at 25°C)[d]	< 1.0[d]	249 [d]	n.a.	n.a.
Perfluorononane sulfonic acid (474511-07-4)	PFNS	$C_9F_{19}SO_3H$	549.126[a]	6.13[b]	n.a.	n.a.	-3.24[b]	n.a.	n.a.	n.a.

Table 1 Physic-chemical properties of selected PFAS (continued).

Compound name (CAS No.)	Acronym	Formula	MW g mol^{-1}	Log K_{ow}	Solubility in water (mg L^{-1})	Vapor pressure	pKa	Boiling point (°C)	Melting point (°C)	Density (g cm^{-3})
Perfluoroalkyl sulfonic acids (PFSAs)										
Long-chain (C_6-C_{14})										
Perfluorodecane sulfonic acid (335-77-3)	PFDS	$C_{10}F_{21}SO_3H$	600.141[b]	6.83[b]	n.a.	n.a.	-3.24[b]	n.a.	n.a.	n.a.
Perfluoroundecane sulfonic acid (749786-16-1)	PFUnDS	$C_{11}F_{23}SO_3H$	n.a.	n.a.	n.a.	n.a.	n.a.	n.a.	n.a.	n.a.
Perfluorododecane sulfonic acid (79780-39-5)	PFDoDS	$C_{12}F_{25}SO_3H$	700.157[a]	8.23[b]	n.a.	n.a.	-3.24[b]	n.a.	n.a.	n.a.
Perfluorotridecane sulfonic acid (n.a.)	PFTrDS	$C_{13}F_{27}SO_3H$	n.a.	n.a.	n.a.	n.a.	n.a.	n.a.	n.a.	n.a.
Perfluorotetradecane sulfonic acid (n.a.)	PFTeDS	$C_{14}F_{29}SO_3H$	n.a.	n.a.	n.a.	n.a.	n.a.	n.a.	n.a.	n.a.
Perfluoroalkane sulfonamides (FASAs)										
Perfluorooctane sulfonamide (754-91-6)	FOSA	$C_8H_2F_{17}NO_2S$	499.142[a]	5.8[d]	$8.04 \cdot 10^{-3}$ (at 25°C)[d]	0.31 mm Hg (at 25°C) [d]	3.37[b]	n.a.	n.a.	n.a.
Potassium salt of 6:2 chlorinated polyfluorinated ether sulfonate (73606-19-6)	F-53B	6:2 Cl-PFAES	570.67[f]	4.84[e]	n.a.	n.a.	< 1[e]	n.a.	n.a.	n.a.

n.a. not available, [a]PubChem (URL: https://pubchem.ncbi.nlm.nih.gov); [b]Chemicalize (URL: https://chemicalize.com/#/); [c] Lide (2007); [d] Hazardous Substances Data Bank (HSDB) (URL:https://toxnet.nlm.nih.gov); [e] predicted by software SPARC Xiao et al. (2017)[3]; [f] Gao et al. (2017)[17].

1.4 PFAS toxicity

PFAS are absorbed in human body after oral ingestion, they are not metabolized and they are detected in human tissue and blood serum at typical concentrations of ng mL^{-1}. Long-chain PFAS are taken up and stored preferentially in the liver. Half-life values of PFOS and PFOA in humans range from 2.3 to 5.4 years [10,18]. Epidemiological studies have shown that the occurrence of PFOA and PFOS in humans is probably linked to a high incidence of thyroid disease, high cholesterol, ulcerative colitis, kidney cancer, testicular cancer, and pregnancy-induced hypertension [19,20]. More details concerning PFAS toxicological properties are reported in literature [21].

Based on WHO's recommendation and on the precautionary principle, the proposal for a recast of the Drinking Water Directive (98/83/CE, Directive on the quality of water intended for human consumption) published on 1st February 2018, has included the group of poly- and perfluoroalkyl substances in the list of regulated chemicals. The proposal recommends the values of 0.5 μg L^{-1} for the total amount of PFAS and 0.1 μg L^{-1} for each single compound. In 2017, the Veneto Region (Italy) set drinking water quality standards for PFAS (Veneto Legislation 1590/201), with a limit value of 90 ng L^{-1} for PFOA and PFOS (with PFOS < 30 ng L^{-1}), and a limit value of 300 ng L^{-1} for the other PFAS (sum of PFBA, PFPeA, PFBS, PFHxA, PFHpA, PFHxS, PFNA, PFDeA, PFUnA, PFDoA). Such regulation came after a large contamination of surface water and GW due to industrial WW discharges, with the subsequent bioaccumulation of PFAS in the serum of the exposed population. As a result, PFAS are emerging contaminants already regulated in Italy.

1.5 PFAS removal

Conventional treatment processes are ineffective for PFAS degradation due to the high straight of the covalent C-F bond of their chain, their low concentration in water and their high hydrophilicity [2,22]. Biological treatment both aerobic and anaerobic are only able to break the C-C bond, and they lead to the formation of short-chain PFAS. When advanced treatment technologies are not implemented, biological WWTPs affect the receiving water bodies and the concentration of PFAS detected in finished water is often higher than in the untreated water [9,12]. This fact gives evidence to recalcitrant behaviour of PFAS to biological treatment and, consequently, their formation via biodegradation of precursor compounds [2]. According to data obtained from monitoring studies, PFAS with long carbon-chain, such as PFOS, tend to accumulate in sludge, whereas perfluorobutane sulfonic acid (PFBS) has been mainly detected in the effluents of WWTPs and in drinking water treatment plants (DWTPs) [2,12].

Under typical water treatment plant conditions, disinfection by free chlorine or UV irradiation are ineffective [2,11]. PFAS are also much more resistant than other micro-contaminants to the oxidation by ozone and hydroxyl radicals due to the strong C-F bond and the electron withdrawing of their functional groups [23,24]. Furthermore, advanced oxidation processes (AOPs) often result in a partial degradation of PFAS, with formation of PFAS with shorter perfluorinated alkyl chain [23,24].

Adsorption, anion-exchange (AE), high pressure nanofiltration and reverse osmosis membrane processes are effective for substantial PFAS removal [8,25,26].

Main issues inherent with PFAS removal through these mentioned techniques are the influence of water matrix (i.e., competing anions, organic matter), frequent regeneration (due to fast breakthrough), and disposal of concentrate with high PFAS concentration [2,25,27].

Adsorption is actually an established technology for PFAS removal, both as single process of point-of-use applications and as step of water treatment plants [12,28,29]. Moreover, it shows a more economical performance compared to high pressure membrane processes [30,31].

As previously mentioned, PFAS exist as anions at ambient pH values and this makes strong base AE resins suitable for their removal. However, AE treatment efficiency depends on the resin properties, including porosity, functional group and polymer matrix [32].

To date, adsorption studies have addressed single long-chain PFAS (i.e., PFOA and PFOS), even though long- and short-chain co-removal requires further investigation [14,33,34]. Moreover, many compounds, commonly present in water bodies, could affect adsorption efficiency and additional studies should regard their potential competition [14,26,35,36].

2. PFAS adsorption and scope of the review

2.1 PFAS adsorption mechanism

Electrostatic and hydrophobic interactions are considered the predominant forces that govern adsorption of PFAS on several adsorbent materials. Other less important mechanisms of PFAS adsorption are hydrogen bonding and covalent bonding. PFAS molecular structure, adsorbent chemistry and physical properties (i.e., surface functional groups, polarity, and porosity), as well as liquid phase composition should be considered as the main factors affecting PFAS adsorption efficiency [26].

Electrostatic interactions occur between anionic PFAS and adsorbent material positively charged. Consequently, any changes in ionic strength (i.e., co-existing inorganic anions and changing solution pH) could affect adsorption efficiency, due to electrostatic repulsions [26]. Change in solution pH has an effect on the charge characteristics of PFAS molecules and surface properties of adsorbents [37,38]. As reported in several studies, an increase in pH solution led to a decrease in adsorption capacity of most adsorbents [17,32,39]. Nevertheless, an increase of ionic strength ascribed to the presence of monovalent and divalent cations (i.e., Na^+, K^+, Ca^{2+}, Mg^{2+}) might enhance the PFAS removal due to the compression of the electrical double layer [26,40]. The salting-out effect should be also mentioned as reported in previous studies [41,42]. This effect occurs at high salt concentrations and it involves a decline of PFAS solubility and, consequently, their adsorption on adsorbent surface could be encouraged [26]. It is clear that the presence of inorganic anions (i.e., Cl^- and SO^{4-}) involves a competition with PFAS for adsorption sites [17,32]. However, the worsening of PFAS removal occurred when solution pH was higher than point of zero charge of the adsorbents, due to the establishment of electrostatic repulsions [43,44].

Electrostatic repulsions between anions PFAS and negatively charged surfaces can be overcome through hydrophobic interactions of fluorinated chain [27]. Moreover, removal efficiency of individual PFAS into adsorbent materials depends on the compound functional groups and C-F chain length. In detail, PFSAs are removed better than PFCAs, and long-chain compounds with the same functional group are more efficiently removed than short-chain ones [11,26,27,33,40].

Hydrophobic effect has been found to increase with the increasing C-F chain length [2,26,33]. This was also demonstrated in a prior work that investigated the competitive adsorption among PFAS with different chain length on kaolinite [40]. The authors argued that, due to a stronger hydrophobic interaction with the tested adsorbent, the longer-chained PFAS outcompeted the shorter during adsorption. Based on PFAS functional group, the presence of one more C-F bond in PFSAs compared to corresponding PFCAs results in stronger hydrophobic properties and increasing adsorption of PFSAs [27,42]. Moreover, strong hydrophobic interactions favour the formation of molecular

aggregates during PFOA and PFOS removal, while highly hydrophilic compounds, such as PFBA and PFBS, are removed as single molecules on adsorbent active sites [26]. Exceeding the critical micelle concentration (c.m.c) may lead to the formation of multilayer structures (i.e., micelles and hemi-micelles) on adsorbent surfaces that may play an important role in PFAS adsorption [11,26,45]. However, at the PFAS environmental level the formation of micelles is unlikely and only aggregates have been observed [27]. McCleaf et al. [33] reported that PFAS adsorption process may include two distinct phases. Initially removal occurs through PFAS adsorption on open sites of adsorbents, gradually pore sites become clogged and removal becomes a function of molecular aggregation of PFAS.

Since electrostatic negativity is originated from PFAS functional head and hydrophobic interaction is linked to C-F chain, the electrostatic interactions seem to be dominant for short-chain PFAS, while longer PFAS are adsorbed through hydrophobic interactions, which favour the formation of molecular aggregate on the active surface [26,27,46].

2.2 Scope of the review

An important limitation of prior research on PFAS adsorption is that the evaluation of adsorption efficiency has been explored at high PFAS concentrations, which are not representative of the environmental concentration level. Furthermore, very high doses of adsorbents have been used which do not reflect the actual water treatment plant adsorption processes [2].

Another relevant limitation of prior researches is that the experiments have often been carried out by using deionized water (DI) spiked with selected PFAS, and the effect of organic matter (OM) was not accounted for [26]. Recent studies have shown that OM may not affect PFAS removal [47] or may positively influence the PFAS adsorption [33]. However, natural organic matter (NOM) and effluent organic matter (EfOM) often play a competitive role in the adsorption process [25,48]. Therefore, a critical review of the published data is needed to better understand the OM effect on long- and short-chain PFAS removal.

Furthermore, the regeneration of adsorbents exhausted by PFAS is not fully addressed [49]. Since PFAS breakthrough is fast, adsorbent regeneration is a very important and challenging task.

Previous published review papers deals with PFAS classification and origins [1,3], their occurrence and fate in aquatic environments [2,7,12] and the treatment technologies for long-chain PFAS removal [8,11]. A critical review concerning PFAS adsorption previously published is mainly concerned with PFOS and PFOA [26] and it does not include recent scientific findings on OM effect as well as the performance and the regeneration of novel adsorbents. Recently, the removal of short-chain PFAS by different processes, including different adsorbents, has been critically reviewed by Ateia et al. [14].

However, such prior review papers concerning PFAS adsorption were not focused on the role of PFAS chain length, OM effect and adsorbents regeneration.

Therefore, the objective of this paper is to critically discuss data concerning PFAS adsorption with particular focus on: 1) recent published data about adsorption capacity of different materials for both long- and short-chain PFAS; 2) effect of OM on the PFAS adsorption; 3) role of adsorbent regeneration.

3. Adsorption of long chain PFAS

3.1 PFOA and PFOS

A number of studies have been carried out worldwide in order to investigate long-chain PFAS removal by adsorption on different materials. PFOA and PFOS are commonly regarded as the most representative PFAS, due to their persistence in the environment and occurrence in industrial applications. A prior review paper indicated that long-chain PFAS (i.e., PFOA and PFOS) have been mainly removed through hydrophobic interactions and adsorbents with amine groups generally have high adsorption capacity [26].

The adsorption of long-chain PFAS on different adsorbents (commercially available or synthetized) obtained from batch adsorption tests is discussed in the following sections. Table 2 reports the adsorption capacity obtained from published data fitting the Langmuir model along with adsorbent material type and dosage, long-chain PFAS initial concentrations and experimental setups.

3.2 Activated carbon and biochar

Among commercial adsorbents, activated carbon (AC) has been widely investigated for PFOS and PFOA removal [50–52]. In detail, powdered activated carbon (PAC) had higher adsorption capacity than granular activated carbon (GAC) for both PFOA and PFOS [43,53].

Results about adsorption of PFOA on bamboo-derived activated carbon (BdAC) have shown that a long time (about 34 h) was required to reach adsorption equilibrium [36]. The comparison between BdAC and microporous AC revealed that the adsorption capacity of BdAC was higher than that of microporous AC [36,54]. This evidence corroborates that microporous adsorbents are not suitable for removing large molecules (i.e., long-chain PFSAs and PFCAs) and it is in agreement with results from fixed-bed column tests, as detailed below [25–27,33,52].

Chlorinated polyfluorinated ether sulfonate (F-53B) is a PFOS alternative compound. Both F-53B and PFOS compounds have been detected at high concentrations in an actual chrome plating WW [55]. Electroplating wastewater treatment plant (EWTP), employing reduction reaction (adding $Na_2S_2O_5$), precipitation (adding $Ca(OH)_2$), and flocculation–sedimentation (adding anionic polyacrylamide, PAM), was unable to effectively remove PFOS and F-53B. Hence, batch adsorption experiments were performed and a commercial coconut shell based GAC (R-CAC), after an activation process at low KOH/C ratio, was selected as adsorbent material for PFOS and F-53B removal [55]. F-53B is more hydrophobic than PFOS, due to an ether unit in the molecular structure, and this led to a much higher adsorption capacity of F-53B (two-fold higher than PFOS) onto R-CAC (Table 2). Single walled carbon nanotubes (SWNT) are hollow cylindrical tubes, made of graphene layers and a lattice of C atoms, and they have been investigated for PFOS and PFOA removal [54].

The comparison of microporous AC efficiency with SWNT, in removing PFOA at the same concentration, revealed that microporous AC has a higher adsorption capacity than SWNT. This difference may be linked to the higher surface area of microporous AC than that of SWNT (Table 2). Moreover, adsorption capacities of SWNT and AC for PFOS were 6 and 2 times higher, respectively, than that of PFOA, probably due to the one more C-F unit of the PFOS molecule [54]. In addition, SWNT exhibited higher adsorption capacity than multi walled carbon nanotubes (MWNT), consistent with their higher Brunauer, Emmett and Teller (BET) surface area [56,57]. PFAS adsorption on biochar has also been investigated because of its cost-effectiveness and affinity with organic compounds [58–60]. Pinewood (PWC) and hardwood (HWC) biochars have been tested for PFOA removal and the adsorption capacity of the biochar was lower than that of AC (Table 2). Guo et al. [58] have demonstrated that the adsorption capacity of corn-straw-derived biochar for PFOS removal increased with the increase of pyrolytic temperature, which is related to BET surface area of biochar (Table 2). Reported data from fixed-bed column tests showed the ability of GAC to remove traces of PFAS (as both complex mixture or single solute) from water intended for human consumption [11,27,33,47,61–63]. GAC (Filtrasorb 400, Calgon) column tested for PFOA removal has shown that the bed volumes were about 55,000 at 90% breakthrough point [61]. The same GAC (Filtrasorb 400, Calgon) has been tested for long-chain PFCAs (i.e., PFOA, PFNA, PFDA, PFUnA, PFDoDA, PFTeDA) and PFSAs (i.e., PFHxS and PFOS) removal, and the observed removal efficiencies were in the range 65-80% [33]. Information about the influence of GAC pore distribution on adsorption capacity of PFOS and PFOA were reported by Zaggia et al. [27]. Results from continuous adsorption experiments have demonstrated the great efficiency of bituminous AC, characterized by meso- and macropores, for PFOA and PFOS removal, whose maximum adsorption capacity was 39.6 and 4.1 μg g^{-1}, respectively [27]. In fact, meso- and macro-porous adsorbent materials are more easily accessed by long-chain PFAS resulting in higher adsorption capacity [27,33,48]. A high dosage of GAC (Filtrasorb 400, Calgon) was tested in a pre-equilibrium batch study for the removal of a complex mixture of long-chain PFSAs (PFHxS and PFOS) and PFCAs (PFOA, PFNA, PFDA, PFUnDA, PFDoDA) from LW [48]. Regardless of OM concentration, long-chain PFAS removal was in the range of 50-90% [48]. However, these results were obtained from a pre-equilibrium study (contact time was 15 min) with a GAC dose (10 g L^{-1}) that is not typically employed at water treatment plants.

3.3 Molecularly imprinted polymers

Several experimental works have explored the PFAS adsorption onto synthetically modified polymers, which are adsorbents conveniently synthetized to have high affinity and selectivity towards the target contaminants [64–66]. The macromolecular imprinted materials (MIMs), containing β-Cyclodextrin (β-CD) within a urethane framework, provide two types of binding sites. One binding

site is a β-CD inclusion site, the second is a non-inclusion (interstitial) site of the cross-linker domains, where aggregates, micelles and other inclusion complexes could be formed [64]. Formation of bilayer and multilayer structures is the dominant adsorption process for both PFOA and PFOS in these materials, as observed in several studies [17,26,64]. The modification of CD-based polymer adsorbents composition may allow an increasing of PFOA removal [65]. Nevertheless, the removal efficiency of cross-linked polymer network, where β-CD substitutes decafluorobiphenyl (DFB-CDP), was comparable with that of biochar tested by Inyang and Dickenson (2017). Adsorption efficiency of non-imprinted carbon microspheres (NIP-CMs) for PFOS removal has been compared with a surface imprinted polymer (MIP-CMs) in which double functional monomers of methacryloyloxyethyl trimethyl ammonium chloride (DMC) and 2-(trifluoromethyl)acrylic acid (TFMA) have been synthetized on carbon microspheres [66]. The adsorption capacity was higher for MIP-CMs than NIP-CMs (Table 2), due to the effect of molecularly imprinting technique in enhancing PFOS removal. The molecular imprinting technique has also been employed in order to prepare a novel adsorbent using chitosan crosslinked for PFOS removal and its adsorption capacity was higher than that observed for non-imprinted ones [38].

3.4 Anion-exchange resin

Several studies have indicated the suitability of the AE process for PFAS removal. Otherwise, PFAS removal efficiency varied greatly among AE resins, due to their properties, such as polymer matrix, functional group and porosity [27]. It was demonstrated that large pores of macroporous resin allow a faster diffusion of PFOS than the gel one [32]. This evidence is confirmed by comparing the adsorption capacity of IRA910 (polystyrene-DVB, macroporous-type) and IRA400 (styrene-DVB, gel-type) for PFOS removal [34,53,54]. Moreover, polymer matrixes led to different intraparticle diffusion and a polyacrylic resin has shown higher efficiency for PFOS removal than polystyrene one [32]. IRA910 exhibited a good selectivity also for PFHxS as demonstrated by Maimaiti et al. [34]. When IRA67 (polyacrylic-DVB, gel-type) has been employed, its adsorption capacity was higher than styrene type resins (Table 2). Gao et al. [17] demonstrated the great applicability of polyacrylic resin for F-53B removal, since the adsorption capacity of IRA67 (about 2400 mg g^{-1}) was higher than that of R-CAC in batch experiments (Table 2). As regards long-chain PFCAs, PFOA removal has been investigated on different kinds of strong AE resins [34,36,53,54]. Based on Table 2, the highest adsorption capacity was obtained when IRA910 (polystyrene-DVB, macroporous-type resin) was employed [34]. The adsorption capacity of IRA67 was higher than that of BdAC, both adsorbents tested at the same PFOA initial concentration (Table 2). The efficiency of IRA67 may be ascribed to the amine groups on the resin surface, which involve the PFOA adsorption via AE mechanisms. Besides, the open pore structure of IRA67 also allowed a better diffusion of PFOA molecules. Moreover, as demonstrated

by Zaggia et al. [27], the selectivity of larger and more hydrophobic anions (i.e., PFOS and PFOA) increased with the increasing of alkyl chain length of the functional group of AE resins. Differences in terms of equilibrium exchange capacity of different type of resins are linked with the strength of hydrophobic interactions between resin functional groups and PFAS molecules. Considering hydrophobicity of resin, highly hydrophobic resins (such as A532E) favour PFOA and PFOS passage from hydrated state to adsorbed state as confirmed by the highest adsorption capacity values obtained on both batch and continuous-flow pilot scale experiments [27]. The comparison between the performance of AE resin and GAC for long-chain PFAS removal has also been carried out by employing the fixed-bed column tests. Particularly, as demonstrated by Chularueangaksorn et al. [61], PFA300 (AE resin, polystyrene crosslinked DVB) could treat a higher amount of water than GAC (Filtrasorb 400, Calgon) before the saturation (at a 90% breakthrough point, bed volumes were 119,880 and 55,080, respectively). A532E (polystyrene-DVB gel-type, bifunctional quaternary amine) exhibited the highest adsorption capacity for both PFOS and PFOA among several adsorbent materials tested (i.e., coconut based GAC, bituminous coal based GAC, mildly hydrophobic and non-hydrophobic resins) during continuous experiments [27]. Removal efficiencies of AE resin (A600, polystyrene-DVB gel-type) for long-chain PFCAs (PFOA, PFNA, PFDA, PFUnA, PFDoDA, PFTeDA) and PFSAs (PFHxS and PFOS) were in the range 33-94% after 50,704 bed volumes (BVs), whereas removal efficiencies of GAC (Filtrasorb 400, Calgon) column were in the range 28-94% after 49,523 BVs [33].

3.5 Synthetized materials

With the purpose of identifying the best suitable adsorbent for PFAS removal, it is currently practice to synthesize new materials with properties and structures easy to control and modify. To date, new adsorbents with higher selectivity and specificity designed towards PFAS removal are also becoming commercially available for water treatment applications. For instance, a porous aromatic framework constructed from benzene rings (PAF-45) was employed for PFOS removal [67]. Despite the remarkable adsorption capacity (Table 2), PAF-45 feasibility was influenced by pH solution and ionic strength since the adsorption capacity was higher at acidic pH values (i.e., pH ~ 3). Moreover, the adsorption isotherm experiments have been carried out at PFOS concentrations in the range of 50-200 mg L^{-1} [67], which are much higher than the PFAS concentrations typically detected in the water environment [2]. Covalent triazine-based framework (CTF) has been investigated for removing different long-chain compounds (PFOA, PFHxS and PFOS), due to its large surface area and rigid pore structure [54]. Among the three long-chain PFAS tested, Wang et al. [54] have demonstrated that the adsorption capacity of CTF was highest for PFOS (Table 2). The electrostatic interaction between PFAS anion head and triazine groups of CTF (positively charged) represents the main driving force

for PFAS adsorption on CTF. Based on electrostatic interactions, which are the main adsorption mechanism of short-chain PFAS, CTF exhibited a good adsorption capacity for PFBS and PFBA removal, as it will be discussed below. Boron nitride, characterized by lightness structure and thermal stability, has been synthesized as porous hexagonal boron nitride nanosheets (h-BNs) for PFOS and PFDA removal [68]. The efficiency of this adsorbent material has been demonstrated to be linked with chain length and functional group of PFAS, since PFDA was more favourable adsorbed than PFOS (adsorption capacity of 0.16 mg m^{-2} and 0.04 mg m^{-2}, respectively). Among novel adsorbent materials investigated, magnetic-nanoparticles attached into fluorographene (2-MNPs@FG, mass ratio of MNPs and FG is 3:5) exhibited the highest adsorption capacity for PFOS instead of PFOA (Table 2). However, adsorbent dosage was not coherent with that really employed in full-scale treatment plants [69]. Quaternized cotton and aminated rice husk (ARH) both prepared with atom transfer radical polymerization (ATRP) technique were tested for PFOS and PFOA removal [45,46]. Results have demonstrated that quaternized cotton had higher adsorption capacity than ARH for both PFOS and PFOA (Table 2). Polyacrylonitrile fiber (PANF)-derived activated carbon fibers (PACFs) showed a remarkable adsorption capacity for PFOS and PFOA [43]. The adsorption affinity could be ascribed to its high specific surface area and micro- and mesoporous structure which allowed the establishment of multilayer adsorption (formation of hemi-micelles and micelles). The latter was also the main adsorption mechanism on crosslinked chitosan beads employed for PFOS removal, as demonstrated by Zhang et al. [70]. Poly(ethylenimine)-functionalized cellulose microcrystals (PEI-f-CMC) have been tested for removing long-chain PFAS at environmentally relevant concentration level [71]. Long-chain PFAS removal percentage was in the range of 80-98%. Despite its low surface area, PEI-f-CMC exhibited a good adsorption affinity both in DI and in the presence of co-existing OM, as discussed in section 5. The main drawback of those synthetized materials is the application at full-scale treatment plants because their production is not industrialized and, probably, they are not commercially available, unlike AC and AE resins. Economic assessment for new synthetized materials is needed.

3.6 Nanoparticles materials

The adsorption of PFAS into nanoparticles (NPs) has recently been investigated due to their co-existing in aquatic environments (i.e., marine debris plastic) or their high surface area and reactivity (i.e., iron oxides). As demonstrated by Lu et al. [72], nano-oxides such as titania (TiO_2), iron oxides (Fe_2O_3), alumina (Al_2O_3) and silica (SiO_2) have the ability to sorb PFOS. Among the different nano-oxides tested, Al_2O_3 showed the highest PFOS adsorption capacity (1.1 μg m^{-2}), whereas SiO_2 exhibited the lower adsorption capacity (0.1 μg m^{-2}). This difference in terms of PFOS removal should be ascribed to the different hydroxyl groups and surface area. Furthermore, the main adsorption

mechanism of PFOS on nano-oxides was not only electrostatic interaction, but also the formation of hydrogen bounds between the PFOS sulfonic terminal group and nano-oxides surface [72]. Magnetite nanoparticles (Fe_3O_4 NP) were used as the substrate of a novel magnetic nanocomposite (Fe_3O_4@SiO_2- NH_2&F_{13}), in which silica membrane functionalized with amino group and octyl-perfluorinated chain was synthesized on the Fe_3O_4 NP surface [73]. Based on kinetic data, the predominant adsorption mechanism between the magnetic adsorbent and PFAS tested was chemisorption, which includes both electrostatic and F-F interaction [73]. In detail, the selective F-F interaction between octyl-perfluorinated chain on the magnetic composite surface and perfluoroalkyl dipole shell in PFAS molecule was enhanced by electrostatic attraction of -NH_2 and the anionic -COOH or -SO_3H of PFCAs and PFSAs molecules, respectively. Due to size exclusion effect, PFCAs were better adsorbed than PFSAs on Fe_3O_4@SiO_2- NH_2&F_{13}. Considering perfluoroalkyl chain length, PFUnDA exhibited the highest adsorption capacity onto Fe_3O_4@SiO_2- NH_2&F_{13}, due to the formation of aggregate structure between long-chain PFAS which could stick together and, consequently, the amount of PFAS adsorbed increased [73]. A recent experimental work investigated the capability of microplastics (MPLs) to sorb a complex mixture of PFAS from RW (Ebro river) and seawater (SeaW), simulating realistic environmental conditions [74]. High-density polyethylene (HDPE), polystyrene (PS) and poly-styrene carboxylic acid (PS-COOH) were selected due to their wide occurrence as marine debris plastic. Results of batch adsorption experiments showed low removal percentages (< 27%) of long-chain PFAS in RW after 7 days (with few exceptions of PFTrA and PFTeA whose percentages were between 65% and 70%). Moreover, MPLs efficiency in SeaW was affected by water chemistry such as salinity and OM concentration. This point will be deeply explained later (see section 5). Overall, carboxylated compounds with more than 11 C atoms were the most removed [74]. In detail, HDPE exhibited the worst adsorption capacity due to its granular shape, which limited the intraparticle diffusion [74]. In RW, PFOA, PFNA, PFHxS and PFOS did not present any adsorption on both HDPE and PS-COOH throughout the experiment period. On the contrary, affinity between carboxylated compounds with less than 10 C atoms and HDPE was higher in SeaW. Adsorption rates of PFCAs on PS-COOH in RW increased with the increasing of chain length. Comparing PFCAs to PFSAs, with the same chain length, the carboxylated compounds were less removed [74]. Whereas, in SeaW, the presence of carboxylic group in the PS-COOH surface implicated an increase of adsorption rates of carboxylated compounds. Adsorption kinetics were influenced by adsorbents size, therefore PS exhibited faster kinetic than HDPE, since it had the smallest particles [74].

Table 2 Batch adsorption experiments of long-chain PFAS fitted by Langmuir model.

Adsorbate		Adsorbent		Water matrix	Experimental setup	Adsorption capacity (mg-PFAS/g-adsorbent)	References
Compound	**$[PFAS]_0$**	**Type and properties**	**Batch dose (mg L^{-1}, except stated otherwise)**				
Activated carbon							
PFOA	15 – 150 mg L^{-1}	**GAC Calgon F400**	1000	DI	T = 30 °C, pH 7.2,	112.1	[50]
	1 – 1000 mg L^{-1}	**PAC**	1000	DI	T = 25 °C, 140 rpm, 48 h	426.49 (1.03 mmol g^{-1})	[52]
	120 mg L^{-1}	**BdAC** S_{BET} = 2450 m^2 g^{-1} Effective size = 0.6–0.85 mm	200	Actual WW (PFOSF WWW)	T=25 °C, 170 rpm, 48 h, pH 4.0	372.6 (0.9 mmol g^{-1})	[36]
	0.01 – 100,000 µg L^{-1}	**Biochar HWC** S_{BET} = 453 m^2 g^{-1} pore volume= 0.11 cm^3 g^{-1}	ratio of biochar:PFOA 1:3 mg mL^{-1}	LW (DOC=2 mg L^{-1})	T= 22 °C, 30 d, pH 7.2	41.2	[59]
				WW (DOC=4.9 mg L^{-1})		31.7	
		Biochar PWC S_{BET} = 413 m^2/g pore volume= 0.10 cm^3/g	ratio of biochar:PFOA 1:3 mg mL^{-1}	LW (DOC=2 mg L^{-1})		41.3	
				WW (DOC=4.9 mg L^{-1})		27.7	
	3.8 – 259 mg L^{-1}	**SWNT** Single walled carbon nanotubes S_{BET} = 468 m^2 g^{-1} pore volume = 0.52 cm^3 g^{-1}	250	DI	Room temperature, 3 d, pH 6	78.67 ± 8.28 (190 ± 20 mmol kg^{-1})	[54]
		AC Calgon, microporous S_{BET} = 825 m^2 g^{-1} pore volume = 0.54 cm^3 g^{-1}				194.6 ± 4.14 (470 ± 10 mmol kg^{-1})	
	20 – 250 mg L^{-1}	**PAC** S_{BET} = 812 m^2 g^{-1} micropore area = 466 m^2 g^{-1}	100	DI	T = 25 °C, 150 rpm, 168 h (12 h for PAC)	277.42 (0.67 mmol g^{-1})	[53]
		GAC S_{BET} = 712 m^2 g^{-1} micropore area = 313 m^2 g^{-1}				161.48 (0.39 mmol g^{-1})	
	0.05 - 10 mg L^{-1}	**MWNT** S_{BET} = 519.7 m^2 g^{-1}	50	DI	T = 25 °C, pH 6.5	2.69 ± 0.29 (0.0065 ± 0.0007 mmol g^{-1})	[57]
	20 – 300 mg L^{-1}	**PAC** S_{BET} = 1227.19 m^2 g^{-1}	100	DI	T= 25 °C, 180 rpm, pH 5	202.9 (0.49 mmol g^{-1})	[43]
		GAC S_{BET} = 815.34 m^2 g^{-1}				178.05 (0.43 mmol g^{-1})	
PFOS	15 – 150 mg L^{-1}	**GAC Calgon F400**	1000	DI	T = 30 °C, pH 7.2	236.4	[50]
		GAC Calgon F300				196.2	
		GAC Calgon URV-MOD1				211.6	
	1 – 1000 mg L^{-1}	**PAC**	1000	DI	T = 25 °C, 140 rpm, 48 h	440.11 (0.88 mmol g^{-1})	[52]
	44.1 µg L^{-1}	**R-CAC** S_{BET} = 1125 m^2 g^{-1} pore volume = 0.90 cm^3 g^{-1}	50 - 250	Effluent EWTP	T= 25 °C, 170 rpm, 48 h	0.345 mg g^{-1} (345 µg g^{-1})	[55]

Table 2 Batch adsorption experiments of long-chain PFAS fitted by Langmuir model (continued).

Adsorbate		Adsorbent		Water matrix	Experimental setup	Adsorption capacity (mg-PFAS/g-adsorbent)	References
Compound	**$[PFAS]_0$**	**Type and properties**	**Batch dose (mg L^{-1}, except stated otherwise)**				
Activated carbon							
PFOS	20 – 250 mg L^{-1}	**PAC** S_{BET} = 812 m^2 g^{-1} micropore area = 466 m^2 g^{-1}	100	DI	T = 25 °C, 150 rpm, 168 h (12 h for PAC)	520.13 (1.04 mmol g^{-1})	[53]
		GAC S_{BET} = 712 m^2 g^{-1} micropore area = 313 m^2 g^{-1}				185.04 (0.37 mmol g^{-1})	
	20 – 300 mg L^{-1}	**PAC** S_{BET} = 1227.19 m^2 g^{-1}	100	DI	T= 25 °C, 180 rpm, pH 5	535.13 (1.07 mmol g^{-1})	[43]
		GAC S_{BET} = 815.34 m^2 g^{-1}				390.1 (0.78 mmol g^{-1})	
	0.5 – 10 mg L^{-1}	**Corn-derived-biochar (T=250 °C)** S_{BET} = 2.5 m^2 g^{-1} total pore volume = 0.013 cm^3 g^{-1}	200	DI + 0.01 mol L^{-1} of $CaCl_2$ + 200 mg L^{-1} of NaN_3	T= 25 ± 1 °C, 150 rpm, 48 h, pH 7	135.53	[58]
		Corn-derived-biochar (T=400 °C) S_{BET} = 3.75 m^2 g^{-1} total pore volume = 0.017 cm^3 g^{-1}				146.52	
		Corn-derived-biochar (T=550 °C) S_{BET} = 41.10 m^2 g^{-1} total pore volume = 0.043 cm^3 g^{-1}				166.42	
		Corn-derived-biochar (T=700 °C) S_{BET} = 297.58 m^2/g total pore volume = 0.199 cm^3/g				169.90	
	59.9 – 415 mg L^{-1}	**SWNT** S_{BET} = 468 m^2 g^{-1} pore volume = 0.52 cm^3 g^{-1}	250	DI	Room temperature, 3 d, pH 6	560.14 ± 40.01 (1120 ± 80 mmol kg^{-1})	[54]
	1 – 500 mg L^{-1}	**SWNT** S_{BET} = 547.2 m^2 g^{-1}	200 - 1200	DI	T= 25 °C, 150 rpm, 2 h, pH 7	712	[56]
		MWNT10 S_{BET} = 324.9 m^2 g^{-1}				656	
		MWNT50 S_{BET} = 97.2 m^2 g^{-1}				514	
	59.9 – 415 mg L^{-1}	**AC Calgon** microporous S_{BET} = 825 m^2 g^{-1} pore volume = 0.54 cm^3 g^{-1}	250	DI	Room temperature, 3 d, pH 6	480.12 ± 10 (960 ± 20 mmol kg^{-1})	[54]
	0.05 - 10 mg L^{-1}	**MWNT** S_{BET} = 519.7 m^2 g^{-1}	50	DI	T = 25 °C, pH 6.5	5.00 ± 0.5 (0.010 ± 0.001 mmol g^{-1})	[57]
	30 – 200 mg L^{-1} (30 – 200 ppm)	**PAC** S_{BET} = 1521.85 m^2 g^{-1}	133.3	DI	T= 25 °C, 170 rpm	360.1 (0.72 mmol g^{-1})	[51]
		40% Ni-PAC S_{BET} = 947.98 m^2 g^{-1}				355.1 (0.71 mmol g^{-1})	
F-53B	102.9 µg L^{-1}	**R-CAC** S_{BET} = 1750 m^2 g^{-1}	50 - 250	Effluent EWTP	T= 25 °C, 170 rpm, 48 h	1.059 (1059.4 µg g^{-1})	[55]

Table 2 Batch adsorption experiments of long-chain PFAS fitted by Langmuir model (continued).

Adsorbate		Adsorbent		Water matrix	Experimental setup	Adsorption capacity (mg-PFAS/g-adsorbent)	References
Compound	**$[PFAS]_0$**	**Type and properties**	**Batch dose (mg L^{-1})**				
Molecularly imprinted polymers							
PFOA	1-12 mg L^{-1}	**DFB-CDP** S_{BET} < 10 m^2 g^{-1}	100	DI	T= 23 °C, 400 rpm, 2 h	34	[65]
PFOS	20 – 550 mg L^{-1}	**Chitosan-based MIP**	100	DI	T = 25 °C, 36 h, pH 5	1455.52 (2910.3 µmol g^{-1})	[38]
		Chitosan-based NIP				1203.51 (2406.4 µmol g^{-1})	
	10 - 80 mg L^{-1}	**MIP-CMS**	250	DI	T= 25 °C, 150 rpm, 2 h, pH 3	75.99	[66]
		NIP-CMS	250			43.94	
Anion-exchange resin							
F-53B	25-400 mg L^{-1}	**IRA67** Polyacrylic-DVB gel-type Polyamine Exchange capacity = 1.6 meq mL^{-1} Effective size = 0.3–1.2 mm	50	Actual WW (chrome plating WW)	T=25 °C, 150 rpm, 48 h, pH 3	2396.84 (4.2 mmol g^{-1})	[17]
PFOA	120 mg L^{-1}	**IRA67** Polyacrylic-DVB gel-type Polyamine Exchange capacity = 1.6 meq mL^{-1} Effective size = 0.3 – 1.2 mm	100	Actual WW (PFOSF WWW)	T=25 °C, 170 rpm, 48 h, pH 4.0	1167.67 (2.82 mmol g^{-1})	[36]
	50 – 400 mg L^{-1}	**IRA910** Polystyrene-DVB macroporous-type Dimethyl ethanol ammonium Exchange capacity = 1.0 meq mL^{-1}	100	DI	T= 25 °C, 160 rpm, 240 h, pH 6	1436.82 (3.47 mmol g^{-1})	[34]
	20 – 250 mg L^{-1}	**IRA400** Styrene-DVB gel-type Quaternary ammonium Exchange capacity = 1.4 meq mL^{-1}	100	DI	T = 25 °C, 150 rpm, 168 h	1209.08 (2.92 mmol g^{-1})	[53]
	3.8 – 259 mg L^{-1}		375	DI	Room temperature, 3 d, pH 6	331.25 ± 8.28 (800 ± 20 mmol kg^{-1})	[54]
PFHxS	50 – 400 mg L^{-1}	**IRA910** Polystyrene-DVB macroporous-type Dimethyl ethanol ammonium Exchange capacity = 1.0 meq mL^{-1}	100	DI	T= 25 °C, 160 rpm, 240 h, pH 6	1364.37 3.41 mmol g^{-1}	[34]
PFOS	25-400 mg L^{-1}	**IRA67** Polyacrylic-DVB gel-type Polyamine Exchange capacity = 1.6 meq mL^{-1} Particle size = 16 – 50 mesh	0.05	Actual WW (chrome plating WW)	T=25 °C, 150 rpm, 48 h, pH 3	2750.71 (5.5 mmol g^{-1})	[17]
	400 mg L^{-1}		35 - 500	DI		2000.52 – 2500.65 (4 – 5 mmol g^{-1})	[32]

Table 2 Batch adsorption experiments of long-chain PFAS fitted by Langmuir model (continued).

Adsorbate		Adsorbent		Water matrix	Experimental setup	Adsorption capacity (mg-PFAS/g-adsorbent)	References
Compound	**$[PFAS]_0$**	**Type and properties**	**Batch dose (mg L^{-1})**				
Anion-exchange resin							
PFOS	400 mg L^{-1}	**IRA958** Polyacrylic macroporous-type Quaternary ammonium Exchange capacity = 3.7 meq g^{-1} Effective size = 0.3 – 1.2 mm	35 - 500	DI	T=25 °C, 150 rpm, 48 h, pH 3	2000.52 – 2500.65 (4 – 5 mmol g^{-1})	[32]
	50 – 400 mg L^{-1}	**IRA910** Polystyrene-DVB macroporous-type Dimethyl ethanol ammonium Exchange capacity = 1.0 meq mL^{-1}	100	DI	T= 25 °C, 160 rpm, 240 h, pH 6	1395.36 2.79 mmol g^{-1}	[34]
	20 – 250 mg L^{-1}	**IRA400** Styrene-DVB gel-type Quaternary ammonium Exchange capacity = 1.4 meq mL^{-1}	100	DI	T = 25 °C, 150 rpm, 168 h	210.05 (0.42 mmol g^{-1})	[53]
	59.9 – 415 mg L^{-1}		375	DI	Room temperature, 3 d, pH 6	165.04 ± 20 (330 ± 40 mmol kg^{-1})	[54]
Other materials							
PFOS	15 – 150 mg L^{-1}	**13X zeolite**	1000	DI	T = 30 °C, pH 7.2	12.0	[50]
		NaY80 zeolite				114.7	
	1 – 500 mg L^{-1}	**Chars from maize straw pyrolysis** S_{BET} = 11.6 m^2 g^{-1}	200 - 1200	DI	T= 25 °C, 150 rpm, 384 h, pH 7	164	[56]
		Chars from willow sawdust pyrolysis S_{BET} = 7.21 m^2 g^{-1}				91.6	
		MA S_{BET} = 38.3 m^2 g^{-1}				811	
Synthesized materials							
PFDA	0.4 – 50 mg L^{-1}	**h-BNs** S_{BET} = 125.5 m^2 g^{-1} pore volume = 0.915 cm^3 g^{-1}	200	DI	T= 23 ± 2 °C, 150 rpm, 5 mM ammonium acetate	0.16 mg m^{-2}	[68]
PFHxS	19.2 – 180 mg L^{-1}	**CTF** S_{BET} = 1270 m^2 g^{-1} pore volume = 0.63 cm^3 g^{-1}	250	DI	Room temperature, 3 d, pH 6	224.06 ± 28 (560 ± 70 mmol kg^{-1})	[54]
PFOS	46.51 – 372.1 mg L^{-1}	**Crosslinked chitosan beads** S_{BET} = 14.1 m^2 g^{-1} Particle diameter = 4 – 5 mm	60.8	DI	T= 25 °C, 150 rpm, 150 h, pH 3	2605.67 (5.21 mmol g^{-1})	[75]
	50 – 200 mg L^{-1}	**PAF-45** S_{BET} = 875.38 m^2 g^{-1} pore volume = 0.40 mL g^{-1}	12.5	DI	T= 25 °C, 180 rpm, 48 h, pH 3	5847.39	[67]

Table 2 Batch adsorption experiments of long-chain PFAS fitted by Langmuir model (continued).

Adsorbate		Adsorbent		Water matrix	Experimental setup	Adsorption capacity (mg-PFAS/g-adsorbent)	References
Compound	**$[PFAS]_0$**	**Type and properties**	**Batch dose (mg L^{-1})**				
Synthesized materials							
PFOS	0.1 – 250 mg L^{-1}	**ARH**	100	DI	T= 25 °C, 150 rpm, 24 h, pH 5	1325.34 (2.65 mmol g^{-1})	[45]
	0.4 – 50 mg L^{-1}	**h-BNs** S_{BET} = 125.5 m^2 g^{-1} pore volume = 0.915 cm^3 g^{-1}	200	DI	T= 25 °C, 180 rpm, 5 mM ammonium acetate	0.04 mg m^{-2}	[68]
	59.9 – 415 mg L^{-1}	**CTF** S_{BET} = 1270 m^2 g^{-1} pore volume = 0.63 cm^3 g^{-1}	250	DI	Room temperature, 3 d, pH 6	665.17 ± 40.01 (1330 ± 80 mmol kg^{-1})	[54]
	95.02 – 460.12 mg L^{-1}	**Quaternized cotton**	100	DI	T= 25 °C, 150 rpm, 24 h, pH 5	1650.43 (3.3 mmol g^{-1})	[46]
	0.5 – 40 mg L^{-1}	**2-MNPs@FG** S_{BET} = 169.85 - 225.42 m^2 g^{-1}	250	DI	220 rpm, 30 min	17.2	[69]
	20 – 300 mg L^{-1}	**PACFs** S_{BET} = 1782 m^2 g^{-1}	100	DI	T= 25 °C, 180 rpm, pH 5	760.2 (1.52 mmol g^{-1})	[43]
PFOA	3.8 – 259 mg L^{-1}	**CTF** S_{BET} = 1270 m^2 g^{-1} pore volume= 0.63 cm^3 g^{-1}	250	DI	Room temperature, 3 d, pH 6	269.14 (650 ± 30 mmol kg^{-1})	[54]
	78.67 – 381 mg L^{-1}	**Quaternized cotton**	100	DI	T= 25 °C, 150 rpm, 24 h, pH 5	1283.61 (3.1 mmol g^{-1})	[46]
	0.1 – 207.03 mg L^{-1}	**ARH**	100	DI	T= 25 °C, 150 rpm, 24 h, pH 5	1031.03 (2.49 mmol g^{-1})	[45]
	0.5 – 40 mg L^{-1}	**2-MNPs@FG** S_{BET} = 169.85 - 225.42 m^2 g^{-1}	250	DI	220 rpm, 30 min	50.4	[69]
	20 – 300 mg L^{-1}	**PACFs** S_{BET} = 1782 m^2 g^{-1}	100	DI	T= 25 °C, 180 rpm, pH 5	302.27 (0.73 mmol g^{-1})	[43]
	2 – 50 µg L^{-1}	**PEI-f-CMC** S_{BET} = 7.8 m^2 g^{-1}	10	DI	T= 25±1 °C, 150 rpm, 24 h	2.32	[71]

S_{BET}: BET surface area; DI: Deionized water; PFSOF WWW: Perfluorooctanesulfonyl fluoride washing wastewater; LW: Lake water; EWTP: Electroplating wastewater treatment plant; GAC: Granular activated carbon; PAC: Powdered activated carbon BdAC: Bamboo-derived activated carbon; 40% Ni-PAC: Ni-compounded PAC with Ni loading an amount of ~40 wt%; R-CAC: reactivated coconut shell-based GAC; HWC: Harwood; PWC: Pinewood; SWNT: Single-walled carbon nanotubes; MWNT: Multi-walled carbon nanotubes; DFB-CDP: cross-linked polymer network where β-CD substitutes decafluorobiphenyl (DFB); MIP-CMS: molecularly imprinted carbon microsphere; NIP-CMS: non-imprinted carbon microsphere; MA: Ash from burning maize straw on stainless steel plate; CTF: Covalent triazine-based framework; h-BNs: porous hexagonal boron nitride nanosheets; PAF-45: porous aromatic framework constructed from benzene rings; ARH: Aminated rice husk; 2-MNPs@FG: Magnetic nano-particles attached into fluorographene (mass ratio of MNPs and FG is 3:5); WW: wastewater; PACFs: Polyacrylonitrile fiber (PANF)-derived activated carbon fibers; PEI-f-CMC: Poly(ethylenimine)-functionalized cellulose microcrystals.

4. Adsorption of short chain PFAS

4.1 Challenges in short chain PFAS adsorption

Short-chain PFAS and their precursors are as persistent as those long-chained. Therefore, although they show less bioaccumulation potential, their environmental occurrence is of concern [14,16,76]. While long-chain PFAS are binding with particles present in solution, those short-chain are mainly in the dissolved phase resulting in long-range transport in aquatic environments [7]. Therefore, short-chain PFAS have higher mobility in water bodies than long-chain compounds. Specifically, short-chain compounds could significantly affect drinking water supplies, increasing the human exposure to PFAS compounds. Considering the properties of short-chain PFAS (Table 1), it is expected that the large-scale remediation treatments, currently suitable for long-chain PFAS, are ineffective for short-chain PFAS [14,16]. This evidence is consistent with data from full-scale drinking water treatment plants [2,12]. Moreover, it is widely reported that carbon-chain length influences adsorption capacities of PFAS onto various materials, since adsorption rate seems to increase with the increase of molecular size [11]. Data collected from full-scale treatment plants (drinking and wastewater facilities) suggested that the removal of short-chain compounds is still a challenge task, due to their early and faster breakthrough [12,27,33]. To date, a restricted number of published data have addressed short-chain PFAS adsorption by using different materials, because most of the experimental works have focused on the removal of long-chain PFAS (i.e., PFOA and PFOS). Adsorption capacities obtained by fitting the Langmuir model along with type and dosage of adsorbent materials, initial concentration of short-chain PFAS and experimental setup are reported in Table 3. Comparisons between several adsorbent materials tested for short-chain PFAS are reviewed based on both batch experiment studies (Table 3) and fixed-bed column tests. The adsorption capacity of materials tested for PFBA removal observed during batch tests (Table 3) follows the order: microporous AC < CTF < IRA910 (strong AE resin). However, results obtained by continuous experiments have demonstrated that the adsorption capacity of meso-porous GAC (meso-porous bituminous coal-derived AC) was higher than A532E (strong AE resin) (4.3 and 3.3 μg g^{-1}, respectively) [27]. In the following sections the removal of short chain PFAS by adsorption is discussed based on the type of adsorbent.

4.2 Activated carbon, biochar and other adsorbents

The performance of BdAC and coal-based AC (microporous type), used for removing PFHxA, has been compared. The adsorption capacity of BdAC was 13 times lower than microporous AC probably due to its low BET surface area and the presence of OM in the solution tested [36,54]. The adsorption capacities of HWC and PWC biochars for PFBA and PFOA removal were investigated by Inyang and Dickenson (2017). Results from adsorption kinetic tests showed that the amount of PFBA

adsorbed on both HWC and PWC was 3-4 times lower than that of PFOA. This evidence suggests the incapability of biochar for short-chain PFAS removal and it may prove the competition between long- and short-chain PFAS for the adsorption sites and/or competition with OM [59]. Short-chain PFAS adsorption on GAC and PAC has also been investigated by using batch test [77]. Tests have been carried out at real concentrations of short-chain PFAS (range about 73 – 320 ng L^{-1}) and using an adsorbent dose comparable to that used in real water treatment plants (range about 25 – 125 mg L^{-1}). Results have demonstrated that PAC has higher adsorption capacity than GAC (more than twice), due to the shorter internal diffusion distances and its higher BET surface area [77]. MWCNTs functionalized in different ways (MWCNTs-PRI, MWCNTs-COOH, MWCNTs-OH) were tested for PFBS removal [78]. Removal percentage of PFBS on MWCNTs was about 30% in DI water, whereas when humic acids (HA) and phenol co-existed in the solution, this percentage was lower than 20% [78]. Moreover, due to the weak hydrophobicity of PFBS, its percentage removal was lower than that of long-chain compounds [78]. Results of adsorption isotherm of PFOS and PFBS on boehmite showed that PFOS was better removed than PFBS, since the effect of surface aggregation enhanced long-chain PFAS removal [79].

Among fixed-bed column experiments carried out in order to assert the short-chain PFAS removal, McCleaf et al. [33] reported faster breakthrough and lower removal percentage of short-chain PFCAs on GAC column (F400, Calgon) than long-chain ones. The removal efficiencies of the short-chain PFCAs tested (i.e., PFBA, PFPeA, PFHxA and PFHpA) were lower than 19% on GAC column after 49,523 BVs. Whereas, the removal efficiency of PFBS (short-chained PFSAs tested) was ~10%. Those results suggest that short-chain PFAS removal depends mainly on the availability of active sites, since they do not bind with other particles and, consequently, the formation of aggregates does not occur [27,33]. Moreover, desorption of short-chain PFAS has been also hypothesized, due to the competition of long-chain PFAS and/or OM. Similar fast breakthrough of short-chain PFAS has also been observed in rapid small-scale column tests (RSSCT) carried out on different types of GAC columns [25]. Among the three activated carbons tested, F300 (microporous bituminous coal-derived) exhibited the lowest efficiency for the short-chain PFCAs tested (i.e., PFBA, PFPeA and PFHxA), due to its pore distribution (mainly microporous type) and BET surface area. Others GAC tested, coconut based GAC (AquaCarb 1240) and bituminous coal based ones (F600), performed better for the removal of selected short-chain PFAS [25]. PFBA uptake on different types of biochar was influenced by BET surface area. Indeed, the highest percentage removal has been found on the hardwood sawdust pellets gasified at 900 °C (HWC), which had the highest BET surface area among the different biochars tested [59]. However, results obtained from batch adsorption kinetic tests have demonstrated that GAC removed PFBA better than HWC [59]. Short-chain PFAS adsorption on

microplastics (HDPE, PS and PS-COOH) has recently been investigated in simulated realistic environmental conditions [74]. Due to the increase in ionic strength, short-chain carboxylates compounds have been better removed by PS-COOH in SeaW than in RW. Whereas, short chain PFAS were almost not adsorbed onto PS and HDPE [74]. Removal of PFBS (short-chain PFSAs) has been investigated at batch mode by means of AC (i.e., microporous AC and Calgon F400) and CTF [50,54]. The difference of adsorption capacity between CTF and AC may be related to their different structure and, consequently, adsorption mechanisms established, since the electrostatic interactions between PFAS anion head and triazine groups of CTF involved short-chain PFAS adsorption on CTF [54]. However, CTF exhibited a lower affinity with PFBA than ARH (Table 3). Adsorption capacity of ARH was 4 times higher than CTF [45,54]. A novel adsorbent poly(ethylenimine)-functionalized cellulose microcrystal (PEI-f-CMC) has been synthetized and its efficiency for short-chain removal has been evaluated at environmental relevant concentration levels [71]. Results have demonstrated that short-chain with sulfonate terminal group were removed better than short-chain PFCAs, in agreement with previous experimental studies [2,33].

4.3 Anion-exchange

The removal efficiency of three PFCAs owning different chain lengths, including PFHxA (with 6 C atoms), PFHpA (with 7 C atoms) and PFOA (with 8 C atoms) from industrial WW (perfluorooctanesulfonyl fluoride washing wastewater, PFSOF WWW) by AE resin has been evaluated during batch experiments conducted by Du et al. [36]. Results demonstrated that adsorption sites on IRA67 were occupied by PFOA molecules prior to the others PFCAs and, therefore, the adsorption rates of short-chain were lower. Consequently, short-chain PFCAs reached the equilibrium very fast [36]. Moreover, comparing the efficiency of two different anion-exchange resins (i.e., IRA910 and IRA67) for removing the same compound (PFHxA), IRA910 (polystyrene-DVB macroporous-type) exhibited higher adsorption capacity than IRA67 (polyacrylic-DVB gel-type) [34,36]. This difference in adsorption capacity for PFHxA may be linked to the resin properties, such as polymer matrix and porosity, and/or to the effect of OM present in the solution. In fact, IRA910 was tested in DI water, whereas IRA67 was employed for PFHxA removal from PFSOF WWW [34,36]. Moreover, when tested for the same actual WW, IRA67 had higher affinity with PFHpA than BdAC, as demonstrated by the adsorption capacity, which was 3 times higher than that of BdAC [36]. Furthermore, amine groups on adsorbent surface improved the short-chain PFAS removal, due to the establishment of electrostatic interactions, which are the main driving force during short-chain adsorption [26,45,75]. Results provided by fixed-bed column tests demonstrated that the adsorption capacity of A532E (strong AE resin) was almost equal to that of GAC (meso-porous bituminous-coal derived AC), when tested for PFBS removal (4.7 μg g^{-1} and 4.1 μg g^{-1}, respectively) [27].

Results from fixed-bed column experiments carried out by McCleaf et al. [33] have shown fast breakthrough and low removal percentage for short-chain PFCAs on AE resin (A600, polystyrene-DVB gel-type). The removal efficiencies of short-chained PFCAs tested were ~11% on A600 column after 50,704 BVs. The same anion-exchange resin better removed PFBS (short-chain PFSAs tested) than other short-chain compounds, and the removal efficiency of PFBS was ~55% [33].

Results from a pre-equilibrium study carried out by Kothawala et al. [48] demonstrated that fresh adsorbent materials (i.e., AE resin, Purolite A600, and GAC, Filtrasorb 400) could remove short-chain PFAS from water solutions. Nevertheless, anion-exchange showed the highest percent of removal. In detail, removal percentages of short-chain PFAS (PFBA, PFPeA, PFHxA, PFHpA, PFBS) were about 90% and 50% on A600 and Filtrasorb 400, respectively. However, those results have been obtained from a pre-equilibrium study (contact time was equal to 15 min) with a high dosage of adsorbent materials [48].

Analysis of transmission electron microscopy (TEM) carried out on AE resins allowed a deep understanding of the predominant adsorption mechanism involved during short-chain PFAS removal [27]. Indeed, TEM images showed that the weak hydrophobic interactions between PFBA (or PFBS) and resin surface did not allow the formation of aggregates and, consequently, AE of single molecules was the main mechanism for short-chain removal.

Overall, AE resins exhibit a remarkable adsorption capacity for both long- and short-chain PFAS. Nevertheless, the possible release of disinfection by-products (DBP) such as N-Nitrosodimethylamine (NDMA) may represent the main drawback for their full-scale application [80]. Particularly, the amount of NDMA and their precursors released upon usage depends on the resin functional group (such as amine groups) and operational conditions (such as regeneration activities and flow interruptions).

Table 3 Batch adsorption experiments of short-chain PFAS fitted by Langmuir model.

Adsorbate		Adsorbent		Water matrix	Experimental setup	Adsorption capacity (mg-PFAS/g-adsorbent)	References
Compound	**$[PFAS]_0$**	**Type and properties**	**Batch dose (mg L^{-1})**				
Activated carbon							
PFBA	6.5 – 204 mg L^{-1}	**AC Calgon** microporous S_{BET} = 825 m^2 g^{-1} pore volume = 0.54 cm^3 g^{-1}	250	DI	Room temperature, 3 d, pH 6	51.36 ± 4.28 (240 ± 20 mmol kg^{-1})	[54]
PFHxA	31.4 mg L^{-1}	**BdAC** S_{BET} = 2450 m^2 g^{-1} Effective size = 0.6–0.85 mm	200	Actual WW (PFOSF WWW)	T=25 °C, 170 rpm, 48 h, pH 4	18.84 (0.06 mmol g^{-1})	[36]
	7.2 – 217 mg L^{-1}	**AC Calgon** microporous S_{BET} = 825 m^2 g^{-1} pore volume = 0.54 cm^3 g^{-1}	250	DI	Room temperature, 3 d, pH 6	235.54 ± 72.23 (750 ± 230 mmol kg^{-1})	[54]
PFHpA	40.04 mg L^{-1}	**BdAC** S_{BET} = 2450 m^2 g^{-1} Effective size = 0.6–0.85 mm	200	Actual WW (PFOSF WWW)	T=25 °C, 170 rpm, 48 h, pH 4	65.53 (0.18 mmol g^{-1})	[36]
PFBS	6 – 247 mg L^{-1}	**AC Calgon** microporous S_{BET} = 825 m^2 g^{-1} pore volume = 0.54 cm^3 g^{-1}	250	DI	Room temperature, 3 d, pH 6	51.01 ± 3 (170 ± 10 mmol kg^{-1})	[54]
	15 – 150 mg L^{-1}	**GAC Calgon F400**	1000	DI	T = 30 °C, pH 7.2	98.7	[50]
Anion exchange resin							
PFBA	50 – 400 mg L^{-1}	**IRA910** Polystyrene-DVB macroporous-type Dimethyl ethanol ammonium Exchange capacity = 1.0 meq mL^{-1}	100	DI	T= 25 °C, 160 rpm, 240 h, pH 6	635.69 (2.97 mmol g^{-1})	[34]
PFHxA	50 – 400 mg L^{-1}	**IRA910** Polystyrene-DVB macroporous-type Dimethyl ethanol ammonium Exchange capacity = 1.0 meq mL^{-1}	100	DI	T= 25 °C, 160 rpm, 240 h, pH 6	1089.76 (3.47 mmol g^{-1})	[34]
	31.4 mg L^{-1}	**IRA67** Polyacrylic-DVB gel-type Polyamine Exchange capacity = 1.6 meq mL^{-1} Effective size = 0.3–1.2 mm	100	Actual WW (PFOSF WWW)	T=25 °C, 170 rpm, 48 h, pH 4	37.68 (0.12 mmol g^{-1})	[36]
PFHpA	40.04 mg L^{-1}	**IRA67** Polyacrylic-DVB gel-type Polyamine Exchange capacity = 1.6 meq mL^{-1} Effective size = 0.3–1.2 mm	100	Actual WW (PFOSF WWW)	T=25 °C, 170 rpm, 48 h, pH 4	192.95 (0.53 mmol g^{-1})	[36]

Table 3 Batch adsorption experiments of short-chain PFAS fitted by Langmuir model (continued).

Adsorbate		Adsorbent		Water matrix	Experimental setup	Adsorption capacity (mg-PFAS/g-adsorbent)	References
Compound	**$[PFAS]_0$**	**Type and properties**	**Batch dose (mg L^{-1})**				
Anion exchange resin							
PFBS	50 – 400 mg L^{-1}	**IRA910** Polystyrene-DVB macroporous-type Dimethyl ethanol ammonium Exchange capacity = 1.0 meq mL^{-1}	100	DI	T= 25 °C, 160 rpm, 240 h, pH 6	1023.32 (3.41 mmol g^{-1})	[34]
Synthesized materials							
PFBA	0.1 – 107.02 mg L^{-1}	**ARH**	100	DI	T= 25 °C, 150 rpm, 24 h, pH 5	363.86 (1.70 mmol g^{-1})	[45]
	6.5 – 204 mg L^{-1}	**CTF** S_{BET} = 1270 m^2 g^{-1} pore volume = 0.63 cm^3 g^{-1}	250	DI	Room temperature, 3 d, pH 6	92.03 ± 4.28 (430 ± 20 mmol kg^{-1})	[54]
PFHxA	7.2 – 217 mg L^{-1}					376.86 ± 94.21 (1200 ± 300 mmol kg^{-1})	
PFBS	6 – 247 mg L^{-1}					141.04 ± 12 (470 ± 40 mmol kg^{-1})	

AC: activated carbon; S_{BET}: BET surface area; DI: deionized water; PFOSF WWW: perfluorooctanesulfonyl fluoride washing wastewater; GAC: granular activated carbon; BdAC: bamboo-derived activated carbon; ARH: aminated rice husk; CTF: covalent triazine-based framework; WW: wastewater

4.4 Comparison between long- and short-chain PFAS adsorption

In order to provide a deeper analysis on the long- and short-chain PFAS removal by adsorption, data from Table 2 and Table 3 have been elaborated to build a box-and-whiskers plot (Figure 1) that allows the comparison between the removals of long- and short-chain PFAS by different adsorbents (classified as activated carbon, resin, and synthetized materials). Figure 1 shows that the adsorption capacity of a wide range of adsorbents is lower for short-chain PFAS compared to that observed for long-chain PFAS. This result emphasizes that the removal of short-chain PFAS by adsorption is very challenging and it will need more research in the future. A comparison in adsorption capacity of the different adsorbents employed have shown that resins are more effective than activated carbons for both long- and short-chain PFAS removal. Activated carbon exhibited the lowest adsorption capacity. A significant variation in adsorption capacity of synthetized materials used for long-chain removal was observed. Such variation ranged from the lowest to the highest adsorption capacity observed for long-chain PFAS removal. However, the latter best results were often obtained at acid pH. For instance, the best adsorption capacity (5847 mg g^{-1}) was found by using the PAF-45 adsorbent at pH 3. Therefore, the real operating conditions may affect the removal efficiency. For instance, the effect OM may significantly influence the performance of adsorbents, as discussed in the next section.

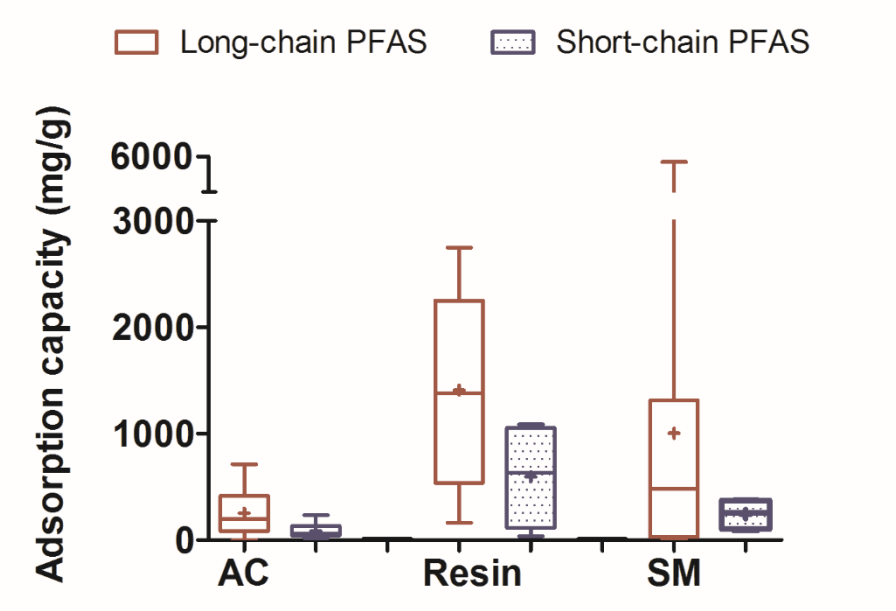

Figure 1 Box-and-whiskers plot concerning the adsorption capacity of long- and short-chain PFAS on different adsorbent materials (AC: activated carbon; Resin; SM: Synthetized materials).

5. Effect of organic matter (OM) on PFAS adsorption

5.1 PFAS adsorption in presence of OM

OM is ubiquitous in the aquatic environment and it can be distinguished between NOM, regarded as OM naturally present in surface water, and EfOM, the OM released from WWTPs [81].

OM could affect adsorption efficiency of adsorbent materials due to binding and adsorption interactions with PFAS, including long- and short-chain compounds. As illustrated by Du et al. [26], NOM could interact with PFAS via electrostatic and/or hydrophobic interactions. Firstly, OM is mostly constituted of anionic species and, after adsorbing on materials, it can lead to repulsive electrostatic interactions. Meanwhile, NOM can also lead to PFAS adsorption via hydrophobic interaction between perfluoroalkyl tail and NOM adsorbed on the adsorbent surfaces. To date, it is not well understood how these effects co-exist and which is predominant.

Most of undertaken experimental works investigated adsorption properties of PFAS on different adsorbent materials in DI [34,46,53,66]. Many researches have selected fulvic and humic acids (FA and HA) as the model DOM in order to evaluate the impact of DOM on PFAS adsorption [34,62,65,78,79,82]. Actually, NOM consists of a wide range of organic compounds, such as hydrophilic acids, proteins, carboxylic and amino acids in addition to the already mentioned HA and FA. When using a synthetic solution of OM during experimental studies, some interactions between PFAS and water matrix have not been described in detail. Table 4 reports the main experimental works published related to the adsorption of PFAS (both long- and short-chain compounds) on different adsorbent materials in the presence of OM. However, some of those studies lacked a detailed discussion on the effect of OM on PFAS adsorption.

Most of these experimental studies [25,55,65,82,83] have investigated the effect of OM on PFAS adsorption through comparison between synthetic OM solution and OM free solution (Table 4). Only few experimental works compared the effect of different DOM sources on PFAS adsorption and tested water had different dissolved organic carbon (DOC) concentrations [47,48,59,69,71] . Furthermore, the simultaneous effect of ionic strength and OM on the PFAS adsorption is very complex. For instance, it was demonstrated that the presence of monovalent and divalent cations increases PFAS adsorption on different materials, i.e. sediments [84], activated carbon [36], synthesized material (PAF-45) [67], resin [36] and kaolite [40]. Particularly, the adsorption of short-chain PFAS (i.e., PFHxA and PFBA) on kaolinite was more thermodynamically favorable at a higher Na^+ concentration due to the compression of the electrical double layer and ensuing reduced electrostatic repulsion between PFAS and kaolite surface [40]. In addition, divalent cations (such as Ca^{2+} and Mg^{2+}) could also improve PFAS removal by divalent cation-bridging effect [26,36]. On the contrary, the presence of inorganic anion negatively affects the adsorption of PFAS due to the competition for adsorption sites [32]. Whereas, it

was observed that the presence of ionic OM (i.e., HA, SDS, FA) compete with both long- [79,85] and short-chain PFAS [34,85]. Specifically, such effect seems more relevant for short-chain PFAS due to the competition for active sites [33,34,85]. On the other hand, hydrophobic DOM was found to improve the PFAS retention in GAC adsorption, while hydrophilic DOM seems do not affect significantly PFAS adsorption in both GAC and AE adsorption experiments [48]. The positive impact of DOM on the adsorption of long-chain PFAS has been ascribed to the formation of PFAS aggregate or DOM-PFAS complexes [33,48] but such bonds have been rarely demonstrated. Consequently, the impact of DOM and ionic strength on the PFAS adsorption need more investigation.

A systematic review concerning the effect of OM on PFAS adsorption for different classes of adsorbents is reported in the following sections.

5.2 Activated carbon

Among adsorbent materials, AC has proven to be effective for PFAS removal and its efficiency in presence of OM has been investigated both in batch and column experiments (Table 4). Contrasting trends have been observed in experimental studies because of the influence of co-existing OM. Indeed, the performance of PFAS adsorption onto AC was found negatively impacted, enhanced or not influenced by the presence of OM. The main interactions that could be established between OM molecules and PFAS (both long- and short-chain) during adsorption on GAC column are illustrated in Figure 2. In detail, hydrophobic interactions mainly concern long-chained C-F molecules, while short-chain PFAS interact with OM molecules through pore blockage and electrostatic repulsions.

In many cases, activated carbon performance was negatively influenced by co-existing OM and its efficiency decreased with the increase of DOC concentrations [35,36,48,55,62,63,77,83,85]. On the contrary, adsorption capacity on GAC did not significantly decrease in the presence of GW NOM probably due to the high concentration of PFAS tested (50 mg L^{-1}) and to the effect of ionic strength [85]. Results from the previously mentioned study demonstrated that PFBA removal was affected by OM since the results from adsorption equilibrium suggested a reduction of 40% [85]. Results from adsorption kinetic experiments provided by Yu et al. [35] suggested that adsorption equilibrium for PFOA and PFOS on PAC was reached at 4 h and 24 h in the absence and in the presence of EfOM, respectively [35]. The competition between PFAS and DOM for AC adsorption sites has also been investigated in RSSCTs [25,33,47,62,63]. Results obtained from the latter mentioned experimental works are in disagreement about the effect of OM. This discrepancy may be related to the different experimental setups, such as PFAS initial concentration, source and concentration of DOM, empty bed contact time (EBCT), and to the kind of AC tested. As suggested by Pramanik et al [62], when DOC concentration increased from 5 to 25 mg L^{-1} the removal efficiency of PFOA and PFOS on PAC decreased by 50% and 35%, respectively. On the contrary, the performance of bituminous coal-based GAC was less influenced

by variation of DOC concentration [62]. Similar results have asserted that proteins resulted in a low retention of PFOA and PFOS through hydrophobic and electrostatic interactions [63]. Moreover, breakthrough > 20% has been reached at 125,000 BVs during DOM-free experiments, and at ~ 11,000 BVs when DOC concentration was equal to 1.7 mg L^{-1}. This observation highlights that faster breakthrough of PFAS takes place during RSSCT experiments in presence of DOM [25]. Nevertheless, Sgroi et al. [47] found that breakthrough curves of some long-chain PFAS (i.e., PFOS, PFOA and PFDA) were similar in column beds packed tests by using Norit Darco 12x40. In those experiments, waters with different DOM concentrations and compositions fed the packed columns (Table 4). The observed behaviour for the investigated long-chain compounds may be ascribed to the hydrophobic interactions occurring between long-chain PFAS and GAC. Indeed, hydrophobic interactions are the main adsorption mechanisms for long-chain PFAS, and the hydrophobic interactions may be only slightly influenced by OM presence.

Results of pre-equilibrium study by Kothawala et al. [48] are in contrast with other findings [35,54,55,85], since the increase in DOC concentration seems to enhance long-chain PFAS removal due to the formation of DOM-PFAS complex and, consequently, their co-adsorption. In detail, removal efficiency of PFAS with a fluorocarbon-chain length of 8 C atoms increased by 50% when DOC concentration of a hydrophobic DOM passed from 0 to 8 mg L^{-1} using GAC [48]. It should be highlighted that these results were obtained in pre-equilibrium conditions (contact time about 15 min), at PFAS initial concentration of about 2.5 μg L^{-1} and at batch dose of GAC of about 10 g L^{-1}, which is much higher than doses typically used in full-scale treatment plants [86]. Performance of BdAC for PFCAs removal from PFSOF WWW has been investigated in the presence of high total organic carbon (TOC) concentration. Co-existing OM competed with PFCAs for adsorption sites on the BdAC [36]. The same achievement was obtained using R-CAC for PFOS and its alternative compound, F-53B, removal from electrochemical WWTP effluent [55]. The high concentration of TOC (78.3 mg L^{-1}) was linked to the high amount of hydrocarbon surfactants which were unfavourable for the adsorption of PFOS and F-53B on R-CAC, since adsorption sites were manly occupied by co-existing organic compounds (Table 4). Depending on OM concentration and source, dose and kind of AC employed (powdered or granular, and its porosity), and PFAS tested (long- or short-chain), the effect of OM is different, due to adsorption mechanisms established. The presence of OM can lead to the enhancement of PFAS adsorption through the formation of agglomerations between long-chain PFAS and OM. Otherwise, OM can negatively influence the adsorption efficiency, due to the reducing of accessible binding sites and pore spaces (i.e., pore blockage) (Figure 2).

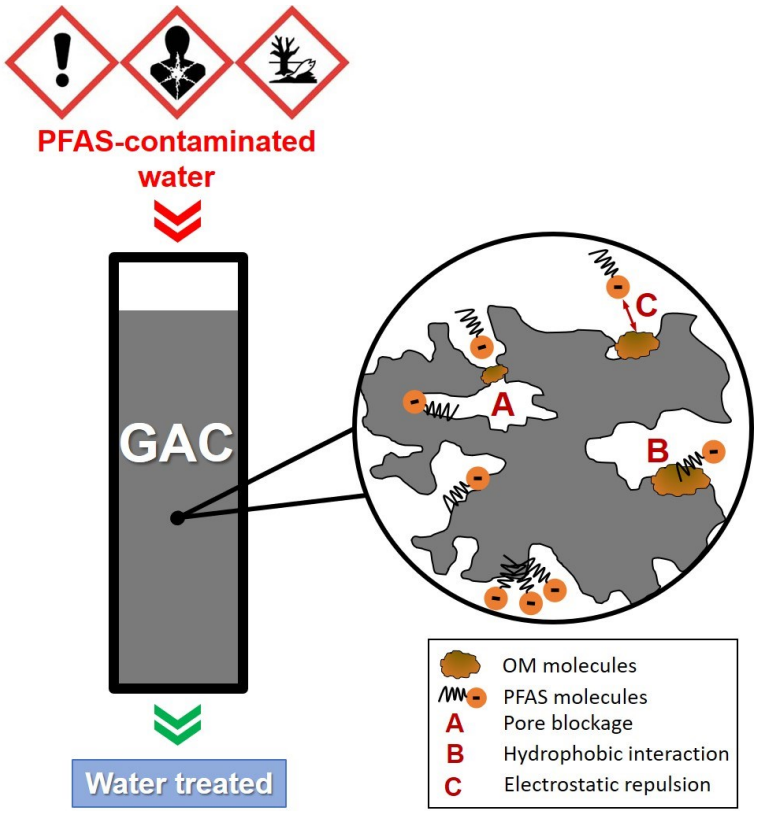

Figure 2 The main interactions established between OM and PFAS molecules during GAC adsorption. A: pore blockage; B: hydrophobic interaction; C: electrostatic repulsion.

5.3 Anion-exchange resin

Main interactions occurring between OM and PFAS molecules during AE process are reported in Figure 3. As previously asserted about the influence of OM on AC performance, the effect of co-existing OM on AE resins for PFAS removal depends on several factors, including OM composition and concentration, kind of resin and PFAS concentration tested.

To date, the competition between OM and PFAS on AE resins is not fully understood. This evidence is confirmed by several experimental studies carried out both on batch and column setups [27,33,34,36,48,54]. Organic compounds, such as HA, tri-chloroethylene (TCE), methylbenzene (MB) and sodium dodecyl sulphate (SDS), have been selected to evaluate their effect on PFHxS removal on AE resin (i.e., IRA910, a macroporous polystyrene resin with a dimethyl ethanol ammonium functional group) during batch experiments [34]. Results suggested that PFHxS retention on IRA910 was not affected by non-ionic co-existing organic compounds (i.e., MB and TCE), regardless of their concentration in the solution. Whereas, IRA910 efficiency decreased with the increasing of HA and SDS concentrations, due to the competition for adsorption sites. A slight effect on PFAS retention has been highlighted under pre-equilibrium condition since AE resin (A600, polystyrene-DVB gel-type with quaternary ammonium functional group) performance was independent from DOM concentration and source [48]. In detail, PFAS removal has been reduced by 10% at the highest DOM

concentration tested. This result is consistent with data reported by previous experimental works which have demonstrated that OM weakly interferes with PFAS removal during AE process [36,54]. Resins gel-type polymer matrixes, such as IRA400 and IRA67, showed a remarkable affinity with PFAS (both long- and short-chain), which was independent of OM present. In an opposed way, the performance of macroporous resins (i.e., IRA910) could be affected by background DOM levels.

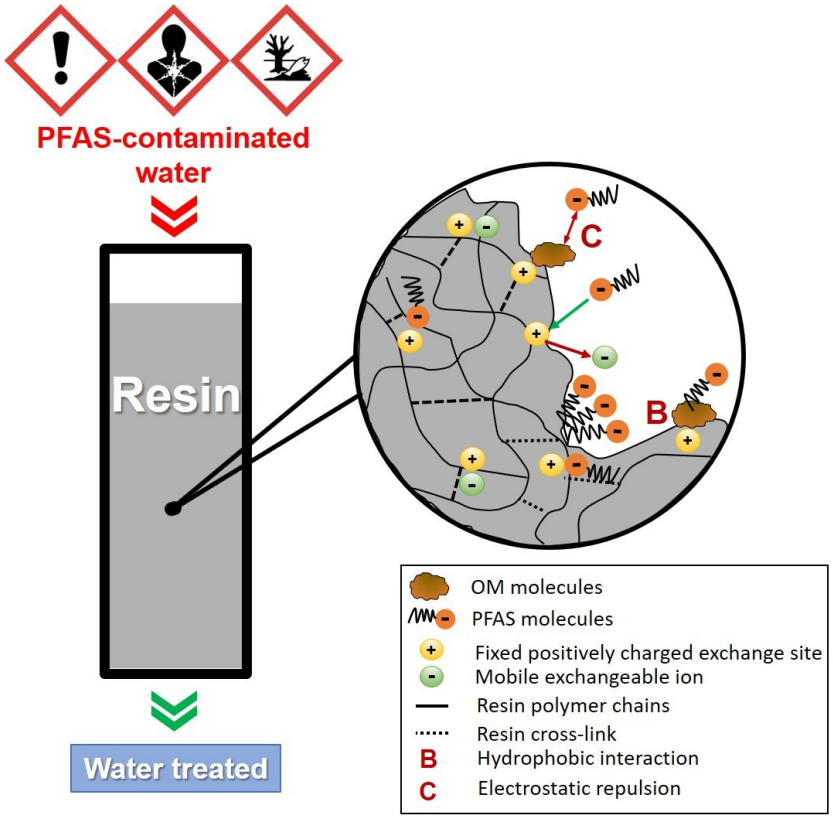

Figure 3 The main interactions established between OM and PFAS molecules during anion-exchange process. B: Hydrophobic interaction; C: Electrostatic repulsion.

5.4 Other adsorbents (biochar, multi-walled carbon nanotubes, mineral materials, nanoparticles)

Effect of co-existing HA on boehmite surface was investigated during PFOS and PFBS batch adsorption experiments [79]. Due to the electrostatic interactions between PFAS and boehmite, strong competition between PFOS (or PFBS) and HA occurred. Electrostatic repulsions increased with the increasing of HA accumulation on boehmite surface [79]. The competition between PFAS and synthetic OM (HA, phenol, 1-naphthol and benzoic acids) has also been investigated on MWCNTs [78]. The pronounced influence on PFOS removal was provided by HA, whereas phenol had a lesser influence. Moreover, PFBS removal was the worst in the presence of HA or phenol [78].

As demonstrated by Inyang and Dickenson (2017), HWC and PWC biochar performances were affected by OM, since adsorption capacities decreased with the increase of DOC concentration. In

particular, OM molecules could lead to pore blockage and may occupy high-energy pore sites. The adsorption capacities were about 41.3 and 27.7 mg g^{-1} when LW (DOC = 2 mg L^{-1}) and tertiary treated WW effluent (DOC = 4.9 mg L^{-1}) were tested, respectively [59]. Results from pilot-scale tests have demonstrated that the breakthrough of some PFAS (i.e., PFPeA, PFHxA, PFOA and PFOS) was faster on biochar HWC filter than on GAC column, since OM adsorbed on biochar surface caused changes on biochar surface charge. Consequently, the electrostatic repulsions between PFAS and biochar surface increased. Adsorption kinetic tests were performed for both PFBA and PFOS, and the observed slow kinetics could have been caused by pre-loaded OM on biochar [59].

The efficiency of novel magnetic adsorbent,2-MNPs@FG, has been investigated for PFOA and PFOS removal from different water matrixes [69]. Its performance was independent of OM content also at the highest DOC concentration tested (1.7 mg L^{-1}). Indeed, the removal efficiencies were always found around 99% for both PFOA and PFOS in all performed experiments. However, it should be noted that those efficiencies have probably been obtained because of a high dosage of adsorbent employed (400 mg L^{-1}). The competition between NOM (both SeaW and RW) and PFAS (both long- and short-chain compounds) has also been investigated during PFAS adsorption onto HDPE, PS and PS-COOH particles [74]. Results asserted that aromatic rings of PS contrasted NOM competition and, consequently, they favoured PFAS adsorption. By contrast, NOM influenced PFAS adsorption on HDPE and its effect was higher in SeaW than in RW [74]. Sun et al. [87] investigated the effect of co-existing organic compounds on GAC biofilter. They reported that more active sites were available for PFAS adsorption in the pre-ozonated regenerated GAC biofilter, due to the oxidation of competitive DOM [87].

Recently, the performance of new synthetized adsorbent (PEI-f-CMC) for PFAS removal (both long- and short-chain) was evaluated using three different NOM solutions [71]. Firstly, experiments were carried out in LW (Hartwell Lake, South Carolina) and PFAS removal efficiency has been compared with that resulted from DOC free solution. PFOA and PFOS removal efficiency was almost equal in both LW and DI. PFAS with longer chain than PFOA and PFOS (C_{12} – C_{13} PFCAs, C_9 – C_{10} PFSAs) were removed better from LW than from DI using PEI-f-CMC. This result can be explained by the co-removal of long-chain PFAS aggregated with OM [26,33]. By contrast, short-chain PFAS removal was higher in DI than in LW. Indeed, OM competed with short-chain PFAS during adsorption process [71]. Overall, lower removal efficiency has been obtained for short-chain PFAS compared with that observed for long-chain ones (removal <20% and >70%, respectively). The effect of different types of NOM (with different hydrophobicity) was also investigated in order to assert the performance of PEI-f-CMC for PFAS removal. The two NOM solutions tested had the same DOC concentration (2 mg L^{-1}) but a different value of specific ultra-violet absorbance at 254 nm ($SUVA_{254}$). Results have

demonstrated that short-chain removal was lower than 30% from both NOM solutions and the competition between short-chain PFAS and hydrophilic NOM ($SUVA_{254}$ = 1.7 L mg^{-1} m^{-1}) was higher than that with hydrophobic NOM ($SUVA_{254}$ = 4.9 L mg^{-1} m^{-1}). The hydrophobicity of NOM does not seem to influence the adsorption of long-chain PFAS on PEI-f-CMC and their removal efficiency was higher than 70% for both NOM solutions.

Table 4 Experimental studies (both batch and column test) of PFAS adsorption performed in the presence of organic matter.

Adsorbate		Adsorbent		Organic matter		Experimental setup	Remarks	References
Target PFAS	**Level**	**Type**	**Batch dose or EBCT**	**Source (Water matrix)**	**Concentration**			
PFOS **PFOA**	200 µg L^{-1} **Spiking** (Single solute)	**PAC**	10 mg L^{-1}	**EfOM** (WWTP effluent)	DOC =7.3 mg L^{-1}	Batch • PFOA or PFOS + EfOM • PFOA or PFOS + PAC loaded of EfOM	PFOA (or PFOS) needs much contact time to reach the equilibrium in the presence of EfOM, in particular onto EfOM-preloaded PAC; EfOM (especially low-molecular-weight compounds) impacts negatively adsorption rate and capacity.	[35]
PFBA **PFPeA** **PFHxA** **PFOA** **PFNA** **PFDA** **PFBS** **PFHxS** **PFOS**	1 µg L^{-1} of each PFAS **Spiking** (Mix)	**GAC** (F300, F600, 1240C)	0.38 min	**DOM (SW)** Clear Creek (Golden, CO)	DOC = 1.7 mg L^{-1}	Column RSSCT experiment	The presence of DOM leads to faster breakthrough of PFAS, in particular shortest chain compounds. Breakthrough of >20% for all PFAS tested has been reached at 11,000 BVs and 125,000 BVs, respectively in the presence and absence of DOM. F300 is less effective with PFBA and PFPeA.	[25]
PFOS **PFOA** **PFBS** **PFHxS**	250.06 µg L^{-1} 207.03 µg L^{-1} 150.04 µg L^{-1} 200.05 µg L^{-1} **Spiking** (Single solute)	**MWCNTs** (MWCNTs-Pri MWCNTs-COOH MWCNTs-OH)	20 mg L^{-1}	**Synthetic OM** (HA, 1-naphthol, phenol, benzoic acid) (Sinopharm Chemical Regent) **in DI**	Range of tested concentration of HA, 1-naphtol, phenol and benzoic acid 0 - 2.5 mg L^{-1}	Batch • PFOS + HA (or 1-naphthol, phenol, benzoic acid) • PFBS (or PFHxS, PFOA) + HA or Phenol	Competition between PFAS and organic compounds on the adsorption sites of the MWCNTs; Effect of co-existing organic compounds on PFOS removal: HA > 1-naphtol > benzoic acid > phenol; % removal in the presence of HA or phenol: PFOS > PFOA > PFHxS > PFBS.	[78]
PFOS **F-53B**	44.1 µg L^{-1} 102.9 µg L^{-1} **Real** (Mix)	**R-CAC**	100 mg L^{-1}	**EfOM** (EWTP effluent)	TOC = 78.3 mg L^{-1}	Batch adsorption experiments of actual WW and synthetic PFAS solution (OM free)	EWTP effluent contains high amount of hydrocarbon surfactants (high concentration of TOC) which are in competition with PFOS and F-53B for active sites on R-CAC; F-53B is better adsorbed on R-CAC than PFOS due to its more hydrophobic chain and its higher concentration in the actual wastewater.	[55]
PFOS **PFOA**	280 ng L^{-1} 550 ng L^{-1} (read from graph)	**PAC** (BET 880 $m^2 g^{-1}$) **GAC** (BET 800 $m^2 g^{-1}$)	10 min	**Synthetic HA and FA** (Sigma-Aldrich) **in DW**	Range of tested concentration of HA and FA 5 – 25 mg L^{-1}	Column	PAC and GAC efficiencies decrease with the increasing of DOC concentration.	[62]

Table 4 Experimental studies (both batch and column test) of PFAS adsorption performed in the presence of organic matter (continued).

Adsorbate		Adsorbent		Organic matter		Experimental setup	Remarks	References
Target PFAS	**Level**	**Type**	**Batch dose or EBCT**	**Source (Water matrix)**	**Concentration**			
C_4 – C_{12}, C_{14} PFCAs (PFBA,PFPeA, PFHxA, PFHpA, PFOA, PFNA, PFDA, PFUnDA, PFDoDA, PFTeDA) **C_4, C_6, C_8 PFSAs** (PFBS, PFHxS, PFOS) **FOSA**	0.1 µg L^{-1} **Spiking** (Mix)	**GAC** (F400)	6.1 min	**DOM (DW)**	DOC = 1.8 mg L^{-1}	Column RSSCT experiment	DOC removal is not linked to PFAS removal from AE or GAC column. DOC loading seems to favour the agglomeration of PFAS on the adsorbent surface.	[33]
		AE resin (A-600, Polystyrene-DVB gel-type Quaternary ammonium)	4.9 min					
PFBS **PFHxS** **PFOS** **PFHxA** **PFHpA** **PFOA** **PFNA** **PFDA**	0.073 ± 0.01 µg L^{-1} 0.47 ± 0.08 µg L^{-1} 1.4 ± 0.2 µg L^{-1} 0.28 ± 0.04 µg L^{-1} 0.32 ± 0.04 µg L^{-1} 1.4 ± 0.13 µg L^{-1} 0.067 ± 0.005 µg L^{-1} 0.04 ± 0.02 µg L^{-1} **Real** (Mix)	**GAC** (coal-based, Silcarbon)	125 mg L^{-1}	**DOM (GW)** (well at 9.5 m depth, downstream a water-resistant clothing manufacture)	DOC = 5.27 ± 0.12 ng L^{-1}	Batch adsorption isotherm for each adsorbent have been measured for the undiluted PFAS contaminated GW	Effect of OM has not been highlighted.	[77]
		PAC (anthracite coal, Silcarbon TH90 extra)	25 mg L^{-1}					
C_4 – C_{12} PFCAs (PFBA, PFPeA, PFHxA, PFHpA, PFOA, PFNA, PFDA, PFUnDA, PFDoDA) **C_4, C_6, C_8 PFSAs** (PFBS, PFHxS, PFOS) **FOSA**	2.5 µg L^{-1} of each PFAS **Spiking** (Mix)	**AE resin** (A600, Polystyrene-DVB gel-type Quaternary ammonium)	10 g L^{-1}	**DOM (LW)** •Görväln (autochtonous DOM, hydrophobic) • Bolmen (terrestrial, algal and bacterial-derived DOM, hydrophilic)	•DOC = 8.3 mg L^{-1} •DOC = 10 mg L^{-1}	Batch Pre-equilibration condition (contact time about 15 min) 4 discrete DOM levels (8, 4, 2, 0 mg DOC L^{-1}) for the two lake waters + PFAS mix	Effect of DOM is weak during PFAS removal by AE, in fact at the highest DOM concentration PFAS percentual removal has been reduced by 10% in comparison with DOC free solution;	[48]
		GAC (Filtrasorb 400, Calgon)					GAC performance is affected by DOC source and concentration. Most hydrophobic long chain PFAS are better removed at highest DOC concentration, in detail the increase of hydrophobic DOM (Görväln) concentration enhances progressively PFAS removal. Whereas, only the absence or presence of hydrophilic DOM (Bolmen) seems to influence PFAS adsorption.	

Table 4 Experimental studies (both batch and column test) of PFAS adsorption performed in the presence of organic matter (continued).

Adsorbate		Adsorbent		Organic matter		Experimental setup	Remarks	References
Target PFAS	**Level**	**Type**	**Batch dose or EBCT**	**Source (Water matrix)**	**Concentration**			
PFOS **PFOA** **PFDA**	0.153 µg L^{-1} 0.138 µg L^{-1} 0.282 µg L^{-1} **Spiking** (Mix)	**GAC** (Norit Darco 12x40)	5.2 min	**Synthetic NOM** (Suwanne river, International Humic Substances Society) **in DI**	DOC = 4.3 mg L^{-1}	Column RSSCT experiment	Similar breakthrough curves of PFAS tested have been obtained despite different DOM composition and concentration. DOM seems not influenced the amount of long-chained PFAS adsorbed since hydrophobic interaction represents the main adsorption mechanism.	[47]
	0.153 µg L^{-1} 0.269 µg L^{-1} 0.238 µg L^{-1} **Spiking** (Mix)			**NOM** (SW)	DOC = 5.4 mg L^{-1}			
	0.556 µg L^{-1} 0.174 µg L^{-1} **Real** (Mix)			**EfOM** (WWTP effluent secondary)	DOC = 7 mg L^{-1}			
PFHxS	200 mg L^{-1} **Spiking**	**AE resin** (IRA910, Polystyrene-DVB macroporous-type Dimethyl ethanol ammonium)	0.1 g L^{-1}	**Synthetic TCE, MB, SDS** (Sinopharm Chemical Reagent) **in DI**	Range of tested concentration of TCE, MB, SDS 0 – 5 mmol L^{-1}	Batch adsorption experiments are carried out by dissolving PFHxS with different organic compounds at varying concentration	Non-ionic co-existing organic compounds (i.e. MB and TCE) do not impacted PFHxS removal, regardless their concentration. Due to the affinity of AE with anionic species, IRA910 performance decreases with the increase of HA and SDS concentrations. In detail, HA and SDS occupies adsorption sites on IRA910 and the latest could form aggregates in competition with PFHxS.	[34]
				Synthetic HA (Sinopharm Chemical Reagent) **in DI**	Range of tested concentration of HA 0 – 200 mg L^{-1}			
PFOA	100 mg L^{-1}	**ACF**	800 mg L^{-1}	**Synthetic FA** (Sinopharm Chemical Regent) **in DI**	Range of tested concentration of FA 0 – 500 mg L^{-1}	Batch adsorption experiments at varying FA concentrations are compared with blank experiments (FA free solution)	FA concentration of 100 mg L^{-1} causes a decrease of PFOA adsorbed (about 75.4% lower than that of FA free solution).	[83]
PFHxA **PFHpA** **PFOA**	31.4 mg L^{-1} 40.04 mg L^{-1} 120.08 mg L^{-1} **Real** (Mix)	**BdAC**	0.2 g L^{-1}	**DOM** (PFOSF WWW)	TOC = 63.2 mg L^{-1}	Batch adsorption experiments of simulated (DI+PFAS) and actual WW	Co-existing organic matter in actual WW has no effect on PFCAs adsorption on IRA67, whereas their presence influences negatively BdAC efficiency.	[36]
		AE resin (IRA67, Polyacrylic-DVB gel-type Polyamine)	0.1 g L^{-1}					

Table 4 Experimental studies (both batch and column test) of PFAS adsorption performed in the presence of organic matter (continued).

Adsorbate		Adsorbent		Organic matter		Experimental setup	Remarks	References
Target PFAS	**Level**	**Type**	**Batch dose or EBCT**	**Source (Water matrix)**	**Concentration**			
PFOA	1 µg L^{-1} **Spiking**	**DFB-CDP**	10 mg L^{-1}	**Synthetic HA** (n.a.) **in DI**	20 mg L^{-1}	Batch kinetic experiments are performed by adding HA to the adsorbent suspension together with PFOA solution. Comparison between PFOA removal by DFB-CDP in the presence or absence of HA	DFB-CDP adsorption efficiency is unaffected by HA.	[65]
PFOS PFBS	50 – 1000 µg L^{-1} **Spiking** (Single compound)	**Boehmite**	5 g L^{-1}	**Synthetic HA** in DI Fluka Co. (Buchs, Switzerland)	Range of tested concentration of HA 2 – 50 mg L^{-1}	Batch adsorption experiments performed for 72 h for achieving the equilibrium	With the increasing of HA adsorbed, boehmite surface becomes negative and electrostatic repulsions cause the reduction in PFOS and PFBS sorption.	[79]
PFOA PFOS	340 ng L^{-1} 520 ng L^{-1} **Real** (Mix)	**GAC** (BET = 800 m^2 g^{-1})	20 min	**Commercial organics**: BSA, sodium alginate and HA (Sigma-Aldrich) **in LW**	DOC= 7.88 ± 0.07 mg L^{-1} Protein = 11.54 ± 0.22 mg L^{-1} Carbohydrate = 8.92 ± 0.28 mg L^{-1}	Column	Removal efficiency is the highest at the lower DOC concentration, due to the competition for adsorption sites. Protein has the greater influence on PFOA and PFOS adsorption behaviour by means of hydrophobic and electrostatic interactions.	[63]
PFOA PFOS	103.5 – 4140.7 µg L^{-1} 125 – 5001.2 µgl L^{-1} **Spiking** (Single compound)	**F-MT**	10 mg L^{-1}	**Synthetic HA** (n.a.) **in DI**	Tested concentration of HA 1 and 10 mg L^{-1}	Batch comparison of PFOA and PFOS adsorbed amounts in absence or in presence of HA	Due to nanoscale interlayers and high hydrophobicity of F-MT, HA macromolecular with hydrophilic groups could not be adsorbed. Consequently, co-existing HA weakly interferes with PFOS and PFOA adsorption (little decrease of PFOS and PFOA adsorption appeared in the presence of 10 mg L^{-1} HA).	[82]
PFOS PFOA PFBA PFBS	50 mg L^{-1} **Spiking** (Mix)	**GAC** (Filtrasorb 600, Calgon)	400 mg L^{-1}	**DOM** (Landfill GW)	Range of tested concentration of TOC 5-20 mg L^{-1}	Batch adsorption isotherm experiments are conducted on both DI and landfill GW	Organic compounds in groundwater can competitive with PFAS for GAC adsorption sites as it is demonstrated by the great equilibrium and fast kinetic adsorption in DI instead of in the landfill groundwater.	[85]

Table 4 Experimental studies (both batch and column test) of PFAS adsorption performed in the presence of organic matter (continued).

Adsorbate		Adsorbent		Organic matter		Experimental setup	Remarks	References
Target PFAS	**Level**	**Type**	**Batch dose or EBCT**	**Source (Water matrix)**	**Concentration**			
C_4 – C_{14}, C_{16}, C_{18} PFCAs (PFBA, PFPeA PFHxA, PFHpA, PFOA, PFNA, PFDA, PFUnDA, PFDoDA, PFTrDA PFTeDA, PFHxDA, PFODA) **C_4, C_6, C_8, C_{10} PFSAs** (PFBS, PFHxS PFOS, PFDS) **FOSA**	10 µg L^{-1} of each PFAS (∑PFAS=180 µg L^{-1}) **Spiking** (Mix)	**HDPE**	5 mg L^{-1}	**NOM** SeaW (Alfacs Bay) RW (Ebro River)	TOC = 7.735 mg L^{-1} TOC = 4.386 mg L^{-1}	Batch Contact time 0, 4, 7, 50 days	PFAS adsorption on HDPE is influenced by the presence of NOM and this effect is more evidence in seawater where NOM concentration is higher than in river water. Percentages of adsorption on HDPE are below 30% and carboxylic acids are adsorbed better than PFSAs (PFOS and PFDS no adsorption).	[74]
		PS	2 mg L^{-1}				Higher adsorption velocity despite HDPE. Aromatic rings of PS monomer favour PFAS adsorption on PS and they go against organic matter competition.	
		PS-COOH	2 mg L^{-1}				PFAS adsorption on PS-COOH is similar to that on PS, but adsorption rate is lower. C_{11} and C_{18} are the most adsorbed compounds. Effect of NOM not assessed.	
PFOA PFOS	180 µg L^{-1} of each compound **Spiking** (Mix)	**MNPs@FG** (1-MNPs@FG, 2-MNPs@FG, 3-MNPs@FG)	400 mg L^{-1}	**Synthetic NOM** (International Humic Substance Society) **in DI**	DOC = 2 mg L^{-1}	Batch adsorption experiments in orbital shaker at room temperature	The performance of MNPs@FG tested is slightly influenced by the presence of synthetic NOM.	[69]
	5 µg L^{-1} of each compound **Spiking** (Mix)	**MNPs@FG** (2-MNPs@FG)	400 mg L^{-1}	**NOM** (LW, RW, DW)	DOC = 1.7 mg L^{-1} DOC = 0.6 mg L^{-1} DOC < 0.1 mg L^{-1}	Batch, investigation of PFOA and PFOS removal from environmental water	After 11 minutes, 2-MNPs@FG exhibits high removal efficiencies (about 99.2 %) for both PFOA and PFOS in all water matrixes tested. The residual concentration of PFOA and PFOS are 11 and 28 ng L^{-1}, 16 and 22 ng L^{-1}, 31 and 18 ng L^{-1}, in lake, river and drinking waters, respectively. Residual combined concentration of PFOA and PFOS (49 ng L^{-1}) in DW is lower than health advisory level of 70 ng L^{-1} (US EPA, 2016)	

Table 4 Experimental studies (both batch and column test) of PFAS adsorption performed in the presence of organic matter (continued).

Adsorbate		Adsorbent		Organic matter		Experimental setup	Remarks	References
Target PFAS	**Level**	**Type**	**Batch dose or EBCT**	**Source (Water matrix)**	**Concentration**			
C_4 – C_8 PFCAs (PFBA, PFPeA PFHxA, PFHpA, PFOA) **C_4 - C_8 PFSAs** (PFBS, PFHxS, PFHpS, PFOS)	3.7 ± 0.9 µg L^{-1} 5.2 ± 0.4 µg L^{-1} 7.6 ± 0.5 µg L^{-1} 1.5 ± 0.1 µg L^{-1} 10.7 ± 0.9 µg L^{-1} 1.8 ± 0.0 µg L^{-1} 21.0 ± 0.3 µg L^{-1} 1.7 ± 0.1 µg L^{-1} 33.1 ± 0.6 µg L^{-1} **Real** (Mix)	**GAC** (Filtrasorb 300, Calgon)	100 mg L^{-1}	**DOM** (AFFF-impacted GW)	DOC = 46.0 ± 0.9 mg L^{-1}	Batch adsorption experiments with unfiltered AFFF-impacted GW for 5 days (no equilibrium reached)	Effect of OM has not been highlighted.	[60]
		Biochar (Mountain Crest Gardens, MCG, pine needle-derived biochar)						
PFOA PFOS	82.8 mg L^{-1} 129.12 mg L^{-1} **Spiking** (Single compound)	**CTF**	250 mg L^{-1}	**Synthetic HA** (soil-extracted) **in DI**	Range of tested concentration of HA 10 – 40 mg L^{-1}	Batch single-point adsorption data (equilibrium pH equal to 6) of each chemical testing the different adsorbent materials	HA do not strongly interfere with CTF adsorption since HA molecules are unable to enter in the internal pores of CTF due to size-exclusion mechanism.	[54]
		AE resin (IRA-400, Amberlite Sinopharm Chemical Regent Co., China)	375 mg L^{-1}				HA present slightly increases PFOA and PFOS adsorbed rates, maybe due to a weak expansion of the polymer matrix and consequently an increase of PFOA and PFOS access to more adsorption sites.	
		Microporous AC (Calgon Carbon Co., USA)	250 mg L^{-1}				Direct competition for adsorption sites on AC and SWNT between dissolved HA and PFOA or PFOS. At the highest concentration of HA (40 mg L^{-1}), the reduction of PFOA and PFOS adsorption rates are 31-48 % and 95% for both AC and SWNT, respectively.	
		SWNT (Nanotech Port Co., China)	250 mg L^{-1}					

Table 4 Experimental studies (both batch and column test) of PFAS adsorption performed in the presence of organic matter (continued).

Adsorbate		Adsorbent		Organic matter		Experimental setup	Remarks	References
Target PFAS	**Level**	**Type**	**Batch dose or EBCT**	**Source (Water matrix)**	**Concentration**			
C_4 – C_{14} PFCAs (PFBA, PFPeA PFHxA, PFHpA, PFOA, PFNA, PFDA, PFUnDA, PFDoDA) **C_4, C_6, C_8 PFSAs** (PFBS, PFHxS PFOS)	212 ng L^{-1} 133 ng L^{-1} 109 ng L^{-1} 24 ng L^{-1} 430 ng L^{-1} <1 ng L^{-1} 1 ng L^{-1} <1 ng L^{-1} <1 ng L^{-1} 171 ng L^{-1} 13 ng L^{-1} 27 ng L^{-1} **Real** (Mix)	**AE resin** (A600E Polystyrene-DVB gel-type Trimethyl quaternary amine A520E Polystyrene-DVB macroporous-type Trimethyl quaternary amine A532E Polystyrene-DVB gel-type Bifunctional quaternary amine)	10.1 min	**DOM** (GW)	n.a.	Column Pilot-scale	Effect of OM has not been assessed.	[27]
		GAC C (mesh: 8x30, iodine number 900 mg g^{-1}) J (mesh: 12x40, iodine number 1100 mg g^{-1}) S (mesh: 12x40, iodine number 1000 mg g^{-1})	10 – 11 min			Column Full-scale		
PFBA PFOA	1 µg L^{-1} **Spiking** (Single compound)	**Biochar** (HWC, PWC)	50 mg in 150 mL 333 mg L^{-1} 1:3 mg mL^{-1} (biochar:PFAA volume ratio)	**EfOM** (Tertiary treated WW effluent)	DOC = 4.9 mg L^{-1}	Batch adsorption kinetic tests, samples are continuously mixed over 30 days on an orbital shaker	Slow kinetics for PFBA and PFOA adsorption may be attributed to pre-loaded EfOM on the biochar surface. At the equilibrium, the amount of PFOA adsorbed is 3-4 times higher than the amount of PFBA sorbed on both HWC and PWC.	[59]
PFOA	0.01 – 100000 µg L^{-1} **Spiking**	**Biochar** (HWC, PWC)	1:3 mg mL^{-1} (biochar:PFAA volume ratio)	**EfOM** (Tertiary treated WW effluent) **NOM** (LW, Lake Mead in Southern Nevada)	DOC = 4.9 mg L^{-1} DOC = 2.0 mg L^{-1}	Batch adsorption isotherm tests using two test waters for evaluating the impact of source water on the adsorption of PFOA on different type of biochar	Effect of OM on PFOA adsorption is more intense in WW in which the higher DOC concentration has been measured. OM molecules occupy high-energy pore sites and consequently they lead to pore blockage during PFOA adsorption. OM adsorbed leads also to a change in surface charge with the increasing of repulsion forces between anionic PFOA molecules and biochar surfaces. PFOA adsorbed in WW is 25% less than that in LW.	

Table 4 Experimental studies (both batch and column test) of PFAS adsorption performed in the presence of organic matter (continued).

Adsorbate		Adsorbent		Organic matter		Experimental setup	Remarks	References
Target PFAS	**Level**	**Type**	**Batch dose or EBCT**	**Source (Water matrix)**	**Concentration**			
PFPeA **PFHxA** **PFOA** **PFOS**	17.6 ± 2.4 ng L^{-1} 9.5 ± 1.4 ng L^{-1} 7.3 ± 0.8 ng L^{-1} 4.1 ± 5.6 ng L^{-1} **Real** (Mix)	**GAC** (Norit 830) **Anthracite** (Leopold) **Biochar** (HWC)	8 min	**EfOM** (Tertiary treated WW effluent)	DOC = 4.9 mg L^{-1}	Column Pilot-scale	Faster breakthrough for PFAS tested is observed in anthracite and biochar filters than GAC. The latter shows the best PFAS removal efficiency in comparison with anthracite and HWC. Effect of OM has not been highlighted.	[59]
PFBS **PFHpA** **PFNA** **PFOA**	32 ng L^{-1} 27 ng L^{-1} 7 ng L^{-1} 26 ng L^{-1}	**Biofilter** (O_3 + GAC)	23 min	**DOM** (water reclamation plant)	DOC = 4.17 mg L^{-1}	Column Pilot-scale	In the pre-ozonated regenerated GAC biofilter more active sites are accessible for PFAS, due to the oxidation of competitive organic compounds. However, short-chain PFAS adsorption amount is lower than long-chain ones.	[87]
C_4 – C_{13} PFCAs (PFBA, PFPeA PFHxA, PFHpA, PFOA, PFNA, PFDA, PFDoDA, PFTrDA) **C_4 – C_{10} PFSAs** (PFBS, PFPeS, PFHxS, PFHpS, PFOS, PFNS, PFDS)	1 µg L^{-1} of each compound **Spiking** (Mix)	**PEI-f-CMC**	25 mg L^{-1}	**DOM** (LW)	DOC = 2 mg L^{-1} $SUVA_{254}$ = 2.0 L mg^{-1} m^{-1}	Batch	The longest PFAS (PFDoDA, PFTrDA, PFNS, PFDS) are better removed in lake water than in DI (removal efficiency is ~100% and ~85%, respectively). Whereas, the removal efficiency of short PFCAs is higher in DI (<20%). Removal efficiency of others PFAS is almost equal in both LW and DI.	[71]
				Isolated NOM (hydrophobic type)	DOC = 2.5 mg L^{-1} $SUVA_{254}$ = 4.9 L mg^{-1} m^{-1}		The removal efficiency of short-chain PFAS is higher at the highest $SUVA_{254}$ (hydrophobic NOM). However, short-chain PFAS removal efficiency is lower than 30%. The difference in NOM composition (different $SUVA_{254}$) does not influence the adsorption of longer PFAS, whose removal efficiency is higher than 70%.	
				Isolated NOM (hydrophilic type)	DOC = 2.5 mg L^{-1} $SUVA_{254}$ = 1.7 L mg^{-1} m^{-1}			

EBCT: Empty bed contact time; PAC: powdered activated carbon; EfOM: effluent organic matter; DOC: dissolved organic carbon; GAC: granular activated carbon; DOM: dissolved organic matter; SW: Surface water; RSSCT: rapid small-scale column tests; MWCNTs: multi-walled carbon nanotubes; HA: humic acids; R-CAC: reactivated coconut shell based GAC; EWTP: electroplating wastewater treatment plant; TOC: total organic carbon; DW: drinking water; FA: fulvic acids; AE: anion-exchange; GW: groundwater; LW: lake water; NOM: natural organic matter; DI: deionized water; WWTP: wastewater treatment plant; TCE: tri- chloroethylene; MB: methylbenzene; SDS: sodium dodecyl sulphate; ACF: activated carbon fiber; BdAC: bamboo-derived AC; PFSOF WWW: perfluorooctanesulfonyl fluoride washing wastewater; DFB-CDP : cross-linked polymer network where β-CD substitutes decafluorobiphenyl; BSA: bovine serum albumin; F-MT: Fluorinated montmorillonite; HDPE: high-density polyethylene; PS: polystyrene; PS-COOH: poly-styrene carboxylic acid; RW: river water; SeaW: seawater; MNPs@FG: magnetic nano-particles attached into fluorographene; AFFF: Aqueous film-forming foam; CTF: Covalent triazine-based framework; SWNT: single-walled carbon nanotubes; HWC: hardwood biochar; PWC: pinewood biochar; PEI-f-CMC: poly(ethylenimine)-functionalized cellulose microcrystals; $SUVA_{254}$: specific ultra-violet absorbance at 254 nm.

6. Regeneration of adsorbents

Despite the widespread use of adsorption and anion-exchange processes for PFAS removal, the main drawback of their application at full-scale is the regeneration of spent materials when their adsorption capacity has been exhausted. Regeneration must allow the removal of adsorbed PFAS in order to restore the adsorption capacity of spent materials by means of technologies, which have economic viability and environmental security.

For instance, chemical regeneration of saturated adsorbents is usually performed in situ at full scale treatment processes. However, it is not always feasible because of the related costs or environmental issues, as discussed in the next section. On the other hand, the thermal regeneration is often performed off-site at the adsorbent manufacturing establishment. Therefore, a direct comparison between the above-mentioned techniques is not easy. Overall, in-situ regeneration should be pursued to avoid the transportation, treatment and/or disposal of exhausted materials.

To date, regeneration and reuse of materials saturated with PFAS is challenging, as discussed in the following sections.

6.1 Chemical regeneration

PFAS anionic head could be desorbed using a solution of sodium salts (such as sodium chloride, NaCl, and sodium hydroxide, NaOH), whereas a solution of organic alcohol is required to desorb the hydrophobic C-F chain [49,88]. Figure 4 depicts a schematic view of PFAS-saturated adsorbent which is regenerated using a chemical solution made of sodium salts and organic alcohol. In Figure 4 the desorption mechanisms related to the use of sodium ions and organic solvents are illustrated as well.

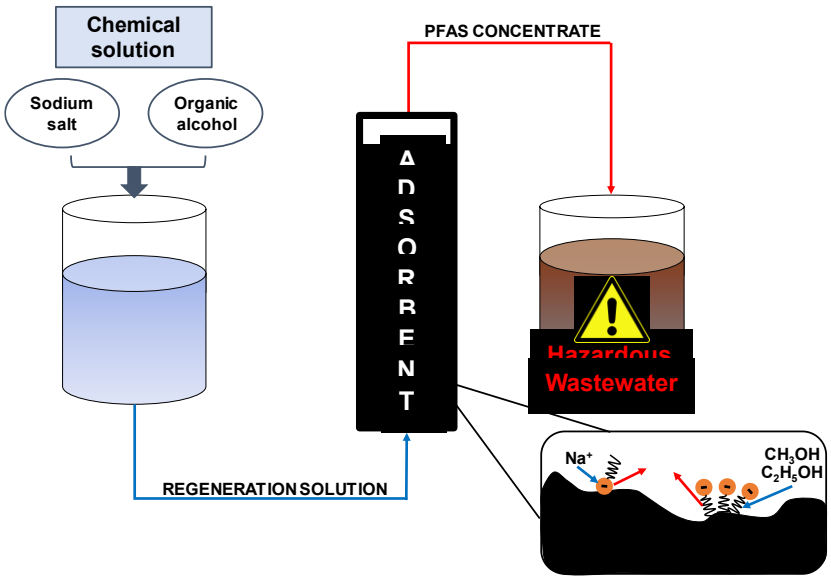

Figure 4 Chemical regeneration of PFAS-exhausted adsorbents using a solution of sodium salt and organic alcohol.

Table 5 reports a compilation of data on chemical regeneration of PFAS-exhausted adsorbents with particular attention to chemical solution employed and regeneration percentage achieved. Due to the lower solubility of PFAS on ionic strength media, conventional solutions of sodium salts were ineffective in regenerating adsorbents exhausted by both long- and short-chain PFAS [89,90]. Regeneration percentages were lower than 10% when regeneration agents, including NaCl and NaOH, were adopted for desorbing PFBS and PFOS from acrylic resins [32,41]. The deprotonation of amine groups on acrylic gel-type resins allowed the desorption of PFOS at a low concentration of NaOH solutions, although a regeneration percentage of about 90% was achieved when a solution of sodium hydroxide and methanol was tested (Table 5).

Mixture of sodium salts and organic solvents (such as CH_3OH, C_2H_5OH and C_3H_6O) have been widely used in order to involve the desorption of PFAS [27,38,90]. Moreover, the efficiency of regenerating solution depends on resin properties and, in particular, on the interactions established between PFAS and resin functional groups [32]. In fact, data from regeneration experiments carried out using different mixtures of inorganic salts with or without organic alcohol demonstrated that the amount of PFAS desorbed from three different types of strong AE resins depends on resin hydrophobicity and, consequently, on the interactions between PFAS and the alkyl chains of the functional exchange group [27]. Solution of ammonium salts (such as NH_4OH and NH_4Cl) showed a good efficiency for the desorption of PFBA, PFBS, PFOA and PFOS from AE resins with trimethyl quaternary amine functional group (i.e., Purolite A600E and A520E). Whereas, the same regenerating solution was totally ineffective in reactivating highly hydrophobic resin (i.e., Purolite A532E), since the solvatation of fluorine chain was needed in order to remove PFAS molecules from the active sites of the resin (Table 5). In that case, the organic solvent could slacken the hydrophobic interactions between PFAS and resin, then the inorganic anions of ammonium salts (OH^- or Cl^-) could replace PFAS (Figure 4), achieving the recovery of the exchange capacity of the resin.

The effect of different temperatures of DI water as regenerating solution on PFOS desorption from BdAC was also investigated [90]. Results from regeneration experiments demonstrated that a higher temperature of DI water (about 80 °C) enhanced the PFOS desorption and the regeneration percentage was about 53% (Table 5). Furthermore, PFOS desorption from PACFs was about 5% when DI water was employed as regenerating solution [43]. By contrast, the regeneration percentage increased with the increase of ethanol concentration in the regeneration solution [43,88,91].

Nevertheless, regenerating solution made of organic solvent is not suitable for the treatment of drinking water on full-scale applications, and consequently on-site regeneration is not feasible. It is noteworthy that the effect of OM co-adsorbed on materials may affect regeneration efficiency. After five successive adsorption-regeneration cycles, the efficiency of BdAC for PFCAs removal (PFHxA,

PFHpA and PFOA) decreased, while AE resin (IRA67) performance was relatively stable [36]. Co-adsorbed organic pollutants on surface or pores of AC could interfere with the regeneration process. It was the case of the R-CAC, which was regenerated through different regenerating solutions (made of 70% ethanol, 90% methanol or 90% acetone). After the regeneration, R-CAC was reused for PFOS and F-53B removal from industrial wastewater [55]. Due to the presence of non-desorbed OM, the adsorption efficiency of regenerated R-CAC decreased after each regeneration cycle. For this reason, persulfate oxidation was tested as alternative regeneration process to the conventional elution with organic solvents. Regeneration results demonstrated that sulphate free radicals were able to diffuse into pores of activated carbon and they allowed the degradation of both PFAS and other organic compounds. However, sulphate free radicals could cause the release of fluorine and short-chained PFAS due to break-down of long-chained PFAS [55]. Consequently, further investigations should be addressed in order to better understand the effect of sulphate and other free radicals on degradation of PFOS. Overall, the need of organic solvents for the chemical regeneration of PFAS saturated adsorbents is a relevant limitation of this technique.

6.2 Thermal regeneration

Thermal regeneration in N_2 gas stream of GAC saturated with long-chain PFAS (PFOS, PFHxS and PFOA) has been investigated in order to evaluate the release of volatile organic fluorine (VOF) or other compounds such as short-chain compounds [92]. Thermal regeneration may be optimized when GAC is maintained at 700 °C and later off-gases will be kept at 1000 °C. Nevertheless, the high temperature needed for thermally regenerating AC may cause the decreasing of their adsorption properties and a change in AC morphology [93]. These described aspect of thermal regeneration of activated carbon deserve a deep investigation. Calcination at 600 °C in air for 20 min has been investigated for the reusability of h-BNs saturated with PFDA and PFOS [68]. A temperature of 600 °C was selected in order to reach the complete decomposition of the investigated PFAS compounds, since PFOS and PFDA are decomposed at about 480 °C and 200 °C, respectively, as inferred from differential scanning calorimetry curves [68]. Moreover, calcium hydroxide ($Ca(OH)_2$) was employed as additive to avoid the formation of short-chain fluorinated gases during calcination process. Results about regeneration experiments of h-BNs via calcining demonstrated that adsorption capacity was maintained approximately constant during different adsorption-regeneration cycles (the amount of PFOS or PFDA on the surface of h-BNs at equilibrium ranged about 0.35 – 0.45 mg m^{-2}) [68].

Recently, microwave (MW) irradiation became an alternative process to conventional thermal regeneration due to its advantages, such as rapidity and selectivity heating [94]. This technique includes the conversion of MW electric field energy adsorbed by the solid medium (i.e., activated carbon) into heat at the molecular level [95]. The dielectric properties of activated carbon combined with PFAS

properties (such as their volatility) could allow the regeneration of PFAS-exhausted AC by means of the interactions between delocalized π-electrons of AC and the MWs. MW regeneration of PFAS-exhausted AC deserve further investigation.

Table 5 Chemical regeneration of PFAS-saturated materials.

Adsorbate	Adsorbent	Water matrix in adsorption experiments	Ratio mass:solution mixture	Experimental setup	Chemical solution	Regeneration percentage (%)	References
PFOS	**PAC** hydrophobic surface S_{BET} = 980 m^2 g^{-1} pore volume = 276 mm^3 g^{-1}	DI	100 mg:50 mL	Batch Adsorbed PFOS is extracted by varying ethanol and Milli-Q water ratios T=25 °C	100% C_2H_5OH	75.41	[91]
					70% C_2H_5OH + 30% DI	87.41	
					50% C_2H_5OH + 50% DI	94.58	
					40% C_2H_5OH + 60% DI	81.46	
					30% C_2H_5OH + 70% DI	80.96	
					20% C_2H_5OH + 80% DI	55.16	
					10% C_2H_5OH + 90% DI	45.22	
	HMS hydrophilic surface S_{BET} = 712 m^2 g^{-1} pore volume = 773 mm^3 g^{-1}				100% C_2H_5OH	101.27	
					70% C_2H_5OH + 30% DI	101.14	
					50% C_2H_5OH + 50% DI	100.16	
					40% C_2H_5OH + 60% DI	74.74	
					30% C_2H_5OH + 70% DI	71.50	
					20% C_2H_5OH + 80% DI	68.47	
					10% C_2H_5OH + 90% DI	58.69	
	OD-HMS hydrophobic surface S_{BET} = 476 m^2 g^{-1} pore volume = 499 mm^3 g^{-1}				100% C_2H_5OH	101.12	
					70% C_2H_5OH + 30% DI	100.72	
					50% C_2H_5OH + 50% DI	101.34	
					40% C_2H_5OH + 60% DI	61.70	
					30% C_2H_5OH + 70% DI	66.07	
					20% C_2H_5OH + 80% DI	60.98	
					10% C_2H_5OH + 90% DI	57.90	
PFOA	**Purosorb PAD 500** Polysyrenic macroporous-type, nonionic Exchange capacity = n.a.	DI	5 g:250 mL	Batch, magnetic stirrer at 250 rpm in a thermostatic oven for 80 h T=20 °C	5% NH_4Cl	0	[89]
					5% NH_4OH	0	
					3% NH_4Cl + 3% NH_4OH	0	
					30% MeOH	20	
					50% MeOH + 3% NH_4OH	90	
	Macronet MN102 Polystyrenic crosslinked macroporous-type, tertiary amine functional groups Exchange capacity = 0.2 meq L^{-1}				5% NH_4Cl	0	
					5% NH_4OH	0	
					3% NH_4Cl + 3% NH_4OH	0	
					30% MeOH	20	
					50% MeOH + 3% NH_4OH	90	
	AE resin **Purolite A600E** Polystyrenic gel-type, quaternary ammonium with trimethyl group functional groups Exchange capacity = 1.4 meq L^{-1}				5% NH_4Cl	20	
					5% NH_4OH	30	
					3% NH_4Cl + 3% NH_4OH	85	
					30% MeOH	< 20	
					50% MeOH + 3% NH_4OH	40	
	AE resin **Purolite A520E** Polystyrenic macroporous-type, quaternary ammonium with trimethyl group functional groups Exchange capacity = 0.9 meq L^{-1}				5% NH_4Cl	35	
					5% NH_4OH	35	
					3% NH_4Cl + 3% NH_4OH	90	
					30% MeOH	20	
					50% MeOH + 3% NH_4OH	50	

* After 5 Adsorption/regeneration cycles. PAC: powdered activated carbon; S_{BET}: BET surface area; DI: deionized water; HMS: hexagonal mesoporous silica; OD-HMS: N-octyldichlorosilane grafted hexagonal mesoporous silica; AE: anion-exchange.

Table 5 Chemical regeneration of PFAS-saturated materials (continued).

Adsorbate	Adsorbent	Water matrix in adsorption experiments	Ratio mass:solution mixture	Experimental setup	Chemical solution	Regeneration percentage (%)	References
PFOS	**BdAC** S_{BET} = 2450 m^2 g^{-1} Effective size = 0.6–0.85 mm	DI	10 g:100 mL	Batch, orbital shaker at 175 rpm for 24 h T = 25 °C	DI	19.8	[90]
					50% CH_3OH	93	
					50% C_2H_5OH	98	
				Batch, orbital shaker at 175 rpm for 7 h T = 80 °C	DI	53	
				Batch, orbital shaker at 175 rpm for 24 h	0.06% NaCl	< 1	
					0.06% NaOH		
				Batch, orbital shaker at 175 rpm for 23 h T = 45 °C	40% C_2H_5OH	89	
					10% C_2H_5OH	46	
					20% C_2H_5OH	71	
					30% C_2H_5OH	80	
				Batch, orbital shaker at 175 rpm for 12 h T = 25 °C	50% C_2H_5OH	70 *	
PFOA	**BdAC** S_{BET} = 2450 m^2 g^{-1} Effective size = 0.6–0.85 mm	Actual WW	25 g:30 mL	Batch, spent adsorbents shake at a thermostatic shaker at 170 rpm for 12 h T = 45 °C	50% CH_3OH	60 *	[36]
PFHpA						< 30 *	
PFHxA						< 10 *	
PFOA	**AE resin** **Amberlite IRA-67** Acrylic gel-type, tertiary amine functional groups Exchange capacity = 1.6 meq mL^{-1}		10 g:30 mL	Batch, spent adsorbents shake at a thermostatic shaker at 170 rpm for 12 h T = 25 °C	1% NaCl/CH_3OH	< 80 *	
PFHpA						< 40 *	
PFHxA						< 10 *	
PFBA **PFOA** **PFBS** **PFOS**	**AE resin** **Purolite A600E** Polystyrene-DVB gel-type, trimethyl quaternary amine functional groups Exchange capacity = 1.6 eq L^{-1}	DW	1 g:1 L	Batch, flash stirred for 18 h and later at controlled temperature for 60 h T= 20 °C	5% NaCl	0	[27]
					5% KCl		
					5% NH_4Cl	0 - 5	
					2% NaOH		
					2% KOH		
					2% NH_4OH		
					0.5% NaOH + 0.5% NaCl	< 10	
					0.5% KOH + 0.5% KCl	40 - 60	
					0.5% NH_4OH + 0.5% NH_4Cl		
					80% CH_3OH + 1% NH_4Cl	60 - 80	
					80% CH_3CH_2OH + 1% NH_4Cl		
	AE resin **Purolite A520E** Polystyrene-DVB macroporous-type, trimethyl quaternary amine functional groups Exchange capacity = 0.9 eq L^{-1}	DW			5% NaCl	0	
					5% KCl		
					5% NH_4Cl	< 10	
					2% NaOH	0 - 5	
					2% KOH		
					2% NH_4OH	< 10	

* After 5 adsorption/regeneration cycles.
BdAC: bamboo-derived activated carbon; S_{BET} = BET surface area; AE: anion-exchange; WW: wastewater; DW: drinking water; DI: deionized water.

Table 5 Chemical regeneration of PFAS-saturated materials (continued).

Adsorbate	Adsorbent	Water matrix in adsorption experiments	Ratio mass:solution mixture	Experimental setup	Chemical solution	Regeneration percentage (%)	References
PFOS	**Chitosan-based MIP**	DI	0.01 g:100 mL	Batch regeneration solution in an orbital shaker for 24 h T = 40 °C	90% NaOH + 10% C_3H_6O	60 *	[38]
PFOS	**AE resin** **Amberlite IRA-458** Acrylic gel-type, quaternary ammonium functional groups Exchange capacity = 1.25 meq mL^{-1}	DI	n.a.	Column Resin loaded with PFOS or PFBS packed in glass column (diameter of 1 cm, height of 10 cm) Flow rate 20 mL/min for 12 h T=22 °C	NaCl (320 mM)	0.0	[41]
					NaOH (320 mM)	0.36	
PFBS					NaOH (320 mM)	4	
PFOS	**AE resin** **Amberlite IRA-958** Acrylic macroreticular-type, quaternary ammonium functional groups Exchange capacity = 0.8 eq L^{-1}	Chromium planting WW (inorganic anions)	20 mg:100 mL	Batch Resin loaded with PFOS and regeneration solution in an orbital shaker for 24 h at 150 rpm T = 25 °C	5% NaCl	< 10	[32]
					5% NaCl + 10% CH_3OH		
					1% NaCl + 10% CH_3OH		
					1% NaCl + 30% CH_3OH		
					100% CH_3OH		
					4% NaOH		
					1% NaCl + 50% CH_3OH	70	
					1% NaCl + 50% CH_3OH	90	
	AE resin **Amberlite IRA-67** Acrylic gel-type, tertiary amine functional groups Exchange capacity = 1.6 meq mL^{-1}				100% CH_3OH	< 5	
					4% NaOH	< 5	
					0.4% NaOH	45	
					0.04% NaOH	50	
					1% NaCl + 30% CH_3OH	20	
					1% NaCl + 50% CH_3OH	85	
					1% NaCl + 70% CH_3OH	95	
					1% NaOH + 30% CH_3OH	95	
					1% NaOH + 50% CH_3OH	90	
					1% NaOH + 70% CH_3OH	90	

* After 5 adsorption/regeneration cycles.
MIP: molecularly imprinted; AE: Anion-exchange; WW: wastewater; DW: drinking water; DI: deionized water.

Table 5 Chemical regeneration of PFAS-saturated materials (continued).

Adsorbate	Adsorbent	Water matrix in adsorption experiments	Ratio mass:solution mixture	Experimental setup	Chemical solution	Regeneration percentage (%)	References
PFBA **PFOA** **PFBS** **PFOS**	**AE resin** **Purolite A520E** Polystyrene-DVB macroporous-type, trimethyl quaternary amine functional groups Exchange capacity = 0.9 eq L^{-1}	DW	1 g:1 L	Batch, flash stirred for 18 h and later at controlled temperature for 60 h T = 20 °C	0.5% NaOH + 0.5% NaCl	10 - 20	[27]
					0.5% KOH + 0.5% KCl	50 - 65	
					0.5% NH_4OH + 0.5% NH_4Cl	70 - 80	
					80% CH_3OH + 1% NH_4Cl	80 - 90	
					80% CH_3CH_2OH + 1% NH_4Cl		
					5% KCl		
	AE resin **Purolite A532E** Polystyrenic macroporous-type, bifunctional quaternary amine functional groups Exchange capacity = 0.85 eq L^{-1}	DW	1 g:1 L	Batch, flash stirred for 18 h and later at controlled temperature for 60 h T = 20 °C	5% NaCl	0	
					5% KCl		
					5% NH_4Cl	0 - 5	
					2% NaOH	0	
					2% KOH		
					2% NH_4OH	0 - 5	
					0.5% NaOH + 0.5% NaCl		
					0.5% KOH + 0.5% KCl		
					0.5% NH_4OH + 0.5% NH_4Cl		
					80% CH_3OH + 1% NH_4Cl	80 - 90	
					80% CH_3CH_2OH + 1% NH_4Cl		
PFOS	**R-CAC** S_{BET} = 1750 m^2 g^{-1}	Actual WW	10mg:20 mL	Batch, shaking at 170 rpm for 12 h T = 50 °C	50% C_2H_5OH	76.0	[55]
					70% C_2H_5OH	89.5	
					90% C_2H_5OH	85.1	
					100% C_2H_5OH	83.1	
				Batch, shaking at 170 rpm for 12 h T = 40 °C	50% CH_3OH	85.3	
					70% CH_3OH	89.5	
					90% CH_3OH	95.1	
					100% CH_3OH	90.2	
					50% C_3H_6O	80.6	
					70% C_3H_6O	85.6	
					90% C_3H_6O	91.6	
					100% C_3H_6O	90.0	
F-53B	**R-CAC** S_{BET} = 1750 m^2 g^{-1}	Actual WW	10mg:20 mL	Batch, shaking at 170 rpm for 12 h T = 50 °C	50% C_2H_5OH	80.4	
					70% C_2H_5OH	96.6	
					90% C_2H_5OH	90.2	
					100% C_2H_5OH	88.3	
				Batch, shaking at 170 rpm for 12 h T = 40 °C	50% CH_3OH	88.3	
					70% CH_3OH	93.1	
					90% CH_3OH	97.7	
					100% CH_3OH	92.6	
					50% C_3H_6O	87.4	
					70% C_3H_6O	92.3	
					90% C_3H_6O	97.6	
					100% C_3H_6O	93.4	

AE: anion-exchange; WW: wastewater; DW: drinking water; DI: deionized water; R-CAC: reactivated coconut shell based GAC; S_{BET} = BET surface area.

Table 5 Chemical regeneration of PFAS-saturated materials (continued).

Adsorbate	Adsorbent	Water matrix in adsorption experiments	Ratio mass:solution mixture	Experimental setup	Chemical solution	Regeneration percentage (%)	References
PFOS **PFHxS** **PFBS**	**PCMAs**	DI	0.5 g/L of PCMAs with 50 mg/L of each PFAS	Adsorbed PFAS are extracted with methanol. Regenerated PCMAs are reused for subsequent PFAS sorption experiments.	CH_3OH	85 - 88 *	[88]
PFOS	**PACFs**	DI	10mg:100 mL	Batch, shaking at 180 rpm for 24 h T = 25 °C	DI	5	[43]
					10% C_2H_5OH	22	
					30% C_2H_5OH	65	
					50% C_2H_5OH	85	
					100% C_2H_5OH	87	

* After 5 adsorption/regeneration cycles
DI: deionized water; PCMAs: permanently confined micelle arrays; PACFs: Polyacrylonitrile fiber (PANF)-derived activated carbon fibers

7. Conclusions and future research recommended

7.1 Conclusions

Poly- and perfluoroalkyl substances (PFAS) are a large group of manmade chemicals characterized by high stability and persistence on environmental compartments. Among interim response measures, adsorption technologies (i.e., by activated carbon or anion-exchange resin) are currently employed for treatment of PFAS-impacted water.

The present critical review of data on PFAS adsorption suggests that:

- To date, most of the experimental works published have been carried out under unrealistic operating conditions, such as high dosage of adsorbent materials, long EBCT, acid pH, and high concentrations of PFAS spiked in DI water. Such conditions are not representative of either full-scale treatment plants or actual environmental contaminations.
- Long-chain PFAS adsorption can involve the formation of aggregates on surface materials that may improve the adsorption efficiency by hydrophobic interactions. Furthermore, when different long-chain PFAS co-exist in solution, the longest PFAS outcompete the shorter due to a stronger hydrophobic interaction between the longest PFAS and the adsorbent surface.
- Meso- and macro-porous adsorbents (both AC and resin) showed high adsorption capacity because long-chain PFAS can easily access.
- Anion-exchange resins are more effective than activated carbon for both long- and short-chain PFAS removal.
- Regardless of the adsorbent used, the adsorption capacity of short-chain PFAS is lower than that observed for long-chain PFAS. Therefore, short-chain PFAS removal is more challenging.
- Adsorption of short-chain PFAS seems related to the availability of active pore sites because the formation of micelles (multi-layer adsorption) does not occur.
- Studies focused on the effect of OM during adsorption process report contrasting results. Overall, co-existing OM negatively affects short-chain PFAS adsorption due to active site competition, whereas the effect of OM seems less relevant during long-chain PFAS adsorption.
- Due to pore blockage and electrostatic repulsions, negative effect of OM on other adsorbent materials (such as biochar, mineral materials and magnetic-nanoparticles) is also reported.
- Effect of co-existing OM should be taken into account during both adsorption and regeneration processes.
- Chemical regeneration of PFAS saturated adsorbents requires the use of organic solvents, which are harmful. Nevertheless, thermal regeneration at high temperature of exhausted

activated carbon causes the decline of adsorption capacity and may release dangerous short-chain fluorinated gases. Overall, the in-situ implementation of either chemical or thermal regeneration is not feasible.

7.2 Research needs

The following specific research needs can be drawn based on the observed gaps in PFAS removal by adsorption:

- The investigation of PFAS removal by adsorption (especially short-chain PFAS) under typical water treatment conditions (i.e., adsorbent dose or EBCT, pH, PFAS concentrations) is strongly advised.
- An advanced characterization of OM before and after the adsorption processes is also advised. In particular, fractionation of OM measuring hydrophobic, transphilic and hydrophilic fractions as well as acid, neutral and base fractions is relevant to better understand the adsorption mechanism and the effect of OM. Size exclusion chromatography (SEC) is also suggested to ascertain the effect of molecular weight of OM.
- Characterization of adsorbent morphology by means of transmission electron microscopy, scanning electron microscopy and Fourier transform infrared spectroscopy before and after PFAS uptake is also useful.
- The simultaneous effect of ionic strength and OM should be considered during PFAS adsorption and further investigations are required in order to better understand the contribution of ionic OM and inorganic ions (i.e., monovalent and divalent cations) on PFAS removal. Further experimental works should be performed at different OM fractions but at the same ionic strength in order minimize the possible effect of inorganic ions.
- Economic assessment of PFAS removal techniques should also address the adsorbent disposal/regeneration. For instance, the management of the eluate produced by chemical regeneration of the resins should be considered.
- Other unconventional techniques, such as microwave irradiation, may help to overcome issues concerning the regeneration of PFAS-saturated adsorbents.
- A novel treatment train, which allows the combination of separation and destructive technologies is expected for the sustainable removal of PFAS.

References

[1] Buck, R.C., Franklin, J., Berger, U., Conder, J.M., Cousins, I.T., Voogt, P. De, Jensen, A.A., Kannan, K., Mabury, S.A., van Leeuwen, S.P.J., **2011**. Perfluoroalkyl and polyfluoroalkyl substances in the environment: Terminology, classification, and origins. *Integrated Environmental Assessment and Management*. 7, 513–541. DOI:10.1002/ieam.258.

[2] Rahman, M.F., Peldszus, S., Anderson, W.B., **2014**. Behaviour and fate of perfluoroalkyl and polyfluoroalkyl substances (PFASs) in drinking water treatment: A review. *Water Research*. 50, 318–340. DOI:10.1016/j.watres.2013.10.045.

[3] Xiao, F., **2017**. Emerging poly- and per fl uoroalkyl substances in the aquatic environment : A review of current literature. *Water Research*. 124, 482–495. DOI:10.1016/j.watres.2017.07.024.

[4] Hu, X.C., Andrews, D.Q., Lindstrom, A.B., Bruton, T.A., Schaider, L.A., Grandjean, P., Lohmann, R., Carignan, C.C., Blum, A., Balan, S.A., Higgins, C.P., Sunderland, E.M., **2016**. Detection of Poly- and Perfluoroalkyl Substances (PFASs) in U.S. Drinking Water Linked to Industrial Sites, Military Fire Training Areas, and Wastewater Treatment Plants. *Environmental Science and Technology Letters*. 3, 344–350. DOI:10.1021/acs.estlett.6b00260.

[5] ITRC, **2017**. Naming Conventions and Physical and Chemical Properties of Per-and Polyfluoroalkyl Substances (PFAS). 1–15. DOI:10.1002/ieam.258.

[6] OECD/UNEP Global PFC Group, **2013**. United Nations Environment Programme: Synthesis paper on per- and polyfluorinated chemicals (PFCs), Environment, Health and Safety, Environment Directorate, OECD. *IOMC: Inter-Organization Programme for the Sound Managment of Chemicals*. 1–58.

[7] Ahrens, L., **2011**. Polyfluoroalkyl compounds in the aquatic environment: A review of their occurrence and fate. *Journal of Environmental Monitoring*. 13, 20–31. DOI:10.1039/c0em00373e.

[8] Kucharzyk, K.H., Darlington, R., Benotti, M., Deeb, R., Hawley, E., **2017**. Novel treatment technologies for PFAS compounds: A critical review. *Journal of Environmental Management*. 204, 757–764. DOI:10.1016/j.jenvman.2017.08.016.

[9] Kaboré, H.A., Vo Duy, S., Munoz, G., Méité, L., Desrosiers, M., Liu, J., Sory, T.K., Sauvé, S., **2018**. Worldwide drinking water occurrence and levels of newly-identified perfluoroalkyl and polyfluoroalkyl substances. *Science of the Total Environment*. 616–617, 1089–1100. DOI:10.1016/j.scitotenv.2017.10.210.

[10] Hölzer, J., Göen, T., Rauchfuss, K., Kraft, M., Angerer, J., Kleeschulte, P., Wilhelm, M., **2009**. One-year follow-up of perfluorinated compounds in plasma of German residents from Arnsberg formerly exposed to PFOA-contaminated drinking water. *International Journal of Hygiene and Environmental Health*. 212, 499–504. DOI:10.1016/j.ijheh.2009.04.003.

[11] Appleman, T.D., Higgins, C.P., Quiñones, O., Vanderford, B.J., Kolstad, C., Zeigler-Holady, J.C., Dickenson, E.R.V., **2014**. Treatment of poly- and perfluoroalkyl substances in U.S. full-

scale water treatment systems. *Water Research*. 51, 246–255. DOI:10.1016/j.watres.2013.10.067.

[12] Arvaniti, O.S., Stasinakis, A.S., **2015**. Review on the occurrence, fate and removal of perfluorinated compounds during wastewater treatment. *Science of the Total Environment*. 524–525, 81–92. DOI:10.1016/j.scitotenv.2015.04.023.

[13] Munoz, G., Labadie, P., Botta, F., Lestremau, F., Lopez, B., Geneste, E., Pardon, P., Dévier, M.H., Budzinski, H., **2017**. Occurrence survey and spatial distribution of perfluoroalkyl and polyfluoroalkyl surfactants in groundwater, surface water, and sediments from tropical environments. *Science of the Total Environment*. 607–608, 243–252. DOI:10.1016/j.scitotenv.2017.06.146.

[14] Ateia, M., Maroli, A., Tharayil, N., Karanfil, T., **2019**. The overlooked short- and ultrashort-chain poly- and perfluorinated substances: A review. *Chemosphere*. 220, 866–882. DOI:10.1016/j.chemosphere.2018.12.186.

[15] Szabo, D., Coggan, T.L., Robson, T.C., Currell, M., Clarke, B.O., **2018**. Investigating recycled water use as a diffuse source of per- and polyfluoroalkyl substances (PFASs) to groundwater in Melbourne, Australia. *Science of the Total Environment*. 644, 1409–1417. DOI:10.1016/j.scitotenv.2018.07.048.

[16] Brendel, S., Fetter, É., Staude, C., Vierke, L., Biegel-Engler, A., **2018**. Short-chain perfluoroalkyl acids: environmental concerns and a regulatory strategy under REACH. *Environmental Sciences Europe*. 30,. DOI:10.1186/s12302-018-0134-4.

[17] Gao, Y., Deng, S., Du, Z., Liu, K., Yu, G., **2017**. Adsorptive removal of emerging polyfluoroalky substances F-53B and PFOS by anion-exchange resin: A comparative study. *Journal of Hazardous Materials*. 323, 550–557. DOI:10.1016/j.jhazmat.2016.04.069.

[18] Stubleski, J., Salihovic, S., Lind, P.M., Lind, L., Dunder, L., McCleaf, P., Eurén, K., Ahrens, L., Svartengren, M., van Bavel, B., Kärrman, A., **2017**. The effect of drinking water contaminated with perfluoroalkyl substances on a 10-year longitudinal trend of plasma levels in an elderly Uppsala cohort. *Environmental Research*. 159, 95–102. DOI:10.1016/j.envres.2017.07.050.

[19] Crawford, N.M., Fenton, S.E., Strynar, M., Hines, E.P., Pritchard, D.A., Steiner, A.Z., **2017**. Effects of perfluorinated chemicals on thyroid function, markers of ovarian reserve, and natural fertility. *Reproductive Toxicology*. 69, 53–59. DOI:10.1016/j.reprotox.2017.01.006.

[20] Domingo, J.L., Nadal, M., **2017**. Per- and polyfluoroalkyl substances (PFASs) in food and human dietary intake: A review of the recent scientific literature. *Journal of Agricultural and Food Chemistry*. 65, 533–543. DOI:10.1021/acs.jafc.6b04683.

[21] Dewitt, J.C., **2015**.Molecular and Integrative Toxicology Toxicological Eff ects of Perfl uoroalkyl and Polyfl uoroalkyl Substances, 2015.

[22] Ross, I., McDonough, J., Miles, J., Storch, P., Thelakkat Kochunarayanan, P., Kalve, E., Hurst, J., S. Dasgupta, S., Burdick, J., **2018**. A review of emerging technologies for remediation of PFASs. *Remediation*. 28, 101–126. DOI:10.1002/rem.21553.

[23] Nzeribe, B.N., Crimi, M., Mededovic Thagard, S., Holsen, T.M., **2019**. Physico-Chemical Processes for the Treatment of Per- And Polyfluoroalkyl Substances (PFAS): A review. *Critical Reviews in Environmental Science and Technology*. 49, 866–915. DOI:10.1080/10643389.2018.1542916.

[24] Trojanowicz, M., Bojanowska-Czajka, A., Bartosiewicz, I., Kulisa, K., **2018**. Advanced Oxidation/Reduction Processes treatment for aqueous perfluorooctanoate (PFOA) and perfluorooctanesulfonate (PFOS) – A review of recent advances. *Chemical Engineering Journal*. 336, 170–199. DOI:10.1016/j.cej.2017.10.153.

[25] Appleman, T.D., Dickenson, E.R. V, Bellona, C., Higgins, C.P., **2013**. Nanofiltration and granular activated carbon treatment of perfluoroalkyl acids. *Journal of Hazardous Materials*. 260, 740–746. DOI:10.1016/j.jhazmat.2013.06.033.

[26] Du, Z., Deng, S., Bei, Y., Huang, Q., Wang, B., Huang, J., Yu, G., **2014**. Adsorption behavior and mechanism of perfluorinated compounds on various adsorbents - A review. *Journal of Hazardous Materials*. 274, 443–454. DOI:10.1016/j.jhazmat.2014.04.038.

[27] Zaggia, A., Conte, L., Falletti, L., Fant, M., Chiorboli, A., **2016**. Use of strong anion exchange resins for the removal of perfluoroalkylated substances from contaminated drinking water in batch and continuous pilot plants. *Water Research*. 91, 137–146. DOI:10.1016/j.watres.2015.12.039.

[28] Eschauzier, C., Beerendonk, E., Scholte-Veenendaal, P., De Voogt, P., **2012**. Impact of Treatment Processes on the Removal of Perfluoroalkyl Acids from the Drinking Water Production Chain. *Environmental Science & Technology*. 46, 1708–1715. DOI:10.1021/es201662b.

[29] Quiñones, O., Snyder, S.A., **2009**. Occurrence of perfluoroalkyl carboxylates and sulfonates in drinking water utilities and related waters from the United States. *Environmental Science and Technology*. 43, 9089–9095. DOI:10.1021/es9024707.

[30] Rizzo, L., Malato, S., Antakyali, D., Beretsou, V.G., Đolić, M.B., Gernjak, W., Heath, E., Ivancev-Tumbas, I., Karaolia, P., Lado Ribeiro, A.R., Mascolo, G., McArdell, C.S., Schaar, H., Silva, A.M.T., Fatta-Kassinos, D., **2019**. Consolidated vs new advanced treatment methods for the removal of contaminants of emerging concern from urban wastewater. *Science of the Total Environment*. 655, 986–1008. DOI:10.1016/j.scitotenv.2018.11.265.

[31] Roccaro, P., Sgroi, M., Vagliasindi, F.G.A., **2013**. Removal of xenobiotic compounds from wastewater for environment protection: Treatment processes and costs. *Chemical Engineering Transactions*. 32, 505–510.

[32] Deng, S., Yu, Q., Huang, J., Yu, G., **2010**. Removal of perfluorooctane sulfonate from wastewater by anion exchange resins: Effects of resin properties and solution chemistry. *Water Research*. 44, 5188–5195. DOI:10.1016/j.watres.2010.06.038.

[33] McCleaf, P., Englund, S., Östlund, A., Lindegren, K., Wiberg, K., Ahrens, L., **2017**. Removal efficiency of multiple poly- and perfluoroalkyl substances (PFASs) in drinking water using granular activated carbon (GAC) and anion exchange (AE) column tests. *Water Research*. 120, 77–87. DOI:10.1016/j.watres.2017.04.057.

[34] Maimaiti, A., Deng, S., Meng, P., Wang, W., Wang, B., Huang, J., Wang, Y., Yu, G., **2018**. Competitive adsorption of perfluoroalkyl substances on anion exchange resins in simulated AFFF-impacted groundwater. *Chemical Engineering Journal*. 348, 494–502. DOI:https://doi.org/10.1016/j.cej.2018.05.006.

[35] Yu, J., Lv, L., Lan, P., Zhang, S., Pan, B., Zhang, W., **2012**. Effect of effluent organic matter on the adsorption of perfluorinated compounds onto activated carbon. *Journal of Hazardous Materials*. 225–226, 99–106. DOI:10.1016/j.jhazmat.2012.04.073.

[36] Du, Z., Deng, S., Chen, Y., Wang, B., Huang, J., Wang, Y., Yu, G., **2015**. Removal of perfluorinated carboxylates from washing wastewater of perfluorooctanesulfonyl fluoride using activated carbons and resins. *Journal of Hazardous Materials*. 286, 136–143. DOI:10.1016/j.jhazmat.2014.12.037.

[37] Liu, L., Liu, Y., Li, C., Ji, R., Tian, X., **2018**. Improved sorption of perfluorooctanoic acid on carbon nanotubes hybridized by metal oxide nanoparticles. *Environmental Science and Pollution Research*. 25, 15507–15517. DOI:10.1007/s11356-018-1728-5.

[38] Yu, Q., Deng, S., Yu, G., **2008**. Selective removal of perfluorooctane sulfonate from aqueous solution using chitosan-based molecularly imprinted polymer adsorbents. *Water Research*. 42, 3089–3097. DOI:10.1016/j.watres.2008.02.024.

[39] Qian, J., Shen, M., Wang, P., Wang, C., Hu, J., Hou, J., Ao, Y., Zheng, H., Li, K., Liu, J., **2017**. Co-adsorption of perfluorooctane sulfonate and phosphate on boehmite: Influence of temperature, phosphate initial concentration and pH. *Ecotoxicology and Environmental Safety*. 137, 71–77. DOI:10.1016/j.ecoenv.2016.11.026.

[40] Xiao, F., Zhang, X., Penn, L., Gulliver, J.S., Simcik, M.F., **2011**. Effects of monovalent cations on the competitive adsorption of perfluoroalkyl acids by kaolinite: Experimental studies and modeling. *Environmental Science and Technology*. 45, 10028–10035. DOI:10.1021/es202524y.

[41] Carter, K.E., Farrell, J., **2010**. Removal of perfluorooctane and perfluorobutane sulfonate from water via carbon adsorption and ion exchange. *Separation Science and Technology*. 45, 762–767. DOI:10.1080/01496391003608421.

[42] Chen, H., Reinhard, M., Nguyen, V.T., Gin, K.Y.H., **2016**. Reversible and irreversible sorption of perfluorinated compounds (PFCs) by sediments of an urban reservoir. *Chemosphere*. 144, 1747–1753. DOI:10.1016/j.chemosphere.2015.10.055.

[43] Chen, W., Zhang, X., Mamadiev, M., Wang, Z., **2017**. Sorption of perfluorooctane sulfonate and perfluorooctanoate on polyacrylonitrile fiber-derived activated carbon fibers: In comparison with activated carbon. *RSC Advances*. 7, 927–938. DOI:10.1039/c6ra25230c.

[44] Zhou, Q., Yu, Q., Zhang, Q., Yu, G., Deng, S., He, H., Huang, J., **2009**. Sorption of perfluorooctane sulfonate on organo-montmorillonites. *Chemosphere*. 78, 688–694. DOI:10.1016/j.chemosphere.2009.12.005.

[45] Deng, S., Niu, L., Bei, Y., Wang, B., Huang, J., Yu, G., **2013**. Adsorption of perfluorinated compounds on aminated rice husk prepared by atom transfer radical polymerization.

Chemosphere. 91, 124–130. DOI:10.1016/j.chemosphere.2012.11.015.

[46] Deng, S., Zheng, Y.Q., Xu, F.J., Wang, B., Huang, J., Yu, G., **2012**. Highly efficient sorption of perfluorooctane sulfonate and perfluorooctanoate on a quaternized cotton prepared by atom transfer radical polymerization. *Chemical Engineering Journal*. 193–194, 154–160. DOI:10.1016/j.cej.2012.04.005.

[47] Sgroi, M., Anumol, T., Roccaro, P., Vagliasindi, F.G.A., Snyder, S.A., **2018**. Modeling emerging contaminants breakthrough in packed bed adsorption columns by UV absorbance and fluorescing components of dissolved organic matter. *Water Research*. 145, 667–677. DOI:10.1016/j.watres.2018.09.018.

[48] Kothawala, D.N., Köhler, S.J., Östlund, A., Wiberg, K., Ahrens, L., **2017**. Influence of dissolved organic matter concentration and composition on the removal efficiency of perfluoroalkyl substances (PFASs) during drinking water treatment. *Water Research*. 121, 320–328. DOI:10.1016/j.watres.2017.05.047.

[49] Woodard, S., Berry, J., Newman, B., **2017**. Ion exchange resin for PFAS removal and pilot test comparison to GAC. *Remediation*. 27, 19–27. DOI:10.1002/rem.21515.

[50] Ochoa-Herrera, V., Sierra-Alvarez, R., **2008**. Removal of perfluorinated surfactants by sorption onto granular activated carbon, zeolite and sludge. *Chemosphere*. 72, 1588–1593. DOI:10.1016/j.chemosphere.2008.04.029.

[51] Liang, X., Gondal, M.A., Chang, X., Yamani, Z.H., Li, N., Lu, H., Ji, G., **2011**. Facile preparation of magnetic separable powdered-activated-carbon/Ni adsorbent and its application in removal of perfluorooctane sulfonate (PFOS) from aqueous solution. *Journal of Environmental Science and Health - Part A Toxic/Hazardous Substances and Environmental Engineering*. 46, 1482–1490. DOI:10.1080/10934529.2011.609066.

[52] Rattanaoudom, R., Visvanathan, C., Boontanon, S.K., **2012**. Removal of concentrated PFOS and PFOA in synthetic industrial wastewater by powder activated carbon and hydrotalcite. *Journal of Water Sustainibility*. 2, 245–258. DOI:10.11912/jws.2.4.245-258.

[53] Yu, Q., Zhang, R., Deng, S., Huang, J., Yu, G., **2009**. Sorption of perfluorooctane sulfonate and perfluorooctanoate on activated carbons and resin: Kinetic and isotherm study. *Water Research*. 43, 1150–1158. DOI:10.1016/j.watres.2008.12.001.

[54] Wang, B., Lee, L.S., Wei, C., Fu, H., Zheng, S., Xu, Z., Zhu, D., **2016**. Covalent triazine-based framework: A promising adsorbent for removal of perfluoroalkyl acids from aqueous solution. *Environmental Pollution*. 216, 884–892. DOI:10.1016/j.envpol.2016.06.062.

[55] Du, Z., Deng, S., Liu, D., Yao, X., Wang, Y., Lu, X., Wang, B., Huang, J., Wang, Y., Xing, B., Yu, G., **2016**. Efficient adsorption of PFOS and F53B from chrome plating wastewater and their subsequent degradation in the regeneration process. *Chemical Engineering Journal*. 290, 405–413. DOI:10.1016/j.cej.2016.01.077.

[56] Chen, X., Xia, X., Wang, X., Qiao, J., Chen, H., **2011**. A comparative study on sorption of perfluorooctane sulfonate (PFOS) by chars, ash and carbon nanotubes. *Chemosphere*. 83, 1313–1319. DOI:10.1016/j.chemosphere.2011.04.018.

[57] Li, X., Chen, S., Quan, X., Zhang, Y., **2011**. Enhanced adsorption of PFOA and PFOS on multiwalled carbon nanotubes under electrochemical assistance. *Environmental Science and Technology*. 45, 8498–8505. DOI:10.1021/es202026v.

[58] Guo, W., Huo, S., Feng, J., Lu, X., **2017**. Adsorption of perfluorooctane sulfonate (PFOS) on corn straw-derived biochar prepared at different pyrolytic temperatures. *Journal of the Taiwan Institute of Chemical Engineers*. 78, 265–271. DOI:10.1016/j.jtice.2017.06.013.

[59] Inyang, M., Dickenson, E.R.V., **2017**. The use of carbon adsorbents for the removal of perfluoroalkyl acids from potable reuse systems. *Chemosphere*. 184, 168–175. DOI:10.1016/j.chemosphere.2017.05.161.

[60] Xiao, X., Ulrich, B.A., Chen, B., Higgins, C.P., **2017**. Sorption of Poly- and Perfluoroalkyl Substances (PFASs) Relevant to Aqueous Film-Forming Foam (AFFF)-Impacted Groundwater by Biochars and Activated Carbon. *Environmental Science and Technology*. 51, 6342–6351. DOI:10.1021/acs.est.7b00970.

[61] Chularueangaksorn, P., Tanaka, S., Fujii, S., Kunacheva, C., **2014**. Adsorption of perfluorooctanoic acid (PFOA) onto anion exchange resin, non-ion exchange resin, and granular-activated carbon by batch and column. *Desalination and Water Treatment*. 52, 6542–6548. DOI:10.1080/19443994.2013.815589.

[62] Pramanik, B.K., Pramanik, S.K., Suja, F., **2015**. A comparative study of coagulation, granular- and powdered-activated carbon for the removal of perfluorooctane sulfonate and perfluorooctanoate in drinking water treatment. *Environmental Technology (United Kingdom)*. 36, 2610–2617. DOI:10.1080/09593330.2015.1040079.

[63] Pramanik, B.K., Pramanik, S.K., Sarker, D.C., Suja, F., **2017**. Removal of emerging perfluorooctanoic acid and perfluorooctane sulfonate contaminants from lake water. *Environmental Technology (United Kingdom)*. 38, 1937–1942. DOI:10.1080/09593330.2016.1240716.

[64] Karoyo, A.H., Wilson, L.D., **2016**. Investigation of the Adsorption Processes of Fluorocarbon and Hydrocarbon Anions at the Solid-Solution Interface of Macromolecular Imprinted Polymer Materials. *Journal of Physical Chemistry C*. 120, 6553–6568. DOI:10.1021/acs.jpcc.5b12246.

[65] Xiao, L., Ling, Y., Alsbaiee, A., Li, C., Helbling, D.E., Dichtel, W.R., **2017**. β-Cyclodextrin Polymer Network Sequesters Perfluorooctanoic Acid at Environmentally Relevant Concentrations. *Journal of the American Chemical Society*. 139, 7689–7692. DOI:10.1021/jacs.7b02381.

[66] Guo, H., Liu, Y., Ma, W., Yan, L., Li, K., Lin, S., **2018**. Surface molecular imprinting on carbon microspheres for fast and selective adsorption of perfluorooctane sulfonate. *Journal of Hazardous Materials*. 348, 29–38. DOI:10.1016/j.jhazmat.2018.01.018.

[67] Luo, Q., Zhao, C., Liu, G., Ren, H., **2016**. A Porous Aromatic Framework Constructed from Benzene Rings Has a High Adsorption Capacity for Perfluorooctane Sulfonate. *Scientific Reports*. 6, 1–9. DOI:10.1038/srep20311.

[68] Feng, Y., Zhou, Y., Lee, P.H., Shih, K., **2016**. Mineralization of perfluorooctanesulfonate (PFOS) and perfluorodecanoate (PFDA) from aqueous solution by porous hexagonal boron nitride: adsorption followed by simultaneous thermal decomposition and regeneration. *RSC Advances*. 6, 113773–113780. DOI:10.1039/C6RA15564B.

[69] Wang, W., Xu, Z., Zhang, X., Wimmer, A., Shi, E., Qin, Y., Zhao, X., Zhou, B., Li, L., **2018**. Rapid and efficient removal of organic micropollutants from environmental water using a magnetic nanoparticles-attached fluorographene-based sorbent. *Chemical Engineering Journal*. 343, 61–68. DOI:10.1016/j.cej.2018.02.101.

[70] Zhang, Q., Deng, S., Yu, G., Huang, J., **2011**. Removal of perfluorooctane sulfonate from aqueous solution by crosslinked chitosan beads: Sorption kinetics and uptake mechanism. *Bioresource Technology*. 102, 2265–2271. DOI:10.1016/j.biortech.2010.10.040.

[71] Ateia, M., Attia, M.F., Maroli, A., Tharayil, N., Alexis, F., Whitehead, D.C., Karanfil, T., **2018**. Rapid Removal of Poly- and Perfluorinated Alkyl Substances by Poly(ethylenimine)-Functionalized Cellulose Microcrystals at Environmentally Relevant Conditions. *Environmental Science and Technology Letters*. 5, 764–769. DOI:10.1021/acs.estlett.8b00556.

[72] Lu, X., Deng, S., Wang, B., Huang, J., Wang, Y., Yu, G., **2016**. Adsorption behavior and mechanism of perfluorooctane sulfonate on nanosized inorganic oxides. *Journal of Colloid and Interface Science*. 474, 199–205. DOI:10.1016/j.jcis.2016.04.032.

[73] Zhou, Y., He, Z., Tao, Y., Xiao, Y., Zhou, T., Jing, T., Zhou, Y., Mei, S., **2016**. Preparation of a functional silica membrane coated on Fe3O4nanoparticle for rapid and selective removal of perfluorinated compounds from surface water sample. *Chemical Engineering Journal*. 303, 156–166. DOI:10.1016/j.cej.2016.05.137.

[74] Llorca, M., Schirinzi, G., Martínez, M., Barceló, D., Farré, M., **2018**. Adsorption of perfluoroalkyl substances on microplastics under environmental conditions. *Environmental Pollution*. 235, 680–691. DOI:10.1016/j.envpol.2017.12.075.

[75] Zhang, Q., Deng, S., Yu, G., Huang, J., **2011**. Removal of perfluorooctane sulfonate from aqueous solution by crosslinked chitosan beads: Sorption kinetics and uptake mechanism. *Bioresource Technology*. 102, 2265–2271. DOI:10.1016/j.biortech.2010.10.040.

[76] Zhao, P., Xia, X., Dong, J., Xia, N., Jiang, X., Li, Y., Zhu, Y., **2016**. Short- and long-chain perfluoroalkyl substances in the water, suspended particulate matter, and surface sediment of a turbid river. *Science of the Total Environment*. 568, 57–65. DOI:10.1016/j.scitotenv.2016.05.221.

[77] Hansen, M.C., Børresen, M.H., Schlabach, M., Cornelissen, G., **2010**. Sorption of perfluorinated compounds from contaminated water to activated carbon. *Journal of Soils and Sediments*. 10, 179–185. DOI:10.1007/s11368-009-0172-z.

[78] Deng, S., Bei, Y., Lu, X., Du, Z., Wang, B., Wang, Y., Huang, J., Yu, G., **2015**. Effect of co-existing organic compounds on adsorption of perfluorinated compounds onto carbon nanotubes. *Frontiers of Environmental Science and Engineering*. 9, 784–792. DOI:10.1007/s11783-015-0790-1.

[79] Wang, F., Shih, K., Leckie, J.O., **2015**. Effect of humic acid on the sorption of perfluorooctane sulfonate (PFOS) and perfluorobutane sulfonate (PFBS) on boehmite. *Chemosphere*. 118, 213–218. DOI:10.1016/j.chemosphere.2014.08.080.

[80] Sgroi, M., Vagliasindi, F.G.A., Snyder, S.A., Roccaro, P., **2018**. Chemosphere N - N itrosodimethylamine (NDMA) and its precursors in water and wastewater : A review on formation and removal. *Chemosphere*. 191, 685–703. DOI:10.1016/j.chemosphere.2017.10.089.

[81] Shon, H.K., Vigneswaran, S., Snyder, S.A., **2006**. Critical Reviews in Environmental Science and Technology Effluent Organic Matter (EfOM) in Wastewater : Constituents , Effects , and Treatment Effluent Organic Matter (EfOM) in Wastewater : *Critical Reviews in Environmental Science and Technology*. 37–41. DOI:10.1080/10643380600580011.

[82] Du, Z., Deng, S., Zhang, S., Wang, B., Huang, J., Wang, Y., Yu, G., Xing, B., **2016**. Selective and high sorption of perfluorooctanesulfonate and perfluorooctanoate by fluorinated alkyl chain modified montmorillonite. *Journal of Physical Chemistry C*. 120, 16782–16790. DOI:10.1021/acs.jpcc.6b04757.

[83] Wang, Y., Niu, J., Li, Y., Zheng, T., Xu, Y., Liu, Y., **2015**. Performance and mechanisms for removal of perfluorooctanoate (PFOA) from aqueous solution by activated carbon fiber. *RSC Advances*. 5, 86927–86933. DOI:10.1039/c5ra15853b.

[84] Higgins, C.P., Luthy, R.G., **2006**. Sorption of perfluorinated surfactants on sediments. *Environmental Science and Technology*. 40, 7251–7256. DOI:10.1021/es061000n.

[85] Zhao, D., Cheng, J., Vecitis, C.D., Hoffmann, M.R., **2011**. Sorption of perfluorochemicals to granular activated carbon in the presence of ultrasound. *Journal of Physical Chemistry A*. 115, 2250–2257. DOI:10.1021/jp111784k.

[86] Ziska, A.D., Park, M., Anumol, T., Snyder, S.A., **2016**. Predicting trace organic compound attenuation with spectroscopic parameters in powdered activated carbon processes. *Chemosphere*. 156, 163–171. DOI:10.1016/j.chemosphere.2016.04.073.

[87] Sun, Y., Angelotti, B., Brooks, M., Dowbiggin, B., Evans, P.J., Devins, B., Wang, Z.W., **2018**. A pilot-scale investigation of disinfection by-product precursors and trace organic removal mechanisms in ozone-biologically activated carbon treatment for potable reuse. *Chemosphere*. 210, 539–549. DOI:10.1016/j.chemosphere.2018.06.162.

[88] Wang, F., Lu, X., Shih, K.M., Wang, P., Li, X., **2014**. Removal of perfluoroalkyl sulfonates (PFAS) from aqueous solution using permanently confined micelle arrays (PCMAs). *Separation and Purification Technology*. 138, 7–12. DOI:10.1016/j.seppur.2014.09.037.

[89] Conte, L., Falletti, L., Zaggia, A., Milan, M., **2015**. Polyfluorinated Organic Micropollutants Removal from Water by Ion Exchange and Adsorption. *Polyfluorinated Organic Micropollutants Removal from Water by Ion Exchange and Adsorption*. 43, 2257–2262. DOI:10.3303/CET1543377.

[90] Deng, S., Nie, Y., Du, Z., Huang, Q., Meng, P., Wang, B., Huang, J., Yu, G., **2015**. Enhanced adsorption of perfluorooctane sulfonate and perfluorooctanoate by bamboo-

derived granular activated carbon. *Journal of Hazardous Materials*. 282, 150–157. DOI:10.1016/j.jhazmat.2014.03.045.

[91] Punyapalakul, P., Suksomboon, K., Prarat, P., Khaodhiar, S., **2013**. Effects of Surface Functional Groups and Porous Structures on Adsorption and Recovery of Perfluorinated Compounds by Inorganic Porous Silicas. *Separation Science and Technology (Philadelphia)*. 48, 775–788. DOI:10.1080/01496395.2012.710888.

[92] Watanabe, N., Takemine, S., Yamamoto, K., Haga, Y., Takata, M., **2016**. Residual organic fluorinated compounds from thermal treatment of PFOA, PFHxA and PFOS adsorbed onto granular activated carbon (GAC). *Journal of Material Cycles and Waste Management*. 18, 625–630. DOI:10.1007/s10163-016-0532-x.

[93] Watanabe, N., Takata, M., Takemine, S., Yamamoto, K., **2018**. Thermal mineralization behavior of PFOA, PFHxA, and PFOS during reactivation of granular activated carbon (GAC) in nitrogen atmosphere. *Environmental Science and Pollution Research*. 25, 7200–7205. DOI:10.1007/s11356-015-5353-2.

[94] Falciglia, P.P., Roccaro, P., Bonanno, L., De Guidi, G., Vagliasindi, F.G.A., Romano, S., **2018**. A review on the microwave heating as a sustainable technique for environmental remediation/detoxification applications. *Renewable and Sustainable Energy Reviews*. 95, 147–170. DOI:10.1016/j.rser.2018.07.031.

[95] Falciglia, P.P., Malarbì, D., Maddalena, R., Greco, V., Vagliasindi, F.G.A., **2017**. Remediation of Hg-contaminated marine sediments by simultaneous application of enhancing agents and microwave heating (MWH). *Chemical Engineering Journal*. 321, 1–10. DOI:10.1016/j.cej.2017.03.097.

Chapter 4: Microwave regeneration of granular activated carbon saturated with PFAS

Abstract

This study investigates the regeneration of PFAS-saturated granular activated carbon (GAC) by microwave (MW) irradiation. For this purpose, two commercially available GACs (Calgon Filtrasorb 400 and Norit Hydrodarco 3000) were saturated with perfluorooctanoic acid (PFOA) and perfluorooctane sulfonic acid (PFOS) and then irradiated at different MW conditions (applied power = 125 - 500 W, irradiation time = 3 - 12 min). The performance of MW regeneration for PFOS- or PFOA-saturated GAC was assessed by evaluating the variation of GAC adsorption capacity (regeneration efficiency, RE) and weight loss percentage (WL). Moreover, the effect of MW irradiation on GAC textural properties (e.g., surface area and pore volume) were evaluated through N_2 adsorption isotherms. Additionally, five successive adsorption/regeneration cycles were carried out at the best MW operational condition (500 W, 3 min). The potential degradation pathways of PFOS and PFOA were also discussed.

Both GACs exhibited a strong ability to convert MW irradiation into a rapid temperature increase (~150 °C min^{-1} at 500 W). The highest values of RE (>90%) for both PFOA- and PFOS-saturated GACs were obtained at MW irradiation of 500 W for 3 min.

It is noteworthy that the highest RE did not occur when the highest temperatures (> 750 °C) were reached (375 W, 6 min) due to the damage of GAC porous structure, particularly for H3000. After five cycles, the observed values of RE (~65%) and a moderate weight loss (<7%) demonstrated the good performance of MW irradiation for regenerating PFOA- and PFOS-saturated F400. Conversely, the higher weight loss obtained for H3000 samples does not recommend its application on several cycles. The obtained findings pointed out that MW irradiation is a promising alternative regeneration technique for PFAS-saturated GAC.

Keywords: Adsorption, granular activated carbon (GAC), microwave (MW) irradiation, Poly- and perfluoroalkyl substances (PFAS), regeneration.

1. Introduction

Poly- and perfluoroalkyl substances (PFAS) are a class of anthropogenic compounds that attracted attention worldwide as contaminants of high concern [1,2]. Over several decades, they have been used in an array of formulations for the manufacture of several commercial products such as fire-fighting foams, food packing, stain repellents, and non-stick cookware [3,4]. The widespread use of PFAS is certainly ascribable to their unique properties such as chemical-thermal stability and hydrophilic-lipophilic nature imparted by chemical composition [5,6]. PFAS structure is made up of a C-F chain of varying length and it also includes a charged functional group attached at one end (e.g., carboxylic or sulfonic acid) [4,7]. Consequently, PFAS are categorized into long-chain and short-chain, according to C-F chain length [8], and into perfluoroalkyl carboxylic acids (PFCAs) and perfluoroalkyl sulfonic acids (PFSAs), according to the type of functional group [4,5].

Recently, PFAS have been called "forever chemicals" due to their persistence and mobility in environment as well as their toxicity for human and wildlife [9,10]. Their occurrence in water bodies is the result of consumer-product degradation, firefighting activities, and discharges of fluorochemical manufacturing facilities [8,11]. Consequently, PFAS have been detected worldwide at μg L^{-1} or even mg L^{-1} levels at some contaminated sites [3,6]. Amongst long-chain PFAS, perfluorooctanoic acid (PFOA) and perfluorooctane sulfonic acid (PFOS) were the most widely used and, although their production has been banned, they are currently detected in groundwater, surface water, wastewater, and even tap water throughout the world [6,12]. The need for efficient PFAS removal from water is growing as a result of increasing regulatory attention and general concern regarding the exposure effects [13,14].

Adsorption using granular activated carbon (GAC) is the most widely applied technique for PFAS removal, employed both as single process of point-of-use applications and as step of water treatment plants [6,15,16]. However, data collected from full-scale treatment plants (both drinking and wastewater facilities) suggested a rapid breakthrough of PFAS, specifically for short-chain compounds, resulting in a fast saturation of GAC [17–19]. Consequently, GAC replacement is required. Conventionally, PFAS-exhausted GACs were incinerated and disposal, which could also lead to a secondary contamination path.

From an environmental and sustainability standpoint the regeneration of exhausted AC is a more attractive alternative.

The regeneration should allow the increase in GAC lifetime, renewing its adsorption capacity by removing the adsorbed PFAS [6]. It is noteworthy that the regeneration of PFAS-exhausted GAC is a very challenging task for both water utilities and activated carbon manufactures. Among regeneration techniques, the chemical regeneration, using a solution of sodium salts and organic alcohol, could

allow the desorption of both PFAS anion head and the hydrophobic C-F chain [20,21]. However, the use of organic alcohol is harmful to full-scale applications and, consequently, on-site regeneration is not feasible [6]. Furthermore, the management of eluate having high PFAS concentration should be also highlighted as a limiting factor for chemical regeneration. Over the years, the thermal regeneration of exhausted GAC has been extensively performed 800 - 1000 °C under mildly oxidizing atmospheric conditions (usually carbon dioxide and steam) [22,23]. However, these conditions lead to a considerable amount of carbon lost (5 - 15%) by attrition, burn-off and washout, and, in turns, to a decline in the adsorption capacity [22]. Furthermore, thermal regeneration under oxidative gases negatively affects carbon porous structure (e.g., a decrease in micropore volume and a shift to pores of narrower sizes) and it may lead to changes in carbon functional groups. The carbonization of adsorbates may also result in pore blockage due to coke formation [24]. The delivery of exhausted GAC through a long distance to a specialized treatment plant along with high energy consumption results in a higher operation cost.

Therefore, the development of alternative regeneration techniques for PFAS-exhausted GAC is strongly encouraged in order to: (i) avoid the harmful secondary pollution after landfill disposal, (ii) save costs related to GAC replacement, (iii) renew GAC adsorption capacity ensuring the preservation of its porous structure [25].

Developed for radar and communication purposes, microwave (MW) irradiation is a well-established technology alternative to conventional heating. Furthermore, it has been recently proposed as potentially viable for regenerating GAC saturated with both organic and inorganic compounds [26–29]. Comparing with conventional thermal heating, MW irradiation offers several advantages: interior heating, higher heating rates, selective heating, greater control of the heating process, no direct contact between the heating source and heated materials, and reduced equipment size and waste [30]. Previous experimental studies have pointed out that the MW regenerated material out-performed the conventionally regenerated carbon [24,31].

The major driving force is the dielectric nature of materials (i.e., activated carbon) which allows the conversion of low power irradiation energy into a rapid temperature increase [32,33]. Its heating capacity at the molecular level leads to a reduction in treatment time and energy consumption [26,27]. Jointly with high GAC dielectric features, high mechanical strength and a good resistance towards heat and radiation are other essential features for promoting GAC regeneration by MW irradiation [28,34,35].

The aim of the present study is to investigate the regeneration of PFAS-saturated GAC by means of MW irradiation. With this purpose, two commercially available GACs were artificially saturated with the main detected long-chain PFAS (i.e., PFOA and PFOS) and successive adsorption/regeneration

cycles were carried out at the bench-scale. MW regeneration was performed at several MW power levels and irradiation times in order to obtain the regeneration efficiency and GAC weight loss. Afterwards, the best operating condition was selected in order to carry out 5 successive adsorption/regeneration cycles. Furthermore, the changes in GAC textural properties (e.g., surface area and pore volume) after MW irradiation were analysed in order to evaluate the MW effect on GAC porous structure.

To the best of our knowledge, this is the first time that the feasibility of MW irradiation is tested for the regeneration of GAC saturated with PFAS.

2. Materials and methods

2.1 Materials

Two commercially available GAC Calgon Filtrasorb 400 (F400) and Norit Hydrodarco 3000 (H3000) were selected for the experiments (Table 1). F400 (microporous) and H3000 (meso/microporous) were obtained from steam activation of bituminous coal and lignite coal, respectively. Both GACs have been extensively tested in PFAS removal studies and they are currently employed at water treatment facilities [13,36–38]. As-received GACs were washed in deionized water several times, dried at 100 °C overnight and then stored in a desiccator until use. The dried GACs were sieved at 10 - 20 mesh size in order to obtain a fraction from 0.85 to 2 mm.

Table 1 Features of GACs used for the experiments.

	Norit Hydrodarco 3000 (H3000)	**Calgon Filtrasorb 400 (F400)**
Base material (-)	Lignite coal	Bituminous coal
Iodine number (mg g^{-1})	500	1000
Abrasion resistance (AWWA) (%)	min. 70	min. 75
Moisture (as packed) (%)	max. 8	max. 2
Apparent density, vibrating feed (g mL^{-1})	0.38	0.49
Uniformity coefficient (-)	2.1	1.9

PFOS (CAS n. 1763-23-1, ≥ 96% purity) and PFOA (CAS n. 335-67-1, ≥ 96% purity) were purchased from Sigma Aldrich. Liquid chromatography (LC) - grade ammonium acetate, acetonitrile and water were purchased from Fischer Scientific. Table 2 reports the physicochemical properties of PFOA and PFOS investigated in this study.

Table 2 The physicochemical properties of long-chain PFAS investigated (i.e., PFOS and PFOA).

Compound name (CAS No.)	**Formula**	**MW (g mol^{-1})**	**Log K_{ow}**	**Solubility in water (mg L^{-1})**	**Vapor pressure (mm Hg at 25 °C)**	**pKa**	**Boiling point (°C)**	**Melting point (°C)**	**Density (g mL^{-1})**
Perfluorooctane sulfonic acid (PFOS) (1763-23-1)	$C_8F_{17}SO_3H$	500.126	4.49	$3.2 \cdot 10^{-3}$ (at 25°C)	$2 \cdot 10^{-3}$	< 1.0	249	n.a.	n.a.
Perfluorooctanoic acid (PFOA) (335-67-1)	$C_7F_{15}COOH$	414.07	4.8	2290 (at 24 °C)	$3.16 \cdot 10^{-2}$	-0.5 – 4.2	192	54.3	3300 (at 24 °C)

n.a. not available.
PubChem (URL: https://pubchem.ncbi.nlm.nih.gov);
Hazardous Substances Data Bank (HSDB) (URL:https://toxnet.nlm.nih.gov).

2.2 Adsorption and MW regeneration experiments

In order to obtain PFOA- and PFOS-saturated GAC (both F400 and H3000), GAC samples were artificially saturated with high concentrated (500 mg L^{-1}) solution of PFOA or PFOS in deionized water, to ensure that the active sites on GAC inner surface were fully occupied [39,40]. Five g of GAC (F400 or H3000) were added to 200 mL of solution (PFOA or PFOS in deionized water), the mixture

was kept stirred (180 rpm) at room temperature (25 ±1 °C) for 24 h to ensure that the equilibrium is established, as also suggested by preliminary tests and in agreement with previous experimental studies reported in literature [37,41]. After the saturation procedure, aqueous samples were withdrawn and centrifugated before analysis through Liquid Chromatography/Mass Spectrometry (LC/MS) (as described in "Analytical methods" section) in order to measure the remaining concentration of compound in solution. Afterwards, the amount of PFOA and PFOS adsorbed by F400 and H3000 was calculated as follows:

$$q=\frac{V(C_0-C_f)}{m} \quad (1)$$

where, q is the adsorption capacity (mg g^{-1}), C_0 (mg L^{-1}) and C_f (mg L^{-1}) are the initial and final concentrations of each compound in the solution, respectively. Whereas, V (L) is the volume of the solution and m (g) is the GAC mass. PFOA- or PFOS-saturated F400 and H3000 were separated from liquid solution through vacuum filtration and transferred into ceramic crucible for the next regeneration phase.

A modified domestic 2.45 GHz - MW oven (Panasonic, NN-SN77HS) equipped with cyclonic inverter owing a maximum power of 1.25 kW was employed for the saturated GAC - regeneration purpose. The temperature (T, °C) reached by GACs after MW irradiation was recorded through a k-type thermocouple.

The main key parameters for the MW regeneration such as irradiation power (W) and irradiation time (min) were selected based on the temperatures reached by GACs during MW irradiation. Indeed, before performing MW regeneration of PFAS-saturated GAC, 5 g of F400 and H3000, separately, were subjected to MW irradiation at different power levels (from 125 to 500 W) and irradiation times (from 3 to 12 min) to study the temperature profiles. Then, the value of 600 °C (or above) was selected as target temperature, which should allow the complete degradation of PFOA and PFOS [42–44]. Consequently, for the regeneration purpose, the MW irradiation conditions (power and irradiation time) were selected to ensure the achievement of target temperature.

The dried regenerated GAC was employed in the next adsorption process and a small amount (~20 mg) was used for GAC characterization (as reported in section 2.3). Subsequent adsorption tests were carried out as reported above.

The efficiency of MW regeneration was evaluated by means of the regeneration efficiency (RE, %) and the single-step desorption efficiency (SSDE, %). Specifically, SSDE allows to understand the desorption of PFOA and PFOS among different cycles, whereas RE enables to study the evolution of the overall yield of MW regeneration.

The RE was calculated as followed:

$$RE=\frac{q_i}{q_0}\cdot 100 \quad (2)$$

Where q_i is the adsorption capacity of the MW regenerated GAC and q_0 is the adsorption capacity of the virgin GAC. Whereas, the SSDE was determined by:

$$SSDE=\frac{q_n}{q_{n-1}}\cdot 100 \quad (3)$$

Where q_n and q_{n-1} are the adsorption capacities of the MW regenerated GAC in a given cycle n and in the previous regeneration cycle (n-1), respectively.

Besides the RE and SSDE, GAC weight loss percentage (WL, %) represents another important parameter could affect the applicability of MW for the regeneration of PFOA- and PFOS-saturated GAC. It was calculated as:

$$WL=\frac{w_0-w_t}{w_0}\cdot 100 \quad (4)$$

Where w_0 and w_t are the mass of GAC (g) before and after MW irradiation, respectively.

The operating conditions (i.e., irradiation power and irradiation time), which allow the achievement of the highest RE and the lowest WL values, were selected for the successive five adsorption-regeneration cycles.

2.3 GAC characterization

The surface areas, pore volumes and pore size distributions of GAC samples (before and after MW irradiation) were measured by nitrogen physisorption data at 77 °K after degassing the samples at 298 °K for 10 h with ASAP 2020 analyzer (Micromeritics Instrument Corp. U.S.). Particularly, Brunauer-Emmett-Teller (BET) theory was used to calculate the specific surface area, whereas the pore size distribution of GAC samples were determined from the nitrogen isotherms using the Density Functional Theory (DFT) [45,46].

2.4 Analytical method

The determination of PFOA and PFOS was conducted using the method described by Park et al. [13], with few modifications. Specifically, the high-volume direct injection was performed using a Liquid Chromatography coupled to ESI-triple Quadrupole Mass Spectrometer (Agilent 6470 LC/TQ) operated in the negative ionization mode. The mobile phase (in LC grade solvents) was: A) 100 mM ammonium acetate in water (pH 10); B) acetonitrile. A combination of 50% of A and 50% of B was delivered at a flow rate of 0.4 mL min^{-1} by the binary pump.

An Agilent ZORBAX RRHD Eclipse Plus C18 column (2.1 × 100 mm, 1.8 µm particle size) was installed at the Binary pump. Moreover, polytetrafluoroethylene-free vials, caps, and septa were used to reduce PFAS background. Data acquisition was performed in Multiple Reaction Monitoring (MRM) mode. For each compound, two MRM transitions (PFOS: 499/80, 499/99; PFOA: 413/169, 413/369) were used for quantification and confirmation, receptively.

Due to the highest concentration used in the present study, samples were diluted with LC grade water to obtain concentrations ranging between 5-500 µg L^{-1}. Afterwards, calibration curves were constructed and the correlation coefficients (R^2) of the calibration curves for PFOS and PFOA were >0.98.

3. Results and discussion

3.1 GAC temperature profiles and weight loss across MW irradiation

The variation of GACs temperature with irradiation times at different power levels is shown in Figure 1. The comparison of the temperature profiles reveals that both F400 and H3000 have the same trend, where temperature increases with increasing the irradiation time and power. However, H3000 reached higher temperature than F400 when the MW power was 375 W for irradiation time longer than 3 min. Moreover, at the highest power investigated (500 W), the increase in temperature (°C) with irradiation time (min) was swifter in H3000 than F400 (156 and 146 °C min^{-1}, respectively). Deeply, among the operational conditions investigated, the irradiation at 500 W for 5 min allowed the achievement of the highest GAC temperatures, which were 730 and 780 °C on F400 and on H3000, respectively. However, the rapid conversation of the MW irradiation into GAC temperature increase is clearly displayed in the initial part of the curves (Figure 1). Regardless of power applied, both GACs reached the minimal value of 250 °C after 1 min of irradiation, which correspond to a T increase ratio of 250 °C min^{-1}. This sharp rise of GAC temperature within short irradiation times is the main key factor in the whole regeneration process. When GAC samples were irradiated at the highest power level (500 W) for 5 min, they reached the highest temperature of ~800 °C, became incandescent with a bright-red colour (Inset Figure1b).

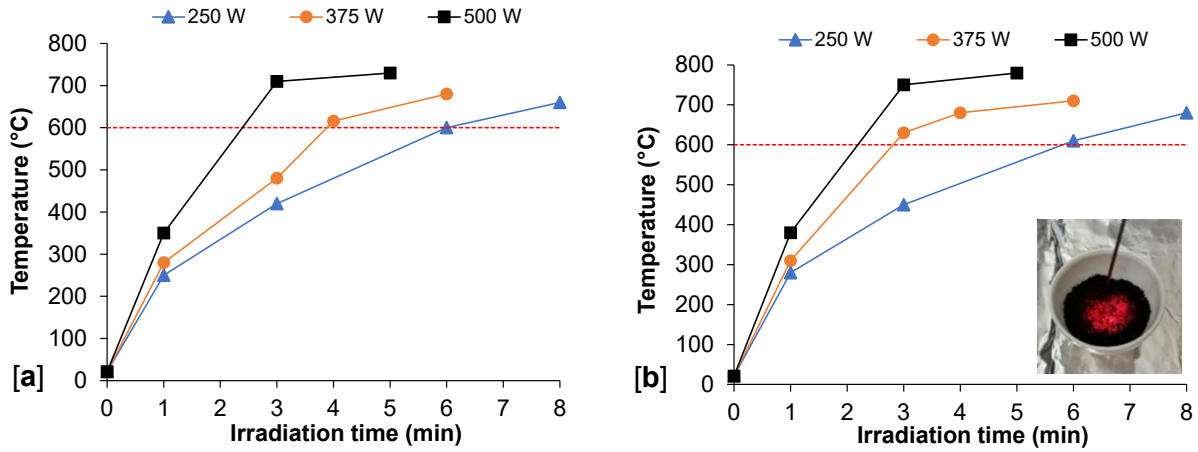

Figure 1 Temperature profiles of F400 [**a**] and H3000 [**b**] at 3 different power levels (250, 375 and 500 W). Inset: image of GAC sample turned red at the highest temperature reached.

The difference in temperature observed for the different GAC samples (F400 and H3000) may be ascribed to their different superficial chemical composition. For instance, the oxygen content of H3000 is higher than that of F400, 8.7% and 5.9% respectively [46,47]. Considering that most of oxygen functionalities are polar functional groups, which are more prone to absorb MW energy than nonpolar

ones [48]. This evidence might explain the highest temperature reached in H3000 by MW dielectric heating.

As previously pointed out by Ania et al. [33], the percentage of carbon weight loss mainly depends on nature of adsorbents (e.g., base material) and the temperature reached by AC during the irradiation, beyond the nature of adsorbate if the irradiation is carried out on saturated AC. Consequently, the variation of WL with T reached on F400 and H3000 samples (irradiated at several power levels and irradiation times) is given in Figure 2.

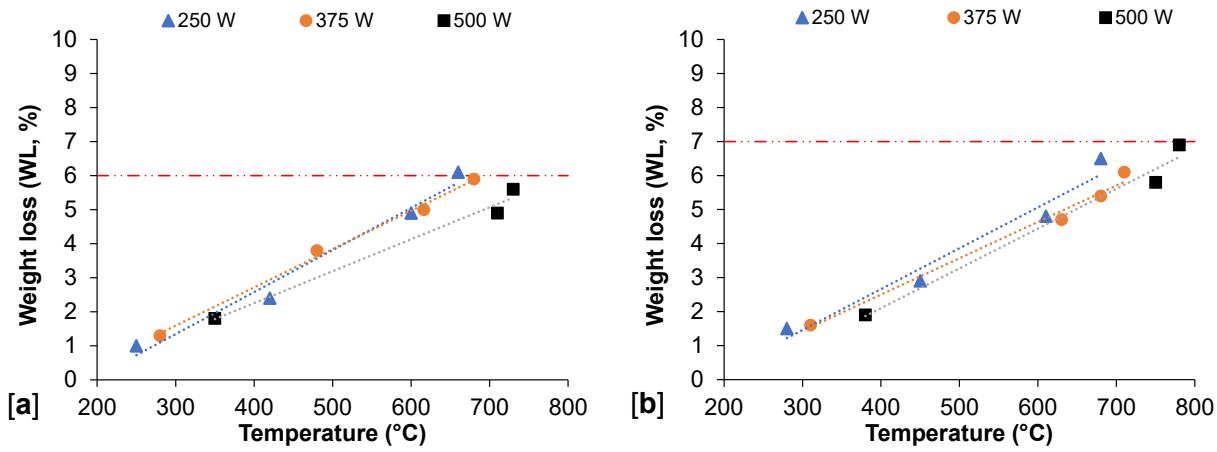

Figure 2 Variation of weight loss with GAC temperature ([**a**] F400, [**b**] H3000).

Figure 2 reveals that the GAC weight loss (WL, %) increases linearly with the increase in T (R^2>0.98). However, the highest WL were 6.1% and 6.9% for F400 and H3000, respectively.

GAC WL is one of the main factor affecting the scaling-up of the investigated technology, especially in order to calculate the cost for GAC replacement, as previously demonstrated by Falciglia et al. [49]. Clearly, WL – T relationship may also be useful in the selection of commercially available GACs. At a comparable value of adsorption capacity for a target compound, AC characterized by lower WL and sharp T rise should be preferred since it is more prone to MW irradiation and to thermal regeneration as a whole.

Among the different experimental conditions investigated, six combinations of power (W) and irradiation time (t, min) were selected for the regeneration of PFAS-saturated GAC. Further details regarding the MW irradiation conditions investigated for PFOA- and PFOS-saturated GACs (both F400 and H3000) are provided in Table 3. Moreover, according to Eq. 12 [50], the selected combinations of power and irradiation time corresponds to a total consumed energy (E) in the 0.025 - 0.038 kWh range. Specifically, the highest E is achievable applying a power of 375 W for an irradiation time of 6 min, whereas the lowest one is attained when GAC samples were irradiated at 125 W for 12 min, 250 W for 6 min, or 500 W for 3 min. Such MW irradiation conditions were based on the criterion of maintaining the GAC (both F400 and H3000) temperature over 600 °C, which

would allow the PFOA and PFOS desorption [42–44]. It should be highlighted that when F400 and H3000 were irradiated at 125 W for 12 min, the GAC temperatures were much lower than 600 °C (~300 °C). However, this combination of power and time (125 W for 12 min) was selected as control experiment to better understand the PFAS desorption process.

Table 3 Experimental conditions of MW irradiation for PFOA- and PFOS-saturated GACs (both F400 and H3000).

Experimental conditions	Power (Watt)	Irradiation time (min)	Total consumed energy (kWh)	Temperature reached ≥ 600 °C
1	125	12	0.025	NO
2	250	6	0.025	YES
3	250	8	0.033	YES
4	375	4	0.025	YES
5	375	6	0.038	YES
6	500	3	0.025	YES

3.2 MW regeneration of PFOA-saturated GACs

The results from batch adsorption experiments pointed out that the adsorption capacity of PFOA was 19.95 mg g^{-1} on virgin F400 and 21.94 mg g^{-1} on virgin H3000. PFOA-saturated F400 samples and PFOA-saturated H3000 samples were irradiated at several MW operational conditions (Table 3). Temperature, weight loss and regeneration efficiency of PFOA-saturated GACs observed are depicted in Figure 3. As expected, PFOA-saturated GAC samples (F400 and H3000) irradiated at 125 W for 12 min reached temperature of 268 and 340 °C, respectively, far from the target temperature of 600 °C (Figure 3a). This also corresponded to the lowest WL found. Specifically, PFOA-saturated F400 sample shown a WL lower than 2%, whereas the WL of PFOA-saturated H3000 sample was 6.5% (Figure 3a). As a whole, PFOA-saturated H3000 samples exhibited higher WL than PFOA-saturated F400 samples, although in some cases the temperatures reached by GAC samples were almost the same (e.g., MW irradiation at 250 W for 6 and 8 min). Moreover, the highest T were reached for both PFOA-saturated H3000 and PFOA-saturated F400 samples (753 and 685 °C, respectively) when the power of 375 W was applied for 6 min.

Overall, the temperatures recorded at the end of the MW regeneration process (for both F400 and H3000) were almost similar to that reached for the virgin GACs when irradiated at the same conditions (Figure). This evidence suggests that the presence of adsorbed PFOA slightly contributes to the conversion of electromagnetic energy into heat during MW irradiation. Consequently, it could be inferred that GAC acts as the major MW-absorbing phase in agreement with previous literature findings [31,51].

The regeneration efficiency (RE) calculated according to Eq.2. for PFOA-saturated F400 and H3000 as a function of different MW powers and irradiation time is shown in Figure 3b. Barring two outliers

(obtained for 125 W - 12 min and 375 W - 6 min, separately discussed), the RE values are in the range of 75-94% for both the PFOA-saturated F400 and H3000.

The lowest values of RE (<30%) were obtained when PFOA-saturated GAC samples (F400 and H3000) were irradiated at 125 W for 12 min. This combination of MW power and irradiation time, which corresponds to a total consumed energy of 0.025 kWh, seems to be unsuitable for regenerating PFOA-saturated GAC due to the low temperatures reached (Figure 3a). The unsatisfactory regeneration at 125 W for 12 min was also proven by GAC textural characterization after MW irradiation, as detailed below. Based on RE values obtained, it can be argued that the highest MW regeneration efficiency did not occur at the highest total power consumed (0.038 kWh), which was obtained for a MW irradiation of 375 W (6 min). At this irradiation condition, the highest temperatures have been reached by PFOA-F400 and PFOA-H3000 (685 and 753°C, respectively). Nevertheless, RE for PFOA-F400 was 74.3% and RE for PFOA-H3000 was 60.3% (Figure 3b).

The RE values of MW irradiation for regenerating PFOA-saturated GAC are similar to that obtained in previous experimental studies after 1 adsorption/regeneration cycles, in which MW irradiation was investigated for the regeneration of AC samples saturated with organic (e.g., methylene blue, phenol, chloramphenicol) [24,39,40] and inorganic compounds (e.g., cesium) [32,49].

Those findings corroborate that MW irradiation could effectively regenerate PFOA-saturated GAC, although further investigations are needed to better understand the desorption mechanisms established due to the unique chemical properties of PFAS. However, the PFOA desorption mechanisms along with its degradation pathways during MW irradiation are theoretically discussed in Section 3.5.

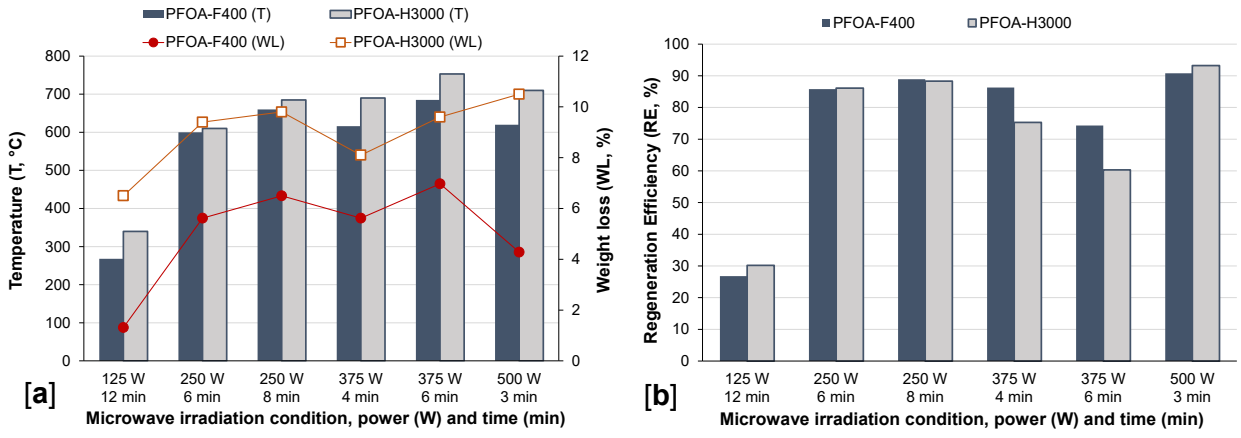

Figure 3 Temperature, weight loss [**a**] and regeneration efficiency [**b**] of PFOA-saturated GAC (F400 and H3000) for the different MW irradiation conditions investigated.

As discussed below, the temperature higher than 600 °C might have a detrimental effect on its porous structure and the damage degree of GAC is related with the regeneration temperature [33]. This evidence corroborates that the temperature reached by GAC during MW irradiation is linked with

MW regeneration efficiency and it represents an important parameter for the whole MW regeneration since GAC porosity can be damaged at high temperature [39]. Further data that supports this statement is provided by the change in textural properties of GAC samples after MW regeneration. With this purpose, the effect of MW regeneration, performed at different irradiation conditions, on GAC samples (PFOA-F400 and PFOA-H3000) was evaluated by means of nitrogen adsorption isotherms. The comparison of BET area and pore volume for regenerated and virgin GAC samples is shown in Figure 4.

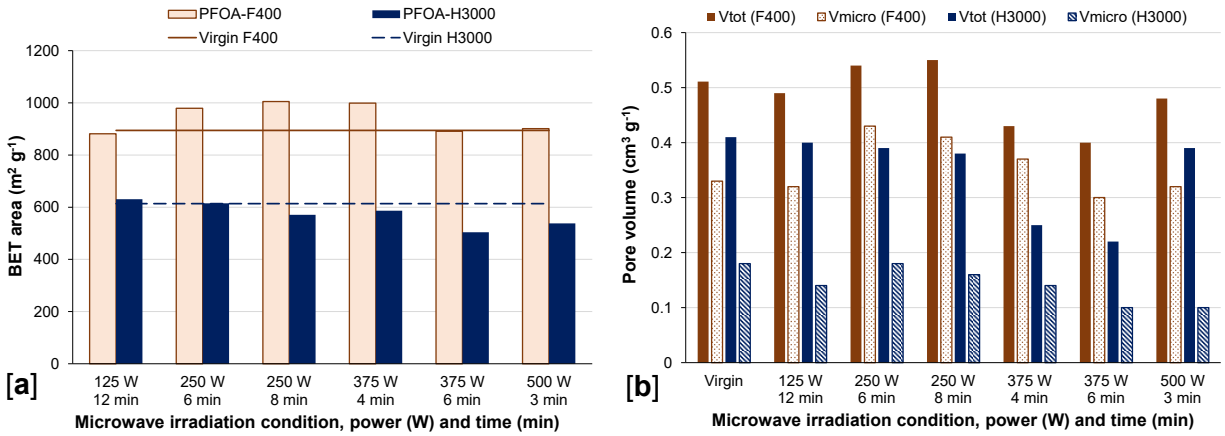

Figure 4 BET area of virgin GAC samples (F400 and H3000) and after MW regeneration at different irradiation conditions (PFOA-F400 and PFOA-H3000) [**a**]; Total pore volume (Vtot) and micropore volume (Vmicro) of virgin GAC samples (F400 and H3000) vs. the regenerated ones (PFOA-F400 and PFOA-H3000) [**b**].

The comparison of BET area reveals that F400 MW regenerated samples had a BET area equal or higher than the virgin ones (Figure 4a), demonstrating a good preservation of the F400 porous structure. Whereas, the BET area of H3000 samples was equal or lower than that of virgin H3000, indicating that H3000 was partially restored to the virgin condition. This difference could be ascribed to the higher impact of MW irradiation on H3000 matrix, due to the larger presence of functional oxygen groups [47]. As reported elsewhere [28,48,52], upon heating, a large amount of gases (coming from desorption of volatiles and the decomposition of oxygen-containing groups) are evolved. As a result, the H3000 porous structure is more modified than F400, also depending on the extent of MW irradiation.

The highest BET area and pore volume (total pore volume and micropore volume) for F400 saturated PFOA were observed for a MW power of 250 W applied for 8 min, whose values exceed those of virgin GAC. At this irradiation condition, the MW regeneration efficiency for PFOA-saturated F400 was ~90% (Figure 3b).

Otherwise, the highest fall of BET area in PFOA-saturated H3000 occurred when MW irradiation was performed at 375 W for 6 min. The decrease in BET area observed for H3000 regenerated samples was also found for total pore volume. This suggests that the MW irradiation created a residual

deposit in H3000 pores, which blocked the porosity and reduced both BET area and total pore volume [53]. The harsh regeneration condition applied, at which the temperature of 753 °C was reached, also contributed to the damage of H3000 porous structure. This deterioration of H3000 sample, irradiated at 375 W for 6 min, negatively affected the adsorption capacity of regenerated H3000, as demonstrated by not high value of RE obtained (~60%, Figure 3b).

3.3 MW regeneration of PFOS-saturated GACs

From batch adsorption experiments, similar PFOS adsorption capacities was obtained on virgin F400 and virgin H3000, they were 19.83 and 19.97 mg g^{-1}, respectively. As reported above, after the saturation procedure, PFOS-saturated F400 samples and PFOS-saturated H3000 samples were subjected to MW regeneration (according to the irradiation conditions provided in Table 3). Temperature, weight loss percentage and regeneration efficiency for PFOS-saturated GACs are reported in Figure 5. As previously obtained for PFOA-saturated GAC samples, H3000 saturated with PFOS reached higher temperature than F400 when both GAC were irradiated at the same MW power and irradiation time.

As a whole, when PFOS-saturated H3000 have been regenerated through MW irradiation it reached a temperature higher than 700 °C, whereas the temperature of PFOS-saturated F400 was lower than 700 °C. However, a power of 125 W and irradiation time of 12 min did not allow the achievement of the target temperature of 600 °C (T=240 °C in PFOS-saturated F400, T=370 °C in PFOS-saturated H3000). This evidence suggests that a higher energy is required to heat GAC samples and consequently to enhance the regeneration of PFOS-saturated GAC, as also demonstrated by the lowest RE obtained (both F400 and H3000, Figure 5b).

By comparing the temperature profiles (Figure 5a vs Figure 1), it can be noted PFOS-saturated GAC samples (both F400 and H3000) reached almost the same temperature of virgin GACs irradiated at the same power and irradiation time. Consequently, it could assert that the impact of PFOS as well as PFOA adsorbed on the heating of F400 and H3000 is negligible. However, further characterizations related to dielectric properties of PFOS and PFOA will be useful to understand the mechanisms heating of PFAS-saturated GAC.

The RE of MW irradiation for PFOS-saturated F400 and PFOS-saturated H3000 are reported in Figure 5b. Despite the higher temperature reached, the RE values for PFOS-saturated H3000 resulted slightly lower than that obtained for F400. Specifically, the RE values for PFOS-saturated F400 were equal or greater than 80% (expect for MW irradiation at 125 W for 12 min due to the low temperature reached by F400). At the highest power (500 W) applied for the shortest irradiation time (3 min), the RE values were higher than 90% for both PFOS-saturated GAC samples (Figure 5b). However, the

lowest WL for F400 samples (4% vs. 10.5% in H3000) encourages its application for the investigation of the 5 successive adsorption/regeneration cycles (Section 3.4).

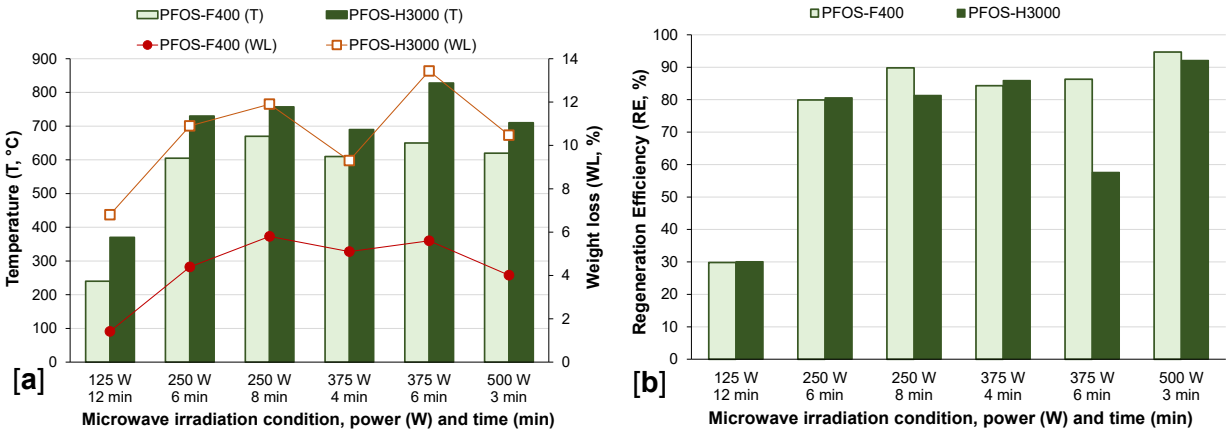

Figure 5 Temperature reached by PFOS-saturated GAC (F400 and H3000) and the percentage of weight loss at several MW irradiation conditions [**a**]; Regeneration efficiency for PFOS-saturated F400 and H3000 samples after MW regeneration [**b**].

As previous pointed out for PFOA-saturated GAC samples, the obtained RE after 1 adsorption/regeneration cycle for PFOS-saturated GAC are in good agreement with those inferred from previous experimental studies carried out on AC saturated with both organic and inorganic compounds [24,32,39,40]. In order to better figure out the PFAS regeneration through MW irradiation, PFOS desorption mechanisms and the potential degradation pathways over MW are conceptually addressed in section 3.5.

The variation of RE across MW regeneration performed at different power and irradiation time reflects the change in BET area and total pore volume of irradiated GAC samples compared to virgin ones. GAC porous structure after MW regeneration depends on PFOS removal rate and also on the deposition of regeneration residues, which blocked carbon pores [31,53]. This statement is supported by obtained results given in Figure 6, related to BET area and pore volume of PFOS-saturated F400 and H3000 before and after MW regeneration.

Looking at PFOS-saturated GAC (both F400 and H3000) irradiated at 500 W for 3 min, a slight increase in total pore volumes and a decrease in the micropore volume could be highlighted (Figure 6). Those decreases indicate that micropores merged to form mesopores [54,55]. However, the BET areas are almost unchanged since the contribution of mesopores to the BET area is small compared to micropores [31]. The development of mesoporosity directly enhances the adsorption kinetics since mesopores are more easily accessible by large molecules (i.e., PFOS and PFOA) than microporous. As a result, the highest RE for PFOA- and PFOS-saturated GAC samples (i.e., F400 and H3000) were obtained at power of 500 W and irradiation time of 5 min (Figure 3b and 5b). The further increase in regeneration temperature for PFOS-saturated H3000 (obtained at 375 W for 6 min) results in damages

to the pore structure of original carbon (decrease of both BET area and pore volume), lowering the adsorption capacity as demonstrating by RE < 60%.

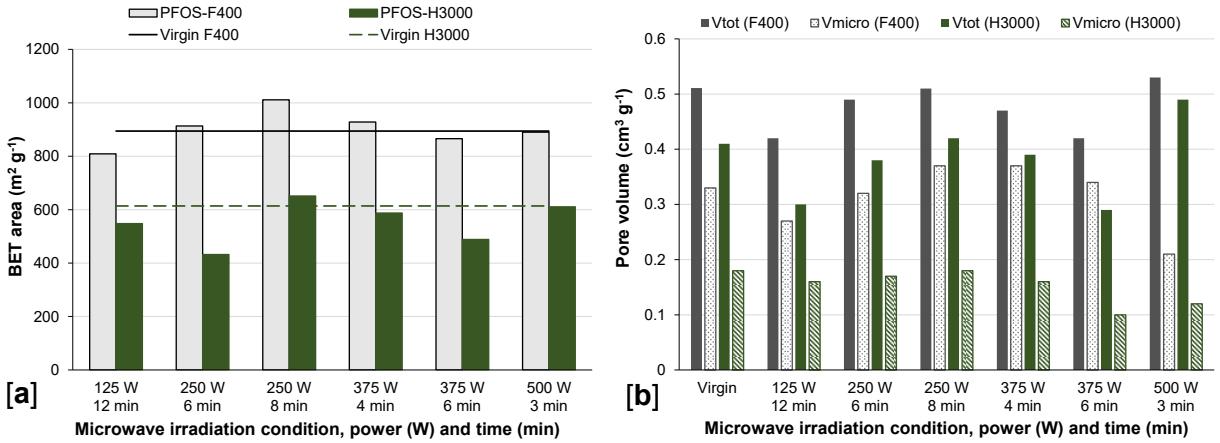

Figure 6 BET area of virgin GAC samples (F400 and H3000) and after MW regeneration at different irradiation conditions (PFOS-F400 and PFOS-H3000) [**a**]; Total pore volume (Vtot) and micropore volume (Vmicro) of virgin GAC samples (F400 and H3000) vs. regenerated ones (PFOS-F400 and PFOS-H3000) [**b**].

The efficiency of MW regeneration (in terms of RE) obtained in the present study could be compared with the regeneration percentages obtained by chemical regeneration of PFOS-saturated AC [56–59]. In previous experimental studies, the regeneration percentages higher than 80% were achieved when PFOS saturated AC samples (e.g., bamboo derived AC and coconut shell based GAC) have been chemically regenerated through a solution of ethanol or methanol (>50%) [56–59]. Indeed, a solution of organic alcohol was required to desorb the hydrophobic C-F chain. However, chemical regeneration using organic solvent is not suitable for the treatment of drinking water on full-scale applications, and consequently on-site regeneration is not feasible [6].

3.4 Investigation of adsorption-regeneration cycles for PFOA- and PFOS-saturated F400

In order to assess the performance of MW irradiation for the regeneration of GAC saturated with PFOA and PFOS, 5 successive adsorption-regeneration cycles were carried out. F400 was selected owing to its lower WL than H3000, which encourages its applicability for MW regeneration.

Among irradiation conditions investigated (Table 3), the MW power of at 125 W applied for 12 min was excluded due to its poor efficacy in terms of GAC final temperature and regeneration efficiency. It seems evident that such power applied is not enough to promote the quantitative desorption both PFOS and PFOA adsorbed on F400 samples. Similar findings were previously obtained by Ania et al. [28,33]. Otherwise, the power of 500 W and irradiation time of 3 min were selected as the best MW operational condition for the regeneration of PFOA- and PFOS-saturated F400. This combination in fact allowed to better preserve F400 porous structure, ensuring a good thermal desorption of PFOS and PFOA (RE > 90%) with the lowest WL (WL < 4.3%).

The trends observed in RE, SSDE and WL values for both PFOA- and PFOS-saturated F400 throughout 5 successive adsorption/regeneration cycles are depicted in Figure 7.

The RE values of PFOA- and PFOS-saturated F400 follow different trends. Specifically, as regards PFOA-saturated F400, the RE increases until the 3rd cycle, at which it reaches the highest value (~95%). Afterward, further adsorption/regeneration cycles led to a gradual decrease in RE, which was ~65% after the 5th cycle. Conversely, PFOS-saturated F400 irradiated at 500 W for 3 min reached the highest RE after the 1st cycle, then RE gradually decreased until 63.5% obtained after the 5th adsorption/regeneration cycle.

The single-step desorption efficiency (SSDE) provides the percentage of PFOA and PFOS desorption in each cycle, allowing to evaluate the desorption yield in the different cycles [28,60] (Figure 7). Regarding PFOS-saturated F400, the SSDE was ~90% and it remained almost constant throughout successive cycles, demonstrating a high rate of PFOS desorption. Conversely, a gradual increase followed by a sharp decrease can be observed in SSDE for PFOA-saturated F400 samples (Figure 7). This evidence suggests that PFOA desorption from regenerated F400 is easier until the 3rd cycle at which the highest RE is also obtained.

As it can be noted from Figure 7, WL increased almost linearly with MW regeneration cycles in both GAC samples (PFOS- and PFOA-saturated F400). Although the greater loss of mass carbon occurred after the 1st cycle (WL ~4%), after 5 successive cycles the WL on PFOS- and PFOA-saturated F400 was < 7%. This percentage is lower than that attributed to conventional thermal regeneration of GAC, which is in the range of 5 - 15% at each regeneration cycle [22]. Moreover, the obtained values of WL are in good agreement with previous findings related to MW regeneration of saturated GAC [32,39,61,62].

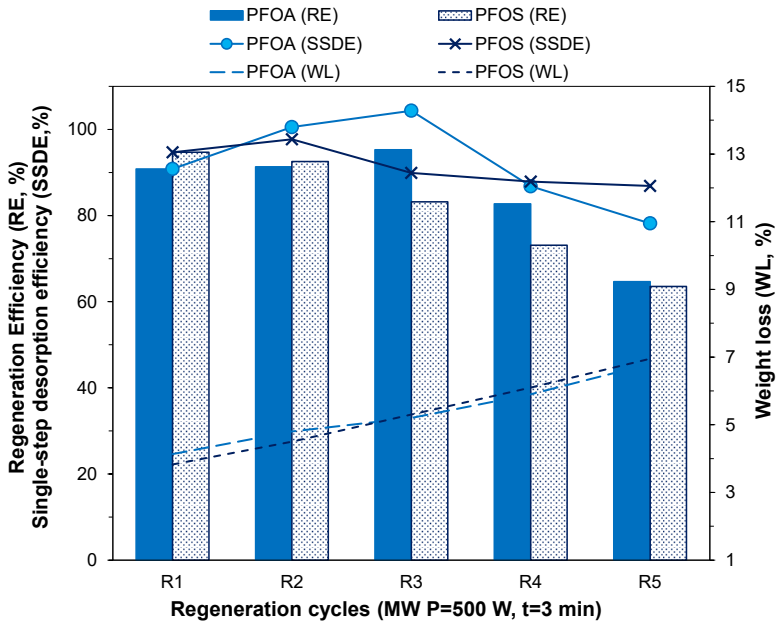

Figure 7 Regeneration efficiency (RE), Single-step desorption efficiency (SSDE) and weight loss (WL) for PFOA- and PFOS-saturated F400 throughout MW regeneration cycles (MW Power=500 W, MW irradiation time=3 min).

Textural properties of PFOA- and PFOS-saturated F400 after several adsorption/regeneration cycles are reported in Table 4.

The relevant surface physical features of the regenerated carbons (i.e., BET area and pore volume) did not differ noticeably from the virgin samples [63], as demonstrated by the percentage variation lower than 20% (Table 4). This evidence demonstrates that the application of short MW irradiation times (i.e., 3 min) could preserve the porous structure of the regenerated carbons throughout several adsorption/regeneration cycles. However, after the 3th cycle, the lack in mesoporosity (Vmeso < 0.05 cm^3 g^{-1}) may delay the migration of the PFOS molecules desorbed from F400. This is also true for the PFOA-saturated F400 after the 5th adsorption/regeneration cycle. Indeed, a fall in mesopore volume (Vmeso = 0.08 cm^3 g^{-1}) and a decrease in average pore size (~3.8 nm) occurred (

Table).

Specifically, the gradual blockage of the porous structure seemed to occur due to the fraction of adsorbed PFOA or PFOS molecules which did not evolve from the carbon surface during the regeneration after successive cycles. These molecules may remain inside the pore network of F400 and give rise to carbonaceous residues [24,29]. Consequently, the formation of coke deposits and damage to porosity may cause the decrease in the adsorption capacity of regenerated F400, as demonstrated by the decrease in RE throughout several cycles [24,32].

Table 4 Textural properties variation of PFOA- and PFOS-saturated F400 with regeneration cycles performed at 500 W for 3 min.

	Virgin F400	PFOA R1	PFOA R3	PFOA R5	PFOS R1	PFOS R3	PFOS R5
BET area (m^2 g^{-1})	894.4	901.4	893.6	1099.3	890.2	1018.1	1052.4
Total pore volume, Vtot (cm^3 g^{-1})	0.51	0.49	0.54	0.47	0.53	0.43	0.52
Micropore volume, Vmicro (cm^3 g^{-1})	0.33	0.32	0.3	0.39	0.21	0.38	0.43
Mesopore volume, Vmeso (cm^3 g^{-1})	0.18	0.17	0.24	0.08	0.32	0.05	0.09
Average pore size (nm)	4.0	4.5	4.8	3.8	5.0	3.6	3.8

R1: after 1 adsorption/regeneration cycle
R3: after 3 adsorption/regeneration cycles
R5: after 5 adsorption/regeneration cycles

3.5 Mechanistic aspects of PFAS degradation over MW irradiation and evidences supporting the feasibility of MW regeneration for PFAS-saturated GAC

In this section the possible degradation mechanisms during MW regeneration of PFAS-saturated GACs have been summarized. Due to the high temperature reached by GACs in short irradiation times, PFAS thermal desorption through volatilization and fluorine mineralization should be considered as the main removal mechanism during MW regeneration. Previous experimental studies reported in literature have been investigated the efficiency of conductive thermal treatment as remediation technique for soil contaminated with PFAS [42,43,64]. For instance, the volatilization of PFAS from soil treated using in situ thermal heating was evaluated by. Results showed that heating soil to 350°C (for 10 days) and 400°C (for 14 days) reduces PFAS soil concentrations by 99.91% and 99.998%, respectively.

Recently, the mineralization behaviour of long-chain PFAS (i.e., PFOA, PFOS and PFHxA) was studied during thermal treatment [43,65]. For instance, Watanabe et al. [43] have identified fluorine mineralization pathways that were established during thermal treatment of PFAS in reagent form and adsorbed onto GAC. Specifically, after thermal treatment under nitrogen atmosphere at 700 °C, the recoveries of mineralized fluorine in the reagent form of PFOA, PFHxA and PFOS (30, 46 and 72%, respectively) were less than that obtained when same compounds were adsorbed on GAC (51,74 and 70%) [43]. This evidence suggests the valuable effect of GAC to enhance the mineralization of PFAS during thermal treatment.

Owing to the strong interaction with MW irradiation and high thermal conductivity, ACs are effective catalysts, able to convert MW energy into thermal energy, which is then transmitted instantaneously to adsorbed chemical compounds. Furthermore, the internal grain temperatures should be higher than the external surface temperature due to the cooling down effect ($\Delta T \sim 400$ °C) [32]. The thermal gradient from the interior of the carbon particle to its cool surface allows the MW-induced reaction to proceed more quickly and effectively at a lower bulk temperature, thus saving energy and

shortening the processing time. In addition, the "hotspots" favour heterogenous reactions between the ACs and the gases taking part in the reaction (i.e., the stripping mechanism of interstitial water) [26,73]. Furthermore, as extensively demonstrated [30,31], ACs are suitable for MW heating due to the delocalized π-electrons from sp2-hybridized carbon materials. Specifically, the motion of electrons generates heat through Joule heating within the grain or arc generation at phase boundaries. Moreover, due to the elimination of the oxygenated surface functional groups after MW irradiation, the π-electron density of the graphene layers increases as well as the chemisorption contribution to the overall loading capacity of target contaminant. Although this statement was demonstrated for phenol [24], similar observation could be addressed for PFAS.

It should be noted that the available values of PFAS physical and chemical properties (e.g., vapour pressure and Henry's law constants) are mostly derived from modelling and not directly measured [5]. Consequently, the lack of consistent information regarding their chemical properties is a limiting factor to deeply understanding the fate of PFAS during thermal treatment. Therefore, further investigations are strongly encouraged.

4. Conclusion and future perspectives

The feasibility of MW irradiation for the regeneration of PFOA- and PFOS-saturated GAC was investigated in terms of regeneration efficiency, carbon weight loss and variation of GAC textural properties. The key findings were summarized as follow:

- During MW irradiation, fast temperature increases were obtained on both GACs (~150 °C min^{-1} at power of 500 W).
- The linear correlation between GAC temperatures and their weight loss percentage provides valuable information to distinguish among several GACs commercially available. The highest weight loss percentages obtained in H3000 samples negatively affects its applicability on several successive adsorption/regeneration cycles.
- Among MW irradiation conditions investigated, a power of 500 W and irradiation time of 3 min was the best performed for both PFOS- and PFOA-saturated GACs, the observed values of RE were higher than 90%.
- The enhancement in the RE may not be exclusively attributed to the complete desorption of PFOA or PFOS, but also to an increase in the overall uptake linked with changes in GAC porous structure (e.g., the development of mesoporosity), as demonstrated by the variation in pore volume.
- After five successive adsorption/regeneration cycles, the observed values of RE (~65%) jointly with a moderate weight loss (<7%) demonstrated the good feasibility of MW irradiation for regenerating PFOA- and PFOS-saturated F400.
- Both thermal desorption through volatilization and fluorine mineralization seem to occur in long-chain PFAS degradation (i.e.: PFOA and PFOS). A stepwise CF_2 flake-off manner toward related short-chain compounds should be also considered.

Consequently, the regeneration of PFAS-saturated GACs through MW irradiation is encouraged. However, due to the complexity of mechanisms established (both thermal treatment and MW-based degradation of PFAS), further investigations in this research topic are advised to overcome some knowledge gaps and to better understand the efficiency of MW regeneration in the presence of co-existing compounds (both organic matter and inorganic compounds).

At last, it should be mentioned that MW regeneration allows the overcoming of many drawbacks related to conventional regeneration techniques (e.g., the use of organic solvent in chemical regeneration, the costs related to landfill disposal of PFAS exhausted GAC).

References

[1] Brendel, S., Fetter, É., Staude, C., Vierke, L., Biegel-Engler, A., **2018**. Short-chain perfluoroalkyl acids: environmental concerns and a regulatory strategy under REACH. *Environmental Sciences Europe*. 30,. DOI:10.1186/s12302-018-0134-4.

[2] Yu, Q., Zhang, R., Deng, S., Huang, J., Yu, G., **2009**. Sorption of perfluorooctane sulfonate and perfluorooctanoate on activated carbons and resin: Kinetic and isotherm study. *Water Research*. 43, 1150–1158. DOI:10.1016/j.watres.2008.12.001.

[3] Rahman, M.F., Peldszus, S., Anderson, W.B., **2014**. Behaviour and fate of perfluoroalkyl and polyfluoroalkyl substances (PFASs) in drinking water treatment: A review. *Water Research*. 50, 318–340. DOI:10.1016/j.watres.2013.10.045.

[4] Buck, R.C., Franklin, J., Berger, U., Conder, J.M., Cousins, I.T., Voogt, P. De, Jensen, A.A., Kannan, K., Mabury, S.A., van Leeuwen, S.P.J., **2011**. Perfluoroalkyl and polyfluoroalkyl substances in the environment: Terminology, classification, and origins. *Integrated Environmental Assessment and Management*. 7, 513–541. DOI:10.1002/ieam.258.

[5] ITRC, **2017**. Naming Conventions and Physical and Chemical Properties of Per-and Polyfluoroalkyl Substances (PFAS). 1–15. DOI:10.1002/ieam.258.

[6] Gagliano, E., Sgroi, M., Falciglia, P.P., Vagliasindi, F.G.A., Roccaro, P., **2020**. Removal of poly- and perfluoroalkyl substances (PFAS) from water by adsorption: Role of PFAS chain length, effect of organic matter and challenges in adsorbent regeneration. *Water Research*. 171, 115381. DOI:10.1016/j.watres.2019.115381.

[7] Du, Z., Deng, S., Bei, Y., Huang, Q., Wang, B., Huang, J., Yu, G., **2014**. Adsorption behavior and mechanism of perfluorinated compounds on various adsorbents - A review. *Journal of Hazardous Materials*. 274, 443–454. DOI:10.1016/j.jhazmat.2014.04.038.

[8] Ateia, M., Maroli, A., Tharayil, N., Karanfil, T., **2019**. The overlooked short- and ultrashort-chain poly- and perfluorinated substances: A review. *Chemosphere*. 220, 866–882. DOI:10.1016/j.chemosphere.2018.12.186.

[9] Hölzer, J., Göen, T., Rauchfuss, K., Kraft, M., Angerer, J., Kleeschulte, P., Wilhelm, M., **2009**. One-year follow-up of perfluorinated compounds in plasma of German residents from Arnsberg formerly exposed to PFOA-contaminated drinking water. *International Journal of Hygiene and Environmental Health*. 212, 499–504. DOI:10.1016/j.ijheh.2009.04.003.

[10] Crawford, N.M., Fenton, S.E., Strynar, M., Hines, E.P., Pritchard, D.A., Steiner, A.Z., **2017**. Effects of perfluorinated chemicals on thyroid function, markers of ovarian reserve, and natural fertility. *Reproductive Toxicology*. 69, 53–59. DOI:10.1016/j.reprotox.2017.01.006.

[11] Hu, X.C., Andrews, D.Q., Lindstrom, A.B., Bruton, T.A., Schaider, L.A., Grandjean, P., Lohmann, R., Carignan, C.C., Blum, A., Balan, S.A., Higgins, C.P., Sunderland, E.M., **2016**. Detection of Poly- and Perfluoroalkyl Substances (PFASs) in U.S. Drinking Water Linked to Industrial Sites, Military Fire Training Areas, and Wastewater Treatment Plants. *Environmental Science and Technology Letters*. 3, 344–350. DOI:10.1021/acs.estlett.6b00260.

[12] Takagi, S., Adachi, F., Miyano, K., Koizumi, Y., Tanaka, H., Mimura, M., Watanabe, I., Tanabe, S., Kannan, K., **2008**. Perfluorooctanesulfonate and perfluorooctanoate in raw and treated tap water from Osaka, Japan. *Chemosphere*. 72, 1409–1412. DOI:10.1016/j.chemosphere.2008.05.034.

[13] Park, M., Wu, S., Lopez, I.J., Chang, J.Y., Karanfil, T., Snyder, S.A., **2020**. Adsorption of

perfluoroalkyl substances (PFAS) in groundwater by granular activated carbons: Roles of hydrophobicity of PFAS and carbon characteristics. *Water Research*. 170,. DOI:10.1016/j.watres.2019.115364.

[14] Kucharzyk, K.H., Darlington, R., Benotti, M., Deeb, R., Hawley, E., **2017**. Novel treatment technologies for PFAS compounds: A critical review. *Journal of Environmental Management*. 204, 757–764. DOI:10.1016/j.jenvman.2017.08.016.

[15] Shivakoti, B.R., Fujii, S., Nozoe, M., Tanaka, S., Kunacheva, C., **2010**. Perfluorinated chemicals (PFCs) in water purification plants (WPPs) with advanced treatment processes. *Water Science and Technology: Water Supply*. 10, 87–95. DOI:10.2166/ws.2010.707.

[16] Du, Z., Deng, S., Bei, Y., Huang, Q., Wang, B., Huang, J., Yu, G., **2014**. Adsorption behavior and mechanism of perfluorinated compounds on various adsorbents-A review. *Journal of Hazardous Materials*. 274, 443–454. DOI:10.1016/j.jhazmat.2014.04.038.

[17] Arvaniti, O.S., Stasinakis, A.S., **2015**. Review on the occurrence, fate and removal of perfluorinated compounds during wastewater treatment. *Science of the Total Environment*. 524–525, 81–92. DOI:10.1016/j.scitotenv.2015.04.023.

[18] Appleman, T.D., Higgins, C.P., Quiñones, O., Vanderford, B.J., Kolstad, C., Zeigler-Holady, J.C., Dickenson, E.R.V., **2014**. Treatment of poly- and perfluoroalkyl substances in U.S. full-scale water treatment systems. *Water Research*. 51, 246–255. DOI:10.1016/j.watres.2013.10.067.

[19] Quiñones, O., Snyder, S.A., **2009**. Occurrence of perfluoroalkyl carboxylates and sulfonates in drinking water utilities and related waters from the United States. *Environmental Science and Technology*. 43, 9089–9095. DOI:10.1021/es9024707.

[20] Wang, F., Lu, X., Shih, K.M., Wang, P., Li, X., **2014**. Removal of perfluoroalkyl sulfonates (PFAS) from aqueous solution using permanently confined micelle arrays (PCMAs). *Separation and Purification Technology*. 138, 7–12. DOI:10.1016/j.seppur.2014.09.037.

[21] Woodard, S., Berry, J., Newman, B., **2017**. Ion exchange resin for PFAS removal and pilot test comparison to GAC. *Remediation*. 27, 19–27. DOI:10.1002/rem.21515.

[22] Zanella, O., Tessaro, I.C., Féris, L.A., **2014**. Desorption- and decomposition-based techniques for the regeneration of activated carbon. *Chemical Engineering and Technology*. 37, 1447–1459. DOI:10.1002/ceat.201300808.

[23] Guo, Y., Du, E., **2012**. The Effects of Thermal Regeneration Conditions and Inorganic Compounds on the Characteristics of Activated Carbon Used in Power Plant. *Energy Procedia*. 17, 444–449. DOI:10.1016/j.egypro.2012.02.118.

[24] Ania, C.O., Parra, J.B., Menéndez, J.A., Pis, J.J., **2005**. Effect of microwave and conventional regeneration on the microporous and mesoporous network and on the adsorptive capacity of activated carbons. *Microporous and Mesoporous Materials*. 85, 7–15. DOI:10.1016/j.micromeso.2005.06.013.

[25] Yuen, F.K., Hameed, B.H., **2009**. Recent developments in the preparation and regeneration of activated carbons by microwaves. *Advances in Colloid and Interface Science*. 149, 19–27. DOI:10.1016/j.cis.2008.12.005.

[26] Falciglia, P.P., Roccaro, P., Bonanno, L., De Guidi, G., Vagliasindi, F.G.A., Romano, S., **2018**. A review on the microwave heating as a sustainable technique for environmental remediation/detoxification applications. *Renewable and Sustainable Energy Reviews*. 95, 147–170. DOI:10.1016/j.rser.2018.07.031.

[27] Ao, W., Fu, J., Mao, X., Kang, Q., Ran, C., Liu, Y., Zhang, H., **2018**. Microwave assisted preparation of activated carbon from biomass : A review. *Renewable and Sustainable Energy Reviews*. 92, 958–979. DOI:10.1016/j.rser.2018.04.051.

[28] Ania, C.O., Parra, J.B., Menéndez, J.A., Pis, J.J., **2007**. Microwave-assisted regeneration of activated carbons loaded with pharmaceuticals. *Water Research*. 41, 3299–3306. DOI:10.1016/j.watres.2007.05.006.

[29] Foo, K.Y., Hameed, B.H., **2012**. A cost effective method for regeneration of durian shell and jackfruit peel activated carbons by microwave irradiation. *Chemical Engineering Journal*. 193–194, 404–409. DOI:10.1016/j.cej.2012.04.055.

[30] Kim, T., Lee, J., Lee, K.H., **2014**. Microwave heating of carbon-based solid materials. *Carbon Letters*. 15, 15–24. DOI:10.5714/CL.2014.15.1.015.

[31] Durán-Jiménez, G., Stevens, L.A., Hodgins, G.R., Uguna, J., Ryan, J., Binner, E.R., Robinson, J.P., **2019**. Fast regeneration of activated carbons saturated with textile dyes: Textural, thermal and dielectric characterization. *Chemical Engineering Journal*. 378, 121774. DOI:10.1016/j.cej.2019.05.135.

[32] Falciglia, P.P., Gagliano, E., Brancato, V., Malandrino, G., Finocchiaro, G., Catalfo, A., De Guidi, G., Romano, S., Roccaro, P., Vagliasindi, F.G.A., **2020**. Microwave based regenerating permeable reactive barriers (MW-PRBs): Proof of concept and application for Cs removal. *Chemosphere*. 251, 126582. DOI:10.1016/j.chemosphere.2020.126582.

[33] Ania, C.O., Menéndez, J.A., Parra, J.B., Pis, J.J., **2004**. Microwave-induced regeneration of activated carbons polluted with phenol. A comparison with conventional thermal regeneration. *Carbon*. 42, 1377–1381. DOI:10.1016/j.carbon.2004.01.010.

[34] Foo, K.Y., Hameed, B.H., **2012**. Microwave-assisted regeneration of activated carbon. *Bioresource Technology*. 119, 41–47. DOI:10.1016/j.biortech.2012.05.061.

[35] Biniak, S., Szymański, G., Siedlewski, J., Światkoski, A., **1997**. The characterization of activated carbons with oxygen and nitrogen surface groups. *Carbon*. 35, 1799–1810. DOI:10.1016/S0008-6223(97)00096-1.

[36] Liu, C.J., Werner, D., Bellona, C., **2019**. Removal of per- and polyfluoroalkyl substances (PFASs) from contaminated groundwater using granular activated carbon: a pilot-scale study with breakthrough modeling. *Environmental Science: Water Research & Technology*. 5, 1844–1853. DOI:10.1039/C9EW00349E.

[37] Ochoa-Herrera, V., Sierra-Alvarez, R., **2008**. Removal of perfluorinated surfactants by sorption onto granular activated carbon, zeolite and sludge. *Chemosphere*. 72, 1588–1593. DOI:10.1016/j.chemosphere.2008.04.029.

[38] Kothawala, D.N., Köhler, S.J., Östlund, A., Wiberg, K., Ahrens, L., **2017**. Influence of dissolved organic matter concentration and composition on the removal efficiency of perfluoroalkyl substances (PFASs) during drinking water treatment. *Water Research*. 121, 320–328. DOI:10.1016/j.watres.2017.05.047.

[39] Sun, Y., Zhang, B., Zheng, T., Wang, P., **2017**. Regeneration of activated carbon saturated with chloramphenicol by microwave and ultraviolet irradiation. *Chemical Engineering Journal*. 320, 264–270. DOI:10.1016/j.cej.2017.03.007.

[40] Foo, K.Y., **2018**. Effect of microwave regeneration on the textural network, surface chemistry and adsorptive property of the agricultural waste based activated carbons. *Process Safety and Environmental Protection*. 116, 461–467. DOI:10.1016/j.psep.2018.01.022.

[41] Yao, Y., Volchek, K., Brown, C.E., Robinson, A., Obal, T., **2014**. Comparative study on adsorption of perfluorooctane sulfonate (PFOS) and perfluorooctanoate (PFOA) by different adsorbents in water. *Water Science and Technology*. 70, 1983–1991. DOI:10.2166/wst.2014.445.

[42] Crownover, E., Oberle, D., Kluger, M., Heron, G., **2019**. Perfluoroalkyl and polyfluoroalkyl substances thermal desorption evaluation. *Remediation*. 29, 77–81. DOI:10.1002/rem.21623.

[43] Watanabe, N., Takata, M., Takemine, S., Yamamoto, K., **2018**. Thermal mineralization behavior of PFOA, PFHxA, and PFOS during reactivation of granular activated carbon (GAC) in nitrogen atmosphere. *Environmental Science and Pollution Research*. 25, 7200–7205. DOI:10.1007/s11356-015-5353-2.

[44] Feng, Y., Zhou, Y., Lee, P.H., Shih, K., **2016**. Mineralization of perfluorooctanesulfonate (PFOS) and perfluorodecanoate (PFDA) from aqueous solution by porous hexagonal boron nitride: adsorption followed by simultaneous thermal decomposition and regeneration. *RSC Advances*. 6, 113773–113780. DOI:10.1039/C6RA15564B.

[45] Lowell, S., Shields, J.E., Morral, J.E., **1985**. Powder Surface Area and Porosity, 2nd Edition. *Journal of Engineering Materials and Technology*. 107, 180. http://dx.doi.org/10.1115/1.3225796.

[46] Dastgheib, S.A., Karanfil, T., Cheng, W., **2004**. Tailoring activated carbons for enhanced removal of natural organic matter from natural waters. *Carbon*. 42, 547–557. DOI:10.1016/j.carbon.2003.12.062.

[47] Cheng, W., Dastgheib, S.A., Karanfil, T., **2005**. Adsorption of dissolved natural organic matter by modified activated carbons. *Water Research*. 39, 2281–2290. DOI:10.1016/j.watres.2005.01.031.

[48] Pi, X., Sun, F., Gao, J., Zhu, Y., Wang, L., Qu, Z., Liu, H., Zhao, G., **2017**. Microwave Irradiation Induced High-Efficiency Regeneration for Desulfurized Activated Coke: A Comparative Study with Conventional Thermal Regeneration. *Energy and Fuels*. 31, 9693–9702. DOI:10.1021/acs.energyfuels.7b01260.

[49] Falciglia, P.P., Gagliano, E., Brancato, V., Finocchiaro, G., Catalfo, A., De Guidi, G., Romano, S., Roccaro, P., Vagliasindi, F.G.A., **2020**. Field technical applicability and cost analysis for microwave based regenerating permeable reactive barriers (MW-PRBs) operating in Cs-contaminated groundwater treatment. *Journal of Environmental Management*. 260, 110064. DOI:10.1016/j.jenvman.2020.110064.

[50] Remya, N., Lin, J.G., **2011**. Current status of microwave application in wastewater treatment-A review. *Chemical Engineering Journal*. 166, 797–813. DOI:10.1016/j.cej.2010.11.100.

[51] Mao, H., Zhou, D., Hashisho, Z., Wang, S., Chen, H., Wang, H.H., **2015**. Constant power and constant temperature microwave regeneration of toluene and acetone loaded on microporous activated carbon from agricultural residue. *Journal of Industrial and Engineering Chemistry*. 21, 516–525. DOI:10.1016/j.jiec.2014.03.014.

[52] Zhang, L., Jiang, H., Ma, C., Yong, D., **2012**. Microwave regeneration characteristics of activated carbon for flue gas desulfurization. *Journal of Fuel Chemistry and Technology*. 40, 1366–1371. DOI:10.1016/S1872-5813(13)60004-3.

[53] Wang, J., Peng, X., Luan, Z., Zhao, C., **2010**. Regeneration of carbon nanotubes exhausted with dye reactive red 3BS using microwave irradiation. *Journal of Hazardous Materials*. 178, 1125–1127. DOI:10.1016/j.jhazmat.2010.01.112.

[54] Yagmur, E., Turkoglu, S., Banford, A., Aktas, Z., **2017**. The relative performance of microwave regenerated activated carbons on the removal of phenolic pollutants. *Journal of Cleaner Production*. 149, 1109–1117. DOI:10.1016/j.jclepro.2017.02.188.

[55] Li, W., Wang, X., Peng, J., **2014**. Effects of microwave heating on porous structure of regenerated powdered activated carbon used in xylose. *Environmental Technology*. 35, 532–540. DOI:10.1080/09593330.2013.796007.

[56] Punyapalakul, P., Suksomboon, K., Prarat, P., Khaodhiar, S., **2013**. Effects of Surface Functional Groups and Porous Structures on Adsorption and Recovery of Perfluorinated Compounds by Inorganic Porous Silicas. *Separation Science and Technology (Philadelphia)*. 48, 775–788. DOI:10.1080/01496395.2012.710888.

[57] Du, Z., Deng, S., Chen, Y., Wang, B., Huang, J., Wang, Y., Yu, G., **2015**. Removal of perfluorinated carboxylates from washing wastewater of perfluorooctanesulfonyl fluoride using activated carbons and resins. *Journal of Hazardous Materials*. 286, 136–143. DOI:10.1016/j.jhazmat.2014.12.037.

[58] Du, Z., Deng, S., Liu, D., Yao, X., Wang, Y., Lu, X., Wang, B., Huang, J., Wang, Y., Xing, B., Yu, G., **2016**. Efficient adsorption of PFOS and F53B from chrome plating wastewater and their subsequent degradation in the regeneration process. *Chemical Engineering Journal*. 290, 405–413. DOI:10.1016/j.cej.2016.01.077.

[59] Deng, S., Nie, Y., Du, Z., Huang, Q., Meng, P., Wang, B., Huang, J., Yu, G., **2015**. Enhanced adsorption of perfluorooctane sulfonate and perfluorooctanoate by bamboo-derived granular activated carbon. *Journal of Hazardous Materials*. 282, 150–157. DOI:10.1016/j.jhazmat.2014.03.045.

[60] Çalişkan, E., Bermúdez, J.M., Parra, J.B., Menéndez, J.A., Mahramanlioğlu, M., Ania, C.O., **2012**. Low temperature regeneration of activated carbons using microwaves: Revising conventional wisdom. *Journal of Environmental Management*. 102, 134–140. DOI:10.1016/j.jenvman.2012.02.016.

[61] Liu, X., Quan, X., Bo, L., Chen, S., Zhao, Y., **2004**. Simultaneous pentachlorophenol decomposition and granular activated carbon regeneration assisted by microwave irradiation. *Carbon*. 42, 415–422. DOI:10.1016/j.carbon.2003.12.032.

[62] Wei, M.C., Wang, K.S., Lin, I.C., Hsiao, T.E., Lin, Y.N., Tang, C.T., Chen, J.C., Chang, S.H., **2012**. Rapid regeneration of sulfanilic acid-sorbed activated carbon by microwave with persulfate. *Chemical Engineering Journal*. 193–194, 366–371. DOI:10.1016/j.cej.2012.04.072.

[63] Cherbański, R., **2018**. Regeneration of granular activated carbon loaded with toluene – Comparison of microwave and conductive heating at the same active powers. *Chemical Engineering and Processing: Process Intensification*. 123, 148–157. DOI:10.1016/j.cep.2017.11.008.

[64] Sörengård, M., Lindh, A.-S., Ahrens, L., **2020**. Thermal desorption as a high removal remediation technique for soils contaminated with per- and polyfluoroalkyl substances (PFASs). *PLOS ONE*. 15, e0234476. DOI:10.1371/journal.pone.0234476.

[65] Wang, F., Shih, K., Lu, X., Liu, C., **2013**. Mineralization behavior of fluorine in perfluorooctanesulfonate (PFOS) during thermal treatment of lime-conditioned sludge. *Environmental Science and Technology*. 47, 2621–2627. DOI:10.1021/es305352p.

[66] Li, S., Zhang, G., Zhang, W., Zheng, H., Zhu, W., Sun, N., Zheng, Y., Wang, P., **2017**.

Microwave enhanced Fenton-like process for degradation of perfluorooctanoic acid (PFOA) using Pb-BiFeO3/rGO as heterogeneous catalyst. *Chemical Engineering Journal*. 326, 756–764. DOI:10.1016/j.cej.2017.06.037.

[67] Liu, F., Hua, L., Zhang, W., **2020**. Influences of microwave irradiation on performances of membrane filtration and catalytic degradation of perfluorooctanoic acid (PFOA). *Environment International*. 143,. DOI:10.1016/j.envint.2020.105969.

[68] Chen, Y., Ai, Z., Zhang, L., **2012**. Enhanced decomposition of dimethyl phthalate via molecular oxygen activated by Fe@Fe2O3/AC under microwave irradiation. *Journal of Hazardous Materials*. 235–236, 92–100. DOI:10.1016/j.jhazmat.2012.07.015.

[69] Gomez-Ruiz, B., Ribao, P., Diban, N., Rivero, M.J., Ortiz, I., Urtiaga, A., **2018**. Photocatalytic degradation and mineralization of perfluorooctanoic acid (PFOA) using a composite TiO2 −rGO catalyst. *Journal of Hazardous Materials*. 344, 950–957. DOI:10.1016/j.jhazmat.2017.11.048.

[70] Yang, L., He, L., Xue, J., Ma, Y., Xie, Z., Wu, L., Huang, M., Zhang, Z., **2020**. Persulfate-based degradation of perfluorooctanoic acid (PFOA) and perfluorooctane sulfonate (PFOS) in aqueous solution: Review on influences, mechanisms and prospective. *Journal of Hazardous Materials*. 393,. DOI:10.1016/j.jhazmat.2020.122405.

[71] Lee, Y., Lo, S., Chiueh, P., Chang, D., **2009**. Efficient decomposition of perfluorocarboxylic acids in aqueous solution using microwave-induced persulfate. *Water Research*. 43, 2811–2816. DOI:10.1016/j.watres.2009.03.052.

[72] Kim, T.H., Lee, S.H., Kim, H.Y., Doudrick, K., Yu, S., Kim, S.D., **2019**. Decomposition of perfluorooctane sulfonate (PFOS) using a hybrid process with electron beam and chemical oxidants. *Chemical Engineering Journal*. 361, 1363–1370. DOI:10.1016/j.cej.2018.10.195.

Chapter 5: Microwave based regenerating Permeable Reactive Barriers (MW-PRBs): proof of concept and application for Cs removal

Abstract

The present study evaluates the concept of permeable reactive barrier (PRB) coupled with microwaves (MWs) as in situ-regenerating technology with focus on Cs-contaminated water. Experimental and modelling results data from batch and column tests were carried out, evaluating several chemical-physical and environmental parameters. Main results showed a very rapid increase in GAC temperature during MW irradiation up to ~680 °C. This highlights the GAC strong ability to transform MW power into heat due to GAC excellent dielectric properties (ε′ = 13.8). Physical characterization revealed that GAC pore volume and specific surface area change with the number of regeneration cycles. GAC regeneration efficiency variation reflects this behaviour with a maximum value of ~112% (5th cycle). The final GAC weight loss of ~7% further demonstrates GAC life span preservation during MW irradiation. Results from column tests confirm that GAC can be regenerated by MW also in dynamic condition, due to sublimation/vaporization and vapour stripping Cs removal mechanisms and that the regeneration effectiveness is time-dependent. The breakthrough curve shape confirms significant benefits from MW irradiation. Overall, obtained finding demonstrated the feasibility of the proposed concept, also providing essential data to guide its scaling-up application.

Graphical abstract

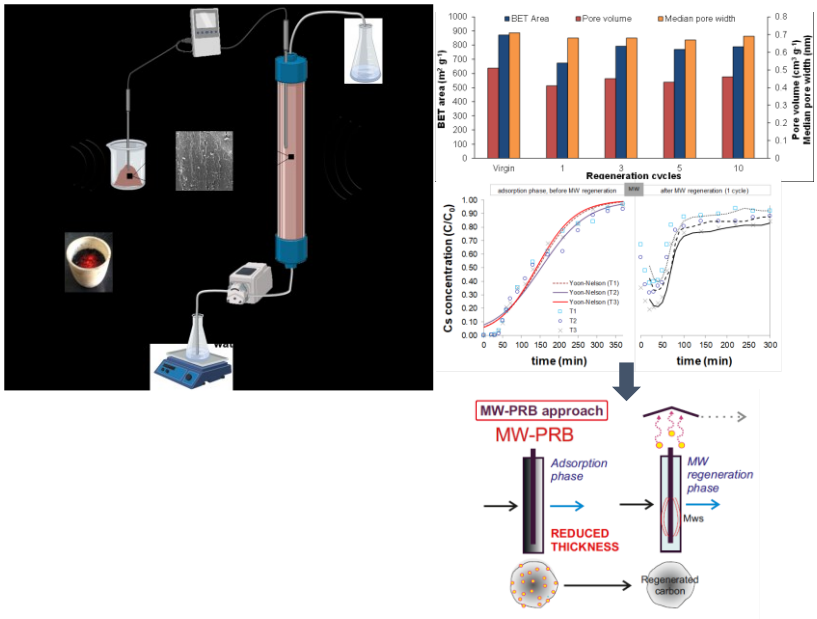

Keywords: Cesium, granular activated carbon, groundwater decontamination, microwave regeneration, permeable reactive barrier.

❖ This chapter have been redrafted from:

Falciglia, P.P., **Gagliano, E.**, Brancato, V., Malandrino, G., Finocchiaro, G., Catalfo, A., De Guidi, G., Romano, S., Roccaro, P., Vagliasindi, F.G.A. "*Microwave based regenerating permeable reactive barriers (MW-PRBs): Proof of concept and application for Cs removal*". **Chemosphere** 251, 126582 (2020).

1. Introduction

Cesium-137 (^{137}Cs) is the most prevalent product of nuclear fission processes of ^{235}U and ^{239}Pu and, consequently, the major radionuclide in spent nuclear fuel processing [1]. Contamination by ^{137}Cs represents the most important risk driver after nuclear accident [2], while nuclear activities (weapon tests, nuclear energy) are other relevant causes [3]. Cesium-137 is a beta (β) and gamma (γ)-emitter radionuclide with high solubility and hazardous long-term radiological effects (half-life 30.2 years) [4,5], representing the major threat for environment and human health [6].

Innovative and cost-effective decontamination alternatives are strictly required for Cs removal from impacted groundwater [6]. Several chemico-physical processes have been proposed for this purpose, namely solvent extraction, ion-exchange, adsorption, chemical precipitation, membrane process, coagulation, and electrochemical. The first three methods are based on ionic selectivity and are in the most widely applied [7]. However, solvent extraction is very restricted due to chemical high costs, while clay minerals or Prussian blue supported materials produce solid waste due to their non-reusable character or very high regeneration costs [8]. On the other hand, adsorption is considered a higher potential solution for Cs removal [5].

In terms of technologies, permeable reactive barrier (PRB) is considered one of the most innovative in-situ alternatives for the effective treatment of contaminated groundwater [9]. PRB is a subsurface emplacement of reactive materials through which a dissolved contaminant plume moves, typically under natural gradient [10]. Activated carbon (AC), mostly in granular form (GAC), is one of the most commonly used materials in PRBs, which are also called permeable adsorptive barriers (PABs) [11,12]. The high surface area and developed porosity of ACs make AC based PRB a low-cost and effective system for a wide range of pollutants among which radionuclides [13–15]. However, very few and unsatisfactory studies on Cs removal have been conducted [3,7,16,17]. Due to reduced longevity of PRB caused by AC saturation, in-situ regeneration (ISR) is very promising but also very challenging [11]. In addition, ISR would avoid early uneconomic incineration or landfill disposal actions, which are also causes of secondary hazardous environmental contaminations. The regeneration of ^{137}Cs-exhausted ACs, would also allow the recovering of the radionuclide that is recognized as an excellent gamma ray source used in nuclear and physics fields [18].

Then the challenge of regenerating PRB during the working phase with the aim of extending the PRB longevity is very interesting. This approach may include the use of barriers coupled with other process or regenerating technologies [19]. Biological PRBs have been proposed by Careghini et al. (2015) [20]. Their regeneration principle includes the use of a permeable porous medium to support autochthonous microorganisms able to biodegrade organic contaminants. The topic has further been investigated more recently in other experimental works [19,21]. A further integration of PRBs with electrokinetic

process has also been studied [11]. However, these alternatives require very long regeneration times and are recognized as ineffective (biological) or uneconomical (chemico-physical) in the presence of metals or radionuclides [20].

In recent years, microwave (MW) irradiation technology has been exploited as a powerful tool in several energy and environmental applications. The growing interest in MW technique is also based on the passive ability of the irradiated matrix to convert a low power energy into a rapid and large temperature increase. This depends on the dielectric features of the media, which undoubtedly represents a major driving force, decreases the energy requirements and makes MW a very cost-effective and sustainable alternative [22]. Other great advantages are the higher ability of MW over conventional thermal remediation to heat the irradiated materials homogenously and rapidly [23]. MW has attracted many attentions on AC regeneration, due to their excellent MW-absorbing properties because of the interactions of the delocalized π-electrons with MWs [24–26]. High mechanical strength and a good resistance towards heat and radiation are other essential features [14,27].

To the best of our knowledge, the regeneration of Cs-exhausted ACs has never been investigated. Furthermore, Cs thermal removal mechanisms is still unclear. Therefore, the present study evaluates the concept of PRB coupled with electromagnetic waves in the frequency of MWs as novel in situ regenerating decontamination technology with the aim of extending the PRB longevity. Laboratory-scaled experiments were focused on radionuclide-contaminated groundwater. The main advantages of the proposed method are the extension of the PRB longevity and then the reduction in PRB thickness and the minimization of GAC final disposal to hazardous landfill. Both advantages allow a significant reduction in both material costs and environment contamination risks.

Batch and fixed-bed column experiments were conducted to assess the AC adsorption/desorption kinetic processes as well as the potentiality of in-situ dynamic regeneration under different constant MW irradiation times. Several chemico-physical (specific surface area, pore volume, pore width, adsorption isotherm parameters) and operating parameters (adsorption capacity, temperature, regeneration efficiency, weight loss) were evaluated jointly with SEM images for the ACs during the adsorption/regeneration phases. Kinetic data were modelled using the most suitable models to describe isotherm adsorption and breakthrough curves. Experimental results from lab-scale tests and parameters from modeling were used to discuss the feasibility of this combined remediation concept and they represent crucial information to guide the scaling-up of application of ACs as adsorptive medium in MW regenerating permeable reactive barriers (MW-PRBs).

2. Materials and methods

2.1 Batch adsorption experiments and isotherm modelling

A series of batch experiments were performed using a ^{133}Cs-contaminated solution at different concentrations [28]. ^{133}Cs (isotope of ^{137}Cs) was selected as the representative but safer targeted contaminant ion, in order to investigate the adsorption behavior of the radioactive ions [29]. Cesium-water samples were prepared by dissolving different amounts of CsCl soluble salt (99% purity, 168.36 g mol^{-1}; *Sigma-Aldrich*, CAS n. 7647-17-8) in deionized water. Commercially available *Norit* Granular Activated Carbon *830* (GAC 830) (Table S1) was selected as adsorbent due to its potential in Cs-adsorption and superior hardness, which is strictly required for thermal reactivation. Before use, AC was washed with deionized water or HCl solution (10^{-3} M), sieved at 2.0 mm, then oven-dried at 100 °C. For the experiments, 5 g of AC were added to 50 mL of Cs-solution at varying concentrations up to 250 mg L^{-1}. The resultant batches were allowed to react on a shaker (180 rpm, 20 °C) for a period of 24 h, sufficient to reach the equilibrium. After the adsorption target period, aliquots were filtered through *Whatman* paper filter (0.20 μm) before analyze Cs concentration using inductively coupled plasma-mass spectrometry (ICP-MS). Initial (C_0, mg L^{-1}) and equilibrium concentration (C_e, mg L^{-1}) were obtained and Cs-uptake at equilibrium, q_e (mg g^{-1}) was calculated as follow:

$$q_e = \frac{(C_0 - C_e)V}{W} \quad (1)$$

where V (L) and W (g) are the volume of the solution and the mass of the adsorbent, respectively. Obtained data were fitted using several models, containing two (Langmuir, Freundlich and Temkin equations) or more (Redlich-Peterson and Sips isotherms) fitting parameters [30] (Table S2). The correlation coefficient (R^2) was employed to evaluate the goodness of mathematical fitting of the isotherm equations in describing the adsorption process [29].

2.2 Batch regeneration of Cs-exhausted activated carbons

For the regeneration tests, Cs-exhausted AC samples from additional adsorption tests were employed. The sample contamination was carried out using the previously described procedure with a Cs-water concentration (C_0) of 250 mg L^{-1}. The regeneration procedure was performed using a 2.45-GHz MW bench-scale oven (maximum power of 1 kW) equipped with a dedicated exhaust vapour capture line (cold traps, AC filter and electric vacuum pump). The Cs removal kinetic within the regeneration process was investigated by MW-irradiating 15 g of AC (dried and water saturated) at 440 W (maximum irradiation time = 10 min). A type-k thermocouple was used for AC temperature recording. ACs were analysed for residual Cs-concentration (C) at different regeneration times by ICP-MS following the procedure previously reported [31]. Tests were carried out in triplicate and mean

and standard deviation values were assessed. Removal (R) was calculated as follow: $R=[(C_0-C)/C_0]*100$ (%). The adsorption/regeneration cycle effect was also assessed for an irradiation time of 3 min and 10 regeneration cycles. The regeneration efficiency (RE, %) [32] and the weight loss percentage (η, %) [25] were calculated using Eqs. 2 and 3, respectively, in order to assess the yield of the whole MW regeneration treatment:

$$RE=\frac{Q_i}{Q_0}\cdot 100 \quad (2)$$

$$\eta=\frac{W_0-W_t}{W_0}\cdot 100 \quad (3)$$

where Q_i is the adsorption capacity (mg g^{-1}) of the regenerated AC, Q_0 is the adsorption capacity (mg g^{-1}) of the fresh AC, W_t is the weight (g) of the AC after the regeneration and W_0 is the weight (g) of the fresh AC.

Characterization of ACs was simultaneously performed before and after the regeneration process. Specifically, nitrogen adsorption isotherms were obtained at 77 K using an automatic volumetric adsorption analyser (Micromeritics ASAP 2020). Prior to gas adsorption measurements, samples were degassed for 3 h under vacuum at 433.15 K in order to remove AC impurities. Brunauer-Emmett-Teller (BET) theory was used in order to calculate the AC specific surface area [33]. The t-plot method and Horvath-Kawazoe (HK) model were employed to estimate the total pore volume and median pore width, respectively [34,35]. Scanning electron microscopy (SEM) analysis were employed in order to assess the effects of washing action (HCl or H_2O) and MW regeneration on the GAC surface structure. For this purpose, a field emission scanning electron microscope (FE-SEM, ZEISS SUPRA 55 VP) was used.

2.3 MW-PRB dynamic regeneration: MW-adsorption column tests and modelling

A series of dynamic adsorption-regeneration tests were conducted for simulating the operating principle of a MW based regenerating permeable reactive barriers (MW-PRB) for Cs removal from groundwater. Experiments were carried out in three distinct and continuous phases (*adsorption – regeneration – adsorption*) using a dedicated setup (Figure S1). It is mainly made up of a Pyrex glass column (50 mm inner and 450 mm high) inserted in a MW oven cavity equipped with a MW generator (1 kW) for the irradiation of the column. The column was filled with the GAC 830, previously washed with HCl solution (10^{-3} M), to produce a bed length of 21 cm and bulk density of 0.53 g cm^{-3} (porosity = 0.48). The system was feed with a peristaltic pump, whereas the outlet section was split in two different hydraulic lines: (i) water line, working during the adsorption phases and (ii) vapour line, which collected the exhaust gas produced during the regeneration phase. Firstly, for the *adsorption*

phase, a solution with a Cs concentration of 100 mg L^{-1} (C_0) was pumped upward at the flow rate of 10 mL min^{-1}, and the outlet effluents were collected at set intervals for Cs concentration (C) analysis. In order to better appreciate the regeneration effect of the MW irradiation, the GAC-column was irradiated (*regeneration phase*) when the GAC was saturated. On the basis of data obtained from batch tests and preliminary column tests, a power of 300 W was selected. Three tests were carried out changing the time of the regeneration phase: T1=5 min, T2=10 min and T3=15 min. The time of the saturation phase was preliminary assessed in a previous test when the Cs effluent concentration was 90% of the inlet Cs concentration. After each regeneration time, a novel *adsorption phase* including the outlet solution collecting was implemented. Breakthrough curves were obtained plotting C/C_0 against the flushing time (t).

Four selected models (Yoon and Nelson, Adams-Bohart, Thomas and Logit models), whose equations are listed in Table S3, were applied to fit the experimental data and to calculate the dynamic parameters. The applicability of these models to evaluate the adsorption rate and mechanisms was assessed by the correlation coefficients (R^2). Data from this MW-PRB dynamic regeneration will allow the achievement of necessary information (design and operation) for the validation of the proposed approach and its potential application [9].

3. Results and discussion

3.1 Adsorption isotherm

All fitting models investigated are in good agreement (R^2 > 0.97) with experimental data from adsorption batch tests (Table S2). Specifically, the Temkin model showed a better applicability than the Freundlich one, suggesting that the binding energy sites of the GAC are uniform [29]. The Sips isotherm model gave the highest R^2 values (~0.99) for unwashed and HCl-washed GAC samples, whereas the Redlich-Peterson model described better the adsorption of Cs on water-washed GAC (Table S2). The α values in the Redlich-Peterson equation (equal to 1) suggest that this "three parameter equation" may be reduced to the Langmuir model [36]. At the highest Cs concentration tested (250 mg L^{-1}), the amount of Cs adsorbed on GAC (unwashed, water-washed and HCl-washed samples) was in the 1.5 - 1.7 mg g^{-1} range (Figure 1).

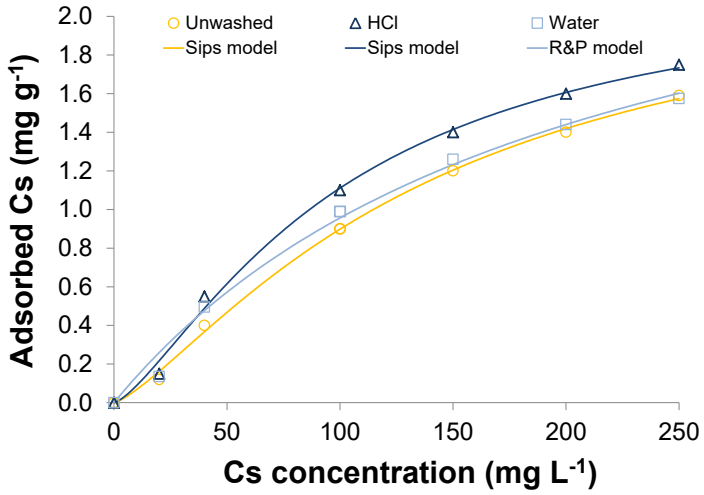

Figure 1. Sorption isotherms of Cs on GAC 830 (unwashed, water- and HCl-washed samples). Solid lines are the best fitting model.

Adsorption of Cs onto GAC 830 is justified by the small dimension of its ions (1.67 Å), which can be easily accommodated into its microporous structure (Table S1, median pore width = ~7.1 Å, as in detail reported in the section 3.3). Albeit mesoporosity (pore width in the 2 - 50 nm range) gives a low contribution, it allows a better connection between micropores and GAC external surface, permitting a more Cs molecule diffusion into carbon porous structure [37]. Despite GAC 830 adsorption capacity found in this study was lower than of that reported for other low-dielectric adsorbent materials [38,39], it is generally comparable with that observed in previous batch experimental studies (0.07 – 0.75 mg g^{-1}), where mesoporous GAC were tested at Cs initial concentration ranging 1.2 – 30 mg L^{-1} [16,17]. The highest Cs adsorption capacities observed in the case of HCl-washed samples were due to the removal of volatile matter and impurities from ACs through hydrochloric acid washing [40]. As a consequence, the need for the use of high dielectric

adsorbents such ACs and the better performance observed for the GAC 830 in Cs removal process, jointly with its cheapness (it does not required specific chemical fabrication [7,41] and resistance to thermal regeneration processes, may widely justify its use in this context.

3.2 AC temperature variation and Cs-removal

The results from MW-regeneration process revealed a very rapid increase in temperature (T) with time (t) (68.2 °C min^{-1}) for dried AC samples. In this case, a maximum T of 682 °C was recorded (Figure 2). This depends on the excellent AC dielectric properties (as confirmed by its dielectric constant, Table S1), which, in turn affect their ability to transform the absorbed power into heat generation following the principle of MW heating [22]. The asymptotic trend observed is related to the dependence of the dielectric constants with the temperature that causes a progressive reduction in the heat generated by the irradiated media. Heat dissipation from AC sample is a secondary cause [42]. Lower T values found in the case of water saturated ACs are due to the higher energy required for the water evaporation (latent heat for phase changing) at the beginning of the treatment [23]. This is clear from the T profile variation analysis. T kept constant (~100 °C) in the range 1-2 min, until the total water evaporation. Thereafter, T tended to the dried AC temperature values. This strong passive ability of ACs to transform a relatively low MW power into a rapid and large T rise represents the main key factor in the whole regeneration process. The observed T profiles corresponded to the removal kinetic depicted in Figure 2. It showed that for dried samples, T values higher than 500 °C resulted in R higher than 60%. When T rose up to ~680 °C, R reached 81%. GAC temperatures reached during the MW regeneration suggest Cs sublimation and partial vaporization as main contaminant removal mechanisms. This observation is in agreement with previous findings, demonstrating that temperatures in the 400-700 °C, are enough to effectively desorb Cs from sediments and clay minerals [43,44]. The enhanced diffusion mechanism given by the partial mesoporosity features of GAC contribute to the Cs removal process. Shimoyama et al. (2014) [45] demonstrated that Cs desorption from saturated vermiculite occurred above 520 °C, with a peak around 660 °C. As a whole, ~40% of Cs was desorbed by vacuum heat treatment at 800 °C for 3 min. In the present study, Cs removal from saturated GAC was higher than 70% when the same irradiation time (~3 min) was applied, demonstrating the good feasibility of MW regeneration for Cs desorption. The complete volatilization of ^{137}Cs occurred at 1150 – 1250 °C when 7:3 soil:limestone mixture was heated for 8 h [46].

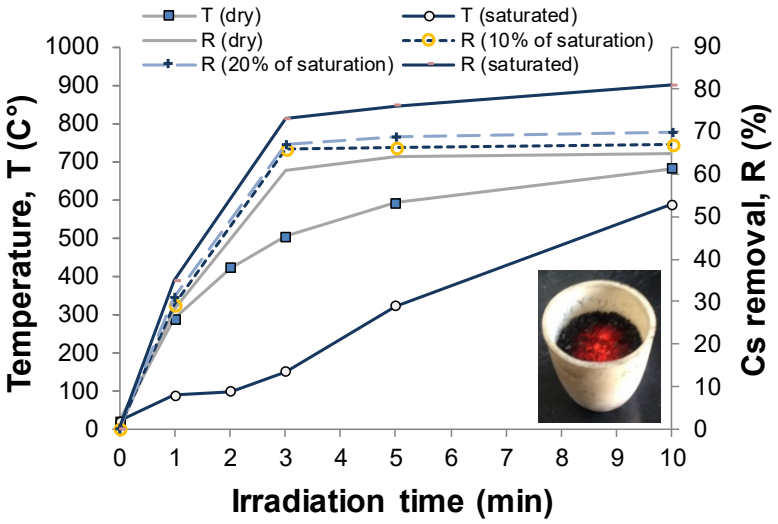

Figure 2. Temperature profiles of GAC samples and Cs removal (%) at different MW irradiation time (batch test, MW power 440 W). Inset: GAC image at the highest temperature reached during MW irradiation.

The overall gradual increase in R observed for increasing moisture values highlights that contaminant stripping due to the occurring of a rapid water distillation represents an important removal co-mechanism during MW regeneration [47,48]. In addition, stripping was shown to be enhanced by a high water solubility of the contaminant as in the case of Cs (1910 g L^{-1} at 25 °C) [47]. This observation confirms that contaminant removal from solid matrices is enhanced by the presence of interstitial water [49].

Based on temperature profiles, an irradiation time of 3 min was selected in order to investigate textural properties of MW regenerated samples and their variation during successive regeneration cycles (until the 10^{th} cycle).

3.3 Textural change of GAC during MW irradiation

N_2-physisorption analysis provides qualitative information regards adsorption mechanisms and porous characteristics of ACs [50]. The nitrogen adsorption-desorption isotherms of virgin and MW-regenerated GAC (440 W, heating time = 3 min) for HCl- and water-washed samples are shown in Figures 3a and 3b, respectively.

Isotherms of virgin and regenerated GACs can be identified as IUPAC type I, which corresponds to a mainly microporous structure [50]. On the other hand, the small hysteresis loop of H4 type in the 0.45 - 1 p/p_0 range observed for all the curves demonstrated the presence of few mesopores [50]. The preservation of the isotherms shape before and after the MW treatment indicates the maintenance of the microporosity condition.

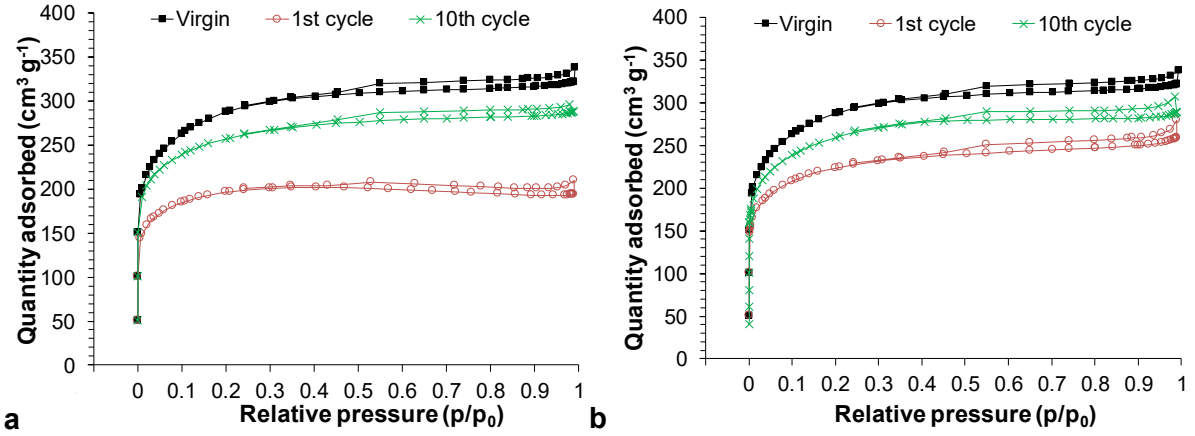

Figure 3. Nitrogen adsorption-desorption isotherms of virgin and MW regenerated GAC after several regeneration cycles (MW irradiation at 440 W for 3 min). (a) HCl- and (b) water-washed samples.

GAC textural properties in term of BET area, pore volume and median pore width obtained from N_2-physisorption analysis are given in Figures 4a and 4b. The modification of porous structure mainly regarded the pore volume and the specific surface area, while pore dimensions of GAC did not change during MW irradiation as demonstrated by constant value of median pore width which was comparable with that of virgin GAC.

The lowest BET area and pore volume occurred at the 1st cycle (on both water- and HCl-washed samples) is probably caused by pore blocking due to interstitial water presence [32]. Then, an irradiation time equal to 3 min is unsatisfactory to provide a sufficient power for a totally water vaporisation. This is also confirmed by BET area and the observed slightly increase in pore volume after the 1st regeneration cycle. After the initial decrease at the end of the 1st cycle, the highest BET area and pore volume were reached at the 5th regeneration cycle, whose values exceeded those of virgin GAC.

This suggests the increase in narrow micropores due to MW irradiation [37,51], and it is ascribable to the reorganization of GAC porous structure due to the interactions between delocalized π-electrons of GAC and MWs [24,25,32].

Moreover, the volumetric and internal heating provided by MWs promotes the elimination of volatile matter and consequently the development of micropore volume which influenced the increment of BET area [51,52]. Then, the MW regenerated GAC developed uniform and well pronounced porous structure with unchanged GAC median pore width. This suggests that GAC microporosity is preserved and MW irradiation does not modify GAC pores dimension as demonstrated by this and previous experimental work [53].

Further regeneration cycles (successive to the 5th) probably led to the partial destruction of some micropores previously formed and consequently the decrease in BET area and pore volume [52,54].

This is in agreement with the variation of GAC textural properties observed with the MW irradiation time (Figure 4c).

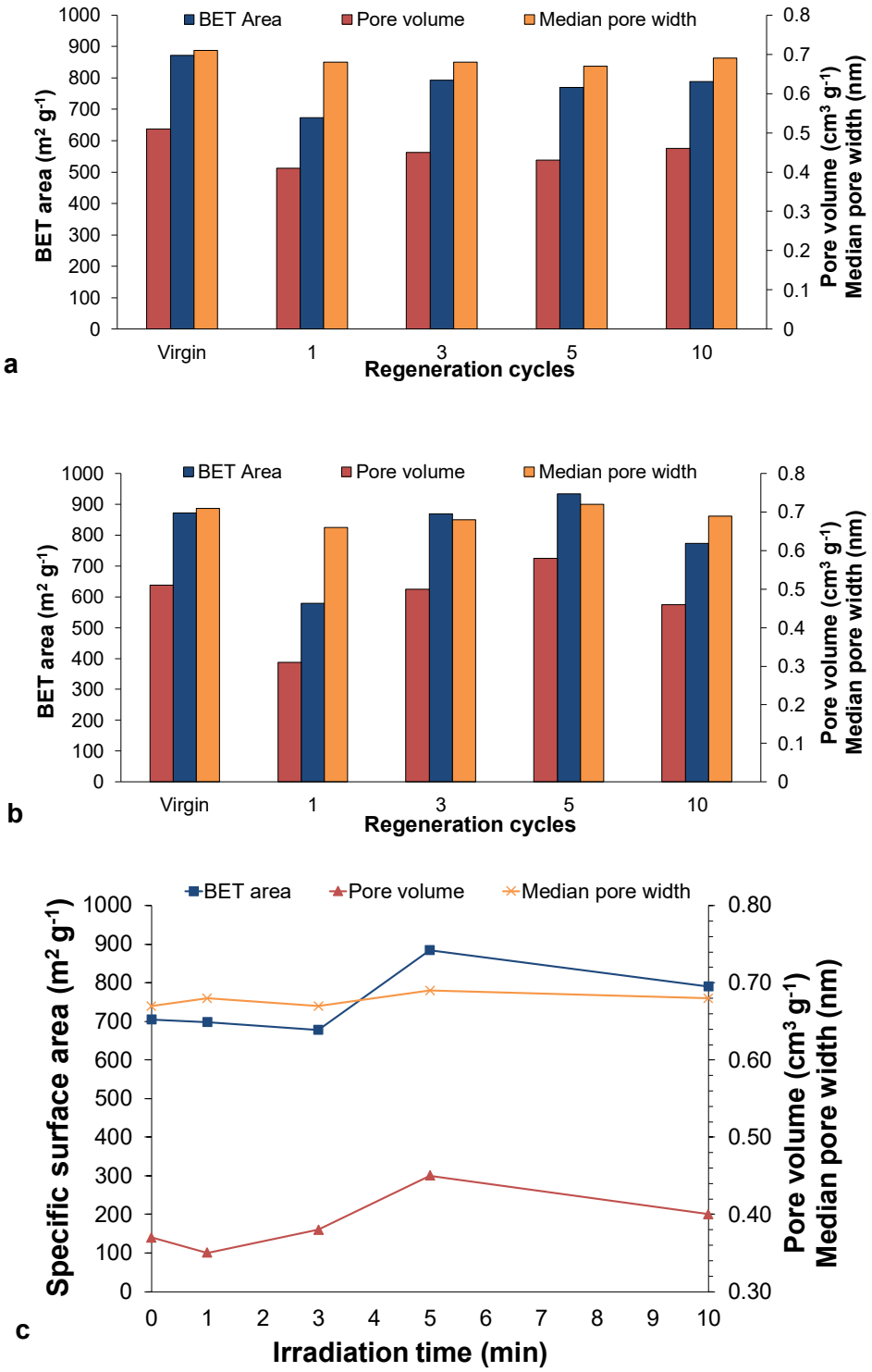

Figure 4. BET area, pore volume and median pore width of virgin GAC and after MW regeneration cycles (a) water- and (b) HCl-washed samples (MW irradiation at 440 W for 3 min); (c) variation of BET area, pore volume and median pore width with irradiation time (MW irradiation at 440 W).

The highest BET area (~900 m^2 g^{-1}) and pore volume (~0.45 cm^3 g^{-1}) were reached at 5 min of MW irradiation, while the median pore width was almost constant during all irradiation time tested. The occurring of a partial micropore destruction after a certain MW power adsorbed by GAC is confirmed by the decrease in pore volume observed after 5-min regeneration. The effect of MW irradiation on GAC porosity is confirmed by SEM analysis images (Figures 5a-5d) where MW regenerated GAC showed an increase in developed pores randomly connected each other.

HCl-washed samples were shown to be more subjected to MW irradiation when compared with water-washed ones as demonstrated by the more marked variation of BET area and pore volume (Figure 4b). BET area and pore volume of HCl-washed GAC were at the end of the 10^{th} cycle about 774 m^2 g^{-1} and 0.46 cm^3 g^{-1}, respectively. A greater reorganization generally occurred on HCl-washed samples and it can be attributed to effect of acid treatment which enhanced the removal of impurities from activated carbon and consequently GAC regeneration as the improvement of surface area and pore volume [55]. This is supported by SEM analysis results (Figures 5e-5h). HCl-washed GAC also revealed a more marked degree of roughness on with intended morphology.

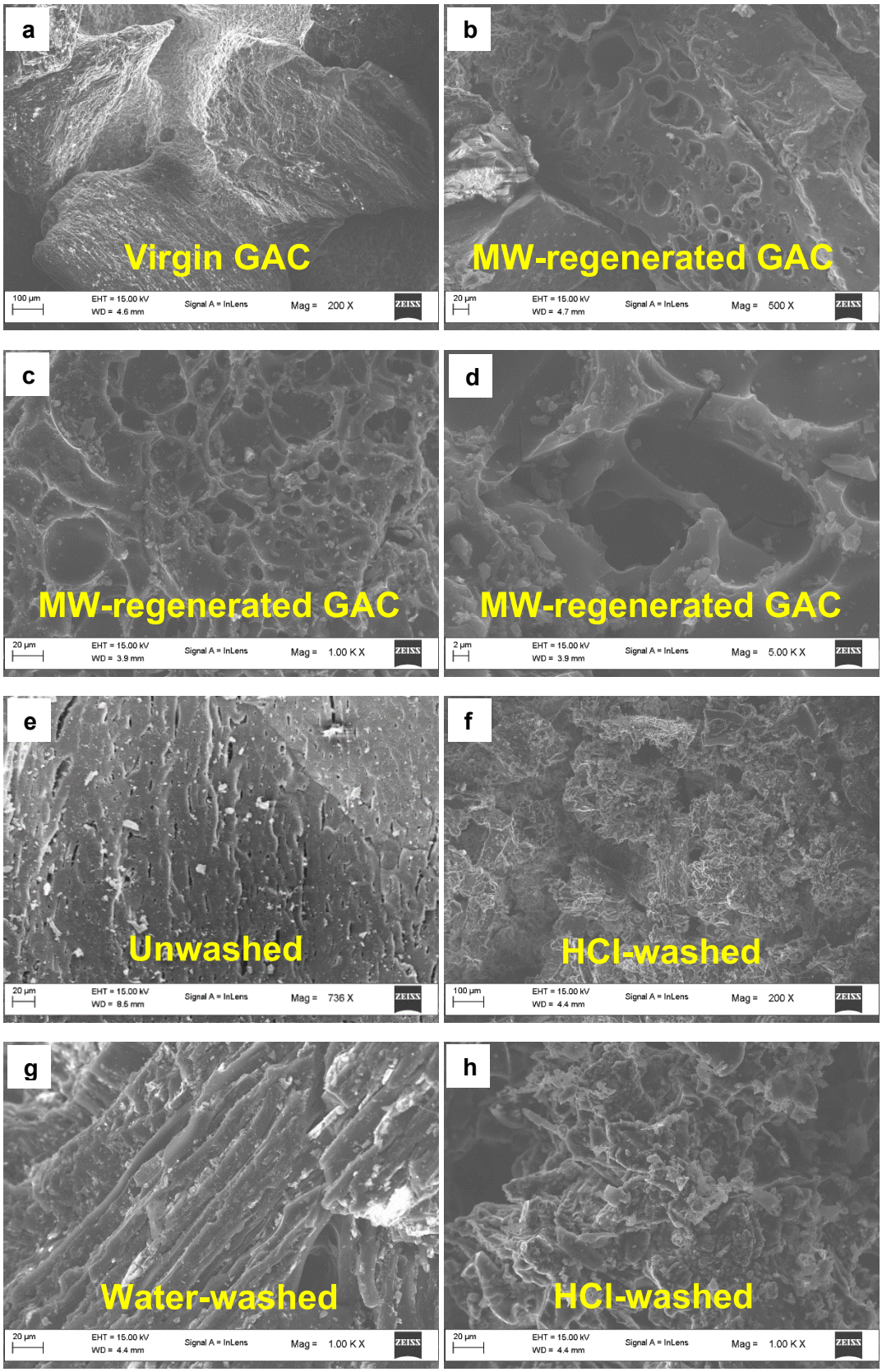

Figure 5. SEM images of (a) virgin GAC 830, (b, c and d) 5 times cycled MW regenerated GAC 830 (MW irradiation at 440 W for 3 min); (e) unwashed GAC 830, (f-h) HCl-washed and (g) water-washed GAC 830.

3.4 Regeneration efficiency (RE) and GAC weight loss (η)

The regeneration efficiency (RE) variation of GAC with regeneration cycles is given in Figure 6a. Overall, an increase in RE occurred until the 5th regeneration cycle with higher values found for HCl-washed samples for which RE was ~112%. This behaviour reflected the GAC structure modification as demonstrated by the BET area and pore volume variation. Then, the observed increase in RE can be ascribed to both Cs desorption mechanism and the internal reorganization of GAC porous structure, as previously commented and confirmed by earlier experimental works [25,32,56]. As it is known, the surface functional groups influence the adsorbate-adsorbent interaction through electrostatic attraction and surface complexation. They can promote bindings by attracting positive charge elements such as Cs anions [57]. Coconut-based GACs such as GAC 830 are mainly characterized by nitrogenous groups and oxygen groups, and the latter resulted from the oxidation of raw material [16]. Microwave regeneration decomposed oxygen functional group due to the elimination of volatile matter, while basic functional groups increased, making GAC more reactive [52,58]. Therefore, MW irradiation enhances GAC adsorption capacity at the increasing of basic groups, which are the active sites where cation adsorption takes place [52]. The modification of surface chemistry after MW regeneration could also be ascribed to the dispersive interaction between the adsorbed Cs with the π-electrons of GAC [59]. The enhanced regeneration effect recorded for HCl-washed samples is ascribable to the removal of impurities from virgin GAC that produces a direct increase in adsorption capacity and a positively influence in the MW penetration. The increase in RE along the GAC regeneration process is in agreement with previous literature [32].

A linear increase in GAC weight loss percentage (η) with MW regeneration cycles has been observed (Figure 6b).

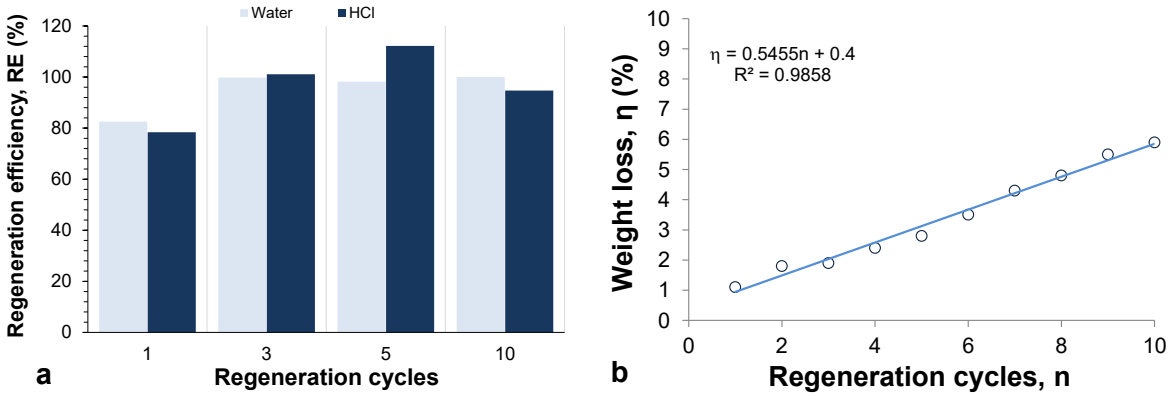

Figure 6. (a) Regeneration efficiency of GAC (water- and HCl-washed samples) after MW regeneration cycles (MW irradiation at 440 W for 3 min); (b) Relationship between GAC weight loss (η) and MW regeneration cycles (MW irradiation at 440 W for 3 min).

At the end of the 10th cycle, η was ~6.78%, much lower than that ascribed to conventional thermal regeneration (5 – 15% for each regeneration cycle) [60]. This evidence demonstrated that MW energy preserves better the life span of activated carbon compared to conventional thermal regeneration [37]. Moreover, the weight loss does not represent a limitation of the technical feasibility of MW regeneration. GAC weight loss can be ascribed to the internal reorganization of its porous structure occurred during MW irradiation [25].

Overall, the observed marked increase in RE jointly with a moderate weight loss represent promising results demonstrating the good feasibility of MW irradiation for regenerating Cs-saturated GAC.

3.5 MW-column tests

Figure 7 shows the breakthrough curves obtained from both the adsorption and adsorption post regeneration phases for the three regeneration times investigated (T1=5 min, T2=10 min and T3=15 min, respectively). As evident, the curves from the adsorption phase can be considered as triplicates. Their mean data revealed that Cs appeared in the effluent solution after ~40 min of flushing (~2 pore volume, PV) and its concentration gradually increased, until the saturation plateau (C/C_0=0.9) that approached to ~300 min (~14 PV). Specifically, the breakthrough time, established when the effluent Cs concentration was 10% of the initial concentration (C/C_0=0.10), was reached at 50 min, which corresponds to 2.5 PV. In order to gain insight in the adsorption dynamics of Cs through GAC column, four mathematical models (Yoon and Nelson, Adams-Bohart, Thomas and Logit) were used to fit the experimental data from the first phase. The prediction of the breakthrough curves throughout the models are essential for the scale-up process and to design a full-scale adsorption process. Obtained fitting parameters and related R^2 values are arranged in Table S3. The highest R^2 (> 0.94) were obtained from Yoon and Nelson model, which can be consequently considered as more satisfactory predictors for the breakthrough curves. The mean value of τ (146.5 min) obtained from Yoon and Nelson model and related to the time required for 50% adsorbate breakthrough (C/C_0=0.5) is almost equal to the experimental ones (~130 min), providing another evidence of the satisfying fitting of Yoon and Nelson model.

Furthermore, the non-linear Thomas equation was used to assess the loading capacity of Cs on GAC. This model showed a maximum amount of Cs loaded on GAC equal to 0.67 mg g^{-1} (mean value). Comparing Cs loading capacity obtained during batch experiments, a lower sorption capacity has been observed under the dynamic conditions. This evidence might be ascribed to the lesser contact time established during fixed-bed column tests [9,61]. A lower contact time causes a weak distribution of the solution through the column leading to a reduced diffusivity of Cs inside GAC active sites [62].

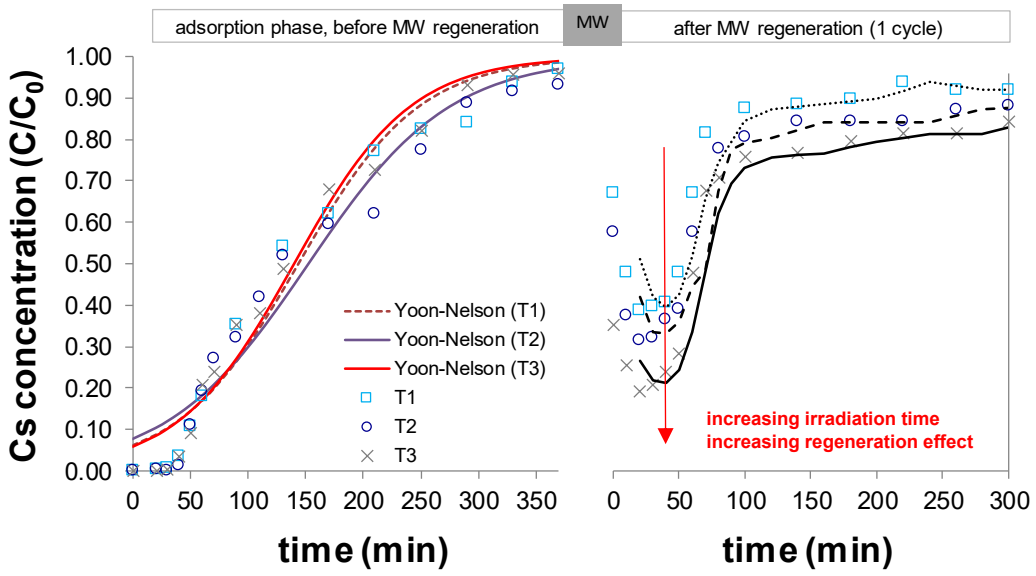

Figure 7. Breakthrough curves from MW-column experiments of both adsorption and adsorption post regeneration phases. T1=5 min-regeneration; T2=10 min-regeneration; T3=15 min-regeneration.

Analysis of Cs concentration from outlet water samples after MW regeneration phase showed that a relevant GAC bed regeneration under all the conditions investigated took place (Figure 7). This demonstrated that the MW energy absorbed by the system was enough to activate Cs removal mechanisms even in a permanent saturation condition. Desaturation was in fact avoided by the constant inlet water flow, which balanced the water vapour flow generated during the heating process. When water-saturated high dielectric medium is MW-irradiated, its grains absorb concentrated MW energy and act as "hot spots" [47]. GAC grain internal temperatures in the 600 – 700 °C range can be consequently achievable, while the external surface temperature presents much lower values (< 200 °C) due to the cooling down effect. This corresponds to a temperature gradient from solid particles to the water phase [47]. Then, the MW energy absorbed by GAC and interstitial water led to the activation of Cs sublimation and vaporization mechanisms, which produced Cs removal, and vapour distillation process. The generated vapour flow also acted as carrier contaminant, which transport both desorbed and dissolved Cs. In addition, the presence of a vapour stream leads to an increase in vapour pressure resulting in a reduction of the temperature needed for the contaminant desorption [63]. In particular, after regeneration, a certain amount of Cs was still revealed by the sampling from outlet water line due to the presence of Cs desorbed during the heating process (water line closed – vapor line open). Then, C/C_0 decreased up to minimum values of 0.39, 0.32, and 0.20, after 20 min, for regeneration times of 5, 10 and 15, respectively, which corresponded to Cs removals from AC of 61, 68 and 80%, respectively (Figure 7: curve related to the MW regeneration phase). It is clear that the effectiveness of the above described removal mechanisms depended on the total MW energy absorbed by the whole system. A longer heating time led to a higher hot spot temperature and a more impetuous water molecule motion. Both led to a faster carrier action that benefited the Cs elimination. Because

higher Cs removals were recorded for 15-min regeneration respect to 10 min, while comparable temperatures were recorded for both the treatments, it is presumable ascribe Cs regeneration enhancement to the more effective vapour stripping mechanism. This is also confirmed by the larger amount of condensed vapour collected along the line. Therefore, the evaporation-contaminant stripping phenomena present a major influence on the removal of contaminants, confirming the key role of the water in MW heating decontamination treatments [47]. After its initial decrease, Cs concentration on effluent solution increased until the saturation plateau which was approached near to 100 min (corresponding to 1 L of flow solution). After MW regeneration, breakthrough curves were more steep than initial ones and this suggests that the mass-transfer flux from bulk solution is rapid [64].

Obtained finding revealed that the MW regeneration efficiency is time-dependent and that regeneration times longer than 15-min would achieve a much higher contaminant removal from GAC. This demonstrated the feasibility of the proposed combined remediation concept, also providing essential data to encourage and guide the scaling-up of the MW-PRB system. A schematic of MW-PRB system includes a MW generation/transmission system inserted in a reduced thickness PRB and a desorbed vapour capture line. More details on antennas for a uniform and effective MW transmission in dielectric media can be found in Falciglia et al. (2018) [65]. On the other hand, the MW-PRB system would avoid contaminant leaching phenomena and disposal costs and, at the same time, allow the reduction of PRB thickness and GAC costs.

Further techno-economic analyses are needed in order to demonstrate the potential of the proposed system in terms of MW penetration, contaminant removal and cost saving.

4. Conclusions

A novel MW based regenerating permeable reactive barrier (MW-PRB) concept has been proposed in this work. Experimental results and modelling data from lab-scale batch and column tests were used to discuss the feasibility of this system.

Data from best fitting curve problem solving reveals that Temkin and Redlich-Peterson adsorption models better describes the process of Cs adsorption on GAC 830 (R^2 >0.99). At the highest Cs concentration of 250 mg L^{-1}, a maximum Cs adsorption capacity in the 1.5 - 1.7 mg g^{-1} range was found. This depended by the observed GAC microporous structure.

Results from MW-regeneration batch tests revealed a very rapid increase in GAC temperature up to a maximum value of ~680 °C, which corresponds to a Cs removal of 81%.

This strong passive ability of the tested GAC to transform a relatively low MW power into a rapid and large temperature increase depends on the excellent GAC dielectric properties, as demonstrated by its dielectric constant $\varepsilon' = 13.8$, and it represents the main key factor in the whole regeneration process. Obtained findings suggest Cs sublimation, partial vaporization and stripping due to water distillation as co-removal mechanisms.

Multiple regeneration cycle tests also revealed that GAC pore volume and specific surface area change with the number of regeneration cycles, while the microporosity condition is preserved. Specifically, the highest BET area (~937 m^2 g^{-1}) and pore volume (0.58 cm^3 g^{-1}) were reached at the 5^{th} regeneration cycle, whose values exceeded those of virgin GAC due to the increase in narrow micropores. Cs regeneration efficiency variation reflects this observed GAC structure modification, with a maximum value of ~112%, in correspondence with the 5^{th} cycle. The final GAC weight loss of ~7% also demonstrates that MW irradiation preserves the GAC life span better than conventional thermal heating.

Overall, despite the observed Cs adsorption values being relatively lower than other materials with poor dielectric features, the need for high dielectric adsorbents, jointly with the noticeable Cs removal performance, low weight loss and cheapness elect GAC 830 as an optimal choice and make MW regeneration of Cs-saturated GAC a high potential effective treatment.

Results from MW-column tests reveal that Cs appeared in the effluent solution after ~40 min of flushing and its concentration gradually increased, until the saturation plateau (C/C_0=0.9) that approached to ~300 min (~14 PV). Data from MW-regeneration phase confirm the effectiveness of the regeneration system also at the larger column scale simulation dynamic condition with a permanent saturation condition. In this case, the GAC fixed bed acts as MW hot spots leading to more powerful and effective vapour stripping removal mechanism. In particular, maximum Cs removals from AC of 61, 68 and 80% were achieved for regeneration times of 5, 10 and 15 min, respectively,

demonstrating that MW duration strictly influences the regeneration effectiveness. The shape of the breakthrough curves obtained after the dynamic regeneration process confirms the regeneration efficiency data from batch-tests, suggesting a benefit in Cs adsorption led from MW irradiation.
Overall, obtained finding demonstrated the feasibility of the proposed system, also providing essential data to guide the scaling-up of application with MW based regenerating permeable reactive barriers. Further techno-economic investigations are still needed for obtaining additional data, such as MW field propagation in PRB, PRB thickness reduction or economic benefits from avoided landfill disposal.

References

[1] De Pourcq, K., Ayora, C., García-Gutiérrez, M., Missana, T., Carrera, J., **2015**. A clay permeable reactive barrier to remove Cs-137 from groundwater: Column experiments. *Journal of Environmental Radioactivity*. 149, 36–42. DOI:10.1016/j.jenvrad.2015.06.029.

[2] Falciglia, P.P., Romano, S., Vagliasindi, F.G.A., **2017**. Application of a γRS index-based method and techno-economic analysis for in situ treatment of 137Cs-contaminated soils by cement-barite based stabilisation/solidification. *Journal of Environmental Management*. 197, 619–630. DOI:10.1016/j.jenvman.2017.04.037.

[3] Li, D., Kaplan, D.I., Knox, A.S., Crapse, K.P., Diprete, D.P., **2014**. Aqueous 99Tc, 129I and 137Cs removal from contaminated groundwater and sediments using highly effective low-cost sorbents. *Journal of Environmental Radioactivity*. 136, 56–63. DOI:10.1016/j.jenvrad.2014.05.010.

[4] Falciglia, P.P., Romano, S., Vagliasindi, F.G.A., **2017**. Stabilisation/solidification of137Cs-contaminated soils using novel high-density grouts: γ-ray shielding properties, contaminant immobilisation and a γRS index-based approach for in situ applicability. *Chemosphere*. 168, 1257–1266. DOI:10.1016/j.chemosphere.2016.10.068.

[5] Khandaker, S., Toyohara, Y., Kamida, S., Kuba, T., **2018**. Adsorptive removal of cesium from aqueous solution using oxidized bamboo charcoal. *Water Resources and Industry*. 19, 35–46. DOI:10.1016/j.wri.2018.01.001.

[6] Zhang, H., Tangparitkul, S., Hendry, B., Harper, J., Kim, Y.K., Hunter, T.N., Lee, J.W., Harbottle, D., **2019**. Selective separation of cesium contaminated clays from pristine clays by flotation. *Chemical Engineering Journal*. 355, 797–804. DOI:10.1016/j.cej.2018.07.135.

[7] Liu, X., Chen, G.R., Lee, D.J., Kawamoto, T., Tanaka, H., Chen, M.L., Luo, Y.K., **2014**. Adsorption removal of cesium from drinking waters: A mini review on use of biosorbents and other adsorbents. *Bioresource Technology*. 160, 142–149. DOI:10.1016/j.biortech.2014.01.012.

[8] Awual, M.R., Yaita, T., Taguchi, T., Shiwaku, H., Suzuki, S., Okamoto, Y., **2014**. Selective cesium removal from radioactive liquid waste by crown ether immobilized new class conjugate adsorbent. *Journal of Hazardous Materials*. 278, 227–235. DOI:10.1016/j.jhazmat.2014.06.011.

[9] Zhang, Y., Jin, F., Shen, Z., Wang, F., Lynch, R., Al-Tabbaa, A., **2019**. Adsorption of methyl tert-butyl ether (MTBE) onto ZSM-5 zeolite: Fixed-bed column tests, breakthrough curve modelling and regeneration. *Chemosphere*. 220, 422–431. DOI:10.1016/j.chemosphere.2018.12.170.

[10] Roehl, K.E., Meggyes, T., Simon, F.-G., Stewart, D.I., **2005**.Long-term permance of permeable reactive barrier, in: J.O. (Univeristy of M. Ngriagu (Ed.), Trace Met. Other Contam. Environ., Elsevier B.V., 2005: pp. 311–321. DOI:10.1016/S0927-5215(05)80016-5.

[11] Ghaeminia, M., Mokhtarani, N., **2018**. Remediation of nitrate-contaminated groundwater by PRB-Electrokinetic integrated process. *Journal of Environmental Management*. 222, 234–

241. DOI:10.1016/j.jenvman.2018.05.078.

[12] Erto, A., Lancia, A., Bortone, I., Di Nardo, A., Di Natale, M., Musmarra, D., **2011**. A procedure to design a Permeable Adsorptive Barrier (PAB) for contaminated groundwater remediation. *Journal of Environmental Management*. 92, 23–30. DOI:10.1016/j.jenvman.2010.07.044.

[13] Montaña, M., Camacho, A., Serrano, I., Devesa, R., Matia, L., Vallés, I., **2013**. Removal of radionuclides in drinking water by membrane treatment using ultrafiltration, reverse osmosis and electrodialysis reversal. *Journal of Environmental Radioactivity*. 125, 86–92. DOI:10.1016/j.jenvrad.2013.01.010.

[14] Marsh, H., Rodríguez-Reinoso, F., **2006**.Activated Carbon, Elsevier S, Elsevier Science & Technology books, 2006.

[15] Mohan, D., Pittman, C.U., **2006**. Activated carbons and low cost adsorbents for remediation of tri- and hexavalent chromium from water. *Journal of Hazardous Materials*. 137, 762–811. DOI:10.1016/j.jhazmat.2006.06.060.

[16] Caccin, M., Giacobbo, F., Da Ros, M., Besozzi, L., Mariani, M., **2013**. Adsorption of uranium, cesium and strontium onto coconut shell activated carbon. *Journal of Radioanalytical and Nuclear Chemistry*. 297, 9–18. DOI:10.1007/s10967-012-2305-x.

[17] Vanderheyden, S.R.H., Van Ammel, R., Sobiech-Matura, K., Vanreppelen, K., Schreurs, S., Schroeyers, W., Yperman, J., Carleer, R., **2016**. Adsorption of cesium on different types of activated carbon. *Journal of Radioanalytical and Nuclear Chemistry*. 310, 301–310. DOI:10.1007/s10967-016-4807-4.

[18] Awual, M.R., Suzuki, S., Taguchi, T., Shiwaku, H., Okamoto, Y., Yaita, T., **2014**. Radioactive cesium removal from nuclear wastewater by novel inorganic and conjugate adsorbents. *Chemical Engineering Journal*. 242, 127–135. DOI:10.1016/j.cej.2013.12.072.

[19] Huang, L., Liu, G., Dong, G., Wu, X., Wang, C., Liu, Y., **2017**. Reaction mechanism of zero-valent iron coupling with microbe to degrade tetracycline in permeable reactive barrier (PRB). *Chemical Engineering Journal*. 316, 525–533. DOI:10.1016/j.cej.2017.01.096.

[20] Careghini, A., Saponaro, S., Sezenna, E., Daghio, M., Franzetti, A., Gandolfi, I., Bestetti, G., **2015**. Lab-scale tests and numerical simulations for in situ treatment of polluted groundwater. *Journal of Hazardous Materials*. 287, 162–170. DOI:10.1016/j.jhazmat.2015.01.028.

[21] Gholami, F., Mosmeri, H., Shavandi, M., Dastgheib, S.M.M., Amoozegar, M.A., **2019**. Application of encapsulated magnesium peroxide (MgO2) nanoparticles in permeable reactive barrier (PRB) for naphthalene and toluene bioremediation from groundwater. *Science of the Total Environment*. 655, 633–640. DOI:10.1016/j.scitotenv.2018.11.253.

[22] Falciglia, P.P., Roccaro, P., Bonanno, L., De Guidi, G., Vagliasindi, F.G.A., Romano, S., **2018**. A review on the microwave heating as a sustainable technique for environmental remediation/detoxification applications. *Renewable and Sustainable Energy Reviews*. 95, 147–170. DOI:10.1016/j.rser.2018.07.031.

[23] Falciglia, P.P., Malarbì, D., Maddalena, R., Greco, V., Vagliasindi, F.G.A., **2017**. Remediation of Hg-contaminated marine sediments by simultaneous application of enhancing agents and microwave heating (MWH). *Chemical Engineering Journal*. 321, 1–10. DOI:10.1016/j.cej.2017.03.097.

[24] Li, W., Wang, X., Peng, J., **2014**. Effects of microwave heating on porous structure of regenerated powdered activated carbon used in xylose. *Environmental Technology*. 35, 532–540. DOI:10.1080/09593330.2013.796007.

[25] Sun, Y., Zhang, B., Zheng, T., Wang, P., **2017**. Regeneration of activated carbon saturated with chloramphenicol by microwave and ultraviolet irradiation. *Chemical Engineering Journal*. 320, 264–270. DOI:10.1016/j.cej.2017.03.007.

[26] Yang, Z., Yi, H., Tang, X., Zhao, S., Yu, Q., Gao, F., Zhou, Y., Wang, J., Huang, Y., Yang, K., Shi, Y., **2017**. Potential demonstrations of "hot spots" presence by adsorption-desorption of toluene vapor onto granular activated carbon under microwave radiation. *Chemical Engineering Journal*. 319, 191–199. DOI:10.1016/j.cej.2017.02.157.

[27] Biniak, S., Szymański, G., Siedlewski, J., Światkoski, A., **1997**. The characterization of activated carbons with oxygen and nitrogen surface groups. *Carbon*. 35, 1799–1810. DOI:10.1016/S0008-6223(97)00096-1.

[28] De Haro-Del Rio, D.A., Al-Joubori, S., Kontogiannis, O., Papadatos-Gigantes, D., Ajayi, O., Li, C., Holmes, S.M., **2015**. The removal of caesium ions using supported clinoptilolite. *Journal of Hazardous Materials*. 289, 1–8. DOI:10.1016/j.jhazmat.2015.02.032.

[29] Wang, K., Ma, H., Pu, S., Yan, C., Wang, M., Yu, J., Wang, X., Chu, W., Zinchenko, A., **2019**. Hybrid porous magnetic bentonite-chitosan beads for selective removal of radioactive cesium in water. *Journal of Hazardous Materials*. 362, 160–169. DOI:10.1016/j.jhazmat.2018.08.067.

[30] Tran, H.N., You, S.J., Hosseini-Bandegharaei, A., Chao, H.P., **2017**. Mistakes and inconsistencies regarding adsorption of contaminants from aqueous solutions: A critical review. *Water Research*. 120, 88–116. DOI:10.1016/j.watres.2017.04.014.

[31] Lepri, F.G., Borges, D.L.G., Araujo, R.G.O., Welz, B., Wendler, F., Krieg, M., Becker-Ross, H., **2010**. Determination of heavy metals in activated charcoals and carbon black for Lyocell fiber production using direct solid sampling high-resolution continuum source graphite furnace atomic absorption and inductively coupled plasma optical emission spectrometry. *Talanta*. 81, 980–987. DOI:10.1016/j.talanta.2010.01.050.

[32] Ania, C.O., Parra, J.B., Menéndez, J.A., Pis, J.J., **2007**. Microwave-assisted regeneration of activated carbons loaded with pharmaceuticals. *Water Research*. 41, 3299–3306. DOI:10.1016/j.watres.2007.05.006.

[33] Lowell, S., Shields, J.E., Morral, J.E., **1985**. Powder Surface Area and Porosity, 2nd Edition. *Journal of Engineering Materials and Technology*. 107, 180. http://dx.doi.org/10.1115/1.3225796.

[34] Lippens, B.C., de Boer, J.H., **1965**. Studies on pore systems in catalysts: V. The t method.

Journal of Catalysis. 4, 319–323. DOI:https://doi.org/10.1016/0021-9517(65)90307-6.

[35] Horvath, G. and Kawazoe, K., **1983**. Method for calclualtion effective pore size distribution in molecular sieve carbon. *J. Chem. Eng. Japan*. 16, 470–475. DOI:10.1252/jcej.16.470.

[36] Febrianto, J., Kosasih, A.N., Sunarso, J., Ju, Y.-H., Indraswati, N., Ismadji, S., **2009**. Equilibrium and kinetic studies in adsorption of heavy metals using biosorbent: A summary of recent studies. *Journal of Hazardous Materials*. 162, 616–645. DOI:10.1016/j.jhazmat.2008.06.042.

[37] Ania, C.O., Parra, J.B., Menéndez, J.A., Pis, J.J., **2005**. Effect of microwave and conventional regeneration on the microporous and mesoporous network and on the adsorptive capacity of activated carbons. *Microporous and Mesoporous Materials*. 85, 7–15. DOI:10.1016/j.micromeso.2005.06.013.

[38] Borai, E.H., Harjula, R., malinen, L., Paajanen, A., **2009**. Efficient removal of cesium from low-level radioactive liquid waste using natural and impregnated zeolite minerals. *Journal of Hazardous Materials*. 172, 416–422. DOI:10.1016/j.jhazmat.2009.07.033.

[39] Chen, G.R., Chang, Y.R., Liu, X., Kawamoto, T., Tanaka, H., Parajuli, D., Chen, M.L., Lo, Y.K., Lei, Z., Lee, D.J., **2015**. Prussian blue non-woven filter for cesium removal from drinking water. *Separation and Purification Technology*. 153, 37–42. DOI:10.1016/j.seppur.2015.08.029.

[40] Machida, M., Mochimaru, T., Tatsumoto, H., **2006**. Lead(II) adsorption onto the graphene layer of carbonaceous materials in aqueous solution. *Carbon*. 44, 2681–2688. DOI:10.1016/j.carbon.2006.04.003.

[41] Abtahi, M., Fakhri, Y., Sarafraz, M., Keramati, H., Conti, G.O., **2018**. Removal of cesium through adsorption from aqueous solutions : a systematic review. *Journal of Advances in Environmental Health Research*. 6, 96–106. DOI:10.22102/jaehr.2018.104959.1048.

[42] Falciglia, P.P., Catalfo, A., Finocchiaro, G., Vagliasindi, F.G.A., Romano, S., De Guidi, G., **2018**. Microwave heating coupled with UV-A irradiation for PAH removal from highly contaminated marine sediments and subsequent photo-degradation of the generated vaporized organic compounds. *Chemical Engineering Journal*. 334, 172–183. DOI:10.1016/j.cej.2017.10.041.

[43] Honda, M., Okamoto, Y., Shimoyama, I., Shiwaku, H., Suzuki, S., Yaita, T., **2017**. Mechanism of Cs Removal from Fukushima Weathered Biotite by Heat Treatment with a NaCl-CaCl2Mixed Salt. *ACS Omega*. 2, 721–727. DOI:10.1021/acsomega.6b00372.

[44] Liu, C., Zachara, J.M., Qafoku, O., Smith, S.C., **2003**. Effect of temperature on Cs+ sorption and desorption in subsurface sediments at the Hanford Site, U.S.A. *Environmental Science and Technology*. 37, 2640–2645. DOI:10.1021/es026221h.

[45] Shimoyana, I., Hirao, N., Baba, Y., Izumi, T., Okamoto, Y., Yaita, T., Suzuki, S., **2014**. Low-pressure sublimation method for cesium decontamination of clay minerlas. *Clay Science*. 18, 71–77.

[46] Spalding, B.P., **1994**. Volatilization of Cesium-137 from Soil with Chloride Amendments

during Heating and Vitrification. *Environmental Science and Technology*. 28, 1116–1123. DOI:10.1021/es00055a022.

[47] Falciglia, P.P., Maddalena, R., Mancuso, G., Messina, V., Vagliasindi, F.G.A., **2016**. Lab-scale investigation on remediation of diesel-contaminated aquifer using microwave energy. *Journal of Environmental Management*. 167, 196–205. DOI:10.1016/j.jenvman.2015.11.046.

[48] De Guidi, G., Falciglia, P.P., Catalfo, A., De Guidi, G., Fagone, S., Vagliasindi, F.G.A., **2017**. Soil contaminated with PAHs and nitro-PAHs: contamination levels in an urban area of Catania (Sicily, southern Italy) and experimental results from simulated decontamination treatment. *Clean Technologies and Environmental Policy*. 19, 1121–1132. DOI:10.1007/s10098-016-1305-x.

[49] Falciglia, P.P., De Guidi, G., Catalfo, A., Finocchiaro, G., Farina, M., Liali, M., Lorenzano, G., Valastro, G., Vagliasindi, F.G.A., **2017**. Glycerol-enhanced microwave heating for ultra-rapid effective remediation of marine sediments highly contaminated with hydrocarbons. *Separation and Purification Technology*. 189, 11–19. DOI:10.1016/j.seppur.2017.07.066.

[50] Groen, J.C., Peffer, L.A.A., Pérez-Ramírez, J., **2003**. Pore size determination in modified micro- and mesoporous materials. Pitfalls and limitations in gas adsorption data analysis. *Microporous and Mesoporous Materials*. 60, 1–17. DOI:10.1016/S1387-1811(03)00339-1.

[51] Mohamad Nor, N., Sukri, M.F.F., Mohamed, A.R., **2016**. Development of high porosity structures of activated carbon via microwave-assisted regeneration for H2S removal. *Journal of Environmental Chemical Engineering*. 4, 4839–4845. DOI:10.1016/j.jece.2016.02.007.

[52] Hoseinzadeh Hesas, R., Wan Daud, W.M.A., Sahu, J.N., Arami-Niya, A., **2013**. The effects of a microwave heating method on the production of activated carbon from agricultural waste: A review. *Journal of Analytical and Applied Pyrolysis*. 100, 1–11. DOI:10.1016/j.jaap.2012.12.019.

[53] Mao, H., Zhou, D., Hashisho, Z., Wang, S., Chen, H., Wang, H.H., **2015**. Constant power and constant temperature microwave regeneration of toluene and acetone loaded on microporous activated carbon from agricultural residue. *Journal of Industrial and Engineering Chemistry*. 21, 516–525. DOI:10.1016/j.jiec.2014.03.014.

[54] Cheng, S., Zhang, L., Zhang, S., Xia, H., Peng, J., **2018**. Preparation of high surface area activated carbon from spent phenolic resin by microwave heating and KOH activation. *High Temperature Materials and Processes*. 37, 59–68. DOI:10.1515/htmp-2016-0042.

[55] Wang, S., Lu, G.Q., **1998**. Effects of acidic treatments on the pore and surface properties of ni catalyst supported on activated carbon. *Carbon*. 36, 283–292. DOI:10.1016/S0008-6223(97)00187-5.

[56] Al-Mutairi, N.Z., **2010**. 2,4-Dinitrophenol adsorption by date seeds: Effect of physico-chemical environment and regeneration study. *Desalination*. 250, 892–901. DOI:10.1016/j.desal.2008.10.035.

[57] Moreno-Castilla, C., **2004**. Adsorption of organic molecules from aqueous solutions on carbon materials. *Carbon*. 42, 83–94. DOI:10.1016/j.carbon.2003.09.022.

[58] Pi, X., Sun, F., Gao, J., Zhu, Y., Wang, L., Qu, Z., Liu, H., Zhao, G., **2017**. Microwave Irradiation Induced High-Efficiency Regeneration for Desulfurized Activated Coke: A Comparative Study with Conventional Thermal Regeneration. *Energy and Fuels*. 31, 9693–9702. DOI:10.1021/acs.energyfuels.7b01260.

[59] Foo, K.Y., Hameed, B.H., **2012**. Microwave-assisted regeneration of activated carbon. *Bioresource Technology*. 119, 41–47. DOI:10.1016/j.biortech.2012.05.061.

[60] Zanella, O., Tessaro, I.C., Féris, L.A., **2014**. Desorption- and decomposition-based techniques for the regeneration of activated carbon. *Chemical Engineering and Technology*. 37, 1447–1459. DOI:10.1002/ceat.201300808.

[61] Lalhmunsiama, Lalhriatpuia, C., Tiwari, D., Lee, S.M., **2014**. Immobilized nickel hexacyanoferrate on activated carbons for efficient attenuation of radio toxic Cs(I) from aqueous solutions. *Applied Surface Science*. 321, 275–282. DOI:10.1016/j.apsusc.2014.09.200.

[62] Metwally, S.S., El-Sherief, E.A., Mekhamer, H.S., **2019**. Fixed-bed column for the removal of cesium, strontium, and lead ions from aqueous solutions using brick kiln waste. *Separation Science and Technology*. 6395,. DOI:10.1080/01496395.2019.1572189.

[63] Falciglia, P.P., Malarbì, D., Maddalena, R., Greco, V., Vagliasindi, F.G.A., **2017**. Remediation of Hg-contaminated marine sediments by simultaneous application of enhancing agents and microwave heating (MWH). *Chemical Engineering Journal*. 321, 1–10. DOI:10.1016/j.cej.2017.03.097.

[64] Chang, S., Fu, H., Wu, X., Liu, C., Li, ZhengDai, Y., Zhang, H., **2018**. Batch and fixed-bed column studies for selective removal of cesium ions by compressible Prussian blue/polyurethane sponge. *RSC Advances*. 8, 36459–36467. DOI:10.1039/c8ra07665k.

[65] Falciglia, P.P., Roccaro, P., Bonanno, L., De Guidi, G., Vagliasindi, F.G.A., Romano, S., **2018**. A review on the microwave heating as a sustainable technique for environmental remediation/detoxification applications. *Renewable and Sustainable Energy Reviews*. 95, 147–170. DOI:10.1016/j.rser.2018.07.031.

Supporting Material

Table S1. Physical properties of GAC 830.

Parameter	Value
Surface area (B.E.T.) ($m^2\ g^{-1}$)	872.09
Apparent density ($kg\ m^{-3}$)	500
Dielectric constant (-)	13.8
Particle size (mm)	0.6 – 2.3
Median pore width (Horvath-Kawazoe model) (nm)	0.71
Pore volume (t-plot method) ($cm^3\ g^{-1}$)	0.51

Table S2. Isotherm equations and kinetic parameters from Cs-adsorption batch tests.

Model	Equation	Parameter	Unwashed	Water-washed	HCl-washed
Langmuir	$q_e=\frac{Q_0 k_L C_e}{1+k_L C_e}$	Q_0 ($mg\ g^{-1}$)	3.665	2.912	3.236
		k_L ($L\ mg^{-1}$)	0.003	0.005	0.005
		R^2 (-)	0.995	0.992	0.992
Freundlich	$q_e=C_e^{\frac{1}{n}}k_F$	k_F ($mg\ g^{-1}$)/($mg\ L^{-1}$)^n	0.026	0.041	0.046
		n (-)	1.334	1.495	1.495
		R^2 (-)	0.987	0.979	0.979
Temkin	$q_e=b_T \ln(k_T C_e)$	k_T ($L\ mg^{-1}$)	0.056	0.061	0.061
		b_T (-)	0.557	0.565	0.628
		R^2 (-)	0.989	0.98	0.989
Redlich-Peterson	$q_e=\frac{k_R C_e}{1+a_R C_e^{\alpha}}$	k_R ($L\ g^{-1}$)	0.011	0.014	0.015
		a_R ($mg\ L^{-1}$)$^{-\alpha}$	0.003	0.005	0.005
		α (-)	1.00	1.00	1.00
		R^2 (-)	0.995	0.995	0.992
Sips	$q_e=Q_s\frac{k_S C_e^{\frac{1}{n_s}}}{1+k_S C_e^{\frac{1}{n_s}}}$	k_S ($mg\ L^{-1}$) $^{1/n_s}$	0.0014	0.0017	0.0017
		n_S (-)	0.754	0.721	0.724
		Q_S ($mg\ g^{-1}$)	2.305	1.996	2.223
		R^2 (-)	0.998	0.984	0.997

Table S3. Mathematical model equations and kinetic parameters from the adsorption phase of MW-column tests.

Model	Equation	Parameter	T1	T2	T3	Mean
Yoon and Nelson	$\frac{C}{C_0}=\frac{1}{1+\exp(k_{YN}\cdot(\tau-t))}$	k_{YN} (min^{-1})	0.0196	0.0163	0.0197	0.0185
		τ (min)	144.3	154.1	141.1	146.5
		R^2 (-)	0.97	0.94	0.97	
Adams-Bohart	$\frac{C}{C_0}=\exp\left(k_{AB}C_0 t-k_{AB}N_0\frac{Z}{v}\right)$	k_{AB} ($L\ mg^{-1}\ min^{-1}$)	$4.95\cdot10^{-5}$	$4.94\cdot10^{-5}$	$4.93\cdot10^{-5}$	$4.94\cdot10^{-5}$
		N_0 ($mg\ L^{-1}$)	809.1	824	802.2	811.76
		R^2 (-)	0.79	0.81	0.8	
Thomas	$\frac{C}{C_0}=\frac{1}{1+\exp\left(\frac{k_{th}q_0 m}{Q}-k_{th}C_0 t\right)}$	k_{th} ($L\ mg^{-1}\ min^{-1}$)	$1.96\cdot10^{-4}$	$1.63\cdot10^{-4}$	$1.97\cdot10^{-4}$	$1.85\cdot10^{-4}$
		q_0 ($mg\ g^{-1}$)	0.660	0.705	0.645	0.67
		R^2 (-)	0.96	0.95	0.97	
Logit	$\frac{C}{C_0}=\frac{\exp(k_L C_0 t-k_L N_L Z/v)}{1+\exp(k_L C_0 t-k_L N_L Z/v)}$	k_L ($L\ mg^{-1}\ min^{-1}$)	$1.96\cdot10^{-4}$	$1.63\cdot10^{-4}$	$1.97\cdot10^{-4}$	$1.85\cdot10^{-4}$
		N_L ($mg\ L^{-1}$)	343.6	366.9	335.9	348.8
		R^2 (-)	0.96	0.94	0.97	

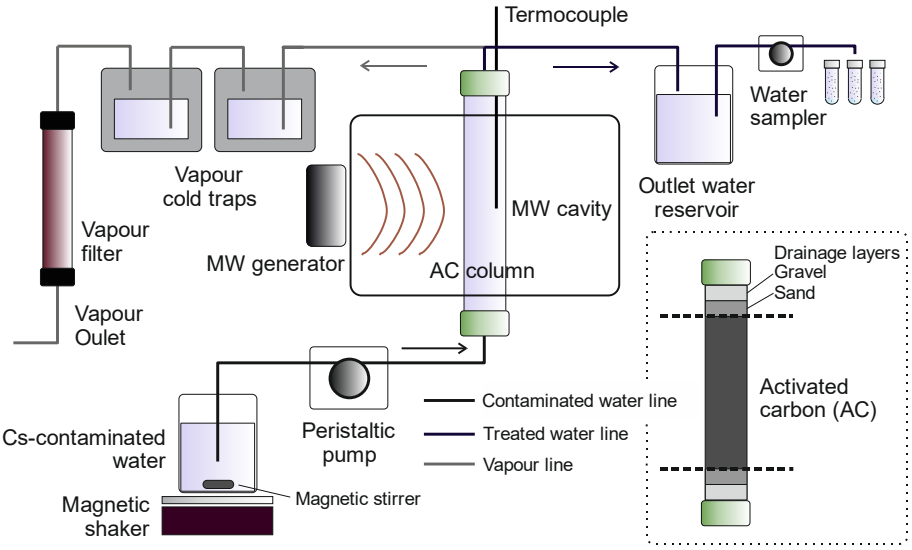

Figure S1. Schematic view of the experimental setup for MW-regeneration column tests.

Chapter 6: Field technical applicability and cost analysis for microwave based regenerating permeable reactive barriers (MW-PRBs) operating in Cs-contaminated groundwater treatment

Abstract

The present study tests the potentiality of a novel microwave based regenerating permeable reactive barrier (MW-PRB) system as combined treatment for Cs-contaminated groundwater. Granular activated carbon (GAC) was selected as adsorptive materials in batch and column MW-regeneration experiments. Experimental and modeling data were elaborated for technical and economic considerations in order to assess the MW-PRB feasibility jointly with essential information regarding its real field applicability. Batch experiments investigated the effects of 10 adsorption-MW regeneration cycles under different MW irradiation conditions (applied electric field = 200–460 V m^{-1}; irradiation times = 1–15 min) by assessing GAC variation properties in term of regeneration yield (δ), specific area and weight loss (WL) variation. Column tests were carried using a dedicated setup essentially including a column filled with GAC implanted in a MW oven cavity (MW electric field of 385 V m^{-1}, irradiation times 5-15 min). Results from techno-economic analysis revealed the MW-PRB viability and its advantages also in comparison with conventional PRB systems, demonstrating the concept of combined MW-PRB treatment. Saved cost obtained demonstrated in fact the potential cost effectiveness of MW-PRB system and, consequently, the implementation of novel approach is encouraged. Calculated PRB longevity vs groundwater velocity curves are useful in order to predict long-term PRB performance and the response of the remediation activities, as well as for guiding the design and the scaling-up of MW-PRB treatment.

Graphical abstract

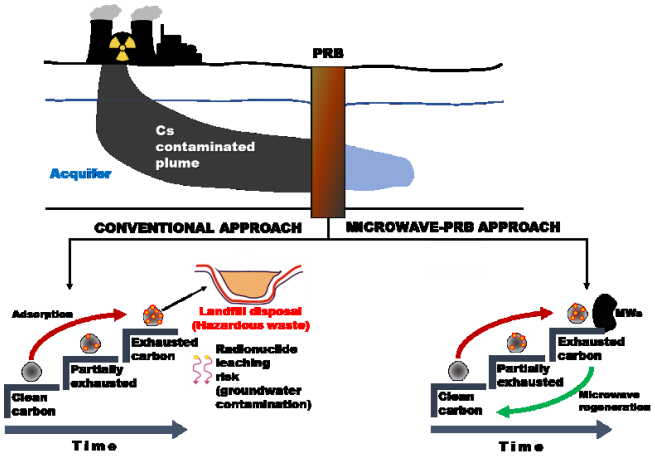

Keywords: Cesium, cost analysis, granular activated carbon, groundwater contamination, microwave regeneration, permeable reactive barrier.

❖ **This chapter have been redrafted from:**

Falciglia, P.P., **Gagliano, E.**, Brancato, V., Finocchiaro, G., Catalfo, A., De Guidi, G., Romano, S., Roccaro, P., Vagliasindi, F.G.A., **2020**. Field technical applicability and cost analysis for microwave based regenerating permeable reactive barriers (MW-PRBs) operating in Cs-contaminated groundwater treatment. *Journal of Environmental Management*. 260, 110064. DOI:10.1016/j.jenvman.2020.110064.

1. Introduction

Over the last decades, past activities with radionuclides created complex environmental challenges of enormous scale worldwide. Common operations or incidental events related to nuclear activities (weapon industry, nuclear energy) are considered severe causes of contamination. The release of radionuclides into surrounding environments produced a severe impact of soils and, especially surface water and groundwater [1]. Water containing radioactive elements introduced a permanent threat to the environment became a high-risk radiation source [2]. Cesium-137 (^{137}Cs) is the most prevalent product of the nuclear fission of ^{235}U and ^{239}Pu and it has problematic long-term radiological effects (half-life 30.2 years) due to beta (β)-particle and strong gamma (γ)-ray emission [3]. Cesium-137 remediation is urgent but challenging due to high solubility of Cs^+ ions in water, mobility through the environment and bioavailability to terrestrial and aquatic organisms through the food chain. It can cause permanent damages among which the irreparable destruction of the biological structure and functions of organisms also leading to cancer, genetic mutation and genetic disorders [4]. This makes the remediation of Cs^+ in groundwater a priority and complex issue. The management of long-lived radionuclide-impacted sites presents in fact a number of important challenges regarding characterization and remedial actions, as well as long-term monitoring to ensure the defence of the environment and human health. Consequently, the need for Cs^+ removal has led to the development of novel methods to accelerate the process of environment decontamination [5].

Permeable reactive barrier (PRB) is considered a valuable innovative technology and potentially applicable for this purpose [6]. PRBs enable physical, chemical or biological in situ treatment of contaminated groundwater by bringing it into contact with reactive/adsorptive materials. The materials are inserted underground in a natural aquifer and intercepts the pollution plume removing the contaminants without water pumping. This makes PRB a cost-effective clean-up technology with much less environmental impact and more economical over the long term than other methods (i.e. pump-and-treat) that require continuous energy input [7,8].

In view of decontaminating Cs-impacted water several processes have been proposed [9]. Solvent extraction, ion-exchange and adsorption are considered the most effective and selective. However, the former is very restricted due to chemical high costs, and ion-exchange with clay minerals or Prussian blue supported materials generates huge amount of solid waste due to their non-reusable character or the very high regeneration costs [10]. Alternatively, adsorption is deemed more cost-effective for Cs-removal from water solutions [4]. Granular activated carbon (GAC) is one of the most commonly used materials in PRB project [11]. GACs are a low-cost and effective adsorptive materials (high surface area and porosity) for several contaminants among which radionuclides [12–14]. Limited data are available on their applicability for Cs removal [9,15–17].

Longevity of PRB is defined as the ability to maintain the contaminant sorption capability in the years [18] and a reduced longevity value due to a GAC saturation is the major problem affecting full-scale treatments [11]. Exhausted AC incineration or landfill disposal are considered further problems, which can also lead to secondary contamination paths. Furthermore, in the case of reusable contaminants such as ^{137}Cs, GAC regeneration would allow the recovery of a precious γ-ray source [10]. However, while wide research has been performed on contaminant/material/process aspects, PRB technological aspects and long-term performance have not been extensively considered. This gap in the knowledge is the most problematic because design life has a decisive influence on the economic viability of PRBs [19].

Consequently, a frontier and active research issue is coupling PRB with other regeneration processes with the aim of extend the PRB longevity [20]. The use of the permeable porous medium to support biodegrading microorganisms in the novel concept study on self-regenerating biological-PRBs has been proposed by Careghini et al. (2015). The same topic has been investigated by other researches [20,22]. The electrochemical-PRB coupled approach is considered another very active research area [11]. However, these coupled-technologies result to be ineffective for metals/radionuclides and/or require very long regeneration times or high costs [21].

Heating by microwave (MW) irradiation is a growing interest issue in several energy and environmental applications [23]. Microwaves (MWs) are electromagnetic radiations (300 MHz - 300 GHz). During MW irradiation, its electric power (E) is partially absorbed by the irradiated medium and converted into heat, generating a consequential exponential E decrease with the distance from the MW source. The presence of an alternating electromagnetic field induces the rotation of the dipoles constituting the media and their intermolecular friction results in heat generation [23]. This offers many advantages such as a uniform heating of the material, an increase in energy transfer efficiency and reductions in the heating time process. It also allows the limits of conventional heating to be overcome [24]. Then the major driving force of MW technique is the passive ability of the irradiated medium to convert the adsorbed energy into heat depending on the media dielectric features (polarity). High dielectric properties intensely decrease the energy requirements and make MW a very cost-effective and sustainable treatment. The rate of heat produced during the irradiation substantially depends on the 'loss tangent' ($\tan \delta = \varepsilon''/\varepsilon'$) of the media. ε' and ε'' are the real part (dielectric constant) and the imaginary parts (dielectric loss factor) of the complex permittivity, respectively. $\tan \delta > 0.5$ categorizes materials as high MW absorbing [23]. The increase of temperature with time is also proportional to the frequency (f) of the MW radiation. However, high f values do not play in favor of the MW penetration into the media. Then, for an effective treatment, the selection of the correct f value is fundamental. The frequency of 2.45 GHz allows a sufficient combination of

both the effects [23]. Regeneration of GACs by MW heating has attracted many attentions due to the excellent MW-absorbing features of activated carbon because the interactions of the delocalized π-electrons with MWs [25–27]. High mechanical strength and a good resistance towards heat and radiation are other essential features [12,28].

The present study tests the potentiality of a novel MW-PRB system as microwave based regenerating PRB installation for the treatment of Cs-contaminated groundwater. Data obtained from fixed-bed column experiments and modelling were used for elaborating technical and economic considerations and, consequently, in order to assess the MW-PRB feasibility jointly with essential information regarding its real field applicability, also in comparison with conventional PRB systems.

2. Experimental

2.1 GAC temperature variation, specific surface area, regeneration yield and the weight loss

Granular activated carbon *830* purchased by *Norit S.p.A.* (GAC 830) was used due to its assumed Cs-adsorption capability and predisposition for MW thermal regeneration processes due to its noticeable dielectric properties (Table 1). GAC samples were washed with a HCl solution (10^{-3} M), sieved at 2.0 mm and dried at 100 °C, then were artificially saturated using a ^{133}Cs-solution as CsCl (99% purity, 168.36 g mol^{-1}, *Sigma-Aldrich*) in deionized water (250 mg L^{-1}) [2,29,30]. Specifically, a Solid:Liquid ratio of 1:10 (mass based) and a shaking speed of 180 rpm (24 h, T = 20 °C) were adopted [31–33]. After the contamination procedure, the exhausted GAC samples were irradiated using a MW oven operating at the frequency of 2.45-GHz (1 kW) under different MW irradiation electric fields (E). The MW cavity was hydraulically connected with a gas line (cold traps, AC filter and electric vacuum pump) to capture the exhaust vapour. In a typical run, 15 g of GAC were irradiated considering different MW electric fields (200 – 460 V m^{-1}) and irradiation times (1 – 15 min). At the end of each run, the GAC temperature (T) was measured with a type-k thermocouple (LT Lutron, TM-946).

Adsorption/regeneration cycle effect was also assessed for 10 regeneration cycles (irradiation time = 3 min) as regeneration yield (δ) [34], Langmuir specific surface area (m^2 g^{-1}) and specific weight loss percentage (WL) (% min^{-1}) [26]. WL was also assessed for increasing MW irradiation times. Regeneration yield is the adsorption capacity recovery percentage and it was calculated by Eq. 1:

$$\delta = \frac{q_i}{q_0} \cdot 100 \quad (1)$$

where q_i is the adsorption capacity (mg g^{-1}) of MW regenerated GAC and q_0 is the adsorption capacity (mg g^{-1}) of fresh GAC. Langmuir specific surface area was obtained from N_2 adsorption isotherm at

77 K using an automatic volumetric adsorption analyser (Micromeritics ASAP 2020) and fitting the experimental data by Langmuir model [35].

Table 1. Physical properties of GAC 830.

Parameter	Value
Surface area (m^2 g^{-1})	872.1
Apparent density (kg m^{-3})	500
Texture (mm)	0.60 - 2.36
Dielectric constant ε' (-)	6.0
Dielectric loss factor ε'' (-)	0.9
Specific heat (J kg^{-1} K^{-1})	1.062
Median pore width (nm)	0.71
Pore volume (T-plot method) (cm^3 g^{-1})	0.43

2.2 Simulation of microwave based regenerating PRB (MW-PRB) process: MW-column tests

Simulation of the MW based regenerating PRB process was carried out in MW-irradiated column tests with Cs removal purpose. Simulation included three different phases: i) adsorption before regeneration; ii) MW regeneration; iii) adsorption after regeneration. The bench-scale apparatus was composed by a Pyrex glass column (∅ = 5 cm, h = 45 cm) implanted in a MW oven cavity (h = 21 cm) provided with a 1-kW magnetron as MW generator for the column irradiation. The column was filled with the GAC 830 (bed length = 21 cm; bulk density = 0.53 g cm^{-3}; packed bed porosity = 0.48) and it was flushed with a peristaltic pump. The outlet section was made up of two different hydraulic lines: water and vapour line. The first worked during the adsorption phases, whilst the second one collected the exhaust vapours produced during the MW regeneration phase. For the adsorption phase i), a Cs solution (C_0 = 100 mg L^{-1}) [29,36] was pumped upward at the flow rate of 10 mL min^{-1} [37,38]. The outlet water samples were collected at set intervals (water line) for Cs concentration (C) analysis. At the end of the phase i), which corresponds with the GAC saturation, the GAC-filled column was MW irradiated at 385 V m^{-1} for 15 min. After regeneration phase, a novel adsorption phase was implemented. The breakthrough curve was expressed in terms of Cs normalized concentration (ratio of effluent Cs concentration to inlet Cs concentration, C/C_0) as a function of flushing time (t, min). Outlet water samples were filtered through *Whatman* paper filter (0.20 μm) before analyse Cs concentration using inductively coupled plasma-mass spectrometry (ICP-MS). The kinetic parameters related to Cs removal from aqueous solution in fixed-bed column tests were obtained from experimental data by fitting Yoon and Nelson model through a non-linear regression [39]. Yoon and

Nelson model assumes that the rate of decrease in the probability of each adsorbate to be adsorbed is proportional to the probability of its adsorption and breakthrough on the adsorbent [40]. This model was chosen because it was developed addressing the sorption and consequently breakthrough of sorbate into activated charcoal. It is generally employed in order to describe the adsorption behaviour of cesium ions in a fixed-bed column [37,41,42].

3. Techno-economic analysis

3.1 Conventional PRB design

From column test data, the minimum thickness (L_{MIN}) of conventional PRB was calculated as follows [43,44]:

$$L_{MIN}=R\cdot\frac{\upsilon\cdot\tau\cdot h\cdot S}{V} \quad (2)$$

where υ (cm min^{-1}) is the linear velocity of water passing through the GAC, equivalent to the adopted flow pump rate (Q = 10 mL min^{-1}), τ (min) is the time that corresponds to the appearance of the contaminant in the effluent, h (cm) is the GAC bed length in the column, S (cm^2) is the cross-sectional area of the column and V (mL) is the volume of the contaminant solution passed through the GAC bed at time τ. R is the scaling-up coefficient taking into account the difference between column and field conditions:

$$R=\frac{C_{0(PRB)}-C_{i(target)}}{C_{0(column)}-C_{i(\tau)}} \quad (3)$$

where $C_{0(PRB)}$ (mg L^{-1}) is the contaminant concentration of groundwater entering the PRB, $C_{i(target)}$ (mg L^{-1}) is target contaminant concentration (regulatory standard). $C_{0(column)}$ (mg L^{-1}) and $C_{i(\tau)}$ (mg L^{-1}) are the initial contaminant concentration of the water solution fluxed through the column (experimental) and the contaminant concentration corresponding to the time τ from the breakthrough curve, respectively. Calculation were performed for different $C_{0(PRB)}$ values (0.1, 1 5, 20 mg L^{-1}) and $C_{i(target)}$ = 3.1 pg L^{-1} (for ^{137}Cs, World Health Organization).

Obtained L_{MIN} values were also compared with finding from the methodology proposed by Gavaskar (1999) and Roehl et al. (2005). In order to discriminate this method from the previous one, the minimum thickness was indicated with letter “b”:

$$b=\upsilon\cdot t_R \quad (4)$$

where t_R is the residence time obtained from kinetic considerations which was calculated as follows [45]:

$$t_R=\frac{-\ln(C_{0(PRB)}/C_{i(target)})}{k} \quad (5)$$

where k (min^{-1}) is the rate constant obtained from breakthrough curve modeling.

Thereafter, PRB longevity (T_L, day) was calculated by Eq. 6 for different fixed L_{PRB} values ($L_{PRB} >> L_{MIN}$) in the range (0.5 – 4 m), groundwater (GW) filtration velocity (0.001 – 1 cm min^{-1}) and $C_{0(PRB)}$ (0.1 – 20 mg L^{-1}).

$$T_L = \frac{L_{PRB} \cdot M_R}{\upsilon \cdot (C_{0(PRB)} - Ci_{(target)})} \quad (6)$$

M_R (mg cm^3) is the total removal efficiency at time τ [43,44]:

$$M_R = \frac{M_T}{h \cdot S} \quad (7)$$

where M_T (mg) is the amount of contaminant removed at time τ:

$$M_T = Q \cdot C_{0(column)} \cdot \tau \quad (8)$$

Finally, from obtained PRB longevity vs GW velocity curves, the PRB design thickness (L) was assessed for two different scenarios: L_{PRB1} and L_{PRB2} for the *Scenario 1* ($T_{L(1)}$ = 600 d, $C_{0(PRB)(1)}$ = 1 mg L^{-1}) and *Scenario 2* ($T_{L(2)}$ = 600 d, $C_{0(PRB)(2)}$ = 5 mg L^{-1}), respectively.

3.2 MW-PRB design

In the case of in-situ microwave regeneration of the PRB (MW-PRB system), the main advantages are given by the potential reduction in PRB dimensions (PRB thickness and GAC weight) and the minimization of final hazardous landfill GAC disposal (Figure 1). Specifically, it is clear that the reduction in PRB thickness is related to the whole MW regeneration process. Based on the above statement, the number of GAC regeneration cycles were calculated for the *Scenarios 1* and *2* ($C_{0(PRB)}$ = 1 and 5 mg L^{-1}, respectively), considering different reduced thickness values ($L_{MW\text{-}PRB}$), the regeneration time (t_R) investigated at the lab-scale (15 min) and the corresponding Cs removal efficiency achieved (RE, %). Calculation were performed by the assessment of the ratio between the longevity values corresponding to the original (L_{PRB}) and the reduced ($L_{MW\text{-}PRB}$) thickness values through the PRB longevity vs GW velocity curves.

The propagation of the MW electric field into the adsorptive material represents another key factor in MW regeneration process. This aspect was evaluated by the assessment of the MW radius of influence (R_{MW}) for different initial electric field (E_0, V m^{-1}) at MW source. Firstly, the spatial variation of the electric field (E_d, V m^{-1}) into the medium with the distance from the MW source (d, m) was calculated by Eq. 9 [23]:

$$E_d = E_0 \cdot e^{-\frac{d}{D_p}} \quad (9)$$

where D_p is penetration depth (m) defined as the distance from d at which E drops to 0.37 from its initial value (E_0):

$$D_p = \frac{\lambda_0}{2\pi} \cdot \frac{\sqrt{\varepsilon'}}{\varepsilon''} \quad (10)$$

where λ_0 is the wavelength of the irradiation, whereas ε' and ε" are the real part (dielectric constant) and the imaginary parts (dielectric loss factor) of the complex permittivity of the media, respectively. Calculation were performed for three E_0 values (500, 1000 and 1500 V m^{-1}) considering the dielectric constants of the GAC reported in Table 1. From obtained E_d vs d curves, R_{MW} was assessed as maximum distance from the source within the average E_d is 385 V m^{-1}. It corresponds to the value used in the MW column tests.

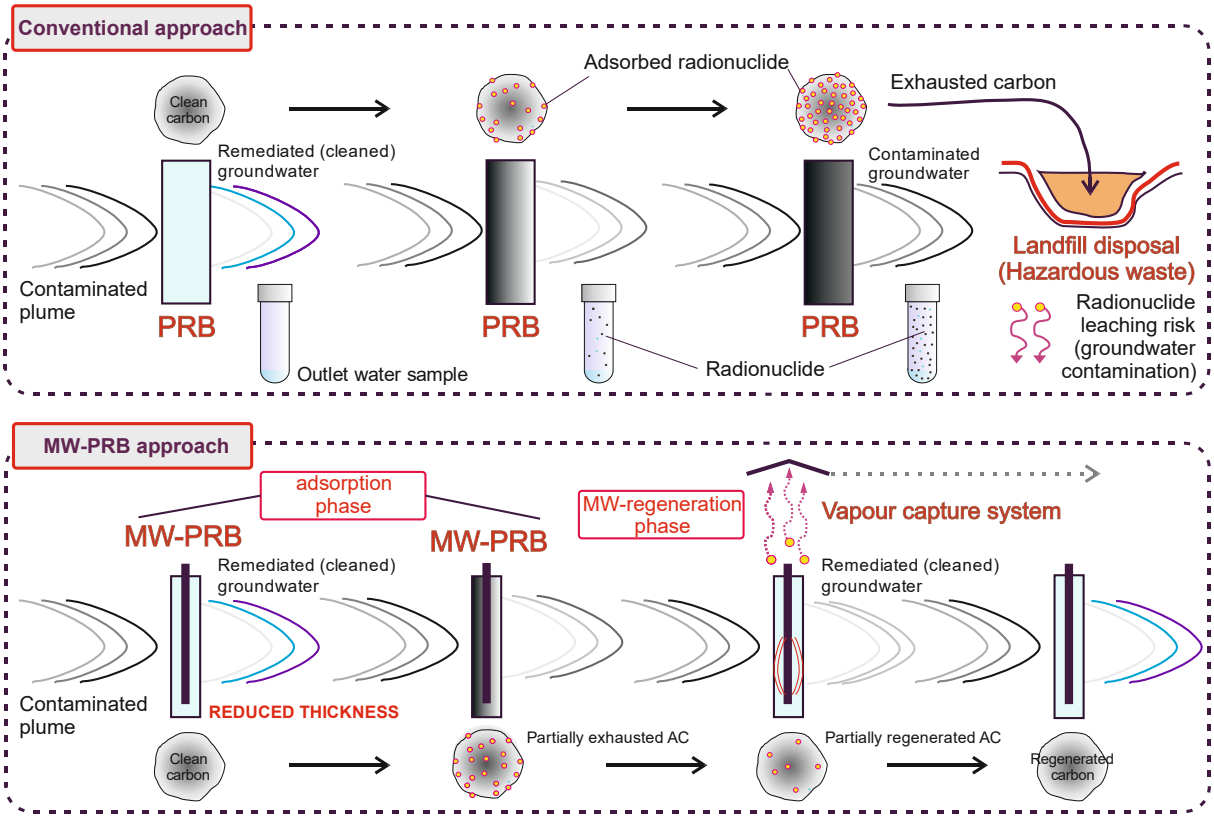

Figure 1. Conventional PRB vs MW-PRB approach.

3.3 Material and energy costs

The feasibility of the MW-PRB approach was evaluated by its comparison with conventional PRB system. Comparison was obtained considering the main specific costs (per unit of plume transversal area, € m^{-2}) that can be identified as variable between the two different approaches: i) GAC reduced cost (due to the reduction in PRB thickness); ii) replacement GAC cost (due to the GAC weight loss during MW regeneration); iii) MW energy cost (due to the MW regeneration). The *Scenario 1* ($C_{0(PRB)}$ = 1 mg L^{-1}) with L reduction from 1 to 0.5 m and *Scenario 2* ($C_{0(PRB)}$ = 5 mg L^{-1}) with L reduction from 4 to 2, 1 and 0.5 m were adopted as design parameters. The cost i) was calculated considering the obtained reduction in PRB specific volume, the GAC specific cost of 1200 € ton^{-1} [19] and density (Table 1). The replacement GAC cost took into account the GAC weight loss per irradiation time unit (% min^{-1}) (from experiments), the corresponding irradiation time for each regeneration cycle (20 min)

and the number of regeneration cycles needed to achieve the PRB thickness reduction. Twenty minutes were selected as safety value respect to the 15 min regeneration time applied during the experiments. The MW energy cost was assessed considering the R_{MW} corresponding to the application of an initial electric field of E_0 (applied power = 6 kW) and an electric energy cost of 0.12 € $k^{-1}W^{-1}h^{-1}$.

4. Results and discussion

4.1 Batch tests: GAC temperature, regeneration yield, specific surface area and the weight loss

The GAC temperature (T) variation with irradiation time during the MW-regeneration process for different applied MW-electric field (E_0) is given in Figure 2. In all cases, T increased with time, due to the passive ability of the GAC, expressed by its considerable dielectric properties, to convert the absorbed E_0 energy into heat ($\dot{Q}$), following the principle of dielectric heating as expressed by Eq. 11 [23].

$$\dot{Q}=\frac{1}{2}\omega\epsilon_0\varepsilon''\left|E_{max}^2\right| = \omega\epsilon_0\varepsilon''\left|E^2\right| \quad (11)$$

where $\dot{Q}$ is the specific heat (per unit of volume) generated during the MW irradiation, ω is the angular frequency ($\omega = 2\pi f$), ε_0 is the permittivity of free space, ε" is the dielectric loss factor of the medium, E_{max} is the electromagnetic field peak value and E is electromagnetic field effective value. The dielectric loss factor expresses the ability of the media to convert the irradiation into heat. The dependence of the dielectric properties with the temperature results in a reduction of this conversion ability as deducible by the asymptotic trend observed for all tests [46].

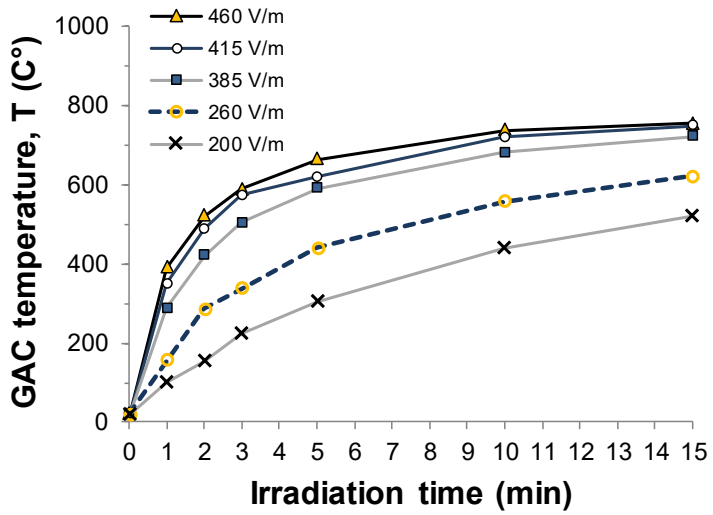

Figure 2. GAG temperature variation with irradiation time for different MW electric field applied (bench-scale tests).

Specifically, T rose rapidly up to about 600 °C within 3 min for the maximum E_0 investigated (460 V m^{-1}) and reached about 700 °C at the end of the MW irradiation. For E_0 = 385 V m^{-1}, a lower T of about 500 °C was achieved in 3-min treatment, whilst a T value almost equal to the previous case was observed after 15 min. The same behaviour but with overall lower T values were progressively found for the lower electric field applied. In general, it is important to remark that the observed strong passive ability of GAC to transform a relatively low MW energy into a rapid and large increase in temperature represents the main key factor in the MW regeneration process. This appears more evident by comparing the obtained findings with temperature profile from MW irradiation of different matrices (i.e.: soils, sediments), which generally produce significantly lower temperatures when irradiated with the same MW power inputs [47,48].

GAC samples from MW regeneration process at E_0 = 385 V m^{-1} (3 min) were analysed for regeneration yield (δ) and Langmuir specific area investigating different regeneration cycles. Results are depicted in Figure 3a. Regeneration yield values higher than ~79% indicate the clear ability of MW irradiation in Cs removal from GAC. The GAC maximum temperature of almost 500 °C achieved at the end of each regeneration cycle (GAC temperature does not significantly vary with increasing the number of the regeneration cycles – data not reported) suggested the Cs thermal desorption as contaminant removal mechanism. Previous studies have demonstrated that temperatures in the 400–700 °C range are sufficient to progressively desorb Cs from clay minerals and sediments [49,50]. At lower temperatures, cesium is prone to sublimate under low pressures [51]. Below 200 °C, water adsorbed on the surface can effectively desorb [51]. Consequently, Cs desorption from GAC was also favoured by stripping mechanism which was demonstrated to be an important removal mechanism during MW regeneration process [47].

It is notably that δ and Langmuir area followed the same trend (Figure 3a), they increased until the 5th cycle and then decreased (at the end of the 10th regeneration cycle). The surface area variation is ascribable to a modification as reorganization of GAC structure [52]. Then, the increase in regeneration yield is not be exclusively attributed to the desorption of Cs [34]. In detail, the π-interactions between GAC and Cs are improved when GAC is irradiated by MW [26]. Further regeneration cycles (successive to the 5th) resulted in a slight decrease in the Langmuir area and, consequently, in regeneration yield. Langmuir area of GAC samples after the 10th regeneration cycle was about 1200 m^2 g^{-1}, which is higher than the virgin GAC (Table 1). The specific weight loss (WL, % min^{-1}) of GAC samples during MW irradiation was assessed, its variation during several regeneration cycles (Figure 3b) and with the irradiation time (Figure 3c) has been investigated. After two regeneration cycles, the specific WL is almost constant and the mean value was 0.226% min^{-1} with the highest values observed within the first two cycles. This is recognized as subordinate effect linked to the

reorganization of GAC porous structure [26]. Considering that MW irradiation time of 3 min and ten regeneration cycles, the overall specific weight loss of GAC was on average about 6.78%. Then, MW energy seems to better preserve the life span of activated carbon comparing with conventional thermal regeneration, in which specific weight loss ranging between 5 – 15% for each regeneration cycle [53]. Figure 3c also demonstrated that the reorganization of GAC porous structure could take place between 2 and 3 min of MW irradiation as suggested by the highest specific weight loss observed (Figure 3c). A regeneration time of 3 min is almost enough to reach the highest temperatures observed during the 385 V m^{-1} test (Figure 2), and allows an important modification of porous structure [52].

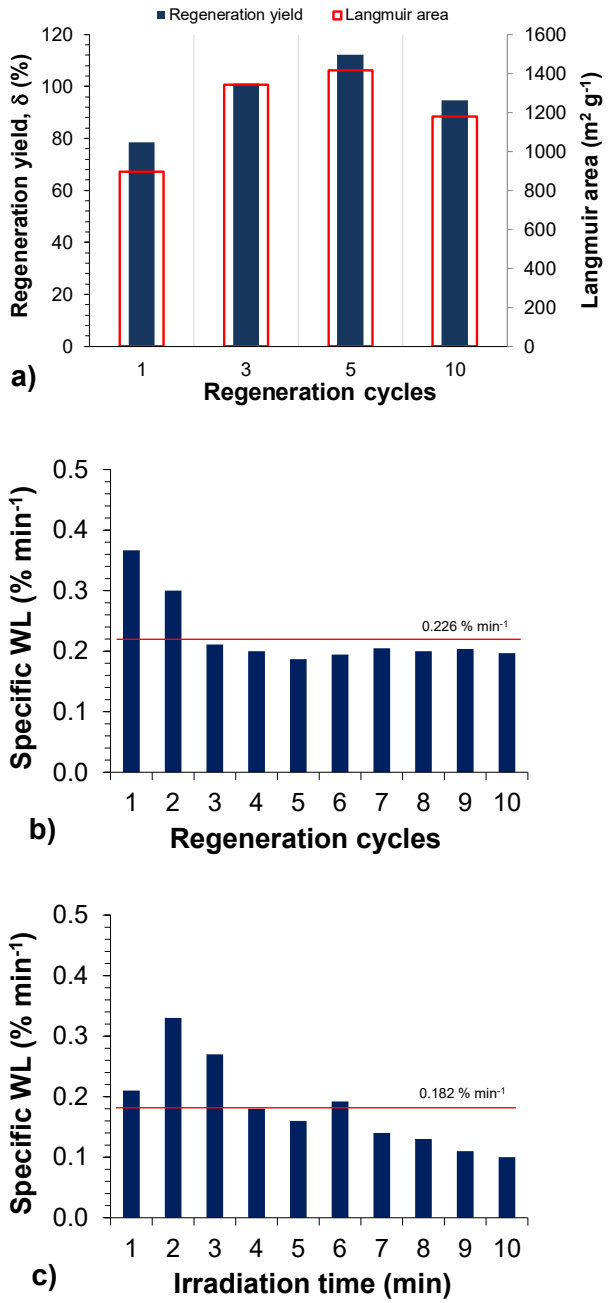

Figure 3. GAC regeneration yield and Langmuir specific area after variable regeneration cycles (bench-scale test, electric field applied = 385 V m^{-1}, MW irradiation time = 3 min) (**a**). Specific weight loss variation with MW regeneration cycles (MW irradiation time = 3 min) (**b**), and MW irradiation time (**c**) (Bench-scale test, electric field applied = 385 V m^{-1}).

4.2 MW column tests: breakthrough curves and Cs-removal efficiency

Figure 4 illustrate the breakthrough curve of Cs adsorption on GAC column (constant flow rate of 10 mL min^{-1} and Cs initial concentration of 100 mg L^{-1}). The slope of observed breakthrough curve is not steep and this suggests a low mass-transfer flux from the bulk solution [41,54]. The saturation plateau was approached near to 3 L of flow solution (corresponding to 300 min) (Figure 4). Kinetic parameters T (min) and k_Y (min^{-1}) obtained from Yoon and Nelson model are given in Table 2. In detail, k_Y (min^{-1}) is the rate constant, related to diffusion characteristics of the mass transfer zone, and T (min) is the time required for 50% adsorbate breakthrough [39,41]. Yoon and Nelson model provided a good fit of the experimental data as confirmed by the coefficient of determination (R^2) and the sum of squared errors (SSE) (Table 2). Obtained data are in agreement with a previous study [37], where Cs sorption (initial concentration = 500 – 1000 mg L^{-1}) on ammonium molybdophosphate-polyacrylonitrile (AMP-PAN) was investigated at different flow rates (5-15 mL min^{-1}) and bed length (14.5-21.5 cm).

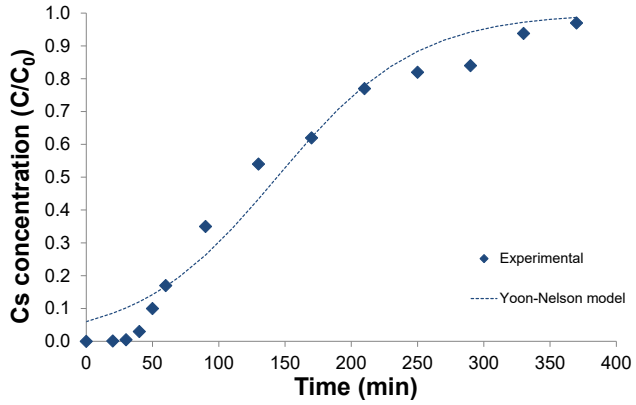

Figure 4. Breakthrough curve from MW-PRB simulated process (MW-column experiments).

Table 2. Kinetic parameters from Yoon and Nelson model fitting.

Equation	Parameters	Values
$t=T+(1/k_Y)\ln\frac{C}{C_0-C}$	T (min)	144.3
	k_Y (min^{-1})	0.019
	R^2	0.96
	SSE	0.064

The effect of the MW regeneration time on Cs removal from GAC observed for the regeneration phase (ii) in MW-column experiments revealed a removal of 80% for 15-min irradiation. GAC temperature recorded for the duration of the regeneration phase indicated values not higher than 150 °C. However, they cannot be considered representative of the GAC real bulk temperature due to the continuous presence of the saturation water or vapor generated during the MW heating. GAC bulk

temperature values in the range of that observed during the batch test are presumable, however in the presence of a water/vapor continuous flow, this kind of measurement is not possible. Bulk temperature of saturated porous media during MW heating is not directly measurable. Observed removals are consequently mainly ascribable to Cs thermal desorption phenomena, which in this case, takes place at higher temperatures (up to ~700 °C). In addition, the continuous, intense and proportional (to the MW irradiation time) production of water vapor, observed during this phase, elects Cs stripping for rapid water distillation as important co-removal mechanism [24]. Cesium stripping was shown to be enhanced by its high water solubility in water [3]. However, the perpetual presence of the saturation water due to the continuous Cs-contaminated solution flushing, and the higher GAC mass irradiated during the column respect to the batch test, resulted in a lower maximum Cs-removal. The different electromagnetic field propagation (different irradiation ways) between batch and column tests also contributed to that result. Furthermore, regeneration yield and removals obtained from experiments suggest that the main adsorption mechanisms established during Cs adsorption are reversible. Consequently, electrostatic interactions and physical adsorption are closely involved during Cs adsorption on GAC. It does not exclude the role of chemisorption (i.e., ion exchange, surface complexation, precipitation) in the removal of Cs from aqueous solution as occurred for others heavy metals [55].

4.3 Technical consideration on PRB/MW-PRB application

Eqs. (2) and (4) were used to calculate the minimum thickness (L_{MIN} and b, respectively) required for conventional PRB design by using column test experimental data. As shown in Table 3, the residence time (t_R) required to ensure the complete degradation and, consequently, the minimum thickness of PRB increases with increasing the Cs field concentration entering the PRB (0.1 – 20 mg L^{-1}). From obtained findings, it is clear that values of minimum thickness calculated with two equations are very different, due to different assumptions on which the methodologies are based [44,45]. Calculation from Eq. (4), based on residence time estimated from kinetic investigation (columns experiments), led to PRB thickness more similar to those generally adopted at the full scale and large enough to achieve the desired degradation of contaminant [18]. Otherwise, very low L_{MIN} values from Eq. (2) confirm that the applied methodology is strongly influenced by experimental conditions established during column tests. Specifically, for R = 1 (means that $C_{0(PRB)} = C_{0(column)}$) L_{MIN} is almost equal to bed length of GAC column.

Table 3. PRB minimum thickness (L_{MIN} and b) calculated for different initial Cs water concentration.

Experimental conditions				Simulated Cs field concentrations		Scaling-up coefficient	Eq. (2)	Eq. (4)	
υ (cm min^{-1})	**k_Y (min^{-1})**	**τ (min)**	**$C_{0(column)}$ (mg L^{-1})**	**$C_{i(target)}$ (pg L^{-1})**	**$C_{0(PRB)}$ (mg L^{-1})**	**R (-)**	**L_{min} (m)**	**t_R (h)**	**b (m)**
0.5	0.019	40	100	3.1	0.1	0.001	$0.02 \cdot 10^{-2}$	9.1	2.74
					1	0.01	$0.22 \cdot 10^{-2}$	11.15	3.34
					5	0.05	$1.08 \cdot 10^{-2}$	12.56	3.7
					20	0.2	$4.3 \cdot 10^{-2}$	13.78	4.13
					100	1	0.21	15.19	4.5

Consequently, calculated PRB longevity (d) vs groundwater (GW) velocity curves were plotted as useful predictor of long-term PRB performance for different assumed L_{PRB} values (0.5, 1, 2, 4 m) (Figure 5). GW filtration velocity and Cs concentration in simulated groundwater were assumed in the 0.001-1 cm min^{-1} [56] and 0.1, 1, 5 and 20 mg L^{-1}, respectively. Curves demonstrate that PRB longevity decreases with the increase of GW velocity. At the highest simulated Cs concentration (20 mg L^{-1}), PRBs with a thickness of 2 and 4 m have a longevity longer than 600 days when the GW velocity is lower than 0.01 cm min^{-1}. Whereas, if the GW velocity is higher than 0.1 cm min^{-1}, all simulated values of PRB thickness are not suitable to treat a Cs concentration of 20 mg L^{-1} (Figure 5a). Assuming a longevity of 600 days and Cs concentration of 5 mg L^{-1}, the several fixed PRB thickness are suitable at lower GW velocity (< 0.01 cm min^{-1}). On the contrary the PRB longevity decreases sharply at increasing GW velocity (Figure 5b). For Cs concentrations of 1 mg L^{-1} and GW velocity ranging between 0.008 and 0.07 cm min^{-1}, simulated PRBs have a longevity longer than 2 years (Figure 5c). At the lowest simulated concentration ($C_{0(PRB)}$ = 0.1 mg L^{-1}) and at the highest simulated GW velocity (1 cm min^{-1}), PRB with the largest thickness (L = 4 m) has a longevity of about 300 days (Figure 5d). As a whole, assuming a longevity (i.e.: 2 years) the establishment of the highest groundwater velocity occurs on PRB having the largest thickness simulated (i.e.: L = 4 m).

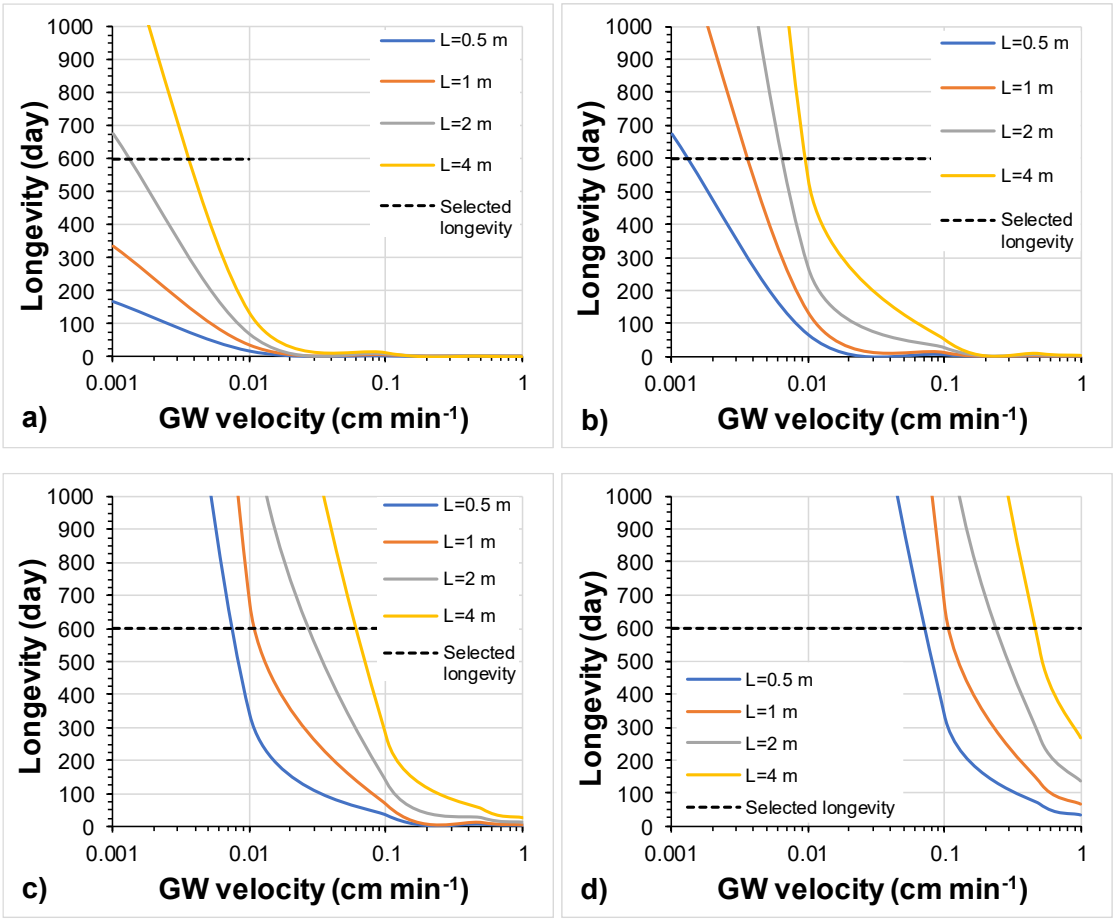

Figure 5. PRB longevity vs groundwater velocity for different fixed PRB thickness (L = 0.5, 1, 2, 4 m) and different Cs concentration in simulated groundwater ($C_{0(PRB)}$) (from calculation). $C_{0(PRB)}$ = 20 mg L^{-1} (**a**), $C_{0(PRB)}$ = 5 mg L^{-1} (**b**), $C_{0(PRB)}$ = 1 mg L^{-1} (**c**), $C_{0(PRB)}$ = 0.1 mg L^{-1} (**d**).

Curves plotted in Figure 5 were used for further technical consideration on PRB and MW-PRB design at the real scale. As also explained in Figure 1, one of the main advantages of the novel approach proposed is the possibility to significantly reduce the thickness (L) of the barrier thanks to the periodical MW regeneration of its filling material (GAC). From calculation (Table 4), it was found that, in the case of lower Cs contamination (C0 = 1 mg L^{-1}), for a L reduction from 1 to 0.5 m, 2 MW regeneration cycles (380 V m^{-1}, 15-min) are required. For the higher Cs concentration (C0 = 5 mg L^{-1}), 2, 4 and 8 cycles were calculated in order to reduce PRB thickness from 4 to 2, 1 and 0.5 m, respectively. Consequently, it is clear that a considerable thickness reduction is possible against a limited number of regeneration cycles, independently from the initial Cs contamination level. As better explained in Section 4.4, this weights significantly on the economy of the whole remediation project.

Table 4. Number of MW-regeneration cycles (380 V m^{-1}, 15-min MW irradiation time) needed to balance PRB thickness reduction in MW-PRB approach for the Scenario 1 and 2 (Calculation from MW-column experimental data).

Scenario	C_0 (mg L^{-1})	L_{PRB} (m)	L_{MW-PRB} (m)	$R_{reg\ (RE\ 100)}$	$R_{reg\ (RE)}$	Reg Cycles
1	1	1	0.5	2	2.5	2
2	5	4	2	2	2.5	2
			1	4	5	4
			0.5	7.5	9.38	8

During the MW irradiation process, the conversion of MW energy into heat (dielectric heating) is balanced by the reduction in electric field (E) during its penetration into the irradiated media. The intensity of the applied incident electric field (E_0) was also shown to significantly influence the ability of the MW penetration [57]. The E reduction curves with the distance from the MW source (d), calculated by Eqs. 9 and 10 for E_0 of 500, 1000 and 1500 V m^{-1}, were shown in Figure 6a. Data confirmed that the MW penetration effect is more considerable for the higher E_0 investigated and that E values are noticeable within a maximum d value of almost 25 cm. This highlights a limited penetration of the MWs into high-dielectric materials such as GAC [23]. Therefore, from E_d - d curves, the radius of influence (R_{MW}) corresponding to an E_d value of 385 V m^{-1} was obtained. A R_{MW} of ~ 2,5, 10 e 15 cm was found for E_0 of 500, 1000 and 1500 V m^{-1}, respectively.

In terms of technical equipment, for the in-situ generation of E values in the range of that considered in this work, a simple MW generation - transmission system is required [23]. It is essentially made up of a power generator equipped with microcontroller for power supply, an air/water cooled magnetron head, an insulator and a slotted coaxial antenna [58]. A 2.45 GHz with 6 kW power is needed to produce an incident electric field of 1500 V m^{-1}. It is connected to an antenna by a dedicated waveguide. The antenna design must ensure a coaxial line with a sufficient number of slots and short-circuited at its end in order to obtain a uniform MW power distribution along the antenna. The system also includes a specific vapour capture system. In addition, based on the obtained R_{MW} values, a such described system should be considered as mobile, due to the impossibility of inserting a very high number of antennas along the PRB.

4.4 Cost analysis

The comparison of main specific costs (per unit of plume transversal area, € m^{-2}) between conventional PRB and novel MW-PRB system was addressed considering two different simulated scenarios. Particular attention was posed on GAC saved cost (due to the potential reduction of MW-PRB thickness compared to conventional one), on MW energy cost required for the regeneration process and cost needed for GAC replacement due to the weight loss during MW regeneration (Table 5). In detail, GAC saved cost was calculated in order to investigate the effect of reducing thickness

on MW-PRB, whereas MW energy and GAC replacement costs are peculiar only for the MW-PRB system. Consequently, it was not included in conventional PRB design.

Input parameter for *Scenario 1* are $C_{0(PRB)}$ = 1 mg L^{-1}, L_{PRB} = 1 m, L_{MW-PRB} = 0.5 m. When thickness is halved, GAC weight needed for the MW-PRB is reduced of 0.25 ton m^{-2}, with a consequent saving of 300 € m^{-2} (Table 5). This effect is more evident looking the *Scenario 2*, whose input parameter are $C_{0(PRB)}$ = 5 mg L^{-1}, L_{PRB} = 5 m, L_{MW-PRB} = 0.5, 1 and 2 m. The amount of filled-GAC decreases with lowering MW-PRB thickness, and a maximum saving weight of 1.7 ton m^{-2} is obtainable when L_{MW-PRB} is 0.5 m. As expected, GAC saved cost is higher (about 2100 € m^{-2}) at the lower simulated thickness of MW-PRB (L_{MW-PRB} = 0.5 m) (Table 5). Among input parameters, regeneration cycles have been included for calculating the specific MW energy (kWh m^{-2}) and the cost required for regeneration process (€ m^{-2}) (Table 5). Considering the *Scenario 1*, the energy needed for two regeneration cycles is about 28.3 kWh m^{-2}, which corresponds to an energy cost of 3.4 € m^{-2}. The *Scenario 2* supposes three different number of regeneration cycles (2, 4, 8). As it can be observed from Table 5, the MW energy necessary for the regeneration of various thickness (L_{MW-PRB} = 0.5, 1, 2 m) of MW-PRB depends on regeneration cycles. In detail, the MW energy consumption depends on both the number of cycles and on the thickness of barrier. Therefore, a MW energy of 113.2 kWh m^{-2} is required during all simulated conditions because with the decrease of MW-PRB thickness increases the number of regeneration cycle, which should be implemented. Another aspect took into account was GAC weight loss (ton m^{-2}) during MW regeneration. MW-PRB design might also considered the cost needed for replacing GAC due to the weight loss during MW irradiation (Table 5). The specific GAC weight loss (% min^{-1}) obtained from experimental data (Figure 3) was used in order to calculate GAC weight loss (ton m^{-2}) during a 20-min MW irradiation time for the two simulated scenarios. Considering the *Scenario 2*, the cost required for replacing GAC weight loss during MW irradiation is about 96 € m^{-2}. This cost is the same at the different configurations assumed due to the constant value of weight loss, which is a function of weight loss per minute (% min^{-1}, Figure 3) and mass of GAC inside the PRB. Based on the peculiar specific costs of MW-PRB, the cost-benefit balance (CBB) was calculated for each scenario as the difference between GAC saved cost (A) and the sum of MW energy cost (B) and GAC replacing cost (C). CBB represents the net saving cost for the MW-PRB system (Table 5). The calculated CBB points out that: i) GAC saved cost is higher than the sum of the two other costs for both simulated scenarios (positive cost balance); ii) the cost balance is lowest at the lowest simulated Cs concentration (1 mg L^{-1}), iii) the cost balance increases with the PRB thickness reducing at the same simulated concentration (5 mg L^{-1}).

Table 5. Calculation for the scenario 1 and 2. Specific weight, weight loss during the MW regeneration process, specific MW energy consumption (E_0 = 385 V m^{-1}, MW irradiation time = 20 min, different cycles) and costs of GAC saved due to the thickness reduction, for the whole regeneration process and GAC replacement.

Scenario	C_0 (mg L^{-1})	L_{PRB} (m)	L_{MW-PRB} (m)	GAC total weight (L_{MW-PRB}) (ton m^{-2})	GAC saved weight (ton m^{-2})	Reg cycles	MW energy (kWh m^{-2})	GAC weight loss (ton m^{-2})
1	1	1	0.5	0.25	0.25	2	28.3	0.02
2	5	4	2	1	1	2	113.2	0.08
			1	0.5	1.5	4	113.2	0.08
			0.5	0.25	1.75	8	113.2	0.08

Scenario	C_0 (mg L^{-1})	L_{PRB} (m)	L_{MW-PRB} (m)	GAC saved cost (A) (€ m^{-2})	MW energy cost (B) (€ m^{-2})	GAC replacing cost (C) (€ m^{-2})	Cost benefit balance (CBB = A-B-C) (€ m^{-2})
1	1	1	0.5	300	3.4	24	272.6
2	5	4	2	1200	13.6	96	1090.4
			1	1800	13.6	96	1690.4
			0.5	2100	13.6	96	1990.4

The comparison of MW-PRB with conventional PRB costs (material and energy) is provided in Figure 6b. Assuming the parameters of *Scenario 2* ($C_{0(PRB)}$ = 5 mg L^{-1}, L_{PRB} = 4 m, L_{MW-PRB} = 2 m and 2 regeneration cycles), fixed depth of 1 m and varied PRB length (1 – 15 m) [59], material cost of conventional PRB has been compared with material and energy costs of MW-PRB (Figure 6b). As it can be noted, saved cost obtained by the application of MW-PRB system (area between the two solid lines in Figure 6b) increases with the increasing of PRB length demonstrating the beneficial effect of the reduced thickness.

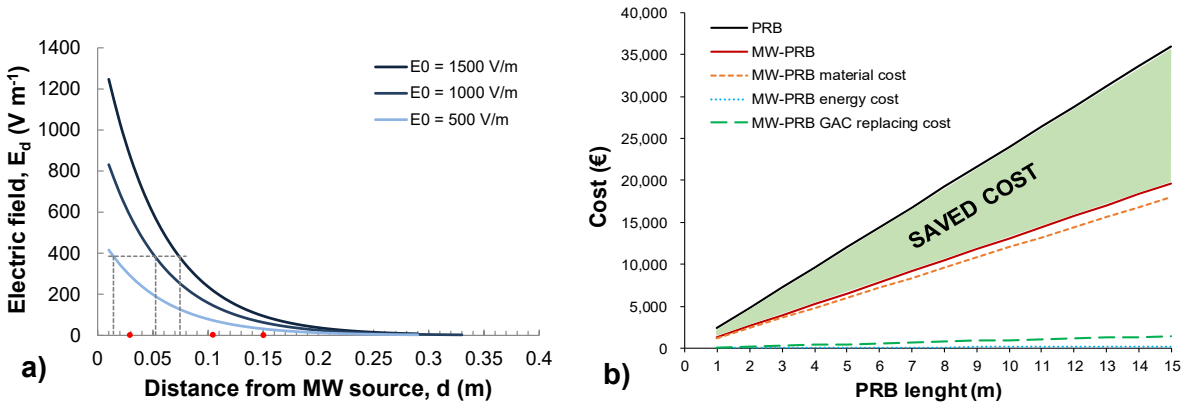

Figure 6. MW electric field variation with distance from MW source for different incident electric field (from calculation) (**a**). Material and energy cost comparison between PRB and MW-PRB at increasing PRB length (**b**).

Considering that material costs represent 40 – 50% of the total capital costs of PRB design and installation [59], saved cost obtained considering the MW-PRB system encourages the implementation of the proposed novel approach. PRB design and installation should also include construction costs, operation and maintenance costs (O&M), and decommissioning costs. Those costs have not been

compared because they are the same on both MW-PRB system and conventional one, however some information are given below. Providing cost data for PRB construction (both MW-PRB and conventional PRB), such as excavation operations (i.e.: conventional trenching vs injection methods) and configuration (i.e.: funnel-and-gate or continuous PRB) based on empirical rules is not feasible due to several site-specific factors [60]. Among those factors, lithologic characteristics of the site, surface/subsurface existing infrastructure, and depth of installation are the most important [19]. Intuitively, the deeper the contaminated plume and the longer the PRB, the greater are the constructions costs. As reported by ITRC (2011), costs for PRB installations using continuous trenching are about € 500 – 1400 for meter ($200–500/linear foot). Moreover, PRB exhibits low O&M costs which mainly regards monitoring since contaminated plume is likely to persists. However, the reactive media longevity and consequently costs of its replacement must be considered among O&M costs.

5. Conclusions

This study investigates the feasibility of a novel microwave based regenerating permeable reactive barrier (MW-PRB) system as combined treatment for Cs-impacted groundwater.

Results from batch experiments demonstrated the good feasibility of MW irradiation for regenerating Cs-saturated GAC as showed by the higher regeneration yield (79 – 110%) and lower GAC weight loss (6.78%) obtained after 10 successive MW regeneration cycles. Data also revealed that GAC life span is better preserved during MW irradiation as demonstrated by Langmuir specific area and pore structure variation. Column experiments results showed a Cs removal of ~80% when the GAC was irradiated for 15 min. Cesium thermal desorption, because the high temperature reached during the regeneration process (up to ~700 °C), and consequential stripping due to water distillation were elected as co-removal mechanisms. Kinetic parameters obtained from column experimental data by fitting Yoon and Nelson model (R^2 ~ 0.97) have been used for calculating PRB minimum thickness and longevity. Results from techno-economic analysis revealed the MW-PRB feasibility and its advantages also in comparison with conventional PRB systems, demonstrating the concept of combined MW-PRB treatment. Saved cost obtained corroborate in fact the potential cost effectiveness of MW-PRB system and, consequently, the implementation of novel approach is encouraged. Calculated PRB longevity vs groundwater velocity curves are useful in order to predict long-term PRB performance and the response of the remediation activities, as well as for guiding the design and the scaling-up of combined MW-PRB treatment. However, further investigations are needed in order to evaluate the feasibility of the proposed proof concept in real groundwater, which are known to be a more complex system.

References

[1] Lee, K.Y., Lee, S.H., Lee, J.E., Lee, S.Y., 2019. Biosorption of radioactive cesium from contaminated water by microalgae Haematococcus pluvialis and Chlorella vulgaris. Journal of Environmental Management. 233, 83–88. DOI:10.1016/j.jenvman.2018.12.022.

[2] Wang, K., Ma, H., Pu, S., Yan, C., Wang, M., Yu, J., Wang, X., Chu, W., Zinchenko, A., 2019. Hybrid porous magnetic bentonite-chitosan beads for selective removal of radioactive cesium in water. Journal of Hazardous Materials. 362, 160–169. DOI:10.1016/j.jhazmat.2018.08.067.

[3] Falciglia, P.P., Romano, S., Vagliasindi, F.G.A., 2017. Stabilisation/solidification of137Cs-contaminated soils using novel high-density grouts: γ-ray shielding properties, contaminant immobilisation and a γRS index-based approach for in situ applicability. Chemosphere. 168, 1257–1266. DOI:10.1016/j.chemosphere.2016.10.068.

[4] Khandaker, S., Toyohara, Y., Kamida, S., Kuba, T., 2018. Adsorptive removal of cesium from aqueous solution using oxidized bamboo charcoal. Water Resources and Industry. 19, 35–46. DOI:10.1016/j.wri.2018.01.001.

[5] Zhang, H., Tangparitkul, S., Hendry, B., Harper, J., Kim, Y.K., Hunter, T.N., Lee, J.W., Harbottle, D., 2019. Selective separation of cesium contaminated clays from pristine clays by flotation. Chemical Engineering Journal. 355, 797–804. DOI:10.1016/j.cej.2018.07.135.

[6] Zhang, Y., Jin, F., Shen, Z., Wang, F., Lynch, R., Al-Tabbaa, A., 2019. Adsorption of methyl tert-butyl ether (MTBE) onto ZSM-5 zeolite: Fixed-bed column tests, breakthrough curve modelling and regeneration. Chemosphere. 220, 422–431. DOI:10.1016/j.chemosphere.2018.12.170.

[7] Faisal, A.A.H., Sulaymon, A.H., Khaliefa, Q.M., 2018. A review of permeable reactive barrier as passive sustainable technology for groundwater remediation. International Journal of Environmental Science and Technology. 15, 1123–1138. DOI:10.1007/s13762-017-1466-0.

[8] Thiruvenkatachari, R., Vigneswaran, S., Naidu, R., 2008. Permeable reactive barrier for groundwater remediation. Journal of Industrial and Engineering Chemistry. 14, 145–156. DOI:10.1016/j.jiec.2007.10.001.

[9] Liu, X., Chen, G.R., Lee, D.J., Kawamoto, T., Tanaka, H., Chen, M.L., Luo, Y.K., 2014. Adsorption removal of cesium from drinking waters: A mini review on use of biosorbents and other adsorbents. Bioresource Technology. 160, 142–149. DOI:10.1016/j.biortech.2014.01.012.

[10] Awual, M.R., Suzuki, S., Taguchi, T., Shiwaku, H., Okamoto, Y., Yaita, T., 2014. Radioactive cesium removal from nuclear wastewater by novel inorganic and conjugate adsorbents. Chemical Engineering Journal. 242, 127–135. DOI:10.1016/j.cej.2013.12.072.

[11] Ghaeminia, M., Mokhtarani, N., 2018. Remediation of nitrate-contaminated groundwater by PRB-Electrokinetic integrated process. Journal of Environmental Management. 222, 234–241. DOI:10.1016/j.jenvman.2018.05.078.

[12] Marsh, H., Rodríguez-Reinoso, F., 2006.Activated Carbon, Elsevier S, Elsevier Science & Technology books, 2006.

[13] Mohan, D., Pittman, C.U., 2006. Activated carbons and low cost adsorbents for remediation of tri- and hexavalent chromium from water. Journal of Hazardous Materials. 137, 762–811. DOI:10.1016/j.jhazmat.2006.06.060.

[14] Montaña, M., Camacho, A., Serrano, I., Devesa, R., Matia, L., Vallés, I., 2013. Removal of radionuclides in drinking water by membrane treatment using ultrafiltration, reverse osmosis and electrodialysis reversal. Journal of Environmental Radioactivity. 125, 86–92. DOI:10.1016/j.jenvrad.2013.01.010.

[15] Caccin, M., Giacobbo, F., Da Ros, M., Besozzi, L., Mariani, M., 2013. Adsorption of uranium, cesium and strontium onto coconut shell activated carbon. Journal of Radioanalytical and Nuclear Chemistry. 297, 9–18. DOI:10.1007/s10967-012-2305-x.

[16] Li, D., Kaplan, D.I., Knox, A.S., Crapse, K.P., Diprete, D.P., 2014. Aqueous 99Tc, 129I and 137Cs removal from contaminated groundwater and sediments using highly effective low-cost sorbents. Journal of Environmental Radioactivity. 136, 56–63. DOI:10.1016/j.jenvrad.2014.05.010.

[17] Vanderheyden, S.R.H., Van Ammel, R., Sobiech-Matura, K., Vanreppelen, K., Schreurs, S., Schroeyers, W., Yperman, J., Carleer, R., 2016. Adsorption of cesium on different types of activated carbon. Journal of Radioanalytical and Nuclear Chemistry. 310, 301–310. DOI:10.1007/s10967-016-4807-4.

[18] ITRC, 2011. Permeable Reactive Barrier : Technology Update PRB-5. Washington, D.C.: Interstate Technology & Regulatory Council, PRB: Technology Update Team. www.itrcweb.org. www.itrcweb.org.

[19] Roehl, K.E., Meggyes, T., Simon, F.-G., Stewart, D.I., 2005.Long-term permance of permeable reactive barrier, in: J.O. (Univeristy of M. Ngriagu (Ed.), Trace Met. Other Contam. Environ., Elsevier B.V., 2005: pp. 311–321. DOI:10.1016/S0927-5215(05)80016-5.

[20] Huang, L., Liu, G., Dong, G., Wu, X., Wang, C., Liu, Y., 2017. Reaction mechanism of zero-valent iron coupling with microbe to degrade tetracycline in permeable reactive barrier (PRB). Chemical Engineering Journal. 316, 525–533. DOI:10.1016/j.cej.2017.01.096.

[21] Careghini, A., Saponaro, S., Sezenna, E., Daghio, M., Franzetti, A., Gandolfi, I., Bestetti, G., 2015. Lab-scale tests and numerical simulations for in situ treatment of polluted groundwater. Journal of Hazardous Materials. 287, 162–170. DOI:10.1016/j.jhazmat.2015.01.028.

[22] Gholami, F., Mosmeri, H., Shavandi, M., Dastgheib, S.M.M., Amoozegar, M.A., 2019. Application of encapsulated magnesium peroxide (MgO2) nanoparticles in permeable reactive barrier (PRB) for naphthalene and toluene bioremediation from groundwater. Science of the Total Environment. 655, 633–640. DOI:10.1016/j.scitotenv.2018.11.253.

[23] Falciglia, P.P., Roccaro, P., Bonanno, L., De Guidi, G., Vagliasindi, F.G.A., Romano, S., 2018. A review on the microwave heating as a sustainable technique for environmental

remediation/detoxification applications. Renewable and Sustainable Energy Reviews. 95, 147–170. DOI:10.1016/j.rser.2018.07.031.

[24] De Guidi, G., Falciglia, P.P., Catalfo, A., De Guidi, G., Fagone, S., Vagliasindi, F.G.A., 2017. Soil contaminated with PAHs and nitro-PAHs: contamination levels in an urban area of Catania (Sicily, southern Italy) and experimental results from simulated decontamination treatment. Clean Technologies and Environmental Policy. 19, 1121–1132. DOI:10.1007/s10098-016-1305-x.

[25] Li, W., Wang, X., Peng, J., 2014. Effects of microwave heating on porous structure of regenerated powdered activated carbon used in xylose. Environmental Technology. 35, 532–540. DOI:10.1080/09593330.2013.796007.

[26] Sun, Y., Zhang, B., Zheng, T., Wang, P., 2017. Regeneration of activated carbon saturated with chloramphenicol by microwave and ultraviolet irradiation. Chemical Engineering Journal. 320, 264–270. DOI:10.1016/j.cej.2017.03.007.

[27] Yang, Z., Yi, H., Tang, X., Zhao, S., Yu, Q., Gao, F., Zhou, Y., Wang, J., Huang, Y., Yang, K., Shi, Y., 2017. Potential demonstrations of “hot spots” presence by adsorption-desorption of toluene vapor onto granular activated carbon under microwave radiation. Chemical Engineering Journal. 319, 191–199. DOI:10.1016/j.cej.2017.02.157.

[28] Biniak, S., Szymański, G., Siedlewski, J., Światkoski, A., 1997. The characterization of activated carbons with oxygen and nitrogen surface groups. Carbon. 35, 1799–1810. DOI:10.1016/S0008-6223(97)00096-1.

[29] El-Kamash, A.M., 2008. Evaluation of zeolite A for the sorptive removal of Cs+ and Sr2+ ions from aqueous solutions using batch and fixed bed column operations. Journal of Hazardous Materials. 151, 432–445. DOI:10.1016/j.jhazmat.2007.06.009.

[30] Mihara, Y., Sikder, M.T., Yamagishi, H., Sasaki, T., Kurasaki, M., Itoh, S., Tanaka, S., 2016. Adsorption kinetic model of alginate gel beads synthesized micro particle-prussian blue to remove cesium ions from water. Journal of Water Process Engineering. 10, 9–19. DOI:10.1016/j.jwpe.2016.01.001.

[31] Liu, X., Quan, X., Bo, L., Chen, S., Zhao, Y., 2004. Simultaneous pentachlorophenol decomposition and granular activated carbon regeneration assisted by microwave irradiation. Carbon. 42, 415–422. DOI:10.1016/j.carbon.2003.12.032.

[32] Kimura, K., Hachinohe, M., Klasson, K.T., Hamamatsu, S., Hagiwara, S., Todoriki, S., Kawamoto, S., 2014. Removal of Radioactive Cesium (Cs-134 plus Cs-137) from Low-Level Contaminated Water by Charcoal and Broiler Litter Biochar Removal of Radioactive Cesium (134 Cs plus 137 Cs) from Low-Level Contaminated Water by Charcoal and Broiler Litter Biochar. Food Science and Technology Research. 6, 1183–1189. DOI:10.3136/fstr.20.1183.

[33] Chang, S.H., Wang, K.S., Liang, H.H., Chen, H.Y., Li, H.C., Peng, T.H., Su, Y.C., Chang, C.Y., 2010. Treatment of Reactive Black 5 by combined electrocoagulation-granular activated carbon adsorption-microwave regeneration process. Journal of Hazardous Materials. 175, 850–857. DOI:10.1016/j.jhazmat.2009.10.088.

[34] Al-Mutairi, N.Z., 2010. 2,4-Dinitrophenol adsorption by date seeds: Effect of physico-chemical environment and regeneration study. Desalination. 250, 892–901. DOI:10.1016/j.desal.2008.10.035.

[35] Langmuir, I., 1916. the Constitution and Fundamental Properties of Solids and Liquids. Part I. Solids. Journal of the American Chemical Society. 38, 2221–2295. DOI:10.1021/ja02268a002.

[36] Attallah, M.F., Borai, E.H., Hilal, M.A., Shehata, F.A., Abo-Aly, M.M., 2011. Utilization of different crown ethers impregnated polymeric resin for treatment of low level liquid radioactive waste by column chromatography. Journal of Hazardous Materials. 195, 73–81. DOI:10.1016/j.jhazmat.2011.08.007.

[37] Mahendra, C., Sathya Sai, P.M., Anand Babu, C., Revathy, K., Rajan, K.K., 2015. Analysis and modeling of fixed bed sorption of cesium by AMP-PAN. Journal of Environmental Chemical Engineering. 3, 1546–1554. DOI:10.1016/j.jece.2015.05.002.

[38] Ararem, A., Bouras, O., Bouzidi, A., 2013. Batch and continuous fixed-bed column adsorption of Cs+ and Sr2+ onto montmorillonite-iron oxide composite: Comparative and competitive study. Journal of Radioanalytical and Nuclear Chemistry. 298, 537–545. DOI:10.1007/s10967-013-2433-y.

[39] Yoon, Y.H., Nelson, J.H., 1984. Application of Gas Adsorption Kinetics I. A Theoretical Model for Respirator Cartridge Service Life. American Industrial Hygiene Association Journal. 45, 509–516. DOI:10.1080/15298668491400197.

[40] Malik, D.S., Jain, C.K., Yadav, A.K., 2018. Heavy Metal Removal by Fixed-Bed Column - A Review. ChemBioEng Reviews. 5, 173–179. DOI:10.1002/cben.201700018.

[41] Chang, S., Fu, H., Wu, X., Liu, C., Li, ZhengDai, Y., Zhang, H., 2018. Batch and fixed-bed column studies for selective removal of cesium ions by compressible Prussian blue/polyurethane sponge. RSC Advances. 8, 36459–36467. DOI:10.1039/c8ra07665k.

[42] Jang, J., Lee, D.S., 2016. Enhanced adsorption of cesium on PVA-alginate encapsulated Prussian blue-graphene oxide hydrogel beads in a fixed-bed column system. Bioresource Technology. 218, 294–300. DOI:10.1016/j.biortech.2016.06.100.

[43] Vukojević Medvidović, N., Nuić, I., Ugrina, M., Trgo, M., 2018. Evaluation of Natural Zeolite as a Material for Permeable Reactive Barrier for Remediation of Zinc-Contaminated Groundwater Based on Column Study. Water, Air, & Soil Pollution. 229–367. DOI:10.1007/s11270-018-4019-3.

[44] Zhou, D., Li, Y., Zhang, Y., Zhang, C., Li, X., Chen, Z., Huang, J., Li, X., Flores, G., Kamon, M., 2014. Column test-based optimization of the permeable reactive barrier (PRB) technique for remediating groundwater contaminated by landfill leachates. Journal of Contaminant Hydrology. 168, 1–16. DOI:10.1016/j.jconhyd.2014.09.003.

[45] Gavaskar, A.R., 1999. Design and construction techniques for permeable reactive barriers. Journal of Hazardous Materials. 68, 41–71.

[46] Falciglia, P.P., Catalfo, A., Finocchiaro, G., Vagliasindi, F.G.A., Romano, S., De Guidi, G.,

2018. Microwave heating coupled with UV-A irradiation for PAH removal from highly contaminated marine sediments and subsequent photo-degradation of the generated vaporized organic compounds. Chemical Engineering Journal. 334, 172–183. DOI:10.1016/j.cej.2017.10.041.

[47] Falciglia, P.P., De Guidi, G., Catalfo, A., Vagliasindi, F.G.A., 2016. Remediation of soils contaminated with PAHs and nitro-PAHs using microwave irradiation. Chemical Engineering Journal. 296, 162–172. DOI:10.1016/j.cej.2016.03.099.

[48] Falciglia, P.P., De Guidi, G., Catalfo, A., Finocchiaro, G., Farina, M., Liali, M., Lorenzano, G., Valastro, G., Vagliasindi, F.G.A., 2017. Glycerol-enhanced microwave heating for ultra-rapid effective remediation of marine sediments highly contaminated with hydrocarbons. Separation and Purification Technology. 189, 11–19. DOI:10.1016/j.seppur.2017.07.066.

[49] Honda, M., Okamoto, Y., Shimoyama, I., Shiwaku, H., Suzuki, S., Yaita, T., 2017. Mechanism of Cs Removal from Fukushima Weathered Biotite by Heat Treatment with a NaCl-CaCl2Mixed Salt. ACS Omega. 2, 721–727. DOI:10.1021/acsomega.6b00372.

[50] Liu, C., Zachara, J.M., Qafoku, O., Smith, S.C., 2003. Effect of temperature on Cs+ sorption and desorption in subsurface sediments at the Hanford Site, U.S.A. Environmental Science and Technology. 37, 2640–2645. DOI:10.1021/es026221h.

[51] Shimoyana, I., Hirao, N., Baba, Y., Izumi, T., Okamoto, Y., Yaita, T., Suzuki, S., 2014. Low-pressure sublimation method for cesium decontamination of clay minerlas. Clay Science. 18, 71–77.

[52] Ania, C.O., Parra, J.B., Menéndez, J.A., Pis, J.J., 2007. Microwave-assisted regeneration of activated carbons loaded with pharmaceuticals. Water Research. 41, 3299–3306. DOI:10.1016/j.watres.2007.05.006.

[53] Zanella, O., Tessaro, I.C., Féris, L.A., 2014. Desorption- and decomposition-based techniques for the regeneration of activated carbon. Chemical Engineering and Technology. 37, 1447–1459. DOI:10.1002/ceat.201300808.

[54] Vincent, C., Hertz, A., Vincent, T., Barré, Y., Guibal, E., 2014. Immobilization of inorganic ion-exchanger into biopolymer foams – Application to cesium sorption. Chemical Engineering Journal. 236, 202–211. DOI:10.1016/j.cej.2013.09.087.

[55] Yang, X., Wan, Y., Zheng, Y., He, F., Yu, Z., Huang, J., Wang, H., Ok, Y.S., Jiang, Y., Gao, B., 2019. Surface functional groups of carbon-based adsorbents and their roles in the removal of heavy metals from aqueous solutions: A critical review. Chemical Engineering Journal. 366, 608–621. DOI:10.1016/j.cej.2019.02.119.

[56] Harter, T., 2003. Basic Concepts of Groundwater Hydrology. University of California, Farm Water Quality Planning (FWQP). 1–6.

[57] Falciglia, P.P., Scandura, P., Vagliasindi, F.G.A., 2017. Modelling of in situ microwave heating of hydrocarbon-polluted soils: Influence of soil properties and operating conditions on electric field variation and temperature profiles. Journal of Geochemical Exploration. 174, 91–99. DOI:10.1016/j.gexplo.2016.06.005.

[58] Pauli, M., Kayser, T., Feiler, J., Wiesbeck, W., 2006.A coaxial Antenna for Microwave Assisted Soil Decontamination, in: 2006 IEEE MTT-S Int. Microw. Symp. Dig., IEEE, 2006: pp. 2027–2030. DOI:10.1109/MWSYM.2006.249852.

[59] Powell, R.M., Powell, P.D., Puls, R.W., 2002. Economic Analysis of the Implementation of Permeable Reactive Barriers for Remediation of Contaminated Ground Water.

[60] Naidu, R., Birke, V., 2015.Permeable Reactive Barrier Sustainable Groundwater Remediation, 2015. DOI:10.1201/9781351228886.

Chapter 7: General discussion and future perspectives

1. Summary of main findings

The adsorption is a well-established technique for CEC removal from aqueous solutions. Amongst adsorbent materials, ACs are perhaps the most cost-effective materials for removing both organic and inorganic compounds, such as PFAS and Cs radionuclide, the two target contaminants investigated in this research. However, one of the limiting factors affecting ACs performance at full-scale treatment plants is the regeneration needed to recover the adsorption capacity and to avoid AC landfill disposal. The key findings of this research are summarized as follow:

- The critical review provided on Chapter 3 highlights relevant limitations of previous published works on PFAS adsorption. Particularly, due to the unrealistic conditions at which experimental studies were carried out (e.g., high dosages of adsorbents, high concentration of PFAS), the investigation of PFAS removal at environmental conditions is strongly advised. Few studies focused on the effect of OM often provide contrasting results, OM seems to negatively affect short-chain PFAS adsorption due to the active site competition. Whereas, the effect of OM on long-chain PFAS adsorption seems to be less relevant. However, future researches are needed to better understand the simultaneous effect of ionic strength and OM. The comparison of previous performed column experiments for PFAS removal (Chapter 3) reveals a rapid breakthrough of PFAS (specifically short-chain ones) through GAC columns which requires a frequent replacement and/or regeneration. To date, the regeneration of PFAS-exhausted GAC is very challenging and further research should investigate regeneration techniques alternative to the chemical regeneration. The latter in fact is unfeasible due to the high related costs and the environmental issues linked to the use of organic solvents required to desorb the hydrophobic C-F chain.
- The obtained findings in Chapter 4 point out that MW irradiation is a promising regeneration technique for PFAS-saturated GAC. Main results show the strong ability of GAC to convert MW irradiation into a rapid temperature increase (~150 °C min^{-1} at power of 500 W). The fast temperature increase jointly with dielectric nature of ACs leads to high MW regeneration efficiency (>90%) for both PFOA- and PFOS-saturated GAC (at MW irradiation of 500 W for 3 min). The observed linear correlation between GAC temperatures reached during MW irradiation and the weight loss may also be useful in the selection of commercially available GACs. At a comparable value of adsorption capacity for a target compound, AC characterized by lower weight loss and sharp temperature rise should be preferred since it is more prone to MW irradiation (Chapter 4, Section 3.1). As a whole, the MW irradiation

slightly affect the GAC textural properties, GAC porous structure is preserved after several MW regeneration cycles.

- Findings from Chapter 5 demonstrate the good feasibility of MW irradiation for the regeneration of Cs-saturated GAC. Specifically, after ten successive adsorption/regeneration cycles, the observed values of regeneration efficiency (RE~90%) jointly with a moderate GAC weight loss (~7%) demonstrates the GAC life span preservation during MW irradiation. Results from column tests confirm that GAC can be regenerated by MW irradiation also in dynamic condition, due to sublimation/vaporization and vapour stripping Cs removal mechanisms and that the regeneration effectiveness is time-dependent (Chapter 5, Section 3.5). The concept of permeable reactive barrier coupled with microwave (MW-PRB) is introduced for the first time as an innovative in situ-remediation technology with focus on Cs-contaminated water.
- The feasibility of novel microwave based regenerating permeable reactive barrier (MW-PRB) has been demonstrated as combined treatment for Cs-impacted groundwater. Batch and column experiments data related to MW regeneration of Cs-saturated GACs were used to the PRB design, as the calculation of minimum thickness and longevity (*Chapter 6*). Calculated PRB longevity vs groundwater velocity curves are useful in order to predict long-term PRB performance and the response of the remediation activities. The techno-economic analysis allowed the comparison of novel MW-PRB and conventional PRB also in terms of materials cost. Saved cost obtained corroborate the potential cost effectiveness of MW-PRB system and, consequently, the implementation of novel approach is encouraged. The obtained results provide essential information to guide the scaling-up of application.

2. Future perspectives

MW irradiation has found relevance in the regeneration of carbonaceous materials due to its unique molecular level heating ability that leads to quick and homogeneous thermal reactions. In few years, it may expect the increase evolution of MW technology turned from an interesting alternative approach into a powerful standard technique due to its several advantages such short processing time, rapid and precise temperature control, selective heating and good performance in terms of adsorption capacity recovery.

In the present research, the efficiency of MW irradiation for the regeneration of GACs saturated with long-chain PFAS and Cs was asserted. The main findings of this research support and promote the feasibility of MW irradiation for the regeneration of saturated ACs. They provide essential information to design and conduct the successive pilot-scale studies. Moreover, some speculations

here provided could be helpful to guide the successive scaling-up and to expand the boundaries of full-scale applications.

Although promising results have been obtained for PFOA and PFOS, further investigations are necessary to demonstrate the efficiency of MW regeneration for other PFAS. Indeed, concern regarding the persistence and bioaccumulation of long-chain PFAS had led manufactures to replace them with shorter chain compounds or alternative ones. Moreover, due to the unique chemical properties of PFAS, further investigations in this research topic are advised to overcome some knowledge gaps and to better understand the efficiency of MW regeneration in the presence of co-existing compounds (both organic matter and inorganic compounds). Moreover, the understanding of PFAS degradation mechanisms under MW irradiation deserves further investigations since a stepwise CF_2 flake-off manner toward related short-chain compounds could also occur.

As regards the novel proposed MW-PRB system, further investigations are needed in order to evaluate its feasibility in real groundwater, which are known to be a more complex system. Although several lab-scale studies demonstrate the possibility to reach high temperatures (> 500 °C) within very short irradiation times (~5 min) also applying relatively low power, full-scale MW application to regenerate activated carbons is still challenging. Indeed, pilot- and full-scale studies are very limited due to the complexity in MW heating plant design, implementation and operation. Moreover, the lack of data related to thermal and physical properties of both adsorbates (e.g., PFAS and Cs) and ACs such as the dielectric properties represents another limiting factor. Despite the novel proposed MW-PRB, two ways (ex-situ and in situ) could be allow the potential field application of MW regeneration for saturated ACs. They ACs would be feasible, of potential interest and, then, worthy of investigation. The ex-situ field application may include a conveyor belt for saturated ACs transportation along a tunnel equipped with MW generator. Conversely, in situ solution would focus on the direct regeneration of GAC column without carbon movement. MW irradiation could be performed by means of specific slotted coaxial antennas inserted along the carbon bed. Furthermore, the well-known benefits of MW heating may be also applied to other environmental matrices for instance to contaminated soil, since conventional thermal treatment often requires long treatment times to reach high temperatures needed for contaminant desorption.

In conclusion material characterization, scaling-up, pilot, modelling, design and demonstration studies are strongly encouraged in order to surround the existing gap between lab-scale findings and full-scale applications, and moving to industrial/production scale.